The Dissertation Committee for Sarena DelVecchio Horava Certifies that this is the approved version of the following dissertation:

Novel Carriers for Oral Delivery of Hemophiliac Factor IX

Committee:

Nicholas A. Peppas, Supervisor

Maria Croyle

Benny Freeman

Jennifer A. Maynard

Donald R. Paul

Novel Carriers for Oral Delivery of Hemophiliac Factor IX

by

Sarena DelVecchio Horava, B.S., M.S.E.

Dissertation

Presented to the Faculty of the Graduate School of

The University of Texas at Austin

in Partial Fulfillment

of the Requirements

for the Degree of

Doctor of Philosophy

The University of Texas at Austin

May 2016

Dedication

To my family for their continued support, inspiration, and encouragement.

Acknowledgements

I would like to thank Dr. Nicholas Peppas for his guidance and support throughout my graduate experience. I would also like to thank my committee members—Dr. Croyle, Dr. Freeman, Dr. Maynard, and Dr. Paul—for their support and feedback.

I have enjoyed being part of the collaborative and supportive environment in the Peppas lab. My research and graduate experience has been positively influenced by the advice and expertise of my colleagues, as well as their friendship. I would like to thank my fellow lab mates, namely, Julia Vela Ramirez, Mary Caldorera-Moore, Brenda Carrillo-Conde, Giulia Pasotti, Brandon Slaughter, Bill Liechty, Jennifer Knipe, Amey Puranik, Diane Forbes, Stephanie Steichen, Michael Koetting, Jonathan Peters, Heidi Culver, Lindsey Sharpe, David Spencer, Angela Wagner, John Clegg, and Marissa Wechsler. I would also like to thank my undergraduate research assistants, Katie Moy and Joel Liou, for their contributions to this work.

I would also like to acknowledge the National Science Foundation, the P. E. O. Philanthropic Organization, the Cockrell School of Engineering, and the National Institutes of Health for providing funding for my research and education.

Novel Carriers for Oral Delivery of Hemophiliac Factor IX

Sarena DelVecchio Horava, Ph.D.

The University of Texas at Austin, 2016

Supervisor: Nicholas A. Peppas

Current treatments for hemophilia B, a hereditary bleeding disorder characterized by the deficiency of coagulation factor IX (FIX), rely on injection-based administration that cause pain and discomfort, leading to noncompliance and risk of subsequent bleeding episodes. A non-invasive protein replacement therapy using an oral delivery system can both overcome such issues and improve access to treatment in developing countries. Oral delivery is a desirable route for protein therapeutics; however, two main challenges—increasing bioavailability and maintaining protein functionality—need to be addressed when designing a delivery platform. The overarching goal of this work presented here is to develop an oral delivery system for human factor IX (hFIX) as a convenient prophylactic treatment. Complexation hydrogels have been engineered to protect biologics from the harsh environment of the GI tract and deliver them to the small intestine for absorption. We have successfully developed pH-responsive hydrogel networks based on poly(methacrylic acid)-grafted-poly(ethylene glycol) [P(MAA-g-EG)] as delivery vehicles for hFIX.

We have focused on optimizing the drug loading and release, as well as evaluating *in vitro* drug absorption and *in vivo* biocompatibility and biodistribution of the microcarrier. Tailoring the networks of P(MAA-g-EG) hydrogels improved the loading of hFIX within the microcarriers, which is critical for minimizing protein degradation.

Optimizing the loading conditions by increasing the incubation time and using a reduced ionic strength buffer further improved the delivery potential of the microcarriers. The presence of the microcarriers significantly improved the *in vitro* absorption of hFIX. As an alternative strategy designed to further increase the delivery potential, we incorporated an enzymatically degradable component into the P(MAA-g-EG) microcarrier system. Evaluation of this degradable system demonstrated the increased levels of hFIX in intestinal conditions, which has the potential to promote the oral bioavailability of hFIX. We performed stability testing of lyophilized hFIX-loaded microparticles to determine the effects of storage conditions on hFIX release and activity. Lastly, *in vivo* biocompatibility and biodistribution studies were performed to establish the safety of multiple oral doses of P(MAA-g-EG) microparticles and to determine the residence time and clearance of these microcarriers. *In vivo* preclinical studies were critical for clinical applications of these drug delivery systems. This works shows that P(MAA-g-EG) microcarriers are promising candidates for the oral delivery of hFIX for treating hemophilia B.

Table of Contents

List of Tables

List of Figures

Chapter 1: Introduction

Hemophilia B is a hereditary bleeding disorder characterized by the deficiency of clotting factor IX (FIX). Protein replacement therapy has successfully improved the patient's life expectancy and quality of life. However, current treatment methods rely on injections and infusions of factor IX concentrates which causes pain and discomfort, leading to noncompliance and risk of subsequent bleeding episodes. Additionally, such treatment regimens are limited to developed countries mainly due to costs of the drug, medical care (e.g. hospital visits, surgery), and possible serious complications from therapy (e.g. severe allergic reactions). A non-invasive treatment for hemophilia B, such as an oral delivery system, is desired both to overcome these issues associated with current methods and to increase global access to protein therapy.

Oral delivery is a desirable route of administration for a diversity of therapeutics for the treatment of systemic and local diseases. The benefits of oral delivery include ease of administration, increased compliance, and lower costs. However, there are two main challenges—maintaining protein functionality and increasing bioavailability—that need to be addressed when designing an oral delivery system. In the oral route, the protein therapeutic must survive the transit along the gastrointestinal (GI) tract. The protein must pass through harsh environment of the stomach before reaching the small intestine where it can be absorbed into the bloodstream. The second challenge to oral delivery is increasing the bioavailability of the protein. In order to reach circulation, the protein must be absorbed in the upper small intestine and pass through the epithelium into the bloodstream. Increasing the permeability of the protein is critical for achieving therapeutically relevant levels in the bloodstream.

Anionic complexation hydrogels have been engineered to protect proteins from the harsh environment of the GI tract and deliver them to the small intestine due to pH-responsive swelling. Our lab has successfully developed environmentally responsive polymeric systems, notably poly(methacrylic acid) grafted with poly(ethylene glycol), denoted as P(MAA-g-EG), as vehicles for the delivery of insulin (5.8 kDa), calcitonin (3.4 kDa), and interferon alpha (23 kDa). However, a polymeric carrier system had not yet been optimized for high molecular weight proteins, such as blood clotting factor IX (57 kDa).

Work presented here considers the development of environmentally responsive hydrogel systems for the oral delivery of clotting factor IX. We cover strategies for tailoring the crosslinked networks of P(MAA-g-EG) hydrogels for loading and release of factor IX, as well as systematically developing methods to improve factor IX loading and release. As an alternative strategy, we explored the use of an enzymatically degradable crosslinking agent in the P(MAA-g-EG) system to improve the site-specific release of factor IX. In addition to the amount of factor IX release, we evaluated the biological activity of factor IX and selected hydrogel systems that maintained protein function, which is essential to therapeutic use.

In addition to preserving biological activity, the overall bioavailability of orally administered factor IX also depends on transport across the intestinal epithelium. We explored the effects of these microparticle drug delivery systems in enhancing the permeability of factor IX across an *in vitro* intestinal epithelium.

For further development of oral delivery systems, we included stability testing and preclinical studies. Stability testing is used for predicting shelf life and recommending storage conditions that maintain the desired release profile while preserving the biological activity of factor IX. Furthermore, evaluating *in vivo* biocompatibility of drug delivery systems is essential to establishing safe use in clinical applications. Knowledge of the *in*

vivo biodistribution of the microcarriers provides information about the residence time in the small intestine and clearance time, which is important for understanding the pharmacokinetics and safety.

Successful outcomes of this work can have positive implications for protein replacement therapy for hemophilia B patients. As a non-invasive method, oral administration of factor IX could change the treatment regimens of hemophilic patients worldwide.

Chapter 2: Background

2.1 Coagulation and Hemostasis

2.1.1 Overview

Knowledge of coagulation and hemostasis is necessary for understanding bleeding disorders, such as hemophilia B, and their treatments. Generally, the coagulation cascade leads to the localized generation of thrombin, then the conversion of fibrinogen to insoluble fibrin polymers that, together with platelet aggregation, functions in maintaining hemostasis (Figure 2-1). Coagulation can be divided into (1) fibrin formation, (2) fibrinolysis, (3) platelet function, and (4) natural anticoagulants.[1]

The coagulation cascade is a series of enzymatic reactions involving activated coagulations proteins and activated platelets designed to amplify the signal from initial trauma into the formation of a fibrin plug. The classic coagulation pathway describes two separate pathways—extrinsic and intrinsic pathways—which were developed based on *in vitro* laboratory tests, but do not match clinical observations. The "new pathway" of coagulation describes the *in vivo* mechanism.[1, 2]

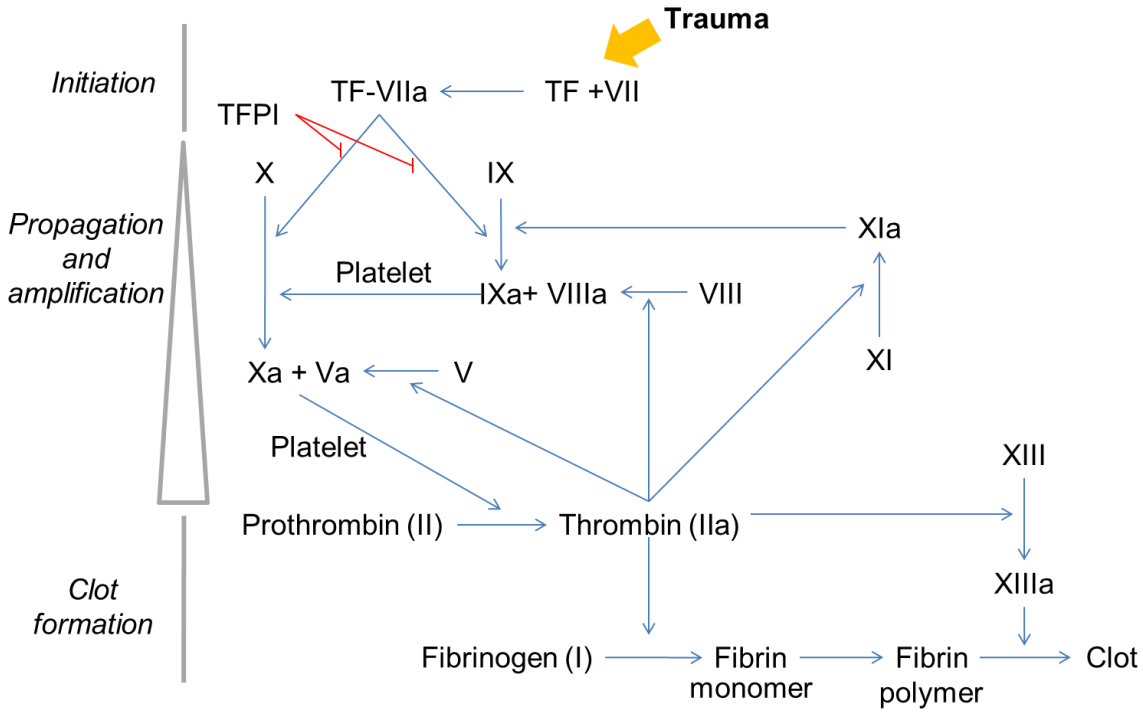

Figure 2-1. Simple diagram of the coagulation cascade. As a result of trauma, tissue factor (TF) initiates the cascade by activating factor VII and binding to factor VIIa. The TF-VIIa complex activates factor X both directly and indirectly via IXa/VIIIa. The initial factor Xa generates a small amount of thrombin, which then begins the propagation and amplification of the cascade. Then, thrombin activates factors VIII and V, which assemble with factors IXa and Xa, respectively, on the platelet surface. The direct activation of factor X is rapidly shut down by tissue factor pathway inhibitor (TFPI). The indirect generation of factor Xa via factor IXa from factor Xia is necessary for effective coagulation to proceed. During the propagation phase, thrombin is amplified and fibrinogen forms the principle structural protein of the clot. Thrombin cleaves fibrinogen into fibrin monomers that form fibrin polymers, which assemble by non-covalent interactions. Factor XIIa covalently crosslinks the fibrin, making a stable clot. (Note: For simplicity, Roman numerals denote coagulation factors and an 'a' indicates the activated form. Figure adapted from *Francischetti*[2].)

2.1.2 Coagulation Proteins

The coagulation cascade involves various coagulation proteins, which are typically either enzymes (serine proteases) or cofactors (Table 2-1). For coagulation proteins classified as enzymes, the protein frameworks consist of a serine protease and various domains with specific functions in clotting. Enzymatic coagulation proteins are synthesized as biologically inactive proenzymes, and most become activated by post-translation modification. For example, factors II, VII, IX, and X, protein C, and protein S have vitamin K-dependent glutamic acid (Gla) domains on the amino terminus. In order to become activated, the 9-11 glutamic acids in the Gla domain are modified by carboxylation of glutamic acid, forming gamma-carboxyglutamic acid. The carboxylation requires vitamin K. The gamma-carboxyglutamic acid residues allow for the binding of calcium. The binding of calcium to the Gla domains serves two functions: (1) inducing a conformational change in the protein necessary for its enzymatic activity, and (2) enabling the protein to bind to the phospholipid surfaces.[3]

The binding of coagulation proteins to phospholipid surfaces of platelets and endothelial cells localizes the coagulation reactions, improving their efficiency. Most coagulation reactions involve a "quaternary complex" containing (1) an active enzyme binding to (2) a cofactor that is bonded by (3) calcium to (4) a phospholipid surface. The cofactors increase the rate of reaction by orders of magnitude.[1]

Table 2-1. Classifications of coagulation proteins.[1]

Enzymes	Cofactors	Miscellaneous
Factor IIa	Tissue factor	Fibrinogen
Factor VIIa	Factor V	Factor XIII
Factor IXa	Factor VIII	$Alpha_2$ antiplasmin
Factor Xa	Protein S	PAI-1
Factor XIa		Antithrombin
Protein C		
tPA		
Plasmin		

2.1.3 Initiation of Coagulation

The coagulation cascade begins with exposure to tissue factor (TF). TF is a membrane-bound glycoprotein that located mainly in the adventitia of a vessel wall. TF is on mostly all cell surfaces except for that of endothelial cells and circulating blood cells.[4] Trauma causing vessel injury exposes TF to factor VII (FVII) and active FVII (FVIIa) present in the circulating blood, forming an active TF-FVIIa complex.[5] The formation of the TF-FVIIa complex initiates the coagulation cascade, by activating FIX and FX. Additionally, FIXa with its cofactor FVIIIa activates FX. Notably, the two most common forms of hemophilia, A and B, are caused by the deficiency in FVIII and FIX, respectively. Then FXa binds with cofactor FVa to generate a small amount of thrombin from prothrombin (FII), marking the final step of the initiation phase. The production of thrombin is the most crucial step in hemostasis.[1]

2.1.4 Propagation and Amplification of Coagulation

The generation of thrombin marks the commencement of the propagation and amplification phase of the coagulation cascade. Thrombin is a multifunctional enzyme

involved in various coagulation reactions. Unlike other coagulation proteins, thrombin does not require a cofactor for enzymatic function, and activated thrombin separates from its Gla domain allowing it to float around to promote clotting. Thrombin provides both positive feedback by activating FV, FVIII, FXI, FXIII, and thrombin-activatable fibrinolysis inhibitor (TAFI) and negative feedback by activating protein C and promoting fibrinolysis. Overall, the propagation phase amplifies the amount of thrombin generated and fibrinogen forms the principle structural protein of the clot.[1, 2]

2.1.5 Fibrin Clot Formation

During clot formation, the fibrinogen is converted into an insoluble, stable fibrin thrombus. Thrombin converts fibrinogen into fibrin monomer by clipping off two peptides (fibrinopeptides A and B) from either end of the fibrinogen molecule. Removal of these peptides exposes the polymerization sites of the fibrin monomer, which can bind to other fibrin monomers producing fibrin polymers. The fibrin polymers assemble by non-covalent interactions, forming a loose clot. FXIIIa then covalently crosslinks the fibrin polymers by forming ε-(γ glutamyl) lysine bonds between the side chains, resulting in a stable thrombus.[6] Additionally, thrombin activates TAFI, inhibiting fibrinolysis and promoting coagulation. TAFI catalyzing the removal of C-terminal lysines of partially degraded fibrin, which are binding sites for plasminogen (see below).[7]

2.1.6 Fibrinolysis

Fibrinolysis is the breakdown of blood clots, which prevents clots from growing too large and becoming problematic, aids in wound healing, and prevents thrombosis in undesired locations. Plasminogen, an inactive precursor to plasmin, is in circulation and becomes incorporated into the clot. Plasminogen is activated by tissue plasminogen activator (tPA), urokinase plasminogen activator (uPA), FXIa, and FXIIa.

The most important plasminogen activator is tPA, which is slowly released from the endothelium of the injured blood vessel. As tPA filters through the clot, it can bind to fibrin to convert plasminogen into plasmin. Plasmin is a serine protease that cleaves bonds in fibrin and fibrinogen, released during clot lysis. The rate at which tPA cleaves plasminogen is significantly higher when both molecules are bound to the fibrin clot. Plasminogen binds to the C-terminal lysine residues of fibrin.[1, 8]

Fibrinolysis is also regulated by several mechanisms. First, uPA and tPA are inhibited by plasminogen activator inhibitors (PAI-1 and PAI-2). Any excess uPA and tPA in the plasma is rapidly bound and inactivated by PAI-1 and PAI-2, which helps confine active fibrinolysis to the thrombus. Additionally, any plasmin free in the plasma is rapidly deactivated by α_2-antiplasmin and α_2-macroglobulin. However, plasmin bound to fibrin is protected from inactivation. Lastly, the fibrin clot is protected by TAFI, an enzyme activated by thrombin, that removes C-terminal lysine residues from the fibrin strand that are required for the binding of plasminogen to the clot.[8]

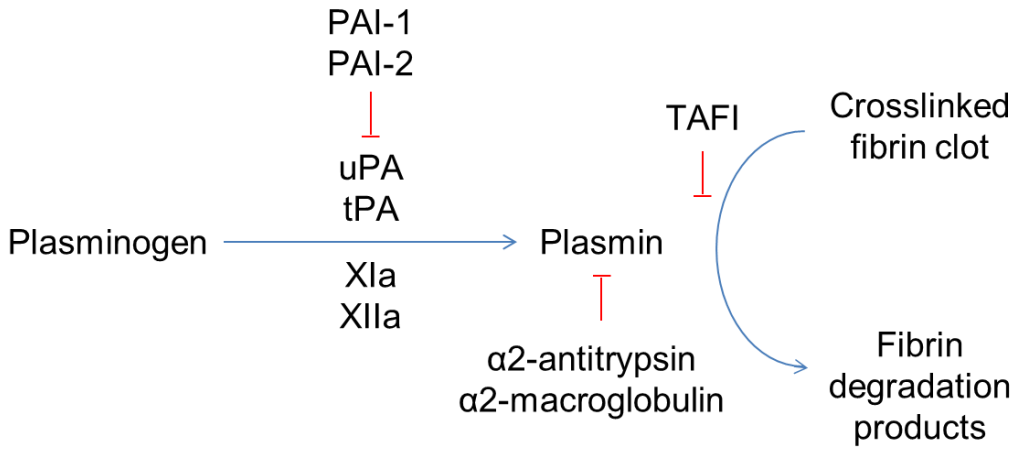

Figure 2-2. Simplified pathway of fibrinolysis.[8]

2.1.7 Function of Platelets

Briefly, platelets are produced in the bone marrow by budding off the edges of megakaryocytes. Platelets are found freely circulating or sequestered in the spleen (one-third of platelets are in the spleen). The four main functions of platelets are to (1) adhere to damaged endothelium, (2) store adenosine diphosphate (ADP) and proteins, (3) aggregate with other platelets, and (4) provide a surface for coagulation reactions ("quaternary complex").

Platelets in circulation survey the integrity of the vascular system, responding to lesions adhering to damaged endothelial cells and to extracellular matrix components exposed to flowing blood. Platelet adhesion to wound sites is mediated by von Willebrand factor (VWF), an adhesive glycoprotein present in plasma. VWF binds to exposed collagen, inducing a structural change in VWF for platelet attachment. The two distinct platelet receptors for VWF are glycoprotein (GP) Ibα in the GP Ib-IX-V complex and the integrin $\alpha_{IIb}\beta_3$ in the GP IIb-IIa complex. Binding of VWF to platelet receptors initiates platelet activation and creates a platelet monolayer over the injured surface.[9]

Platelets contain granules for storage functions. Alpha granules store proteins, such as vWF and FV, and dense granules store chemicals, such as serotonin and ADP. Release of ADP activates nearby platelets, and further platelet activation also leads to the production of another platelet activator/agonist, thromboxane A_2. Such platelet agonists play an important role in platelet aggregation.[1]

After platelets have formed a monolayer on an injured surface by adhering to the vasculature, they release platelet agonists such as ADP, which activates the platelet receptors GP IIb/IIIa of nearby platelets. Activation of GP IIb/IIIa can occur due to various processes including: (1) binding of vWF to GP Ib, (2) binding of platelet agonist such as ADP and thromboxane A_2 to platelet receptors, and (3) binding of thrombin to platelet

thrombin receptor. Thrombin is known as the most potent physiologic activator of platelets. Furthermore, thrombin links the humoral phase of coagulation (e.g. tissue factor, etc.) to platelet activation. Activation of GP IIb/IIIa leads to platelet aggregation. Active GP IIb/IIIa receptors exposed on the platelet surface bind to fibrinogen (abundant in the plasma), which acts as glue for platelet aggregation. As the platelets aggregate into a large mass, they form a platelet plug to stop bleeding.[1]

Furthermore, as part of the "quaternary complexes", activated platelets serve as a surface on which coagulation reactions occur. Activation of platelets exposes a negatively charged phospholipid called phosphatidylserine which augments the binding of coagulation proteins to the injured site. Additionally, blebs called platelet microparticles bubble off the surface of activated platelets to increase the surface area for coagulation reactions.[1]

2.1.8 Natural Anticoagulants

Natural anticoagulants regulate the coagulation cascade, ensuring that excess thrombosis does not occur. These protein inhibitors are tissue factor pathway inhibitor (TFPI), protein C, protein S, and antithrombin. TFPI rapidly shuts down the activation of FX by binding to FXa. This TFPI-FXa complex then forms a quaternary complex with TF-FVIIa, which also stops the activation of FIX. However, the coagulation cascade can still proceed through thrombin activation of FXI, which then actives FIX and leads to more thrombin generation. Protein C is serine protease that cleaves FVa and FVIIIa specifically. Protein S is a cofactor that is critical for the function of protein C. Protein S circulates in two forms, a free form and a form bound to C4B-binding protein, and free form (normally around 40% of protein S) serves as a cofactor to protein C. Lastly, antithrombin is a serine protease inhibitor that binds and inactivates all serine proteases in the coagulation cascade

(see Table 2-1). Heparan (a glycosaminoglycan in extracellular matrix produced by all cell types) and heparin (a glycosaminoglycan produced only by mast cells) are anticoagulants that dramatically increase the function of antithrombin.[1]

2.2 HEMOPHILIA B

2.2.1 Overview

Hemophilia, the oldest known hereditary bleeding disorder, is characterized by spontaneous and prolonged bleeding in the joints, muscle and internal organs [10]. It is potentially life-threatening and is often associated with disabling arthropathy resulting from recurring joint bleeding episodes. Hemophilia A and hemophilia B are congenital X-chromosome linked coagulation disorders, which arise from the deficiency in coagulation factor VIII (FVIII, MW=264 kDa) or factor IX (FIX, MW=57 kDa), respectively, normally expressed in the liver. Hemophilia A is the most common with approximately 80% of hemophilia cases.[11, 12] However, hemophilia B affects 80,000 males worldwide.[10] We have selected hemophilia B as the target disease for developing an oral delivery system of FIX, taking into consideration protein size.

2.2.2 Causes

Hemophilia B is a genetic disorder caused by a mutation in the F9 gene encoding FIX located on the X chromosome. (See Section 2.3.2 Mutations in F9 Gene for more details about the genetic causes.) Hemophilia B is usually inherited; however, in 30% of the cases, hemophilia B is caused by a sporadic mutation.[11-13] In the inherited cases, hemophilia B is inherited in an X-linked recessive manner, meaning that males (XY) with one mutated X chromosome and females (XX) with two mutated X chromosomes (although rare) have hemophilia B. A female with a single mutated X chromosome is a

genetic carrier. In the case of a father without hemophilia and a mother who is a carrier, 50% of their sons will have hemophilia and 50% of their daughters will be carriers (Figure 2-3). In the case of a father with hemophilia and mother without hemophilia, none of their sons will have hemophilia, but all their daughters will be carriers. Female carriers may exhibit symptoms of hemophilia B due to the lyonization (X-inactivation). Lyonization is a normal phenomenon in which one of the two haploid sets of X-linked genes in a cell are inactivated at random and have no phenotypic expression. On average, carriers have about 50% of the normal amount of clotting factor due to suppression of about half of the normal F9 gene. However, some carriers have far lower levels of FIX.[12]

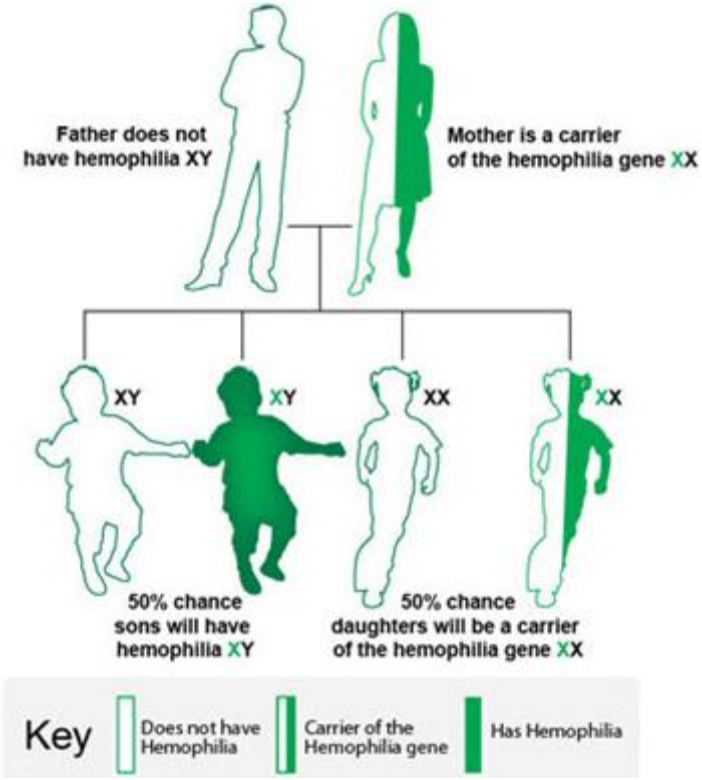

Figure 2-3. Inheritance of hemophilia in the case of a father without hemophilia and a mother who is a carrier.[11]

2.2.3 Symptoms

The clinical severity of hemophilia is related to level of factor IX deficiency in the blood, which affects the symptoms. The classifications of hemophilia B and associated symptoms are outlined in Table 2-2.[2, 10, 13-16] Generally, patients with severe disease often have unprovoked bleeding, while patients with moderate disease tend to bleed with trauma. Patients with severe disease often only bleed as a result of severe trauma, surgery, or dental procedures.

Table 2-2. Classification of hemophilia B. Classifications are based on *in vitro* clotting activity (1 % = 1 IU/dL).[13]

Clinical severity	Factor IX clotting activity	Cases by severity	Symptoms	Typical age of diagnosis
Severe	< 1%	60%	Frequent spontaneous bleeding (2-5/mo.); spontaneous joint bleeding; bruises and hematomas not due to trauma	≤ 2 years
Moderate	1% - 5%	15%	Rare spontaneous bleeding (1/mo.–1/yr.); joint bleeding; bruises and hematomas not due to trauma	< 5 – 6 years
Mild	>5%- 30%	25%	No spontaneous bleeding (< 1/yr.); often no outward signs	Often later in life

Hemarthrosis, bleeding into joint spaces, is a common symptom of hemophilia. The knee and elbow are the most common sites of joint bleeding, but the ankle and shoulder can also be affected. Typically, the bleeding starts with hemorrhage into the synovial space, where the presence of intrasynovial blood causes an inflammatory reaction. Inflammation leads to pain, warmth, and swelling. Subsequently, synovium hypertrophies (inflammation) and increased vascularity lead to the recurrence of joint bleeding. Patients

can develop “target joints” where recurrent bleeding episodes can occur, leading to permanent damage and chronic pain. Untreated hemarthroses commonly results in crippling arthritis and ultimately joint failure, typically requiring joint replacement. Furthermore, hemophilia patients have a 15-40 times greater incidence rate of developing septic arthritis than the general population.[17]

Another common symptom of hemophilia is intramuscular hematomas caused by muscle bleeding. Muscle bleeding in any limb can be further complicated by compartment syndrome (excessive pressure build up caused by internal bleeding and swelling), which may require surgical decompression if they progress despite factor replacement. Iliopsoas (inner hip muscles) muscle hematomas are particularly devastating to the patient, and may also be life-threatening. If compartment syndrome is developed in the psoas muscle as result of iliopsoas muscle hematomas, compression of the femoral nerve can result in paralysis of the quadriceps muscle group.[1]

Internal bleeding in the brain is a very serious complication of hemophilia may be a result of minor trauma or may occur spontaneously, particularly in patients with severe disease. Associated symptoms include long-lasting headaches, repeated vomiting, sleepiness, behavioral changes, double vision, convulsions, and seizures.[11] Cerebral hemorrhages are the leading case of hemorrhagic death.[1]

About one third of carriers are classified as a symptomatic carrier, meaning she has 40-60% of FIX activity levels and experiences abnormal bleeding. In most cases, the symptoms of symptomatic carriers are similar to that of men with mild hemophilia. However, symptomatic carriers often have heavier, more prolonged menstrual bleeding (termed menorrhagia) and are more likely to require an iron supplement. Females are also more likely to experience pain during menstrual bleeding (termed dysmenorrhea), as well as experience some internal bleeding during ovulation causing mid-cycle pain. Mid-cycle

bleeding can become severe or even life-threatening, especially in carriers with very low FIX levels. Carriers also have a higher risk of developing hemorrhagic ovarian cysts due to increased internal bleeding during ovulation. These cysts are typically painful and may require urgent medical care. Additionally, carriers are also at higher risk to develop endometriosis.[12]

Additionally, labor and delivery can affect carriers (and females with hemophilia B), as well as male babies with hemophilia B. Male babies with hemophilia are at an increased risk of head bleeding during labor and delivery, particularly if the process is prolonged. Carriers of hemophilia, especially symptomatic carriers and women with hemophilia, have an increased risk of postpartum hemorrhage. In developing countries, postpartum hemorrhage is a major cause of maternal death and disability.[12]

2.2.4 Diagnosis

The typical age at diagnosis depends on the clinical severity of hemophilia B (Table 2-2). In the United States, most people with hemophilia are diagnosed at a young age. Over the past decade, increased awareness and improved recognition has resulted in over 50% of cases being diagnosed in the newborn period.[18] In the United States, the median age at diagnosis is 36 months for mild hemophilia, 8 months for moderate hemophilia, and 1 month for severe hemophilia, which is particularly affected by known family history.[19]

Diagnosis includes screening tests to determine if the blood is clotting properly and clotting factor tests (factor assays) to diagnose the specific bleeding disorder. Various screening tests are complete blood count (CBC), activated partial thromboplastin time (APTT) test, prothrombin time (PT) test, and fibrinogen test. CBC is a common test used to measure the amount of hemoglobin, the size and number of red blood cells, and the amounts of different types of white blood cells and platelets. Typically, the CBC results

are normal in hemophilia patients; however, the hemoglobin and red blood cell count might be low due to unusually heavy or prolonged bleeding.[11] APTT tests measure clotting time, primarily based on the clotting abilities of FVIII, FIX, FXI, and FXII. Normal times are 25-35 seconds, while deficiency of FIX prolongs clotting by up to 2.5 times. PT tests measure clotting time, primarily based on the clotting abilities of fibrinogen, prothrombin, FV, FVII, and FX. Results for hemophilia B patients are not affected. Fibrinogen tests, which measure clotting time based on fibrinogen activity, are used when APPT and PT results are abnormal. Specific clotting factor tests are used to determine the activity of individual clotting factors, which determine the type of hemophilia and severity.[11]

Given a known family history of bleeding disorders, many families elect to have their male babies tested after delivery. If a mother is a known carrier of hemophilia, testing can be performed during pregnancy. Options for prenatal diagnosis include chorionic villus sampling at 9 to 11 weeks or amniocentesis (amniotic fluid sampling) at 15 to 20 weeks.[12] Immediately after birth, a blood sample is drawn from the umbilical cord and tested for clotting factor levels. While low levels of FVIII are strongly indicative of hemophilia A, results for FIX are not as conclusive. FIX takes longer to develop, taking about 6 months of age to reach normal levels. Mildly low FIX level at birth are not necessary due to hemophilia B, but significantly decreased levels are indicative of hemophilia B. Repeating the test is recommended when the baby is older.[11] Without knowledge of family history or in the case of sporadic hemophilia, the time of diagnosis is based on outward signs and symptoms.

Genetic testing is also available; however, accessibility may be limited by cost and regulatory bodies, and are associated with ethical and cultural concerns. Genetic testing may be useful for carrier testing, treatment of hemophilia patients, and, in the future, determination of eligibility for gene therapy. Genetic testing for factor IX mutations require

scanning the entire gene, since there are no common mutations causing hemophilia B. In the case of a potential carrier, the National Hemophilia Foundation's Medical and Scientific Advisory Council recommends carrier testing before becoming pregnant. Carrier testing will first use clotting factor tests. However, if these test results are inclusive, genetic testing is recommended.[13]

In the case of known family history, especially if the female is a known carrier, families should consider genetic counseling when family planning. Female carriers have options available for conception, prenatal diagnosis, and fetal sex determination. To minimize or eliminate the risk of having a child with hemophilia, there are currently three conception options:

- In vitro fertilization (IVF) with pre-implantation diagnosis: embryos are genetically tested and ones without the mutated gene are implanted
- IVF with egg donation: donor eggs from a woman that is not a carrier
- Sperm sorting: only sperm carrying an X chromosome are used, ensuring the birth of a female child

All these procedures are expensive and not available in many parts of the world, as well as have ethical, cultural, and religious implications. Additionally, they have other associated risks. The success rate of IVF is approximately 30%. For the pre-implantation diagnosis, prenatal testing is still recommended. In the case of sperm sorting, this method is only available in specialized centers as a research tool and is still under evaluation. Furthermore, sperm sorting will only ensure a female child, but this child may still inherit the altered gene and be a carrier. For a female carrier, male babies will inherit the mutated gene for hemophilia. Determining the sex can provide options regarding the pregnancy, as well as allow for planning of labor and delivery to minimize bleeding of the male fetus. Fetal sex

determination can be tested by fetal sex typing from maternal plasma at 8 weeks or by ultrasound scan at 15 weeks.[12]

Genetic testing for F9 mutations requires sequencing of the entire F9 gene. A well-standardized method is DNA amplification by PCR followed by direct sequencing. However, PCR is generally not able to detect large deletions or other gross abnormalities in carriers due to the presence of the other allele (normal F9 gene). Although such mutations are uncommon, they are nearly always associated with severe disease, making the carrier status important.[20] Recently new techniques, such as multiplex ligation-dependent probe amplification (MLPA) and multiplex amplification and probe hybridization (MAPH), have been successfully applied to sequencing the F9 gene.[21, 22]

2.3 FACTOR IX

2.3.1 Structure and Function

Factor IX (also known as Christmas factor) is a vitamin K-dependent coagulation glycoprotein (17 wt. % carbohydrate). The average plasma concentration of FIX is 2.5-5 μg/mL, and its half-life in circulation is 24 hours. hFIX is a single chain consisting of 415 amino acid (aa) residues with a molecular weight of 57 kDa (note that recombinant hFIX is 55 kDa). F9 gene (for FIX) was fully sequenced in 1985.[23] F9 is located at Xq27.1, spanning 33 kbp (kilo-base pair). The gene contains eight exons which are transcribed into a 2802-bp mRNA. This mRNA is then translated into a 461-amino acid (aa) sequence from which a 28-aa signal peptide and a 18-aa propeptide are removed, leaving a 415-aa mature protein. The primary translocation product has an approximate molecular weight of 52-kDa.[20]

The structure of FIX can be broken down into six domains: (1) γ-carboxylation acid (Gla), (2) short hydrophobic stack, (3) epidermal growth factor 1 (EGF1), (4) EGF2, (5) activation peptide, and (6) serine protease (Figure 2-4). [24, 25] The activation of FIX, either by TF-FVIIa or FXIa, occurs after the double cleavage of peptide bonds after the Arg192 and Arg 266, releasing the activation peptide (MW=11 kDa). Activated FIX (FIXa) has a light chain, (Gla, EGF1, and EGF2 domains) and a heavy chain (serine protease) held together by a single disulfide bond (Cys178-Cys335). FIXa has catalytic activity due to the exposed catalytic triad of the serine protease domain. [24]

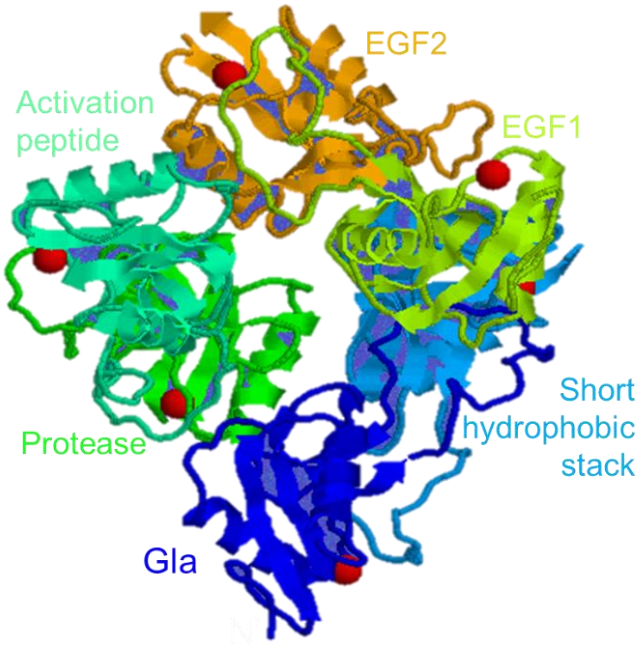

Figure 2-4. Structure of factor IX. Individual domains are color coded. Note that the red spheres are calcium ions. (Adapted from *College*.[25])

The Gla domain contains 11 glutamic acid residues that are post-translationally modified to 4-carboxyglutamate. As previously mentioned, these modified residues are

necessary for the binding of calcium ions. The binding of calcium ions give the Gla domain a positive charge which interacts with the negatively charged phospholipid membrane.[20]

The catalytic triad, which is characteristic of serine proteases, is made up of His267, Asp315, and Ser411.[20] FIXa on its own is relatively inefficient in activating its preferred substrate, FX. However, when FIXa is non-covalently bound to its cofactor, FVIIIa, and forms a macromolecular intrinsic tenase complex, its specific activity is increased by 50,000-fold.[26] Additionally, docking on a phospholipid membrane (forming a "quaternary complex") further enhances its catalytic activity. While the structure of the FIXa-FVIIIa complex has not been determined, it can be inferred from published crystal structures of porcine FIXa,[27] individual domains of hFIXa,[28-30] and hFVIII.[31, 32] Based on the porcine FIXa structure shown in Figure 2-5, the light chain (Gla, EGF1, and EGF2 domains) of FIXa forms a stalk with the Gla domain at bottom end, allowing the Gla domain to attach to the phospholipid membrane. The top of the stalk is the serine protease (catalytic domain), which has a globular structure.[20] Interactions with FVIIIa include critical residues in the EGF1, EGF2, and catalytic domains of FIXa.[32, 33]

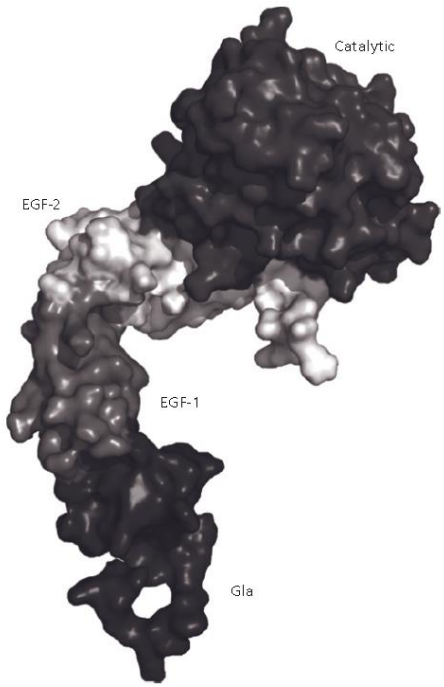

Figure 2-5. Structure of porcine activated factor IX. Individual domains are shown in shades of grey. (PDB ID: 1PFX)[20]

2.3.2 Mutations in F9 Gene

Approximately 900 distinct mutations in the F9 gene are reported across three public databases (Haemophilia B Mutation Database; Coagulation Serine Protease Mutation Database; The Human Gene Mutation Database). The different types of genetic defects reported in hemophilia B are categorized in Figure 2-6.

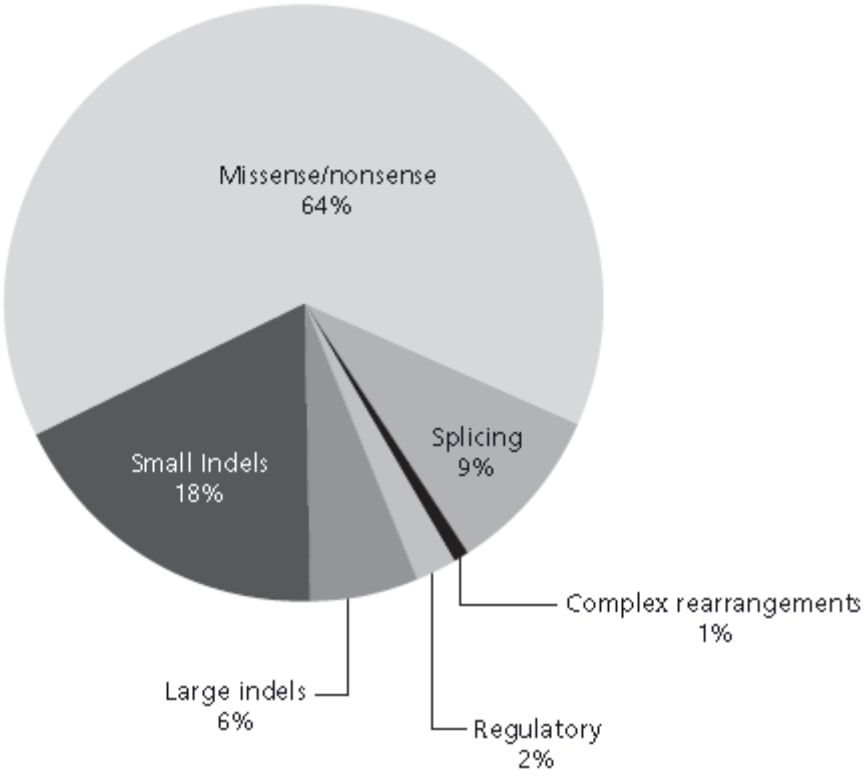

Figure 2-6. Categories of genetic defects reported in hemophilia B. (Note that indel means insertion or deletion of bases in DNA.)[20]

Point mutations are the most common type of abnormality found in hemophilia B (64% of all mutations). Analysis of the number of mutations reported at each position showed that certain nucleotides are more frequently mutated ("mutation hotspots"). One example of "mutation hotspots" is the overexpression of arginine residues, which can be explained by the effect of CpG islands (increased mutation rate in the regions with a high frequency of cytosine and guanine nucleotides typically found near transcription start sites of genes).[34] Furthermore, point mutations causing hemophilia B that occur during meiosis are more frequent in the male gamete.[35] The location of the point mutation affects the

severity of the disease. Point mutations can result in missense mutations, premature stop codons, or splicing.

Missense mutations can provide information about the function of specific regions of the protein. Missense mutations are classified into two broad types:

- Type I: quantitative mutations resulting in reduced levels of an otherwise normal protein
- Type II: qualitative mutants of the protein having reduced function that may be presence at either normal or reduced amount.

Many missense mutations can belong to both categories.

Type I mutations can be a result of a mutation in the signal peptide (residues 1-28), which directs intracellular trafficking of the protein and has no effect on the function of the circulating form. Defects in the signal peptide can lead to reduced levels of secretion, producing a full spectrum of disease severity. Most Type I defects are caused by impairment of transcription or protein secretion.[20]

However, approximately 60% of the mutations that cause hemophilia B are predominantly type II, which is unusual in coagulation factor deficiency. Type II mutations that occur in triad of residues forming the active site render the protein in incapable of catalytic activity, resulting in severe hemophilia B. Another example of type II defects is mutations in the propeptide (residues 29-46), which mediates the interaction with the vitamin K-dependent γ-carboxylase. Mutations in this region produce proteins with reduced function due to impaired phospholipid binding.[36]

A nonsense mutation is a single point mutation that results in a premature stop codon. Generally, nonsense mutations result in a severe type I defect with no protein production. However, nonsense mutations can occur near the C-terminal end which results in the production of a truncated, non-functional protein (type II defect).

Splicing defects accounts for 9% of all mutations and can results in a range of disease severity. One cause of splicing mutations is a single point mutation that destroys a splice donor site, generally resulting in a nonsense mRNA. Secondly, a point mutation in the sequence of an intron can create an alternative splice acceptor site which may result in a nonsense mRNA.[20]

Other occurrences of "mutation hotspots" can be explained by the founder effect where specific mutations occur more frequently in a particular, geographically restricted hemophilia B population. Such mutations indicate the inheritance of a discrete rare haplotype, which has become more prevalent in population with a relatively restricted gene pool. Examples of mutations due to the founder effect have been reported in North America,[37] the United Kingdom,[38] and Ireland.[39]

Unlike the previously described mutations in the coding sequence, mutations in the gene's regulatory elements in the non-coding sequence (2% of all mutations) can result in type I defects. There are several known mutations that affect transcription factor binding sites in the F9 promoter. Some of these mutations cause a type I defect with FIX levels at a stable low level throughout life. However, mutations in the F9 promoter region can also cause hemophilia B Leyden. The hemophilia B Leyden phenotype is characterized by a severe deficiency in FIX at birth, then FIX levels starts to increase during the second decade of life, and FIX levels near normality are achieved in the third decade. After that, normal or near-normal levels are maintained through life. The mutations that cause hemophilia B Leyden occur in promoter regions not associated with the androgen response element (ARE), which regulates transcription levels following the hormonal changes associated with puberty. Transcription of the F9 gene is upregulated as testosterone levels increase, which therefore produces more FIX after puberty.[40, 41]

The insertion or deletion of a few nucleotides can result in hemophilia B (indels are 18% of all mutations). These mutations, which often occur in sequences of dinucleotide repeats, are commonly in the intron sequence and, therefore, have no effect. However, indels can occasionally occur in regulatory elements or result in frame-shifts. Frame-shift errors likely result in a severe FIX deficiency.[20]

Gross genetic abnormalities, which include gene rearrangements or large deletions, account for 7% of hemophilia B cases. In hemophilia B, deletions are more common than inversions in F9. A complete deletion of F9, or null allele, results in severe hemophilia B. Since the probability of inhibitor formation is related to severity and type of genetic defect, a null allele results in the greatest risk of inhibitor formation.[42]

2.4 HEMOPHILIA B TREATMENTS

2.4.1 Treatment

In the late 1950s and early 1960s, hemophilia B was treated using fresh frozen plasma (FFP) or prothrombin complex concentrates (PCC). PCCs were prepared by absorbing plasma from the vitamin K-dependent proteins and the final product not only contained FIX, but prothrombin, FVII, and FX. Due to the lack of purity, these products were associated with numerous complications including excessive activation of the coagulation pathway and large volumes (especially for FFP) to achieve desired FIX levels.[1, 13] By the 1970s, lyophilized powder concentrates of FIX became available, allowing for home storage and self-infusion.[13] However, these blood factors were originally plasma derived. Until relatively recently, procuring a safe blood supply was difficult, with risks of transmitting hepatitis and HIV viruses to patients receiving blood-derived products. Specifically, over 60% of hemophiliac patients were accidently

infected.[43] Due to the advancements in blood screening for infectious agents and methods for viral inactivation, the production process for deriving factors from human plasma is now significantly safer.[43] In the 1990s, plasma-derived FIX products with improved purity and safety entered the market.[13] In 1997, the first recombinant FIX (granted to Genetics Institute; now a Pfizer product under the tradename BeneFIX®) was approved by the FDA.[43] Additionally, use of prophylaxis in children became more common during the mid-1990s, which has improved patients' quality of life and life expectancy. Now, fusion proteins are engineered to improve pharmacokinetics in order prolong circulation time. In March 2014, the FDA approved the first long-lasting recombinant FIX Fc fusion protein (ALPROLIX® by Biogen Idec®).[44]

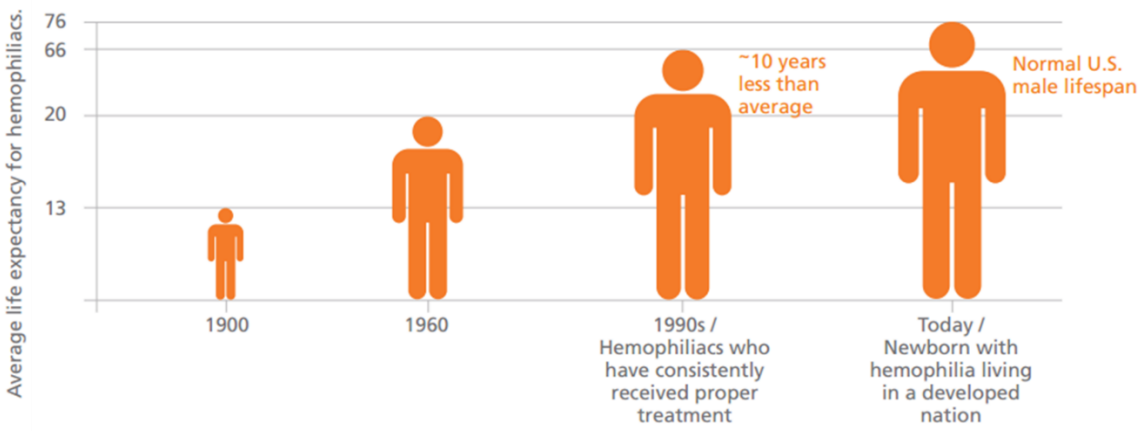

Figure 2-7. Average life expectancy of hemophilia patients. Better treatments have increased the life expectancy of hemophilia patients.[13]

Current treatment for hemophilia B consists of protein replacement therapy of plasma-derived or, more recently, recombinant factor IX concentrates. On-demand treatment, required after a bleeding event, is given as an intravenous (IV) injection or by

continuous infusion. Advancements in hemophilia treatments have significantly increased the life expectancy of hemophilia patients (Figure 2-7). Although this treatment markedly improves both the life expectancy and the quality of life of the hemophilia patients, it suffers from low patient compliance due to fear, pain, and embarrassment associated with needle-based treatments.[45]

Prophylactic therapy is the administration of replacement therapy in the absence of bleeding as a protective measure. Regimens are tailored on a per patient basis with intervals typically ranging from every other day to two or three infusions per week [45]. ALPROLIX® (Biogen Idec®), a recombinant FIX Fc fusion protein with a longer half-life in the circulation, only requires infusions once per week (at maximum) for hemophilia B prophylactic therapy. [44] The benefits of a prophylaxis regimen include:

- Greatly reduced or ceased spontaneous bleeding episodes by a one to five percent increase in circulating factor IX [45]
- Prevention of future joint disease by early initiation (1-2 years of age) of prophylaxis [46]
- More effective than on-demand treatment, even at a later start (> 2 years of age). [47, 48]

In 2007, the National Hemophilia Foundation Medical and Scientific Advisory Council recommend prophylactic treatments as optimal therapy for children with severe hemophilia B.[13] In 2013, about 33% of patients with severe hemophilia B used prophylaxis, while patients with moderate and mild hemophilia B mainly relied on on-demand treatments. The average prophylaxis rates were 15% globally and 27% in the United States in 2013.[49]

However, the major challenge, especially with children, is the need for venous access. Central venous access devices must be surgically implanted and have associated risks of infection and thrombosis. An alternative is using an arteriovenous fistula to treat

children, but long-term effects are not well established.[48] Issues with venous access, as well as variability in severe hemophilic phenotype, can result in unnecessary invasive procedures for children.

Overall, therapies, both on-demand and prophylactic, are not getting to those who need them due to economic, societal, and practical hindrances. Global accessibility is limited due to costs associated with the drug, medical care, and possible complications with therapy.[45] Without modern treatments, the median life expectancy is 11 years, which is still the case in many developing countries.[14] In order to improve the worldwide use of prophylactic therapy and prevent invasive procedures in children, alternative delivery methods and less expensive treatment approaches are necessary.

2.4.2 Commercially Available Products and Market

Current products for the treatment of hemophilia B include plasma-derived FIX, recombinant FIX, and long-lasting recombinant FIX, as outlined in Table 2-3.

Table 2-3. Current commercially available products for hemophilia B treatment.[49]

Company	Product	Type	Use	FDA Approval
CSL Behring	Mononine/Berinin-P	Plasma-derived	On-demand	1992
Baxter/Baxalta	Immunine	Plasma-derived	On-demand and prophylaxis	Not for use in US
Grifols	AlphaNine SD	Plasma-derived	On-demand	1996
Octapharma	Octanine	Plasma-derived	On-demand	Not for use in US
Pfizer	BeneFIX	Recombinant	On-demand	1997
Baxter/Baxalta	RIXUBUS	Recombinant	On-demand and prophylaxis	June 2013
Biogen Idec	ALPROLIX	Long-lasting recombinant, Fc fusion	On-demand and prophylaxis	March 2014
Cangene/Emergent BioSolutions	IXINITY	Recombinant	On-demand	May 2015
CSL Behring	IDELVION	Long-lasting recombinant, albumin fusion	On-demand and prophylaxis	March 2016

The global market for hemophilia B in 2013 was $1.2B for the 80,000 patients worldwide. Currently, it is estimated that 30% of individuals with hemophilia B have been diagnosed and are receiving treatment. Additionally, more patients are seeking out prophylactic treatments, especially as new products are entering the market. As a result, the global market is projected to grow at an average rate of 9% to reach over $1.8B by 2016.[49]

Pfizer is the market share leader in hemophilia B treatment. BeneFIX® is one of Pfizer's major products with an annual revenue of $213M worldwide and $97M in the United States in 2013. Baxter/Baxalta released RIXUBIS™, the first recombinant FIX product for prophylaxis (FDA approved in June 2013), which resulted in a short term market advantage.[49] However, the emergence of long-lasting products with reduced

injection frequency and therefore increased patient compliance are expected to capture a significant share of the market. For example, Biogen Idec's ALPROLIX® is a long-lasting therapy that offers the convenience of less frequent injections. As the first long-lasting factor IX to reach the market, ALPROLIX® is expected to capture a significant share of the market. Since receiving FDA approval in March 2014, Aprolix has brought in $10M in revenue for Q2. Barclays Capital analysis forecasted $75M in annual sales for ALPROLIX® in 2014, reaching $581M in 2020.[50] The market for hemophilia B treatments is beginning to shift to therapies that offer improved patient compliance and convenience (Figure 2-8).

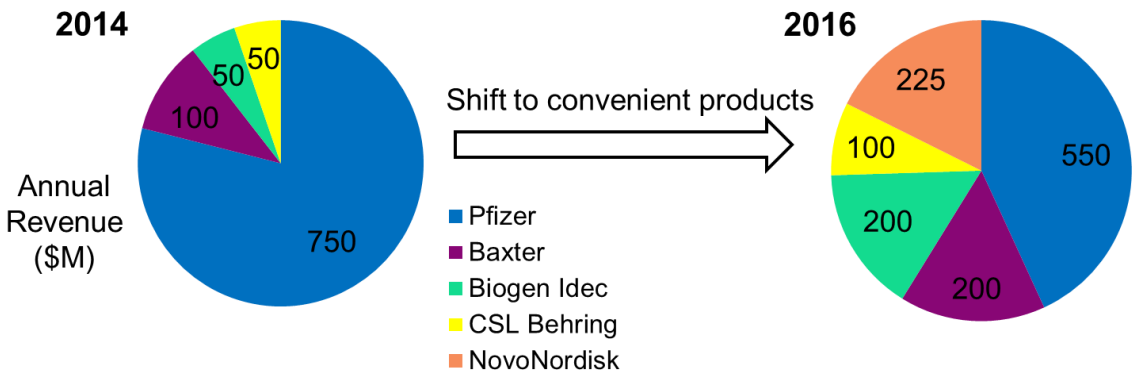

Figure 2-8. The market share for recombinant factor IX products. Based on 2016 estimates, the market is expected to shift to emerging long-lasting products.[49]

2.4.3 Product Pipeline and Recently Approved Products

The trend in emerging products for hemophilia is engineering FIX for improved pharmacokinetics with prolonged circulation times. Increasing the half-life ($t_{1/2}$) of a recombinant FIX product can reduce the frequency of injections and improve patient

compliance. Table 2-4 summarizes the FIX products that have been recently FDA approved, as well as products that are currently in the development pipeline.

One strategy for prolonging circulation time is based on the widespread approach of Fc fusion proteins. The complete fusion protein molecule can be expressed recombinantly, eliminating the need for a chemical modification step (i.e. PEGylation).[43] Notably, ALPROLIX™ is a recombinant factor IX-Fc fusion protein (rFIXFc) that was designed to contain a single FIX molecule recombinantly attached to the constant region (Fc) of immunoglobulin G (IgG). The purpose of the Fc domain is to protect the fusion protein from catabolism by using the natural pathway mediated by Fc receptor (FcRn) that protects IgG antibodies from degradation.[51]

PEGylation of proteins is another strategy to improve intestinal delivery by minimizing activity loss and extending circulation time.[52-54] Novo Nordisk has post-translationally modified FIX by using the GlycoPEGylation™ technology. Using this method, site-specific PEGylation was achieved by targeting native N-glycans as attachment sites for PEG (40 kDa). The PEG is covalently attached to the activation peptide, which is released when FIX is activated. PEGylation of FIX in this site-specific manner preserves its biologic activity while prolonging circulation time.[52-54]

Table 2-4. Recently marketed products and pipeline product for hemophilia B treatment. (Adapted from CHS[55])

Company	Product	Type	Clinical Trials	Description
Baxter/Baxalta	RIXUBUS	Recombinant	FDA approved in June 2013. In October 2014, received pediatric indication from FDA for children (< 12 years).	3rd generation rFIX manufactured without exposure to human and animal proteins, and with a normal half-life
Biogen Idec	ALPROLIX (rFIXFc)	Recombinant, Fc fusion	Phase III trial (B-Long) ended in June 2012; In July 2012, Phase III trial was extended to children under 12. FDA approved in March 2014 for prophylaxis and to treat bleeding in patients (≥ 12 years).	rFIX fused with Fc to extend half-life; Phase II/III trials showed a 2.5 times increase in half-life
Emergent BioSolutions (previously Cangene)	Ixinity	Recombinant (trenonacog alfa)	Phase III trials showed similar pharmacokinetics to BeneFIX with 24-h half-life, 84% of bleeds were controlled with 1-2 infusions, and no inhibitors or thrombotic events were observed. FDA approved in May 2015.	3rd generation rFIX manufactured in a Chinese Hamster Ovary cell line without exposure to human and animal proteins, and with a normal half-life
Baxter/Baxalta	RIXUBUS	Recombinant	FDA approved in June 2013. In October 2014, received pediatric indication from FDA for children (< 12 years).	3rd generation rFIX manufactured without exposure to human and animal proteins, and with a normal half-life.
CSL Behring	IDELVION	Recombinant, albumin fusion	Granted orphan drug status by FDA in June 2012. Phase III trials in previously treated patients were completed. No serious adverse reactions were reported. FDA approved in March 2016.	rFIX fused with recombinant human albumin. Phase III trials showed a 5 times increase in half-life.
Novo Nordisk	NN79 (N9-GP)	Recombinant, PEGylated	Phase III trial (paradigm 2) was completed in May 2013. No inhibitors formed. In January 2016, filed a license application with the European Medicines Agency.	Site-specific PEGylation for prolonged half-life. Reported a 5 times increase in half-life.

2.4.4 Cost of Treatment

The cost of treatment depends on the clinical severity, and therefore the use of prophylaxis. Generally, the total cost of treatment (including medications, inpatient, and outpatient care) increases with increasing severity. In a recent study with hemophilia A patients, patients with severe disease receiving prophylaxis had a total annual cost of about $300,000 on average, while the total annual cost for patients with mild disease was about $60,000. However, 94% of total costs for the patients with severe disease receiving prophylaxis was for clotting factors, while only 54% of total costs for patients with mild disease was for clotting factors.[56] This cost breakdown showed that patients on prophylactic therapy have fewer bleeding episodes and less ER visits, especially compared to patient with severe disease only using on-demand treatment. Similar trends in costs based on severity and treatment type can be expected for hemophilia B patients.

A recent study also showed that treatment costs vary with age. For hemophilia B patients with moderate and severe disease (not including patients with inhibitor formation) in the United States, the total cost of treatment increases during the first three decades of life, peaking at an annual cost of $453,179 at age 29, and then decreasing during the fourth and fifth decades of life (Figure 2-9).[57] However, the annual out-of-pocket costs per patient remain relatively steady at an average of $1,838 per year. In 2012, the breakdown of the payer cost (insurance cost) was on average $206,027 for medications, $109,401 for inpatient care, and $34,702 for outpatient care.[57]

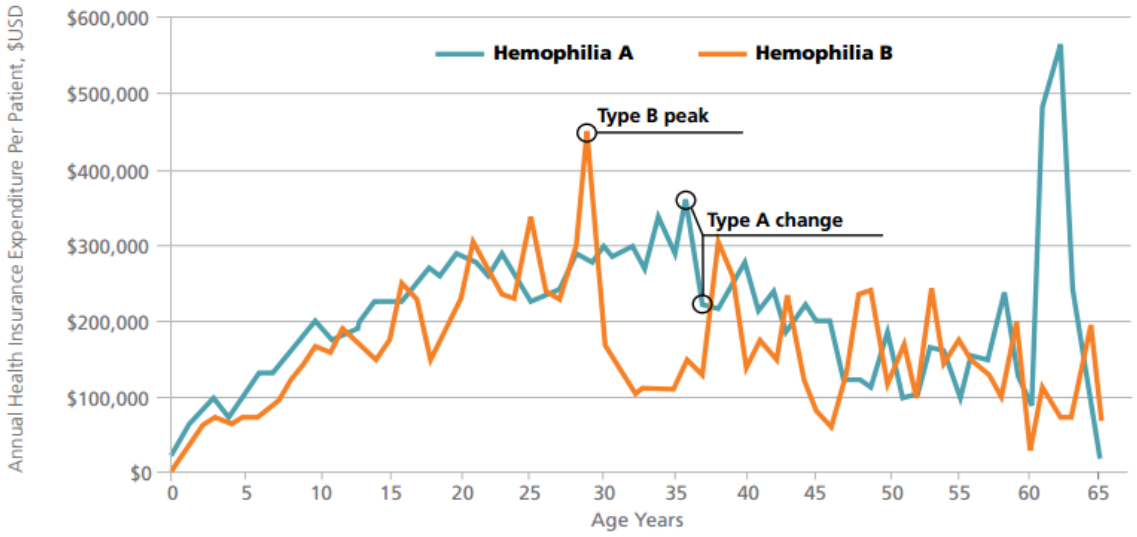

Figure 2-9. Payer costs for hemophilia A and hemophilia B patients by patient age. (Data from Eldar-Lissai *et al.*[57], figure from OptumRx [58]).

2.4.5 Inhibitors

Another serious complication associated with protein replacement therapy is the development of humoral immune (Th2) responses to functional clotting factors in some hemophilia patients.[59] As a result of a helper-T-cell-dependent (Th2) response, inhibitory antibodies (inhibitors) form against the replaced clotting factor, which, in turn, increases the risk of bleeding-related morbidity, specifically nephrosis, and mortality. Furthermore, high-titer inhibitors (>5 Bethesda units, BU/mL) prevent treatment with coagulation factor products. Immune tolerance induction (ITI) protocols, requiring frequent high dose IV infusions for months to several years, can eliminate inhibitor development. ITI costs can reach up to several million US dollars annually, [59] which is significantly greater than treating patients without inhibitor development. Although the overall incidence of inhibitors for hemophilia B is relatively low (1.5-3% of all cases), 9-23% of patients with

severe hemophilia form high-titer inhibitors. In addition, ITI protocols are less effective in treating FIX inhibitors than FVIII inhibitors.[42, 60] Up to 50% of patients with FIX inhibitors may experience potentially life-threatening anaphylactic reactions.[42]

2.4.6 Exploratory Treatments

Gene therapy is one of the approaches currently under investigation for treatment of the disease. For hemophilia, this alternative can potentially provide constant, sustained FIX synthesis within the patient, thereby obviating the risk of spontaneous bleeding and the need for repeated injections or infusions. Gene therapy for hemophilia thus could completely cure the disease,[61] but it is plagued by challenges related to safety, ethical issues, accessibility, and cost. Some of the issues with gene therapy, particularly with adeno-associated virus (AAV)-mediated options, include:

- Human uncertainty with gene therapy, especially due to limited long-term studies and possible development of side effects [62, 63]
- High prevalence of neutralizing antibodies to AAV[62-64]
- As a result, restricted access to the three ongoing clinical trials of AAV-mediated gene therapy for severe hemophilia B patients [62, 65-67]
- Issue with manufacturing, such as product-related impurities and limited production size. [63, 68]

Additional overarching challenges deal with accessibility and affordability of gene therapy in both advanced and developing countries. According to one report, the cost of gene therapy is currently unknown. In the US, policy and insurance coverage also contribute to the uncertainties associated with gene therapy as a potential treatment for hemophilia B.[69] Despite recent advantages in gene therapy for hemophilia, the clinical realization of this treatment is limited by challenges related to safety, ethical issues,

accessibility, and cost. Gene therapy has not met the need for a new method of treating hemophilia B, and an innovative treatment approach is still desired.

Another exploratory treatment is an oral delivery method developed by Dr. Daniell, Dr. Herzog, and collaborators for FIX fused with cholera toxin B (CTB) (CTB-FIX) in the chloroplasts of transgenic tobacco plants for ITI therapy. Treatment by this method demonstrated suppression of an immune response and prevention of anaphylactic reactions to systemically delivered proteins in humanized hemophilia B mice.[70] The CTB-FIX proteins orally administered in transgenic plant cells were non-functional, indicating that they serve only as antigens that prevent inhibitor responses and cannot function as protein replacement therapy. [70, 71] Additionally, possible genetic instability of transgenic plants could lead to unexpected side effects. [72] This approach only offers an alternative to ITI therapy, but does not treat nor prevent bleeding episodes and other symptoms associated with hemophilia.

Further testing of this oral tolerance induction method showed effective inhibitor suppression in hemophilia B mice. Delivery of bioencapsulated CTB-FIX fusion protein to the Peyer's patches of the intestinal epithelium induced an immune response that results in cytokine-mediated suppression,[73] as well as regulation involving tolerogenic dendritic cells and T cell subsets.[74] To further improve the safety of this bioencapsulated system, the investigators generated transplastomic lettuce cells for CTB-hFIX expression and demonstrated the suppression of inhibitor formation with orally delivered CTB-hFIX in lettuce cells. Furthermore, they have successfully generated transplastomic lettuces plants at an industrial scale that is highly efficient, cost-effective, and environmentally friendly. This study demonstrates the first clinical advancement of a protein drug made in edible plant cells for oral delivery. Additionally, these results are promising for developing a clinical ITI protocol in hemophilia patients.[75]

2.4 Oral Delivery of Proteins

2.4.1 Oral Route of Administration

The oral delivery of protein therapeutics is an ideal route of administration which offers a means to overcoming the issues with injections. The benefits of oral delivery include ease of administration, increased compliance, and lower costs. However, there are two main challenges—maintaining protein functionality and increasing bioavailability—that need to be addressed when designing an oral delivery system. In the oral delivery route, the protein therapeutic must first pass through the harsh environment of the gastrointestinal (GI) tract. The protein structure must be maintained in the stomach which contains a large quantity of gastric juice and proteolytic enzymes to denature proteins. The second challenge to oral delivery is increasing the bioavailability of the protein. In order to reach circulation, the protein must be absorbed in the upper small intestine and pass through the epithelium into the bloodstream. There is a narrow absorption window (4-6 hours) within the upper small intestine (pH ~5-7). Due to its large surface area, the small intestine is the site of 95% of nutrient absorption. However, the epithelial layer can act as physical barrier and not readily uptake large molecules, such as proteins (~5-5000 kDa). Furthermore, the tight junctions between the epithelial cells are specifically designed to prevent the transfer of foreign material from the intestinal epithelium into the blood stream.[76] Addressing the issues of the narrow absorption window and the barrier of the epithelium is necessary for increasing the bioavailability of orally delivered protein therapeutics.

2.4.2 Complexation Hydrogels

Hydrogels are three dimensional polymer networks that are insoluble due to the presence of physical and/or chemical crosslinks.[77] In addition, hydrogels are often used in biomedical applications due to their biocompatibility and ability to imbibe large amounts

of water. Complexation hydrogels are a specific class of hydrogels that form physical crosslinks through non-covalent interactions, such as hydrogen bonding.[78] Our lab has successfully developed a class of environmentally sensitive complexation hydrogels capable of swelling and deswelling in response to the pH gradient found in the GI tract.

Previous work by *Peppas and collaborators* has focused on the use of pH-responsive anionic complexation hydrogels, specifically ones consisting of a poly(methacrylic acid) (PMAA) backbone with poly(ethylene glycol) (PEG) tethers (designated as P(MAA-g-EG)) crosslinked with PEG dimethacrylate (PEGDMA), as vehicles for oral protein delivery.[79-83] Anionic complexation hydrogels have been engineered to overcome the challenges of an oral administration route by protecting proteins from the harsh environment of the stomach and delivering them to the small intestine (Figure 2-10). Their pH-responsive swelling, imparted by ionization of acid pendant groups, exploits the physiological changes along the gastrointestinal (GI) tract. At a low pH, hydrogen bonding between the carboxyl group of MAA and the etheric oxygen of the PEG chains results a collapsed polymer network with a small mesh size, ξ. As the environmental pH increases above the pKa of MAA (~4.8), deprotonation disrupts these interpolymer complexes and causes ionization and electrostatic repulsion of the acid groups of MAA, resulting in hydrogel swelling and increased mesh size.[77, 84] Such hydrogels have been evaluated for the oral delivery of insulin (5.8 kDa),[79, 81-83] calcitonin (3.4 kDa),[85, 86] interferon beta (23 kDa),[85] and growth hormone (22 kDa).[86] However, a polymeric carrier system has not been optimized for high molecular weight coagulation proteins, such as hFIX (57 kDa).

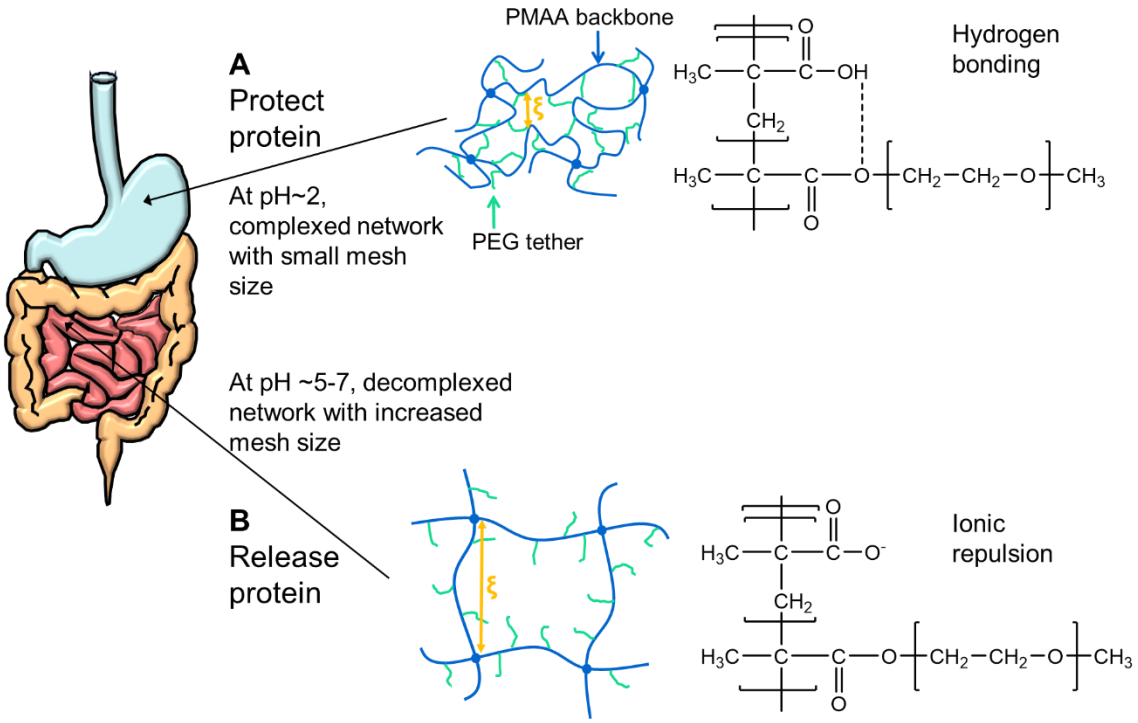

Figure 2-10. Complexation hydrogels are engineered to exploit the pH changes in the GI tract in order to (A) protect proteins from the harsh gastric conditions and (B) deliver them to the small intestine, where they can be absorbed into the bloodstream.

2.5 REFERENCES

1. DeLoughery, T. G., *Hemostasis and Thrombosis*. Springer Verlag: Cham, 2015; Vol. 3;3;3rd 2015;.
2. Francischetti, I. M. B., Does activation of the blood coagulation cascade have a role in malaria pathogenesis? *Trends in Parasitology* **2008,** *24* (6), 258-263.
3. Stenflo, J., Contributions of Gla and EGF-like domains to the function of vitamin K-dependent coagulation factors. *Critical reviews in eukaryotic gene expression* **1998,** *9* (1), 59-88.
4. Wilcox, J. N.; Smith, K. M.; Schwartz, S. M.; Gordon, D., Localization of tissue factor in the normal vessel wall and in the atherosclerotic plaque. *Proceedings of the National Academy of Sciences* **1989,** *86* (8), 2839-2843.

5. Banner, D. W.; D'Arcy, A.; Chene, C.; Winkler, F. K.; Guha, A.; Konigsberg, W. H.; Nemerson, Y.; Kirchhofer, D., The crystal structure of the complex of blood coagulation factor VIIa with soluble tissue factor. *Nature* **1996,** *380*, 41-46.

6. Mosesson, M. W.; Siebenlist, K. R.; Meh, D. A., The structure and biological features of fibrinogen and fibrin. *Annals of the New York Academy of Sciences* **2001,** *936* (1), 11-30.

7. Bajzar, L., Thrombin activatable fibrinolysis inhibitor and an antifibrinolytic pathway. *Arteriosclerosis, thrombosis, and vascular biology* **2000,** *20* (12), 2511-2518.

8. Fantony, J. J.; Inman, B. A., Thromboembolism and bleeding in bladder cancer. *Oncology* **2014,** *28* (10), 847-847.

9. Ruggeri, Z., Von Willebrand factor, platelets and endothelial cell interactions. *Journal of Thrombosis and Haemostasis* **2003,** *1* (7), 1335-1342.

10. Kessler, C. M., Mariani G, Clinical manifestations and therapy of the hemophilias. In *Hemostasis and Thrombosis: Basic Principles and Clinical Practice*, 5 ed.; Colman, R. W., J Hirsh, VJ Marder, AW Clowes, JN George, Ed. Lippincott-Raven: Philadelphia, 2006; pp 887-904.

11. Hemophilia. http://www.cdc.gov/ncbddd/hemophilia/facts.html.

12. About Bleeding Disorders: Hemophilia. http://www.wfh.org/en/page.aspx?pid=646.

13. Hemophilia B. https://www.hemophilia.org/Bleeding-Disorders/Types-of-Bleeding-Disorders/Hemophilia-B.

14. Darby, S. C.; Kan, S. W.; Spooner, R. J.; Giangrande, P. L. F.; Hill, F. G. H.; Hay, C. R. M.; Lee, C. A.; Ludlam, C. A.; Williams, M.; Doctors, U. K. H. C., Mortality rates, life expectancy, and causes of death in people with hemophilia A or B in the United Kingdom who were not infected with HIV. *Blood* **2007,** *110* (3), 815-825.

15. White, G. C., 2nd; Rosendaal, F.; Aledort, L. M.; Lusher, J. M.; Rothschild, C.; Ingerslev, J., Definitions in hemophilia. Recommendation of the scientific subcommittee on factor VIII and factor IX of the scientific and standardization committee of the International Society on Thrombosis and Haemostasis. *J. Thromb. Haemost.* **2001,** *85* (3), 560.

16. Colman, R. W., Are hemostasis and thrombosis two sides of the same coin? *J Exp Med* **2006,** *203* (3), 493-5.

17. Manco-Johnson, M. J.; Abshire, T. C.; Shapiro, A. D.; Riske, B.; Hacker, M. R.; Kilcoyne, R.; Ingram, J. D.; Manco-Johnson, M. L.; Funk, S.; Jacobson, L., Prophylaxis versus episodic treatment to prevent joint disease in boys with severe hemophilia. *New England Journal of Medicine* **2007,** *357* (6), 535-544.

18. Chalmers, E. A., Haemophilia and the newborn. *Blood reviews* **2004,** *18* (2), 85-92.

19. Kulkarni, R.; Soucie, J.; Lusher, J.; Presley, R.; Shapiro, A.; Gill, J.; MANCO-JOHNSON, M.; Koerper, M.; Mathew, P.; Abshire, T., Sites of initial bleeding episodes, mode of delivery and age of diagnosis in babies with haemophilia diagnosed before the age of 2 years: a report from The Centers for Disease Control and Prevention's (CDC) Universal Data Collection (UDC) project. *Haemophilia* **2009,** *15* (6), 1281-1290.

20. Lee, C. A.; Berntorp, E. E.; Hoots, K.; Ebooks, C., *Textbook of Hemophilia*. John Wiley & Sons, Ltd: Chichester, 2010; Vol. 2nd;2;.

21. Sellner, L. N.; Taylor, G. R., MLPA and MAPH: new techniques for detection of gene deletions. *Human mutation* **2004,** *23* (5), 413-419.

22. KWON, M. J.; YOO, K. Y.; KIM, H. J.; KIM, S. H., Identification of mutations in the F9 gene including exon deletion by multiplex ligation-dependent probe amplification in 33 unrelated Korean patients with haemophilia B. *Haemophilia* **2008,** *14* (5), 1069-1075.

23. Yoshitake, S.; Schach, B. G.; Foster, D. C.; Davie, E. W.; Kurachi, K., Complete nucleotide sequences of the gene for human factor IX (antihemophilic factor B). *Biochemistry* **1985,** *24* (14), 3736-3750.

24. Schmidt, A. E.; Bajaj, S. P., Structure–Function Relationships in Factor IX and Factor IXa. *Trends in Cardiovascular Medicine* **2003,** *13* (1), 39-45.

25. College, D. o. B. D. Coagulation Factor IX. Structure–Function Relationships in Factor IX and Factor IXa.

26. Fay, P. J., Activation of factor VIII and mechanisms of cofactor action. *Blood reviews* **2004,** *18* (1), 1-15.

27. Brandstetter, H.; Bauer, M.; Huber, R.; Lollar, P.; Bode, W., X-ray structure of clotting factor IXa: active site and module structure related to Xase activity and hemophilia B. *Proceedings of the National Academy of Sciences* **1995,** *92* (21), 9796-9800.

28. Hopfner, K.-P.; Lang, A.; Karcher, A.; Sichler, K.; Kopetzki, E.; Brandstetter, H.; Huber, R.; Bode, W.; Engh, R. A., Coagulation factor IXa: the relaxed conformation of Tyr99 blocks substrate binding. *Structure* **1999,** *7* (8), 989-996.

29. Rao, Z.; Handford, P.; Mayhew, M.; Knott, V.; Brownlee, G. G.; StuartZ, D., The structure of a Ca 2+-binding epidermal growth factor-like domain: its role in protein-protein interactions. *Cell* **1995,** *82* (1), 131-141.

30. Huang, M.; Furie, B. C.; Furie, B., Crystal structure of the calcium-stabilized human factor IX Gla domain bound to a conformation-specific anti-factor IX antibody. *Journal of Biological Chemistry* **2004,** *279* (14), 14338-14346.

31. Shen, B. W.; Spiegel, P. C.; Chang, C.-H.; Huh, J.-W.; Lee, J.-S.; Kim, J.; Kim, Y.-H.; Stoddard, B. L., The tertiary structure and domain organization of coagulation factor VIII. *Blood* **2008,** *111* (3), 1240-1247.

32. Ngo, J. C. K.; Huang, M.; Roth, D. A.; Furie, B. C.; Furie, B., Crystal structure of human factor VIII: implications for the formation of the factor IXa-factor VIIIa complex. *Structure* **2008,** *16* (4), 597-606.

33. Autin, L.; Miteva, M.; Lee, W.; Mertens, K.; RADTKE, K. P.; Villoutreix, B., Molecular models of the procoagulant factor VIIIa–factor IXa complex. *Journal of Thrombosis and Haemostasis* **2005,** *3* (9), 2044-2056.

34. Koeberl, D. D.; Bottema, C.; Buerstedde, J.; Sommer, S. S., Functionally important regions of the factor IX gene have a low rate of polymorphism and a high rate of mutation in the dinucleotide CpG. *American journal of human genetics* **1989,** *45* (3), 448.

35. Green, P.; Saad, S.; Lewis, C.; Giannelli, F., Mutation rates in humans. I. Overall and sex-specific rates obtained from a population study of hemophilia B. *The American Journal of Human Genetics* **1999,** *65* (6), 1572-1579.

36. Saunders, R. E.; Perkins, S. J., CoagMDB: a database analysis of missense mutations within four conserved domains in five vitamin K–dependent coagulation serine proteases using a text-mining tool. *Human mutation* **2008,** *29* (3), 333-344.

37. Thompson, A.; Bajaj, S. P.; Chen, S.-H.; MacGillivray, R., " Founder" effect in different families with haemophilia B mutation. *The Lancet* **1990,** *335* (8686), 418.

38. Anagnostopoulos, T.; Morris, A.; Ayres, K. L.; Giannelli, F.; Green, P., DNA variation in a 13-Mb region including the F9 gene: inferring the genealogical history and causal role of a hemophilia B mutation (IVS 5+ 13 A→ G). *Journal of Thrombosis and Haemostasis* **2003,** *1* (12), 2609-2614.

39. Jenkins, P.; Egan, H.; Keenan, C.; O'SHEA, E.; Smith, O.; Nolan, B.; White, B.; O'DONNELL, J., Mutation analysis of haemophilia B in the Irish population: increased prevalence caused by founder effect. *Haemophilia* **2008,** *14* (4), 717-722.

40. Ljung, R.; Nilsson, I. M., Hemophilia B Leyden and a similar variant of hemophilia A. *The New England journal of medicine* **1982,** *307* (14), 897.

41. Crossley, M.; Ludwig, M.; Stowell, K. M.; De Vos, P.; Olek, K.; Brownlee, G. G., Recovery from hemophilia B Leyden: an androgen-responsive element in the factor IX promoter. *Science* **1992,** *257* (5068), 377-379.

42. DiMichele, D., Inhibitor development in haemophilia B: an orphan disease in need of attention. *British Journal of Haematology* **2007,** *138* (3), 305-315.

43. Jameel, F.; Hershenson, S., *Formulation and Process Development Strategies for Manufacturing Biopharmaceuticals*. John Wiley & Sons: Hoboken, 2010; Vol. 1.

44. Biogen-Idec Press Release. http://www.biogenidec.com/press_release_details.aspx?ID=14712&Action=1&NewsId=2303&M=NewsV2&PID=61997.

45. Berntorp, E.; Shapiro, A. D., Modern haemophilia care. *Lancet* **2012,** *379* (9824), 1447-56.

46. Ljung, R. C., Aspects of haemophilia prophylaxis in Sweden. *Haemophilia* **2002,** *2*, 34-7.

47. Yee, T. T.; Beeton, K.; Griffioen, A.; Harrington, C.; Miners, A.; Lee, C. A.; Brown, S. A., Experience of prophylaxis treatment in children with severe haemophilia. *Haemophilia* **2002,** *8* (2), 76-82.

48. Mancuso, M. E.; Berardinelli, L.; Beretta, C.; Raiteri, M.; Pozzoli, E.; Santagostino, E., Improved treatment feasibility in children with hemophilia using arteriovenous fistulae: the results after seven years of follow-up. *Haematologica* **2009,** *94* (5), 687-92.

49. Healthcare Observer Jan 2013: The Hemophilia B Market. *Morningstar* **2013**.

50. Mullard, A., Biogen Idec enters hemophilia B market. *Nature biotechnology* **2014,** *32* (6), 506-506.

51. Peters, R. T.; Low, S. C.; Kamphaus, G. D.; Dumont, J. A.; Amari, J. V.; Lu, Q.; Zarbis-Papastoitsis, G.; Reidy, T. J.; Merricks, E. P.; Nichols, T. C., Prolonged activity of factor IX as a monomeric Fc fusion protein. *Blood* **2010,** *115* (10), 2057-2064.

52. Østergaard, H.; Bjelke, J. R.; Hansen, L.; Petersen, L. C.; Pedersen, A. A.; Elm, T.; Møller, F.; Hermit, M. B.; Holm, P. K.; Krogh, T. N.; Petersen, J. M.; Ezban, M.; Sørensen, B. B.; Andersen, M. D.; Agersø, H.; Ahmadian, H.; Balling, K. W.; Christiansen, M. L. S.; Knobe, K.; Nichols, T. C.; Bjørn, S. E.; Tranholm, M., *Prolonged half-life and preserved enzymatic properties of factor IX selectively PEGylated on native N-glycans in the activation peptide*. 2011; Vol. 118, p 2333-2341.

53. Karpf, D. M.; Sørensen, B. B.; Hermit, M. B.; Holmberg, H. L.; Tranholm, M.; Bysted, B. V.; Groth, A. V.; Bjørn, S. E.; Stennicke, H. R., Prolonged half-life of glycoPEGylated rFVIIa variants compared to native rFVIIa. *Thrombosis Research* **2011,** *128* (2), 191-195.

54. Stennicke, H. R.; Ostergaard, H.; Bayer, R. J.; Kalo, M. S.; Kinealy, K.; Holm, P. K.; Sørensen, B. B.; Zopf, D.; Bjørn, S. E., Generation and biochemical characterization of glycoPEGylated factor VIIa derivatives. *Thrombosis and haemostasis* **2008,** *100* (5), 920-928.

55. Product Pipeline: Factor IX. http://www.hemophilia.ca/en/.

56. Zhou, Z.-Y.; Koerper, M. A.; Johnson, K. A.; Riske, B.; Baker, J. R.; Ullman, M.; Curtis, R. G.; Poon, J.-L.; Lou, M.; Nichol, M. B., Burden of illness: direct and indirect costs among persons with hemophilia A in the United States. *Journal of medical economics* **2015,** *18* (6), 457-465.

57. Eldar-Lissai, A.; Hou, Q.; Krishnan, S., The Changing Costs of Caring for Hemophilia Patients in the US: Insurers' and Patients' Perspectives. *Blood* **2014,** *124* (21), 199-199.

58. Hemophilia Insight Report. https://www.optum.com/content/dam/optum/resources/brochures/Rx/m53018_n_hemophilia_insight_report_0424a.pdf.

59. Dimichele, D. M., Immune tolerance: critical issues of factor dose, purity and treatment complications. *Haemophilia* **2006,** *12*, 81-86.

60. Thorland, E. C.; Drost, J. B.; Lusher, J. M.; Warrier, I.; Shapiro, A.; Koerper, M. A.; Dimichele, D.; Westman, J.; Key, N. S.; Sommer, S. S., Anaphylactic response to factor IX replacement therapy in haemophilia B patients: complete gene deletions confer the highest risk. *Haemophilia* **1999,** *5* (2), 101-105.

61. Pannier, A. K.; Shea, L. D., Controlled release systems for DNA delivery. *Mol Ther* **2004,** *10* (1), 19-26.

62. Ginn, S. L.; Alexander, I. E.; Edelstein, M. L.; Abedi, M. R.; Wixon, J., Gene therapy clinical trials worldwide to 2012 – an update. *The Journal of Gene Medicine* **2013,** *15* (2), 65-77.

63. High, K. H.; Nathwani, A.; Spencer, T.; Lillicrap, D., Current status of haemophilia gene therapy. *Haemophilia* **2014,** *4*, 43-9.

64. Kotterman, M. A.; Schaffer, D. V., Engineering adeno-associated viruses for clinical gene therapy. *Nat Rev Genet* **2014,** *15* (7), 445-451.

65. Dose-escalation study of a self complementary adeno-associated viral vector of gene transfer in hemophilia B. In *ClinicalTrials.gov*, 2009; Vol. Identifier: NCT00979238.

66. Hemophilia B gene therapy – Spark. In *ClinicalTrials.gov* 2012; Vol. Identifier: NCT01620801.

67. Open-Label Single Ascending Dose of Adeno-associated Virus Serotype 8 Factor IX Gene Therapy in Adults with Hemophilia B. In *ClinicalTrials.gov*, 2012; Vol. Identifier: NCT01687608.

68. Wright, J., Product-Related Impurities in Clinical-Grade Recombinant AAV Vectors: Characterization and Risk Assessment. *Biomedicines* **2014,** *2* (1), 80-97.

69. Skinner, M. W., Gene Therapy for Hemophilia: Addressing the Coming Challenges of Affordability and Accessibility. *Mol Ther* **2013,** *21* (1), 1-2.

70. Verma, D.; Moghimi, B.; LoDuca, P. A.; Singh, H. D.; Hoffman, B. E.; Herzog, R. W.; Daniell, H., Oral delivery of bioencapsulated coagulation factor IX prevents inhibitor formation and fatal anaphylaxis in hemophilia B mice. *Proc. Natl. Acad. Sci. U.S.A.* **2010,** *107* (15), 7101-6.

71. Kwon, K.-C.; Verma, D.; Singh, N. D.; Herzog, R.; Daniell, H., Oral delivery of human biopharmaceuticals, autoantigens and vaccine antigens bioencapsulated in plant cells. *Adv. Drug Deliv. Rev.* **2013,** *65* (6), 782-799.

72. Guan, Z. J.; Guo, B.; Huo, Y. L.; Guan, Z. P.; Dai, J. K.; Wei, Y. H., Recent advances and safety issues of transgenic plant-derived vaccines. *Appl. Microbiol. Biotechnol.* **2013,** *97* (7), 2817-40.

73. Sherman, A.; Su, J.; Daniell, H.; Herzog, R. W., Mechanism Of Oral Tolerance Induced By Bioencapsulated Coagulation Factor IX In Hemophilia B Mice. *Blood* **2013,** *122* (21), 30-30.

74. Wang, X.; Su, J.; Sherman, A.; Rogers, G. L.; Liao, G.; Hoffman, B. E.; Leong, K. W.; Terhorst, C.; Daniell, H.; Herzog, R. W., Plant-based oral tolerance to hemophilia therapy employs a complex immune regulatory response including LAP+ CD4+ T cells. *Blood* **2015,** *125* (15), 2418-2427.

75. Su, J.; Zhu, L.; Sherman, A.; Wang, X.; Lin, S.; Kamesh, A.; Norikane, J. H.; Streatfield, S. J.; Herzog, R. W.; Daniell, H., Low cost industrial production of coagulation factor IX bioencapsulated in lettuce cells for oral tolerance induction in hemophilia B. *Biomaterials* **2015,** *70*, 84-93.

76. Daugherty, A. L.; Mrsny, R. J., Transcellular uptake mechanisms of the intestinal epithelial barrier - Part one. *Pharmaceutical Science & Technology Today* **1999,** *2* (4), 144-151.

77. Peppas, N. A.; Bures, P.; Leobandung, W.; Ichikawa, H., Hydrogels in pharmaceutical formulations. *Eur. J. Pharm. Biopharm.* **2000,** *50* (1), 27-46.

78. Lowman, A. M.; Dziubla, T.; Bures, P.; Peppas, N. A., Structural and dynamic response of neutral and intelligent networks in biomedical environments. In *Advances in Chemical Engineering: Molecular and cellular foundations of biomaterial*, Peppas, N. A.; Sefton, M., Eds. Elsevier: San Diego, 2004; Vol. 29, pp 75-130.

79. Lowman, A. M.; Morishita, M.; Kajita, M.; Nagai, T.; Peppas, N. A., Oral delivery of insulin using pH-responsive complexation gels. *J. Pharm. Sci.* **1999,** *88* (9), 933-937.

80. Nakamura, K.; Murray, R. J.; Joseph, J. I.; Peppas, N. A.; Morishita, M.; Lowman, A. M., Oral insulin delivery using P(MAA-g-EG) hydrogels: effects of network morphology on insulin delivery characteristics. *J. Control. Release* **2004,** *95* (3), 589-599.

81. Morishita, M.; Goto, T.; Nakamura, K.; Lowman, A. M.; Takayama, K.; Peppas, N. A., Novel oral insulin delivery systems based on complexation polymer hydrogels: Single and multiple administration studies in type 1 and 2 diabetic rats. *J. Control. Release* **2006,** *110* (3), 587-594.

82. Wood, K. M.; Stone, G. M.; Peppas, N. A., Wheat Germ Agglutinin Functionalized Complexation Hydrogels for Oral Insulin Delivery. *Biomacromolecules* **2008,** *9* (4), 1293-1298.

83. Wood, K. M.; Stone, G. M.; Peppas, N. A., The effect of complexation hydrogels on insulin transport in intestinal epithelial cell models. *Acta Biomater.* **2010,** *6* (1), 48-56.

84. Sharpe, L. A.; Daily, A. M.; Horava, S. D.; Peppas, N. A., Therapeutic applications of hydrogels in oral drug delivery. *Expert Opin. Drug Deliv.* **2014,** *11* (6), 901-15.

85. Kamei, N.; Morishita, M.; Chiba, H.; Kavimandan, N. J.; Peppas, N. A.; Takayama, K., Complexation hydrogels for intestinal delivery of interferon beta and calcitonin. *J. Control. Release* **2009,** *134* (2), 98-102.

86. Carr, D. A.; Gomez-Burgaz, M.; Boudes, M. C.; Peppas, N. A., Complexation Hydrogels for the Oral Delivery of Growth Hormone and Salmon Calcitonin. *Ind. Eng. Chem. Res.* **2010,** *49* (23), 11991-11995.

Chapter 3: Specific Aims

Hemophilia B is a hereditary bleeding disorder caused by the deficiency of clotting protein factor IX (FIX), affecting 80,000 males worldwide. Protein replacement therapy can prevent spontaneous bleeding episodes and restore hemostasis, significantly improving the patient's lifespan and quality of life. However, current treatment is limited to injection-based methods which are associated with noncompliance, increased risk of needle injury, costly medical care (e.g. hospital visits, surgeries), and other complications (e.g. severe allergic reactions). As a result, such treatments are not readily available worldwide, and without treatment the median life expectancy drops to 11 years. Oral delivery of clotting factors can improve patients' quality of life by ensuring safety, convenience, and ease of administration. A non-invasive oral delivery therapy is a highly desirable alternative and has the potential to make hemophilia treatment globally available. Development of a pH-responsive polymeric microcarrier system for the oral delivery of human FIX (hFIX) has the potential to provide a novel method for treating hemophilia B patients and was accomplished by completing the following specific aims:

- **Specific Aim 1. Synthesize and characterize pH-responsive polymeric carriers composed of methacrylic acid and ethylene glycol as vehicles for the oral delivery of factor IX.** P(MAA-g-EG) hydrogels were synthesized by bulk UV polymerization. Purified, dried polymer films were crushed and sieved into microparticles. Physical characterization included SEM for surface morphology and size distribution, potentiometric titration and FTIR for polymer composition, swelling studies for pH-responsive behavior, and *in vitro* cytotoxicity for

cytocompatibility. Formulations that exhibited the desired pH-responsive swelling and cytocompatibility were selected for further analysis.

- **Specific Aim 2. Evaluate the performance of P(MAA-g-EG) carriers in delivering active factor IX, and evaluate the formulation stability.** Microparticles were loaded with hFIX by swelling in a protein solution at pH 7.4, and were then collapsed with acid to trap the protein in the polymer network. Loading efficiency was optimized by tailoring loading conditions, such as temperature, time, and buffer ionic strength. Release studies were performed using two-stage dissolution in biorelevant media mimicking the GI tract. hFIX was quantified by ELISA, and its activity was measured by a chromogenic activity assay. *In vitro* permeability of hFIX was assessed in transport studies using intestinal epithelial models. Stability testing of hFIX-loaded microparticles was conducted using three conditions specified by the FDA. An optimal formulation was selected for further *in vivo* analysis.
- **Specific Aim 3. Develop and characterize enzymatically degradable, pH-responsive P(MAA-g-EG) carriers, and evaluate the performance in delivering active factor IX.** An enzymatically degradable system was designed to improve hFIX release in the small intestine and therefore improve overall bioavailability. Uncrosslinked P(MAA-g-EG) polymer was synthesized by UV polymerization, and then purified uncrosslinked polymer was crosslinked with a peptide by EDC-NHS chemistry. The peptide-based crosslinking agent was designed to resist degradation by gastric enzymes, such as pepsin, and target degradation by intestinal enzymes, such as trypsin. The pH-responsive swelling and enzymatic degradation was confirmed by bright-field microscopy. *In vitro* cytotoxicity studies was performed to quantify the cytocompatibility of degradation

products. Loading efficiency of hFIX was determined for such carriers, and release studies were conducted using simulated gastric and intestinal conditions containing relevant enzymes. The effects of these microparticles and their degradation products on hFIX permeability was assessed using *in vitro* transport studies.

- **Specific Aim 4. Determine the *in vivo* biocompatibility and biodistribution of P(MAA-g-EG) carriers.** For all *in vivo* studies, mice were administered microparticles by oral gavage. The acute and long-term toxicity of P(MAA-g-EG) carriers was evaluated by cytokine analysis, biochemical analysis for kidney and liver function, and tissue histology. For biodistribution and clearance, fluorescently-tagged microparticles were tracked over time using the IVIS® in vivo imaging system. For further analysis of biodistribution and bioadhesion, the gastrointestinal tract was removed and imaged.

Chapter 4: Design and Development of pH-Responsive Delivery Systems[1]

4.1 INTRODUCTION

This work focused the development of pH-responsive biomaterials to enable the oral route of human factor IX (hFIX). Previous work by *Peppas and collaborators*[1-5] has focused on the use of pH-responsive anionic complexation hydrogels, specifically ones consisting of a poly(methacrylic acid) (PMAA) backbone with poly(ethylene glycol) (PEG) tethers (designated as P(MAA-g-EG)) crosslinked with PEG dimethacrylate (PEGDMA), as vehicles for oral protein delivery.

Anionic complexation hydrogels have been engineered to overcome the challenges of an oral administration route by protecting proteins from the harsh environment of the stomach and delivering them to the small intestine. Their pH-responsive swelling, imparted by ionization of acid pendant groups, exploits the physiological changes along the gastrointestinal (GI) tract. At a low pH, hydrogen bonding between the carboxyl group of MAA and the etheric oxygen of the PEG chains results a collapsed polymer network with a small mesh size, ξ. As the environmental pH increases above the pKa of MAA (~4.8), deprotonation disrupts these interpolymer complexes and causes ionization and electrostatic repulsion of the acid groups of MAA, resulting in hydrogel swelling and increased mesh size.[6, 7] Such hydrogels have been evaluated for the oral delivery of insulin (5.8 kDa),[1, 3-5] calcitonin (3.4 kDa),[8, 9] interferon beta (23 kDa),[8] and growth hormone (22 kDa).[9] However, a polymeric carrier system has not been optimized for high molecular weight coagulation proteins, such as hFIX (57 kDa).

[1] Portions of this chapter have been previously published in Horava, S. D.; Peppas, N. A., Design of pH-Responsive Biomaterials to Enable the Oral Route of Hematological Factor IX. Annals of Biomedical Engineering 2016, 1-13.

Here, we outline the synthesis and characterization of P(MAA-g-EG) hydrogels. In order to tailor the delivery system for hFIX loading and release, P(MAA-g-EG) hydrogels were formulated with different mesh sizes, by varying the length of the PEGDMA crosslinking agent. All formulations were evaluated for surface morphology and size distribution of microparticles, polymer composition, and swelling behavior.

4.2 METHODS

4.2.1. Materials

Methacrylic acid (MAA) and Irgacure 184® (1-hydroxy-cyclohexyl-phenylketone) were purchased from Sigma-Aldrich (St. Louis, MO). Poly(ethylene glycol) (MW=1000) mono methyl ether monomethacrylate (PEGMMA1000), poly(ethylene glycol) (MW=400) dimethacrylate (PEGDMA400), PEGDMA600 (MW=600), and PEGDMA1000 (MW=1000) were purchased from Polysciences (Warrington, PA).

4.2.2 Polymer Synthesis

P(MAA-g-EG) hydrogels were synthesized by bulk UV-polymerization. MAA and PEGMMA1000 were added at a 2:1 molar ratio of hydrogen bonding groups to a 1:1 (w/w) mixture of deionized water and ethanol to result in a 1:1 (w/w) ratio of total monomer to solvent. A PEGDMA crosslinking agent, varying in molecular weight (MW of PEG= 400, 600, or 1000), was added at 1.0 mol % of total monomers, and the Irgacure 184® photoinitiator was added at 1.0 wt. % of total monomers. After the addition of all components (shown in Figure 4-1), the pre-polymer mixture was sonicated for 20 minutes in a Bransonic® CPX3800 ultrasonic digital bath (Branson Ultrasonics Corporation, Danbury, CT).

In an oxygen-deficient environment of a MBRAUN LABmaster 130 glove box (Garching, Germany), the pre-polymer mixture was needle purged with nitrogen for 5 minutes to remove residual oxygen (a free radical scavenger). The mixture was then dispensed between two quartz glass plates, which were separated with a 0.7 mm Teflon® spacer, and then polymerized for 30 minutes under 35 mW cm^{-2} UV light using a UV flood source. After synthesis, the resulting polymer was removed from the glass plates, and 10 mm diameter disks were punched for swelling studies. The polymer was washed in 1 L of deionized water, changed daily 10 times, to remove any unreacted monomer. After washing, the polymer was air dried for 3 days, followed by drying at 37°C under vacuum for 3 days. Dried films were crushed using a mortar and pestle and sieved into microparticles, sized 30-45 µm. Figure 4-2 shows a schematic of the synthesis process.

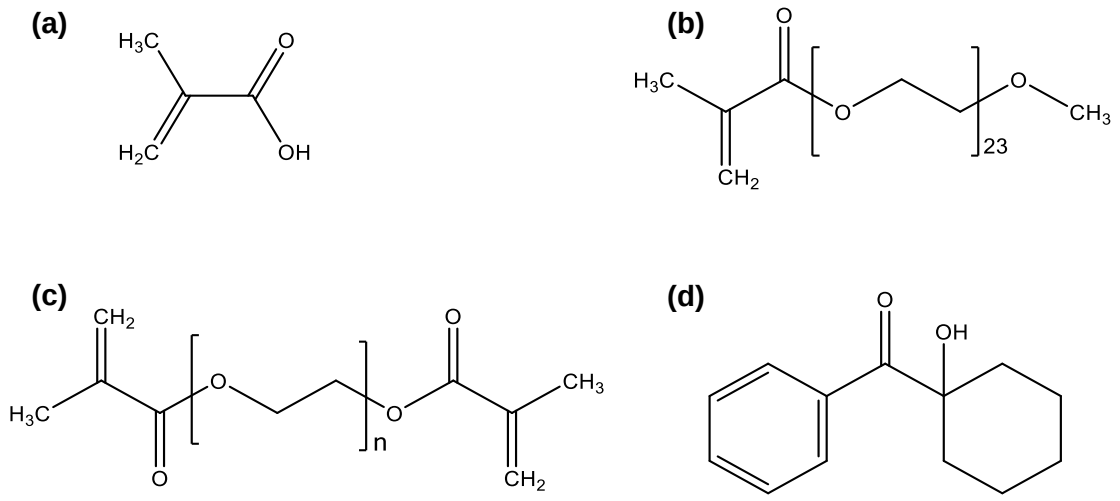

Figure 4-1. Components of the monomer solution. The two monomers are (a) methacrylic acid and (b) poly(ethylene glycol) monomethylether monomethacrylate. The crosslinking agent is (c) poly(ethylene glycol) dimethacrylate, and the photoinitiator is (d) Irgacure184 ®.

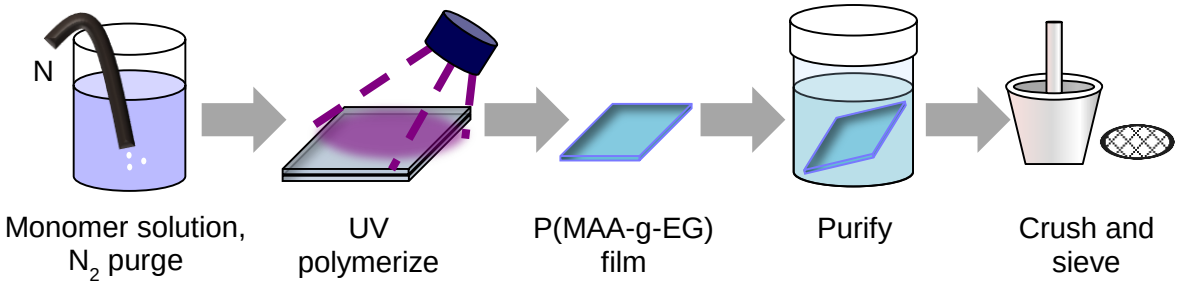

Figure 4-2 Schematic of the synthesis of P(MAA-g-EG) hydrogels.

4.2.3 Scanning Electron Microscopic (SEM) Studies

Scanning electron microscopy (SEM) was used to examine the surface morphology and size distribution of the microparticles. For SEM sample preparation, vacuum-dried microparticles were dusted onto carbon tape-covered aluminum stubs. Samples were coated with 10 nm of Pt/Pd using a Cressington 208 Benchtop sputter coater (Watford, England, UK). SEM images were obtained using a Zeiss Supra 40VP Scanning Electron Microscope (Oberkochen, Germany).

4.2.4 Potentiometric Titration

Potentiometric titration was used to quantify the MAA content of the microparticles. P(MAA-g-EG) microparticles were suspended in 10 mM NaCl at a concentration of 2 mg/mL, and then titrated to a pH of 10.5 using 0.2 N NaOH at 25°C with constant stirring. HCl was added (10-60 µL) to the polymer solution, and the pH was measured until reaching a steady value (three consecutive readings within ± 0.02) at each step using a Thermo Scientific Orion Star A211 pH benchtop meter (Waltham, MA). The molar amount of MAA was calculated based on equivalence point and a charge balance.

4.2.5 Fourier Transform Infrared (FTIR) Spectroscopy

FTIR is a surface analysis technique that was used to confirm the polymer composition. Vacuum dried microparticles were added at 1-2.5 wt. % to crushed and dried potassium bromide (KBr), and samples were pressed into disks. FTIR spectra were obtained using a Thermo Mattson Infinity Gold spectrometer. Background spectra of KBr only were subtracted from all sample spectra. FTIR was performed for all formulations. For each sample, 512 scans were performed with a resolution of 2 cm^{-1} and a gain of one.

4.2.6 Thermogravimetric Analysis (TGA)

Thermogravimetric analysis (TGA) was conducted using a TA Instruments TGA Q500 (New Castle, DE) to determine the thermal stability of the polymers (2-5 mg of vacuum dried microparticle samples). Decomposition profiles were recorded from 25°C ramped at 10°C/min to 550°C in nitrogen and then isothermal at 550°C for 5 minutes.

4.2.7 Dynamic and Equilibrium Swelling Studies

Swelling studies were conducted to quantify the water uptake into the networks during the initial contact process and determined the associated structural changes which affect the overall loading and release behavior. Dried 10 mm disks were weighed prior to all swelling studies. Dynamic swelling studies were performed using a series of 0.1 M 3,3-dimethylglutaric acid (DMGA) buffers between pH 1.2 and 7.6 at constant ionic strength at 37°C. The disks were stepped through the buffers in order of increasing pH, spending 30 minutes in each buffer. Between each step, the disks were blotted and weighed.

For equilibrium swelling, the relaxed weight of the polymer disks was measured in air and heptane immediately after the disks were punched from the freshly polymerized film. Dried weights in air and heptane were obtained prior to the start of the study. Dried disks were placed in a pH 2.0 buffer solution at 37°C for at least 72 hours, then blotted and

weighed in air and heptane. The same disks were then placed in a pH 6.5 buffer solution at 37°C for at least 72 hours, then blotted and weighed in air and heptane. Equilibrium swelling studies were at constant ionic strength using 167 mM NaCl as the pH 2 buffer and the 1x PBS as the pH 6.5 buffer. The buffered solutions were selected to represent the gastric (pH 2.0) and the intestinal (pH 6.5) conditions.

4.2.8 Turbidimetric Studies

The timescale of microparticle swelling, which is critical to drug release, was measured by kinetic turbidity. Microparticles suspensions of 5 mg mL^{-1} were prepared with 1x PBS with 2% (v/v) 1 N NaOH at 37°C. Immediately following suspension, 200 μL of solution, including all particle suspensions and buffer only, was added in quadruplicate to a 96-well plate. The absorbance was then measured at 520 nm in 1 minute intervals over 60 minutes at 37°C, with 20 seconds of shaking prior to each measurement, using a BioTek Cytation 3 multi-mode reader (Winooski, VT).

4.2.9 *In Vitro* Cytocompatibility Studies

To examine the cytocompatibility of the newly developed systems with biological systems, we conducted basic studies of compatibility with well-known cell lines. Human epithelial colorectal adenocarcinoma (Caco-2) and mucus-secreting goblet-like human colorectal adenocarcinoma (HT29-MTX) cells were obtained from American Type Culture Collection (ATCC, Rockwell, MD). Both cell lines were cultured in modified Dulbecco's Eagle Medium (DMEM) supplemented with 10% fetal bovine serum (FBS). Cells, either Caco-2 cells (at passages 65-75) or HT29-MTX cells (at passages 15-20), were plated on a 96-well plate at an initial seeding density of 10^5 cells per well and then cultured to 80% confluence. Separately, microparticles were sterilized under UV exposure for 10 minutes and then added to DMEM without phenol red with 2% FBS at concentrations of 1.25, 2.5,

and 5 mg mL^{-1} and allowed to swell overnight. After reaching 80% confluence, growth media was removed, and 100 µL of solution—microparticle suspensions (n=4 for each formulation and concentration), media (positive control, n=8), or water/lysis solution (negative control for MTS/LDH, n=8)—was applied to the cells. The cells were then incubated for 6 hours.

For the CellTiter 96® Aqueous One Solution Cell Proliferation (MTS) assay (Promega Corporation, Madison, WI), MTS reagent (20 µL $well^{-1}$) was added, and then incubated for an additional 90 minutes. The absorbance was read at 490 nm for MTS and 690 nm for background using a BioTek Cytation 3 multi-mode reader (Winooski, VT). For the CytoTox ONE Homogeneous Membrane Integrity (LDH) assay (Promega Corporation), lysis solution (2 µL $well^{-1}$) was added to the negative control wells after the 6-hour incubation. After equilibrating to room temperature, cell solution (50 µL $well^{-1}$) was removed and added to a black-wall 96-well plate with CytoTox ONE reagent (50 µL $well^{-1}$). After a 30-second shaking period and a 10-minute incubation, the fluorescence was measured at 560 nm excitation and 590 nm emission.

4.2.10 Statistical Analysis

Data are reported as mean ± standard error. All statistical analysis, either a Student's two-tailed t-test for two groups or an ANOVA for multiple groups, were computed using GraphPad Prism 6. Significant differences were considered when $*p < 0.05$ and $**p < 0.01$.

4.3 Results and Discussion

4.3.1 Polymer Synthesis

P(MAA-g-EG) hydrogels were successfully synthesized as films and then purified and dried. Dried polymer films were crushed into microparticles using a mortar and pestle, and then sieved into the desired size ranges. The three formulations of P(MAA-g-EG) hydrogels were synthesized 1 mol% PEGDMA crosslinking agent, which varies in the length of the PEG chain as outlined in Table 4-1.

Table 4-1. P(MAA-g-EG) formulations vary in the length of the PEGDMA crosslinking agent.

Crosslinking agent	# EG repeat units
PEGDMA400	9
PEGDMA600	14
PEGDMA1000	23

4.3.2 SEM Studies

P(MAA-g-EG) hydrogels were successfully synthesized and crushed into microparticles. SEM micrographs of dried P(MAA-g-EG) microparticles (35-45 μm) shows the irregular morphology due to the crushing process (Figure 4-3). Additionally, the wide polydispersity of microparticle size can be attributed to sieving, which only defines two of the three dimensions. The difference in formulation shows no observable effect on the physical characteristics of the microparticles.

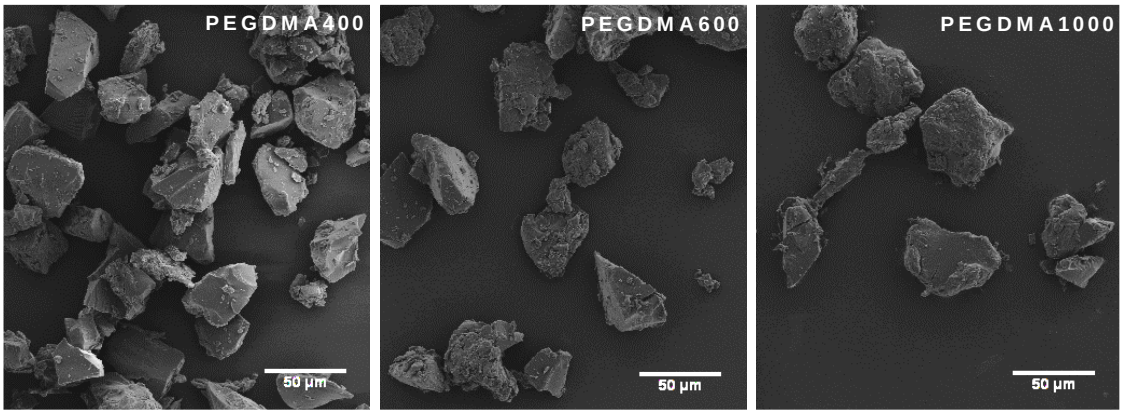

Figure 4-3. SEM images of crushed, dried P(MAA-g-EG) microparticles (30-45 µm) shown for each formulation—PEGDMA400, PEGDMA 600, and PEGDMA1000 (scale bar = 50 µm).

4.3.3 Potentiometric Titration

Microparticle suspensions were titrated with 0.2 N NaOH to quantify the amount of MAA. Calculated based on equivalence point and a charge balance, the molar amount of MAA in each formulation is reported in Table 4-2. The initial feed of MAA in the monomer solution prior to polymerization was 97.8 mol%, and the resulting polymers have a MAA content that closely matches that of the feed composition.

Table 4-2. Molar methacrylic acid content of the P(MAA-g-EG) polymers based on titration.

Crosslinking agent	MAA (mol %)
PEGDMA400	96.9 ± 0.1
PEGDMA600	95.7 ± 0.1
PEGDMA1000	95.8 ± 0.1

4.3.4 Fourier Transform Infrared (FTIR) Spectroscopy

FTIR spectra of crosslinked P(MAA-g-EG) shows characteristics of both MAA and PEG. As shown in Figure 4-4, the wide band in the 2800-3600 cm^{-1} is attributed to stretching of hydrogen bonded carboxylic acid dimers (2800-3100 cm^{-1}) of MAA and stretching of hydroxyl groups (3200-3600 cm^{-1}) of MAA. The characteristic peaks around 1700 cm^{-1} are attributed to the stretching of carbonyl groups (1725-1700 cm^{-1}) of MAA, which shifted toward 1730 cm^{-1} due to hydrogen bonding interactions. An additional contribution to this peak is due to the carbonyl stretching of the ester group (1750-1735 cm^{-1}) of PEG. The peaks in the 1500- 1300 cm^{-1} are characteristic of hydroxyl in-plane bending (1440-1395 cm^{-1}) of the carboxylic acid and in-plane methylene bending (1450 cm^{-1}). The peak around 1350 cm^{-1} can be attributed to methylene wagging, mostly attributed to PEG.[10]

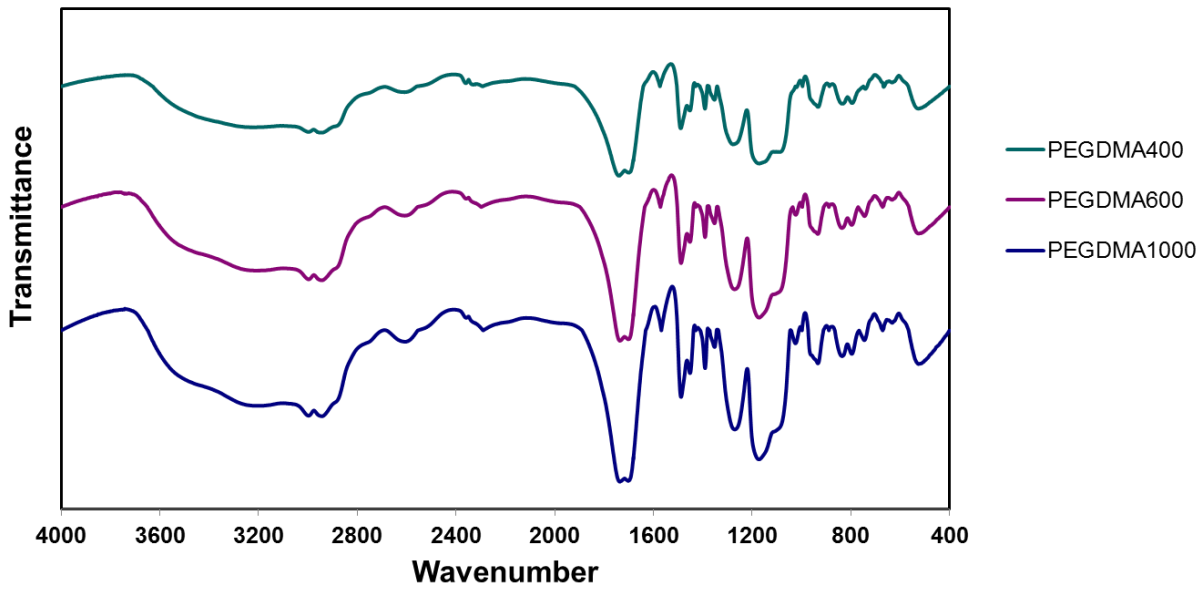

Figure 4-4. FTIR spectra of crosslinked P(MAA-g-EG) microparticles.

4.3.5 Thermogravimetric Analysis (TGA)

The thermal decomposition shows that the P(MAA-g-EG) polymer is stable at temperatures at which it can be exposed during processing and storage. The thermal degradation of the P(MAA-g-EG) formulations is shown by TGA curves (Figure 4-5). The first drop in the decomposition curves around 100°C is due to the removal of residual water. The first decomposition region at 240°C is a result of the conversion of PMAA into poly(methacrylic anhydride). The second decomposition region at 470°C is the degradation of poly(methacrylic anhydride) due to ring fragmentation and further decomposition into CO, CO2, and various carbonyls.[11]

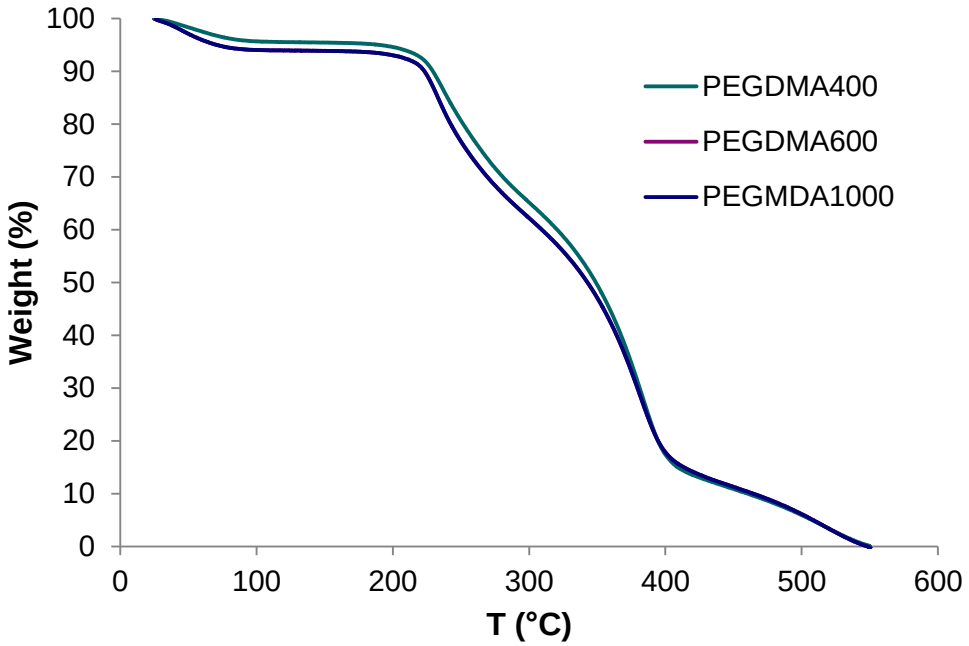

Figure 4-5. Thermal decomposition of P(MAA-g-EG) polymers.

4.3.6 pH-Responsive Swelling

Swelling behavior is critical for proper protein loading and release. To prevent degradation, protein is loaded post synthesis and processing. Therefore, the microparticles are loaded by swelling, and then collapsed to entrap the protein. Then the targeted release of protein relies on the pH-responsive swelling characteristics to provide protection in the stomach and release in the small intestine. Dynamic swelling studies were conducted to determine effect of buffer pH on the hydrogel's swelling response on a short timescale (30 minutes per buffer). Weight swelling ratios, q, were calculated at each pH condition according to:

$$q = \frac{W_S}{W_D} \qquad \text{(Eq. 4-1)}$$

where W_S is the swollen weight (mg) and W_D is the initial dry weight (mg) of the disk. All formulations remained collapsed at low pH (1.2-4.2), which is critical for protecting the payload in the stomach. As the pH increased to ~5.2, all formulations started to swell, with q increasing as pH increased (Figure 4-6). The effect of the PEGDMA crosslinking agent type (i.e. the length of the PEG unit) was not apparent on the short timescale (30 minute intervals) for the macroscopic level (10-mm diameter disks).

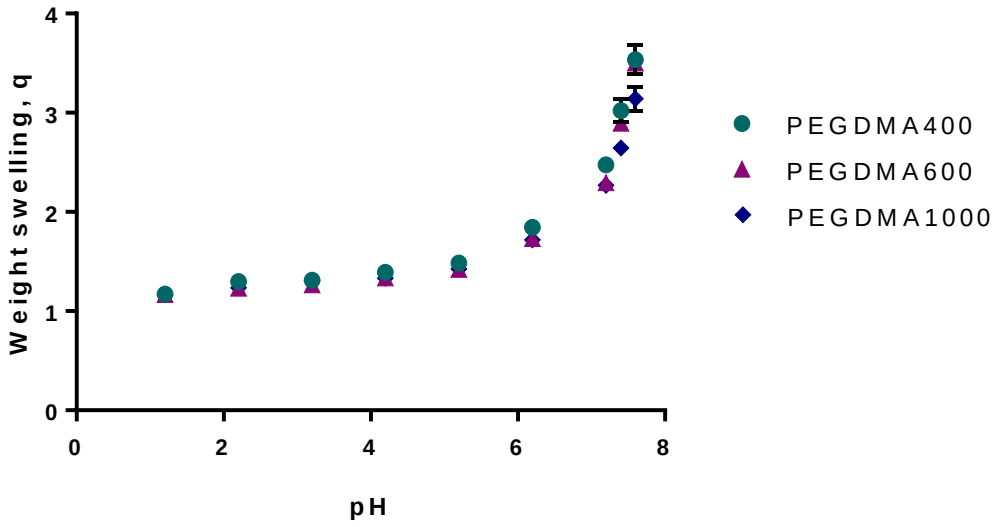

Figure 4-6. Dynamic swelling curves show the weight swelling ratio of hydrogel disks in response to change in buffer pH (n=3, mean ± SE).

4.3.7 Equilibrium Swelling and Mesh Size

Equilibrium swelling studies were conducted to determine the maximum water imbibition at both gastric and intestinal conditions, as well as determine the effect of the PEGMDA length on swelling and mesh size. As shown in Figure 4-7, all formulations remained collapsed at pH 2 (q≈1.4) due to hydrogen-bonding forming interpolymer

complexes between the protonated carboxylic acid groups of MAA and the etheric oxygen of the PEG. This collapsed state is desired to prevent premature release in the stomach. At pH 6.5, all formulations swell significantly due to the deprotonation of the carboxylic acid group, which causes disruption of interpolymer complexes and increased mesh size, as well as ionization and electrostatic repulsion resulting in water imbibition [6, 7]. This swollen state is critical for the release of protein in the small intestine. Hydrogel disks were monitored over the initial 24 h exposure to the pH 6.5 buffer. The PEGDMA400 and PEGDMA600 formulations began to burst at 6-8 h, which may be due to stresses caused by the shorter length of the crosslinking agents. However, the PEGDMA1000 formulation remained intact for the first 24 h, which may be attributed to the increased crosslinking length allowing increased water imbibition before breaking. The equilibrium swelling at pH 6.5 (Figure 4-7) shows a significant increase in the weight swelling ratio at pH 6.5 (measured after 5 days). The PEGDMA600 formulation shows a significantly reduced weight swelling ratio at pH 6.5, which is likely an artifact of mass loss (i.e. difficulty collecting all the small pieces of the broken hydrogel). Instead, it is expected that the equilibrium weight swelling ratio of the PEGDMA600 formulation would fall in between that of the PEGDMA400 and PEGDMA1000.

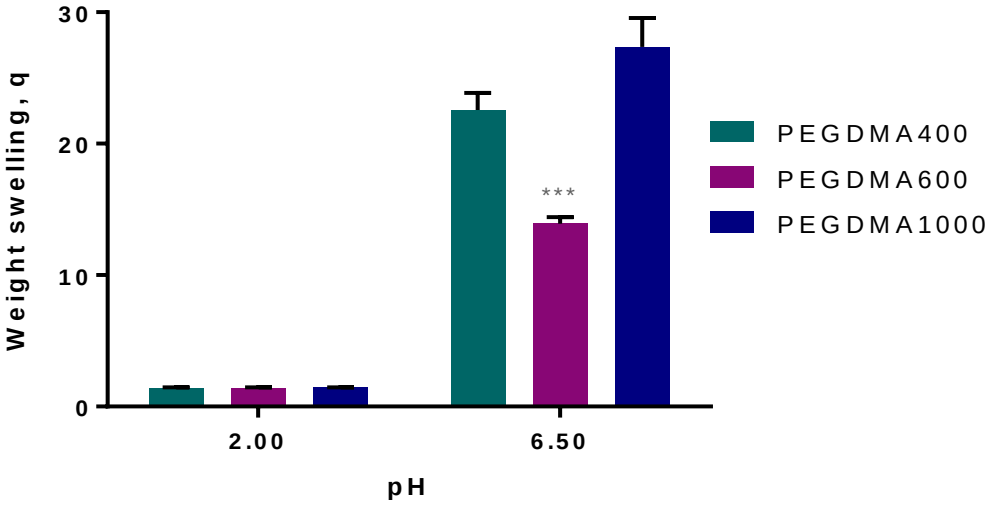

Figure 4-7. Equilibrium swelling studies show the weight swelling ratio of P(MAA-g-EG) hydrogel disks. ***Note that the weight swelling of the PEGDMA600 at pH 6.5 is likely reduced due to mass loss (n=3, mean ± SE).

Data from the equilibrium swelling studies can also be used to determine the mesh size of the hydrogel network. The mesh size, ξ, can be expressed as:

$$\xi = \nu_{2,s}^{-\frac{1}{2}} \left(\frac{2C_n\bar{M}_c}{M_r}\right)^{1/2} l \qquad \text{(Eq. 4-2)}$$

where $\nu_{2,s}$ is the volume fraction of the polymer in the swollen state, C_n is the characteristic ratio of the polymer (14.6 for PMAA),[12] $\bar{M}_c$ is the average molecular weight between crosslinks, M_r is the molecular weight of the repeat unit (calculated as a weighted average of the molecular weights of the monomers), and l is the bond length (1.54 Å for carbon-carbon bond).[13]

Based on Archimedes' principle, the volume fraction for *x* state (swollen or relaxed) can be expressed as:

$$\nu_{2,x} = \frac{w_{a,d} - w_{h,d}}{w_{a,x} - w_{h,x}} \quad \text{(Eq. 4-3)}$$

where $w_{a,d}$ is the weight of the polymer in air in the dried state, similarly the subscript *h* is for heptane, and the subscript *x* can be substituted for either *r* or *s* for the relaxed or swollen state, respectively.

The Peppas-Merrill theory is a modification of the Flory-Rehner model of the equilibrium swelling of polymer networks that takes into account the preparation of a polymer network in the presence of a solvent. The average molecular weight between crosslinks, $\bar{M}_c$, can be calculated using the Peppas-Merrill equation:

$$\frac{1}{\bar{M}_c} = \frac{2}{\bar{M}_n} - \frac{(\bar{v}/V_1)[\ln(1-\nu_{2,s}) + \nu_{2,s} + \chi_1 {\nu_{2,s}}^2]}{\nu_{2,r}\left[\left(\frac{\nu_{2,s}}{\nu_{2,r}}\right)^{1/3} - \frac{\nu_{2,s}}{2\nu_{2,r}}\right]} \quad \text{(Eq. 4-4)}$$

where $\bar{M}_n$ is the average molecular weight of the linear polymer, $\bar{v}$ is the specific volume of the polymer, V_1 is the molar volume of water (18.0 mL/mol), and χ_1 is the Flory interaction parameter.[13] Specific volume of polymer, $\bar{v}$:

$$\bar{v} = \frac{1}{\rho_h}\frac{w_{a,d} - w_{h,d}}{w_{a,d}} \quad \text{(Eq. 4-5)}$$

where ρ_h is the density of heptane (0.668 g/mL).

Flory interaction parameter, χ_1, is an indicator of how good a solvent is for a particular polymer ($\chi_1 < 0.5$ is a good solvent and $\chi_1 > 0.5$ is a poor solvent). The Flory-Rehner theory and the Peppas-Merrill theory require $\chi_1 < 0.5$. For PMAA, χ_1 can be expressed as a function of the polymer volume fraction in the swollen state as:

$$\chi_1 = 0.44 + 0.6\nu_{2,s} \quad \text{(Eq. 4-6).}$$

However, the Peppas-Merrill model is applicable for neutral polymer networks. To take into account the ionic contribution of swelling, the Brannon-Peppas equation must be used.[14] For polyelectrolyte networks with monoprotic ionizable moieties, the average

molecular weight between crosslinks, $\bar{M}_c$, can be calculated using the Brannon-Peppas equation:

$$\frac{V_1}{4I}\left(\frac{10^{-pKa}}{10^{-pH}+10^{-pKa}}\right)\left(\frac{\nu_{2,s}X}{\bar{\nu}M_r}\right) = \left[\ln(1-\nu_{2,s}) + \nu_{2,s} + \chi_1{\nu_{2,s}}^2\right] + \left(\frac{V_1}{\bar{\nu}\bar{M}_c}\right)\left(1-\frac{2\bar{M}_c}{\bar{M}_n}\right)\nu_{2,r}\left[\left(\frac{\nu_{2,s}}{\nu_{2,r}}\right)^{1/3} - \frac{1}{2}\left(\frac{\nu_{2,s}}{\nu_{2,r}}\right)\right] \quad \text{(Eq. 4-7)}$$

where I is the ionic strength of the buffer (in units of mol/mL), the pKa is 4.8 for MAA, X is the molar fraction of the ionizable groups in the polymer (determined by titration).[14]

The average molecular weight between crosslinks, $\bar{M}_c$, for P(MAA-g-EG) polymers was calculated using the Brannon-Peppas equation, where the average molecular weight of the linear polymer, $\bar{M}_n$, was determined empirically. By varying $\bar{M}_n$, nonlinear regression was used to solve for $\bar{M}_c$. $\bar{M}_n$ reaches a critical threshold where increasing its value has no significant effect on the value of $\bar{M}_c$. In this case $\bar{M}_n$= 50,000 g/mol, the average values for $\bar{M}_c$ as calculated by the Brannon-Peppas equation shown in Figure 4-8. Based on these $\bar{M}_c$ values, the mesh size, ξ, of the networks can be calculated by Equation 4-2 (Figure 4-9).

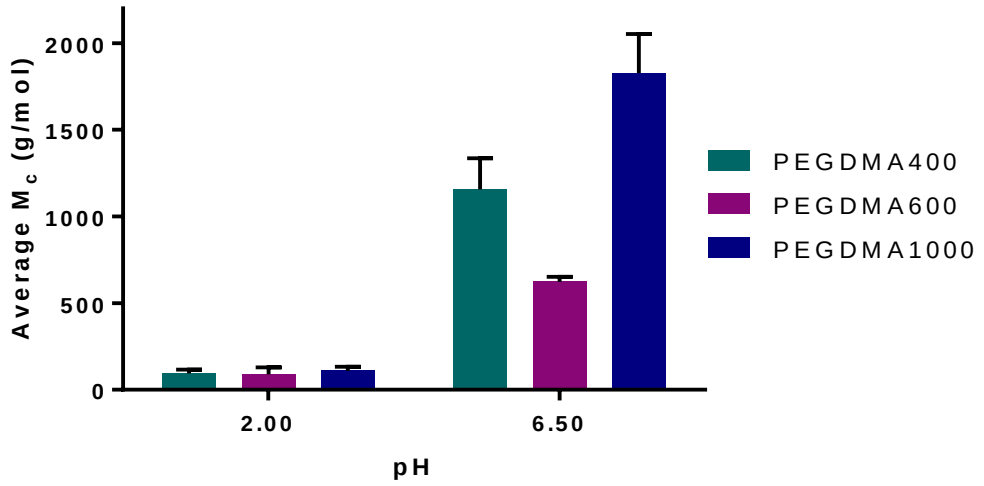

Figure 4-8. The average values for the average molecular weight between crosslinks, $\bar{M}_c$, for P(MAA-g-EG) polymer networks were calculated using the Brannon-Peppas equation, where $\bar{M}_n$= 50,000 g/mol (n=3, mean ± SE).

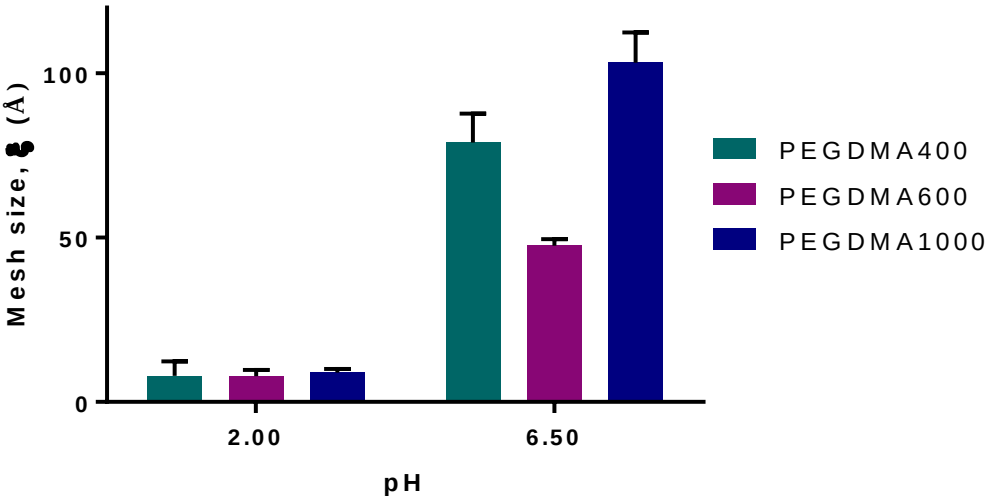

Figure 4-9. The average values for mesh size, ξ, for P(MAA-g-EG) polymer networks were calculated using the Brannon-Peppas equation, where $\bar{M}_n$= 50,000 g/mol (n=3, mean ± SE).

Based on the mesh size calculations using the Brannon-Peppas equation to determine $\bar{M}_c$, the mesh sizes of the swollen hydrogel networks at pH 6.5 range from 78.9 ± 5.1 Å for the PEGDMA400 formulation to 103.3 ± 5.2 Å for the PEGDMA1000 formulation. Previously reported mesh sizes for P(MAA-g-EG) polymers crosslinked with tetraethylene glycol dimethacrylate (TEGDMA, n=4) are approximately 200 Å under neutral conditions. However, these mesh size calculations used the Peppas-Merrill equation to determine $\bar{M}_c$. In order to compare mesh size values, the $\bar{M}_c$ must be calculated using the Peppas-Merrill equation ($\bar{M}_c$ = 1.95 x 10^4 Å for the PEGDMA1000 formulation). Based on the Peppas-Merrill equation, the mesh size for the PEGDMA1000 formulation is 338.0 ± 13.8 Å at pH 6.5. However, use of the Peppas-Merrill equation is inappropriate for an ionizable polymer network, and the $\bar{M}_c$ values are an order of magnitude higher than that calculated from the Brannon-Peppas equation (1.83 x 10^3 Å for the PEGDMA1000 formulation). This significant difference in $\bar{M}_c$ values accounts for the significant difference in the mesh size. Another limitation for both the Brannon-Peppas and Peppas-Merrill equations is that these models assume that the crosslinks are just a single point; however, in this case, the crosslinks contain PEG chains of various lengths.

Tailoring the mesh size of the swollen hydrogel is important for selecting a formulation that can properly load and release factor IX. The hydrodynamic radius of a 50-kDa protein is approximately 3.2 nm (32 Å).[15] By increasing the PEGDMA length, the mesh size of the polymer in the swollen state (intestinal pH conditions) increases, while the mesh size under acidic conditions (gastric pH conditions) remains relatively unaffected. Increasing the PEGDMA length can help improve factor IX release under intestinal conditions, while still preventing release under gastric conditions.

4.3.8 Timescale of Microparticle Swelling

The timescale of microparticle swelling, which affects drug release, was quantified by kinetic turbidimetric measurements.[16, 17] As microparticles swell, the dispersions become more optically transparent, and the refractive index of the swollen microparticle dispersion approaches that of the solvent. Therefore, the swelling of microparticle dispersions reduces the turbidity. Theoretically, turbidity is defined as:

$$\tau = \frac{cQ_{ext}}{2d\rho} \quad \text{(Eq. 4-8)}$$

where c is the mass concentration of particles, Q_{ext} is the Mie extinction coefficient, d is the particle diameter, and ρ is the particle density. The value of Q_{ext} is a function of the relative refractive index of the particles and solvent, n_p/n_0.[17] As the microparticles swell, the relative refractive index decreases (i.e. approaches one), reducing the turbidity. The degree of microparticle swelling is related to the relative turbidity of the particle dispersion to the solvent, defined as:

$$\tau = -\ln(I_t/I_0) \quad \text{(Eq. 4-9)}$$

where I_t is the transmittance of the sample at time t and I_0 is that of the pure solvent. With A being the absorbance, transmittance is defined as:

$$I = 10^{(2-A)} \quad \text{(Eq. 4-10)}$$

where, the turbidity can be expressed as:

$$\tau = [A_t - A_0]\ln(10) \quad \text{(Eq. 4-11).}$$

To monitor the change in turbidity over time for an individual sample, the relative turbidity is defined as:

$$\tau_{rel} = \frac{\tau_t}{\tau_{t=0}} \quad \text{(Eq. 4-12).}$$

By converting the turbidity data to relative swelling, as defined as:

$$Relative\ swelling = \frac{\tau_t - \tau_{t=0}}{\tau_\infty - \tau_0} \quad \text{(Eq. 4-13)}$$

where τ_∞ is the average τ values at long times (e.g. t= 50-60 minutes).

P(MAA-g-EG) microparticle swelling occurred within the first 5-10 minutes, with relative turbidity values and relative swelling values remaining stable for the remainder of the 60 minutes (Figures 4-10 and 4-11). Differences in the relative turbidity values across the different formulations cannot be easily discerned due to the irregular particle morphology and wide polydispersity in size.

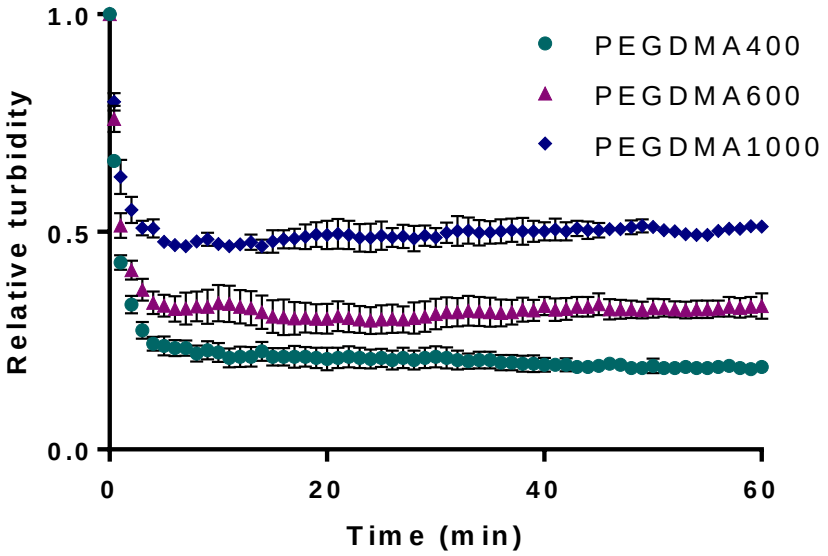

Figure 4-10. Relative turbidity curves of P(MAA-g-EG) microparticles show the kinetics of the decreasing turbidity as microparticles swell (n=4, mean ± SE).

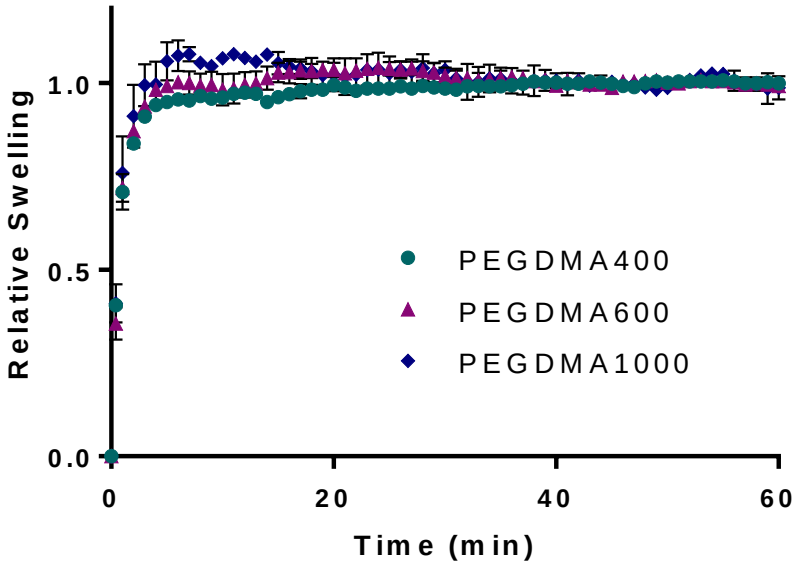

Figure 4-11. Relative swelling curves show the timescale of microparticles swelling (n=4, mean ± SE).

4.3.9 Cytocompatibility Studies

Microparticle cytotoxicity was assessed in Caco-2 and HT29-MTX cells to screen for potentially harmful carriers. Both the effect on cellular metabolic activity (MTS assay) and membrane integrity (LDH assay) were evaluated to determine the concentration dependence of microparticle cytotoxicity after a 6-hour exposure, where the average transit time in the small intestine is 2-6 hours. For this evaluation, 80% cell viability is considered cytocompatible. At a low concentration (1.25 mg particles mL^{-1}), there is no significant effect on the metabolic activity across all formulations for both cell types (Figures 4-12 and 4-13).

The metabolic activity is reduced due to increasing the microparticle concentration, with particularly inhibitory effects observed for 5 mg mL^{-1} for Caco-2 cells. However, one

limitation of these cytotoxicity studies is that the microparticles have settled into a stagnant layer on the cells, possibly creating a barrier to nutrient transport. As a secondary method, the cell membrane integrity was assessed. For all conditions, cell viability is approximately 100% indicating that a 6-hour exposure to the microparticles is not membrane disruptive (Figure 4-14 and 4-15).

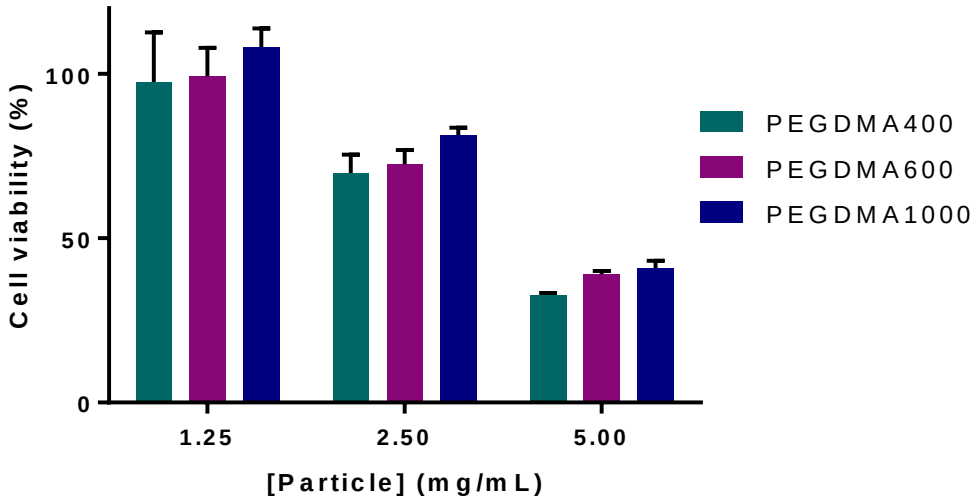

Figure 4-12. Cytocompatibility of P(MAA-g-EG) microparticles was evaluated in Caco-2 cells using a cellular metabolic activity MTS assay (n=3, mean ± SE).

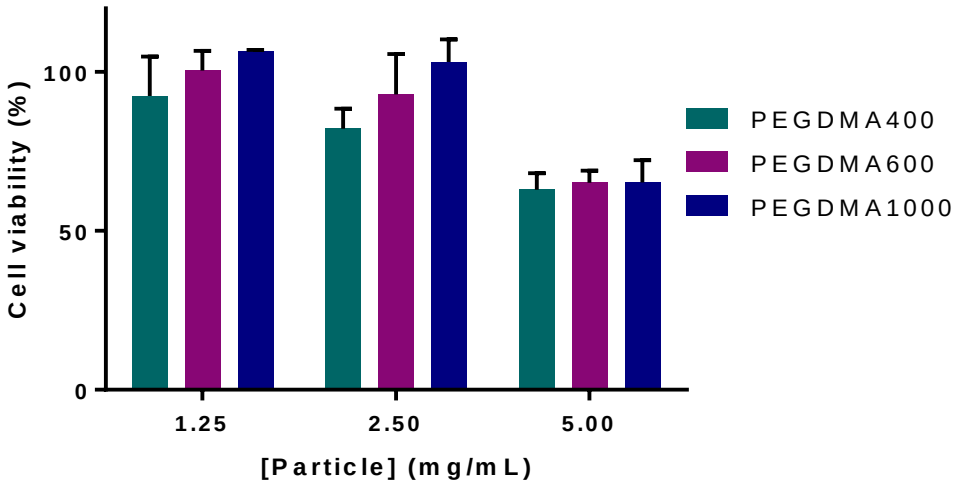

Figure 4-13. Cytocompatibility of P(MAA-g-EG) microparticles was evaluated in HT29-MTX cells using a cellular metabolic activity MTS assay (n=3, mean ± SE).

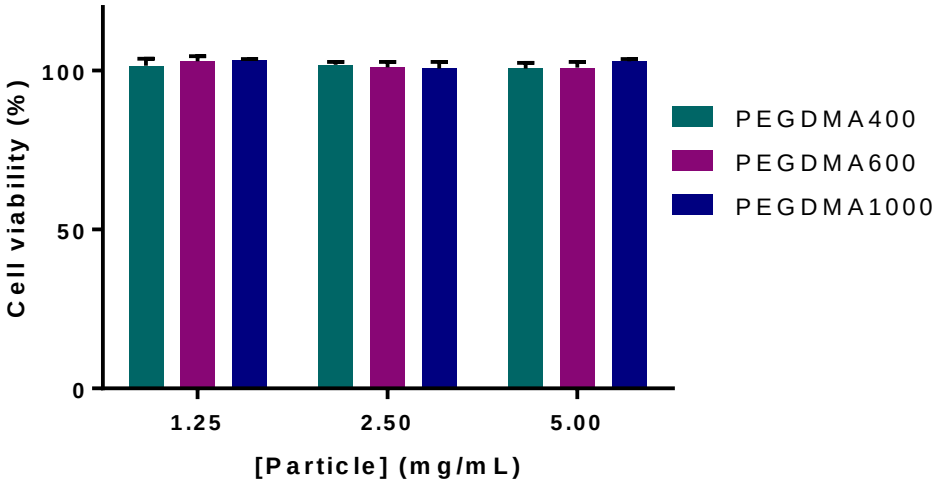

Figure 4-14. Cytocompatibility of P(MAA-g-EG) microparticles was evaluated in Caco-2 cells using a cell membrane integrity LDH assay (n=3, mean ± SE).

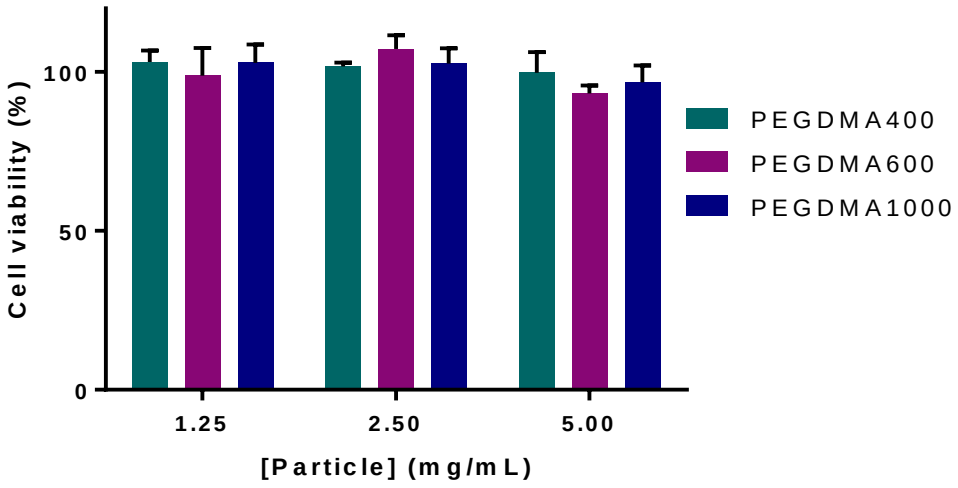

Figure 4-15. Cytocompatibility of P(MAA-g-EG) microparticles was evaluated in HT29-MTX cells using a cell membrane integrity LDH assay (n=3, mean ± SE).

4.4 CONCLUSIONS

In order to achieve the overarching goal of developing an oral delivery system for factor IX, we first designed, synthesized, and characterized pH-responsive P(MAA-g-EG) hydrogels. As confirmed by physical characterization, we synthesized hydrogels with the desired composition. Methacrylic acid was incorporated to achieve the desired pH-responsive behavior due to the ionization of pendant carboxylic acid groups (pKa=4.8). The PEG tethers serve as hydrogen-bonding acceptors to form interpolymer complexes in the collapsed state in gastric conditions. Additionally, the hydrophilicity of the PEG chains improves the water uptake in the swollen state. The pH-responsive behavior, as demonstrated by various swelling studies, is critical to providing protection of the hFIX in gastric conditions and allowing for targeted intestinal release. Furthermore, tailoring the

mesh size of the polymer networks by varying the PEGDMA length is critical for determining the effect of mesh size on the drug delivery performance of the microcarriers.

Furthermore, selection of polymeric components, such as methacrylic acid (currently used in enteric coating formulations) and PEG (considered a "FDA-friendly" polymer),[18] minimizes safety concerns of our P(MAA-g-EG) hydrogel systems. The combination of these polymeric components in the P(MAA-g-EG) systems were also found to be cytocompatible as evaluated in intestinal epithelial cells. Such hydrogels exhibited the desired characteristics—pH-responsive swelling and cytocompatibility—necessary for therapeutic applications.

4.5 REFERENCES

1. Lowman, A. M.; Morishita, M.; Kajita, M.; Nagai, T.; Peppas, N. A., Oral delivery of insulin using pH-responsive complexation gels. *J. Pharm. Sci.* **1999**, *88* (9), 933-937.
2. Nakamura, K.; Murray, R. J.; Joseph, J. I.; Peppas, N. A.; Morishita, M.; Lowman, A. M., Oral insulin delivery using P(MAA-g-EG) hydrogels: effects of network morphology on insulin delivery characteristics. *J. Control. Release* **2004**, *95* (3), 589-599.
3. Morishita, M.; Goto, T.; Nakamura, K.; Lowman, A. M.; Takayama, K.; Peppas, N. A., Novel oral insulin delivery systems based on complexation polymer hydrogels: Single and multiple administration studies in type 1 and 2 diabetic rats. *J. Control. Release* **2006**, *110* (3), 587-594.
4. Wood, K. M.; Stone, G. M.; Peppas, N. A., Wheat Germ Agglutinin Functionalized Complexation Hydrogels for Oral Insulin Delivery. *Biomacromolecules* **2008**, *9* (4), 1293-1298.
5. Wood, K. M.; Stone, G. M.; Peppas, N. A., The effect of complexation hydrogels on insulin transport in intestinal epithelial cell models. *Acta Biomater.* **2010**, *6* (1), 48-56.
6. Peppas, N. A.; Bures, P.; Leobandung, W.; Ichikawa, H., Hydrogels in pharmaceutical formulations. *Eur. J. Pharm. Biopharm.* **2000**, *50* (1), 27-46.

7. Sharpe, L. A.; Daily, A. M.; Horava, S. D.; Peppas, N. A., Therapeutic applications of hydrogels in oral drug delivery. *Expert Opin. Drug Deliv.* **2014**, *11* (6), 901-15.

8. Kamei, N.; Morishita, M.; Chiba, H.; Kavimandan, N. J.; Peppas, N. A.; Takayama, K., Complexation hydrogels for intestinal delivery of interferon beta and calcitonin. *J. Control. Release* **2009**, *134* (2), 98-102.

9. Carr, D. A.; Gomez-Burgaz, M.; Boudes, M. C.; Peppas, N. A., Complexation Hydrogels for the Oral Delivery of Growth Hormone and Salmon Calcitonin. *Ind. Eng. Chem. Res.* **2010**, *49* (23), 11991-11995.

10. Torres-Lugo, M.; Peppas, N. A., Preparation and characterization of P (MAA-g-EG) nanospheres for protein delivery applications. *Journal of Nanoparticle Research* **2002**, *4* (1-2), 73-81.

11. Ho, B.-C.; Lee, Y.-D.; Chin, W.-K., Thermal degradation of polymethacrylic acid. *Journal of Polymer Science Part A: Polymer Chemistry* **1992**, *30* (11), 2389-2397.

12. Brandrup, J.; Immergut, E. H., Polymer handbook. Wiley: New York, **1989**; Vol. 3rd.

13. Lowman, A. M.; Peppas, N. A., Analysis of the complexation/decomplexation phenomena in graft copolymer networks. *Macromolecules* **1997**, *30* (17), 4959-4965.

14. Brannon-Peppas, L.; Peppas, N. A., Equilibrium swelling behavior of dilute ionic hydrogels in electrolytic solutions. *J. Control. Release* **1991**, *16* (3), 319-329.

15. Erickson, H. P., Size and shape of protein molecules at the nanometer level determined by sedimentation, gel filtration, and electron microscopy. *Biological procedures online* **2009**, *11* (1), 32.

16. Knipe, J. M.; Chen, F.; Peppas, N. A., Enzymatic Biodegradation of Hydrogels for Protein Delivery Targeted to the Small Intestine. *Biomacromolecules* **2015**, *16* (3), 962-972.

17. Klinger, D.; Landfester, K., Enzymatic- and light-degradable hybrid nanogels: Crosslinking of polyacrylamide with acrylate-functionalized Dextrans containing photocleavable linkers. *J. Polym. Sci. A Polym. Chem.* **2012**, *50* (6), 1062-1075.

18. Hoffman, A. S., Stimuli-responsive polymers: Biomedical applications and challenges for clinical translation. *Advanced Drug Delivery Reviews* **2013**, *65* (1), 10-16.

Chapter 5: Evaluation of pH-Responsive P(MAA-g-EG) Delivery Systems for Factor IX[2]

5.1 INTRODUCTION

Hemophilia B, a hereditary bleeding disorder caused by the deficiency of clotting factor IX (FIX), affects 80,000 males worldwide.[1] Protein replacement therapy by intravenous (IV) injection or continuous infusion can prevent spontaneous bleeding episodes and restore hemostasis, significantly improving the patient's lifespan and quality of life. Prophylactic treatments, requiring multiple injections per week, are recommended for 75% of hemophilia B patients, classified as severe (<1% FIX clotting activity) or moderate (1-5% FIX clotting activity).[1-2] However, current treatments are limited by noncompliance, increased risk of needle injury, costly medical care, and potential complications (e.g. severe allergic reactions).

A major challenge for prophylactic regimens, especially in children, is the need for a surgically implanted venous access port, which may lead to risks of infection and thrombosis.[3] As a result, such treatments are not readily available worldwide. Without treatment, the median life expectancy of a hemophilia B patient drops to 11 years.[4] Therefore, a non-invasive alternative is highly desirable to overcome such limitations and promote the global availability of hemophilia treatment.

Oral delivery of coagulation proteins can improve the patients' quality of life by ensuring safety, convenience, and ease of administration. In this work, we focus on developing an oral delivery system for a therapeutically effective prophylactic treatment

[2] Portions of this chapter have been previously published in Horava, S. D.; Peppas, N. A., Design of pH-Responsive Biomaterials to Enable the Oral Route of Hematological Factor IX. Annals of Biomedical Engineering 2016, 1-13.

for hemophilia. There is currently no commercially available oral delivery method of factor IX for protein replacement therapy.

In this chapter, we focus on the evaluation of pH-responsive biomaterials as delivery vehicles to enable the oral route of hematological factor IX.[5] The mesh size of the hydrogel networks was tailored to optimize the diffusional processes necessary for improving protein loading and release. Additionally, loading conditions were modified to further adjust the therapeutic delivery potential. An evaluation of delivery system's performance, including loading, release, protein activity, and *in vitro* transport, is detailed herein.

5.2 Materials and Methods

5.2.1 Materials

Methacrylic acid (MAA) and Irgacure 184® (1-hydroxy-cyclohexyl-phenylketone) were purchased from Sigma-Aldrich (St. Louis, MO). Poly(ethylene glycol) (MW=1000) mono methyl ether monomethacrylate (PEGMMA1000), poly(ethylene glycol) (MW=400) dimethacrylate (PEGDMA400), PEGDMA600 (MW=600), and PEGDMA1000 (MW=1000) were purchased from Polysciences (Warrington, PA). Plasma-derived human factor IX (hFIX) was purchased from Haematologic Technologies Inc. (Essex Junction, VT). Human factor IX ELISA kits were purchased from AssayPro LLC. (St. Charles, MO), and the BIOPHEN factor IX activity assays were purchased from HYPHEN Biomed SAS (Neuville-sur-Oise, France). FaSSIF, FeSSIF & FaSSGF Powder was purchased from Biorelevant.com (London, England, UK). All reagents were used as received. All other solvents and buffers were purchased from Fisher Scientific (Waltham, MA).

5.2.2 Factor IX Activity Assay

The biological activity of hFIX was determined using hFIX chromogenic activity assays according to the manufacturer's protocol (BIOPHEN factor IX activity assay, HYPHEN Biomed SAS). This chromogenic activity assay relies on a portion of the coagulation cascade (Figure 5-1), where the enzymatic activity is directly related to hFIX, the limiting factor. The generated factor Xa (FXa) can be quantified with high sensitivity (detection range 0.1-30 ng/mL) based on its specific activity on factor Xa chromogenic substrate (SXa-11). FXa can cleave the substrate to release a pNA chromophore. The free pNA can be quantified by color development at 405 nm. The amount of active FIX in the sample is linearly related to the FXa activity, as measured by the amount of pNA released.

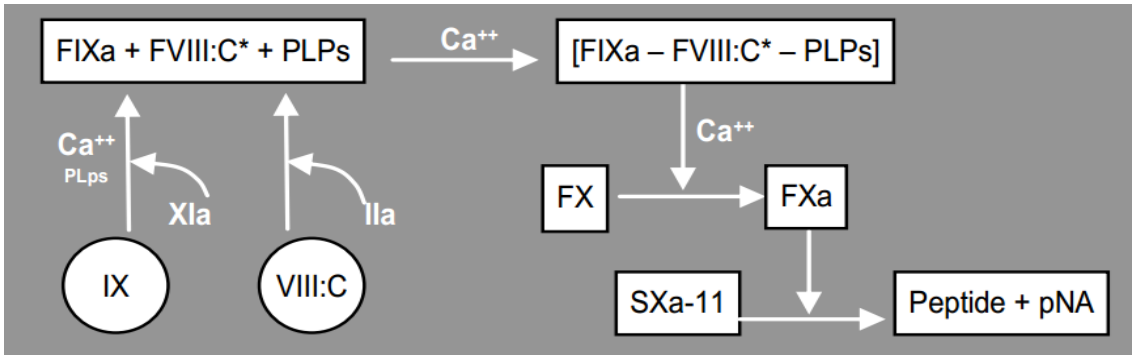

Figure 5-1. Reaction scheme for the BIOPHEN factor IX chromogenic activity assay.

5.2.3 Equilibrium Swelling Studies at Reduced Ionic Strength

Ionic strength of the buffer affects the swelling of P(MAA-g-EG) hydrogels, which may also affect the protein loading. For equilibrium swelling, dried disks were placed in a pH 2.0 buffer solution at 37°C for at least 72 hours, then blotted and weighed. The same disks were then placed in a pH 7.4 buffer solution at 37°C for at least 72 hours, then blotted

and weighed. Equilibrium swelling studies were conducted using buffers of two different ionic strengths—5 mM and 167 mM. The lower ionic strength buffers were 5 mM NaH_2PO_4 and the pH was adjusted using 1 N NaOH and 1 N HCl as necessary. For the higher ionic strength buffers, the pH 2 buffer was 167 mM NaCl and the pH 7.4 buffer was 1x PBS. The buffered solutions at pH of 2.0 and 7.4 were selected because these values represent the loading (pH 7.4) and collapse (pH 2.0) conditions.

5.2.4 Protein Stability

In order to optimize loading, the stability of the hFIX was evaluated in two different buffers (pH 7.4)—1x PBS and 5 mM NaH_2PO_4— at three different temperatures—4, 20, and 37°C—over a 7-day period. For the study duration, 0.5 mg mL^{-1} hFIX solutions in either buffer were stored at the designated controlled temperature under constant end-to-end rotation. The activity of hFIX was quantified at days 1, 2, 5, and 7, as compared to a freshly prepared stock of hFIX in the same buffer, using hFIX chromogenic activity assays according to the manufacturer's protocol (BIOPHEN factor IX activity assay, HYPHEN Biomed SAS).

5.2.5 Protein Loading Studies

Dried particles were added to a 0.5 mg mL^{-1} hFIX solution (1x PBS with 2% 1(v/v) N NaOH) to a final concentration of 5 mg mL^{-1} and pH of 7.4. hFIX loading was carried out by equilibrium partitioning for 24 hours with particle/protein suspensions under constant end-to-end rotation at 37°C. After 24 hours, particles were collected by Buchner filtration using Whatman 50 filter paper. Particles were then collapsed with 0.1 N HCl and then triple rinsed with 0.1 N HCl, DI water, and 0.1 N HCl. Samples were collected after each step—end of loading, collapse, and rinse—for protein quantification using hFIX ELISAs. Protein-loaded particles were then lyophilized overnight.

To optimize loading, the ionic strength of the loading, length of loading time, and temperature at which loading occurs were modified, while other parameters remained constant. Loading was increased to 5 days at 4°C using two different buffers (pH 7.4)—1x PBS and 5 mM NaH_2PO_4.

5.2.6 Protein Distribution Studies

To visually confirm the distribution of protein within the loaded microparticles, loading studies were completed using fluorescein isothiocyanate (FITC)-conjugated hFIX. hFIX was labeled with FITC (MW=389) using Thermo Scientific™ Pierce™ FITC Antibody Labeling Kits according to the manufacturer's protocol. The isothiocyanate of FITC reacts with primary amines of proteins. The molar ratio of FITC to protein was calculated from the absorbance measurements at 280 nm and 495 nm.

Loading studies were conducted as previously described at 37°C for 24 hours. Following the collapse and rinse steps, microparticles were collected and then added to microscope slides with Molecular Probes™ ProLong™ Gold Antifade Mountant, which was allowed to cure for 24 hours at room temperature. Confocal images, both fluorescent and bright field channels, were captured using an Olympus All-in-one Confocal Laser Scanning Microscope FV10i (Shinjuku, Tokyo, Japan).

5.2.7 Protein Release Studies

Protein release studies were conducted following a two-stage dissolution procedure using biorelevant media. Biorelevant media were prepared using a FaSSIF, FeSSIF & FaSSGF Powder which contains bile salts and phospholipids. Fasted-state simulated gastric fluid (FaSSGF) was prepared at a 1x concentration with a final pH of 1.6 according to the manufacturer's protocol (Biorelevant). Fasted-state simulated intestinal fluid (FaSSIF) was prepared at 2x concentration with a final pH of 6.9. For the two-stage

dissolution procedure, a 1:1 (v/v) FaSSGF:FaSSIF mixture at a final pH of 6.5 is required for the intestinal condition.

Dissolution testing was performed using an USP apparatus 2 (with paddles) setup for small volume (100 mL vessel) with low evaporation mini vessel covers using a Distek 2100B dissolution apparatus (North Brunswick, NJ). A 5 mg sample of hFIX-loaded microparticles was added to a Sigmacoted (i.e., siliconized) vessel containing 30 mL of SGF (1x, pH 1.6) at 37°C. After 30 minutes, 30 mL of FaSSIF (2x) at 37°C was added, raising the pH to 6.5. The solution was continuously stirred at 75 rpm and maintained at 37°C for both stages. The FaSSIF stage was carried out for up to 6 h. Over the course of the dissolution, 1 mL samples were taken using a 1/8 cannula sample probe (Distek, Inc.) with a 10 micron polyethylene filter tip (Agilent Technologies, Santa Clara, CA). Samples were replaced with an equal volume of appropriate prewarmed media. hFIX released was quantified by hFIX ELISAs and its activity was measured by hFIX chromogenic activity assays.

5.2.8 Endotoxin Depletion

For *in vitro* use, hFIX was endotoxin-depleted using Thermo Scientific™ Pierce™ High-Capacity Endotoxin Removal Spin Columns according to the manufacturer's protocol. After endotoxin removal, the amount of endotoxin in hFIX samples was measured using a Thermo Scientific™ Pierce™ LAL Chromogenic Endotoxin Quantification Kit. To verify the lack of product inhibition, a spiked hFIX sample was included in the assay.

5.2.9 In Vitro Transport Studies

In vitro transport studies using an intestinal epithelial model were conducted to determine the effect of the presence of the microcarriers on protein transport. Caco-2 and

HT29-MTX cells were cultured with DMEM with 10% FBS in separate flasks. For the transport studies, cells (either Caco-2 cells only or 1:1 Caco-2:HT29-MTX cell mixture) were seeded on the apical side of 12-well Transwell® plates (12 mm diameter, 0.4 μm pores, Corning, Corning, NY) at 10^5 cells per well. Monolayers were cultured for 21-25 days to allow the cells to fully differentiate and reach confluence. Every other day, media (DMEM supplemented with 10% FBS, 1% L-glutamine, and 1% penicillin/streptomycin) was changed, and the transepithelial electrical resistance (TEER) was monitored with an EVOM^2 epithelial voltohmmeter and a chopstick electrode (World Precision Instruments, Sarasota, FL).

One hour prior to the transport experiment, the medium was removed and replaced with Hank's balanced salt solution (HBSS) at 37°C with 0.5 mg mL^{-1} bovine serum albumin (BSA) to allow the cells to equilibrate. After removing the HBSS/BSA solution from the apical side, the cells were exposed to one of the following conditions: HBSS/BSA, neat protein (0.04 mg mL^{-1} hFIX), and microparticles (0.875 mg mL^{-1}= 0.391 mg cm^{-2}) with protein (0.04 mg mL^{-1} hFIX). Over the course of the 4-hour experiment, the TEER was measured, and then 200 μL samples were collected from the basolateral side and replaced with HBSS/BSA at 37°C for each time point. After 4 hours, final samples from both the apical and basolateral sides were collected, then cells were rinsed with media, and fresh media was added to both sides. At 24 hours post study completion, final TEER measurements were collected to determine the recovery of the monolayers. The amount of hFIX on the basolateral side was quantified using hFIX ELISAs.

5.2.10 Statistical Analysis

Data are reported as mean ± standard error. Comparisons between groups were performed using a Student's two-tailed t-test, and comparisons among multiple groups

were performed using an ANOVA. Significant differences were considered when *$p < 0.05$ and **$p < 0.01$. All statistical analysis was computed using GraphPad Prism 6.

5.3 Results and Discussion

5.3.1 Protein Loading and Release Studies

High molecular weight proteins, like factor IX, have difficulty being transported in molecular structures, including polymer networks. For factor IX, we investigated the effect of the mesh size, by varying the length of the PEGDMA crosslinking agent, on loading and release. The final amount of protein loaded was calculated based on the concentration of the supernatant after incubation, collapse, and triple rinse. Protein lost during the collapse and rinse was likely surface loaded. The loading level (μg hFIX mg^{-1} particles) was calculated as:

$$Loading = \frac{c_0 V_0 - c_f V_f}{c_p V_0} \quad \text{(Eq. 5-1)}$$

where c_0 is the initial protein concentration (μg mL^{-1}), V_0 is the initial volume (mL), c_f is the final protein concentration (μg mL^{-1}) after rinsing, V_f is the final volume (mL) after rinsing, and c_p is the particle concentration (mg mL^{-1}).

As shown in Figure 5-2, increasing the PEGDMA length increased the amount of hFIX loaded, with significantly higher loading achieved with both the PEGDMA600 and PEGDMA1000 formulations than the PEGDMA400 formulation. To further investigate the effect of PEGDMA length on loading, FITC-hFIX (0.37 mol FITC per mol hFIX) was loaded to visualize the protein distribution within the microparticles. As confirmed by confocal microscopy (Figure 5-3), hFIX was surface loaded on microparticles for both the PEGDMA400 and PEGDMA600 formulations. However, hFIX was loaded uniformly

throughout the microparticles for the PEGDMA1000 formulation as shown in Figure 5-4. Protein loading within the microparticle can be achieved by increasing the mesh size (i.e. longer PEGDMA crosslinking agent), which can lead to improved protection of the protein.

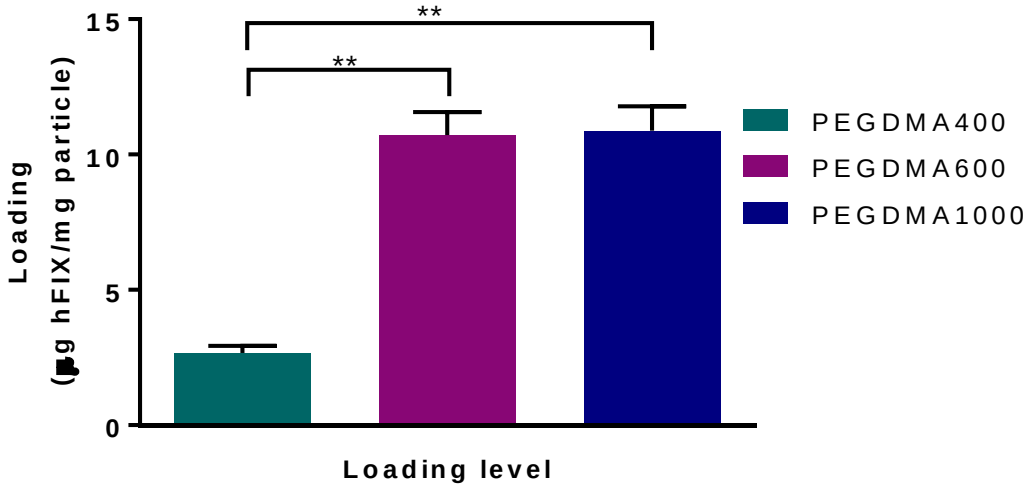

Figure 5-2. Loading level of hFIX is dependent on the PEGDMA crosslinking agent length of P(MAA-g-EG) hydrogels (n=3, mean ± SE, **p<0.01).

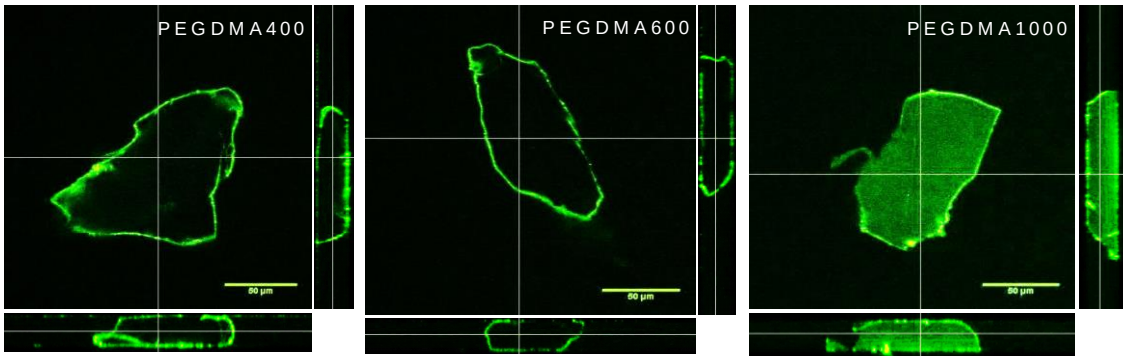

Figure 5-3. The distribution of hFIX loaded is improved by increasing the PEGDMA crosslinking agent length. Confocal images of FITC-hFIX loaded microparticles (orthogonal view, fluorescence channel) show that hFIX surface loaded for the PEGDMA400 and PEGDMA6000 formulations, and hFIX loaded throughout the microparticles for the PEGDMA1000 formulation (scale bar = 50 µm).

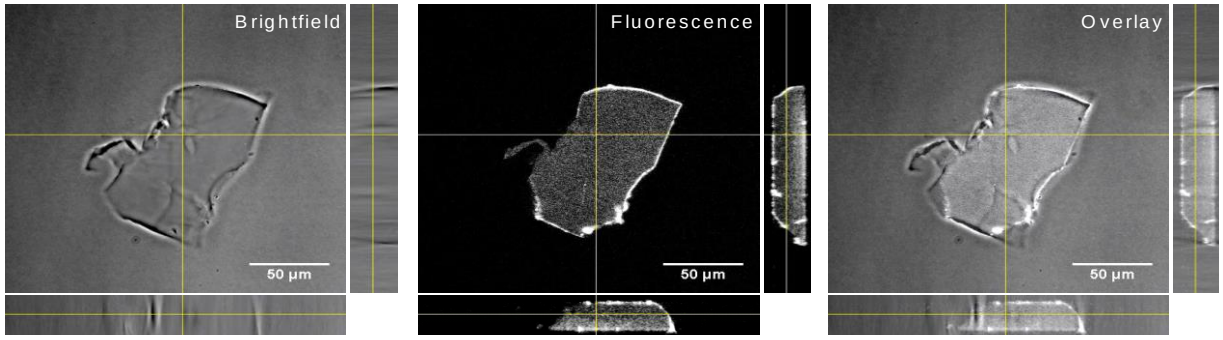

Figure 5-4. Confocal image of FITC-hFIX loaded P(MAA-g-EG) crosslinked with 1 mol% PEGMDA1000 microparticle (channels: bright field, fluorescence, and overlay) (scale bar = 50 µm).

The release of hFIX from P(MAA-g-EG) microparticles was tested using a two-stage dissolution procedure in biorelevant media. For all formulations, hFIX release was minimal in the simulated gastric conditions (FaSSGF), while release significantly increased in the simulated intestinal conditions (FaSSIF) (Figure 5-5). The cumulative release in the FaSSIF conditions was higher for the PEGDMA400 and PEGDMA600 formulations, as compared to PEGDMA1000, due to hFIX being surface loaded and therefore released faster. Release from the PEGDMA100 formulation is expected to be sustained over longer periods as the hFIX must diffuse out of the hydrogel network. While the cumulative protein release showed the desired release profile, the activity of the released protein is critical for its therapeutic use. The activity of released hFIX is better maintained as the length of the PEGDMA crosslinking agent increases (Figure 5-6). Protein released from P(MAA-g-EG) microparticles crosslinked with 1 mol % PEGDMA1000 maintained approximately 100% of its activity, which was significantly higher than the other two formulations. For the PEGDMA1000 formulation, hFIX loading within the microparticle improved protection as confirmed by the activity of released protein. To compare the overall performance among the three formulations, the amount of active hFIX released (Figure 5-7) was calculated as the product of the total release of hFIX and the activity percentage of released hFIX at a given time point. The PEGDMA1000 formulation is the most promising due to significantly higher release of active hFIX.

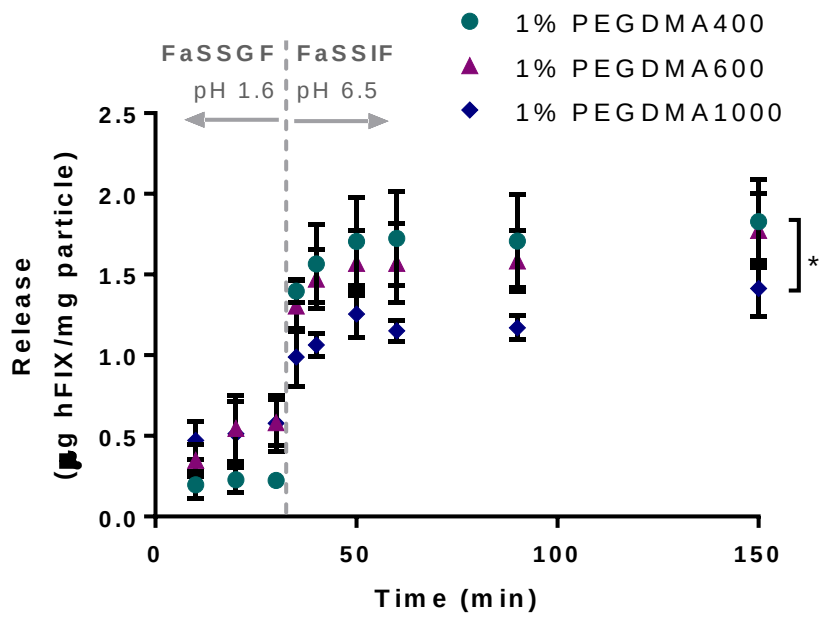

Figure 5-5. Release of hFIX from P(MAA-g-EG microparticles using two-stage dissolution in biorelevant conditions shows the desired release profile. (n=3, mean ± SE, *p<0.05, **p<0.01).

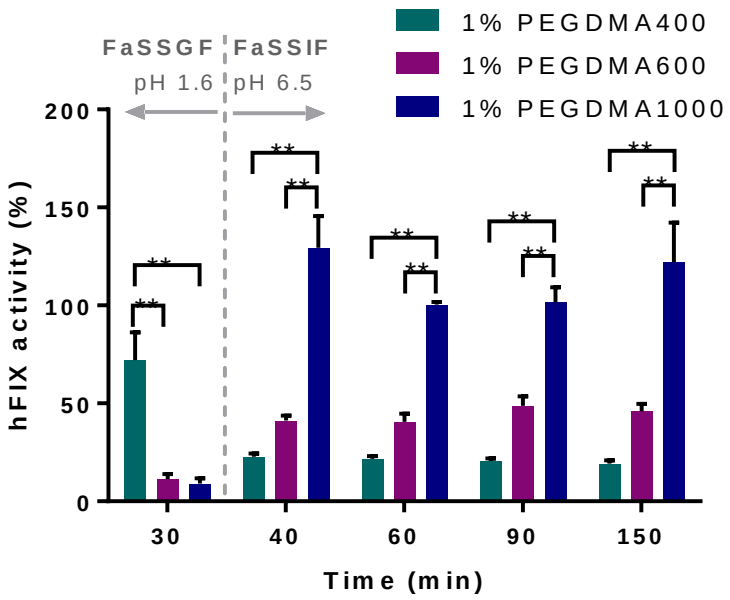

Figure 5-6. Activity of release hFIX is better maintained as the length of the PEGDMA crosslinking agent increases. (n=3, mean ± SE, *p<0.5, **p<0.01).

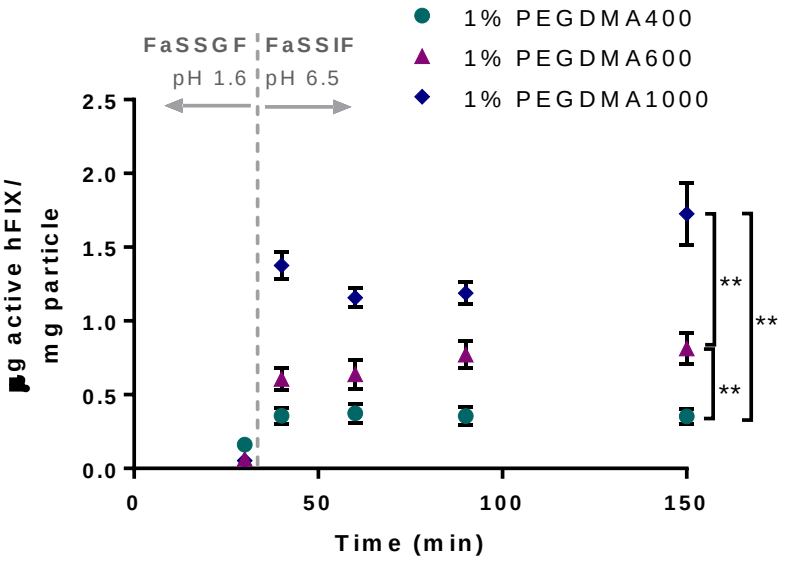

Figure 5-7. The amount of active hFIX released (the product of the total release and its activity) shows that the PEGMDA1000 formulation is the most promising candidate. (n=3, mean ± SE, *p<0.5, **p<0.01).

5.3.2 Optimization of Loading and Release

To further optimize the loading efficiency, three parameters—ionic strength of the buffer, time, and temperature—were modified. As previously described,[6] reducing the ionic strength of the buffer increases the swelling of anionic hydrogels. Increasing swelling can result in higher protein loading.[7] Additionally, increasing both time and temperature can increase the rate of diffusion to increase the amount of protein loaded. However, increasing time and temperature can also reduce the protein stability. A balance between increasing loading and maintaining the protein stability/activity is necessary for determining improved loading conditions.

In order to analyze these parameters, two buffers—1x PBS (162.7 mM) and 5 mM NaH_2PO_4—were evaluated for their effects on hydrogel swelling and protein stability. Equilibrium swelling studies using the PEGDMA1000 formulation showed minimal swelling at pH 2 and significantly increased swelling at pH 7 (Figure 5-8). At pH 7, the weight-swelling ratio was ~2.3-fold higher for the reduced ionic strength buffer. Additionally, the effect of temperature and time on the stability of hFIX in both buffers at pH 7 was assessed to determine the time and temperature that maintained at least 95% of its activity. After 5 days at 4°C, hFIX was stable in both buffer conditions; however, at higher temperatures, the stability of hFIX dropped over time down to 12% of its relative activity (in 5 mM NaH_2PO_4 at 37°C) (Figure 5-9).

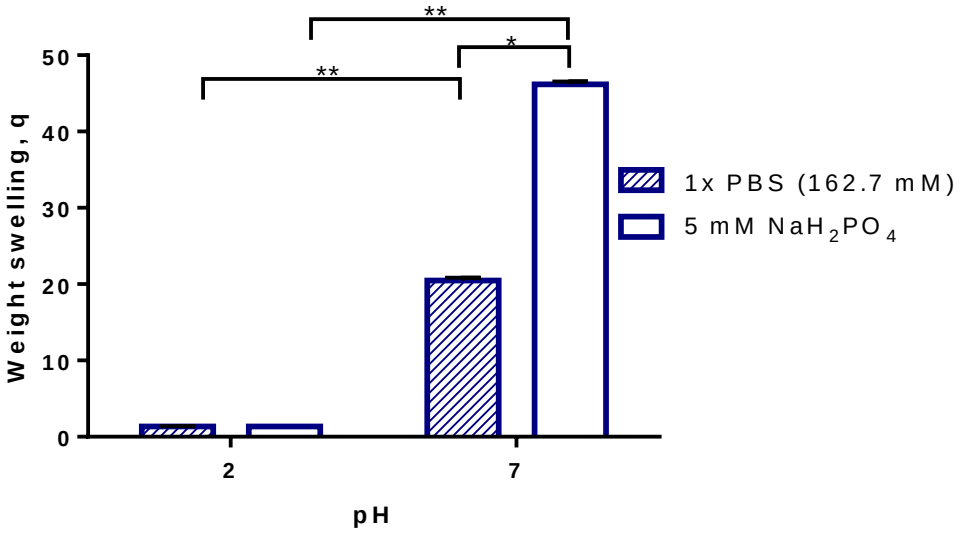

Figure 5-8. Hydrogel disks show increased equilibrium swelling in a reduced ionic strength buffer. (n=3, mean ± SE, *p<0.05, **p<0.01).

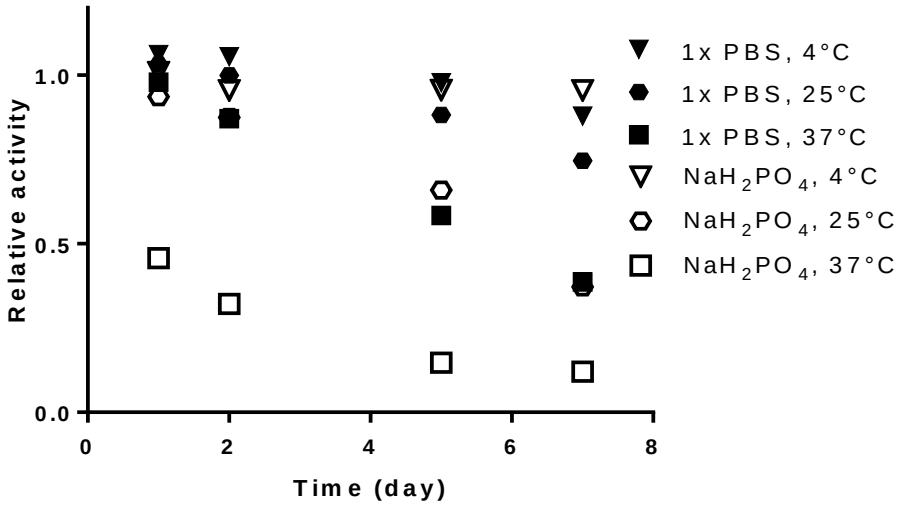

Figure 5-9. Time, temperature, and ionic strength affect hFIX stability. (n=3, mean ± SE, *p<0.05, **p<0.01).

Loading studies were conducted at 4°C for 5 days in both buffers to determine if hFIX loaded can be improved for the PEGDMA1000 formulation. Compared to loading at 37°C for 1 day, the new loading conditions resulted in significantly higher hFIX loading levels (Figure 5-10). Reducing the buffer's ionic strength also improved hFIX loading. Release of hFIX from P(MAA-g-EG) particles showed the desired profile with minimal release in gastric conditions and significantly higher release in intestinal conditions (Figure 5-11).

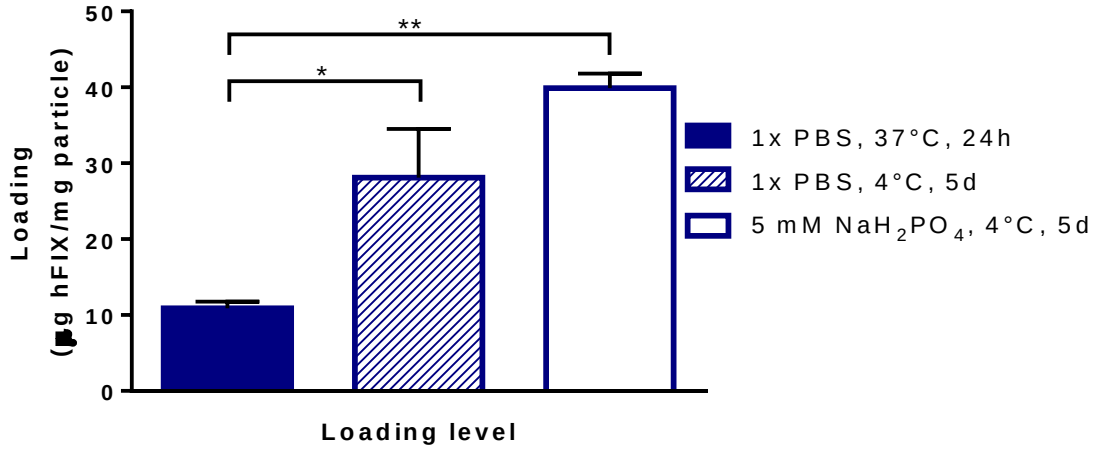

Figure 5-10. Optimized loading conditions (5 days at 4°C) significantly improved hFIX loading into P(MAA-g-EG) microparticles, and a reduced ionic strength buffer further improved loading. (n=3, mean ± SE, *p<0.05, **p<0.01).

The particles loaded in the reduced ionic strength buffer (5mM NaH_2PO_4) have higher delivery potential likely due to a higher loading level compared to those using a higher ionic strength buffer (1x PBS). Additionally, released hFIX maintained approximately 80% of its activity in intestinal conditions (Figure 5-12). Overall, improving the amount of hFIX loaded in P(MAA-g-EG) microparticles (PEGDMA1000 formulation)

increased the amount of active hFIX released in intestinal conditions (Figure 5-13), which can lead to improved bioavailability of orally delivered therapies.

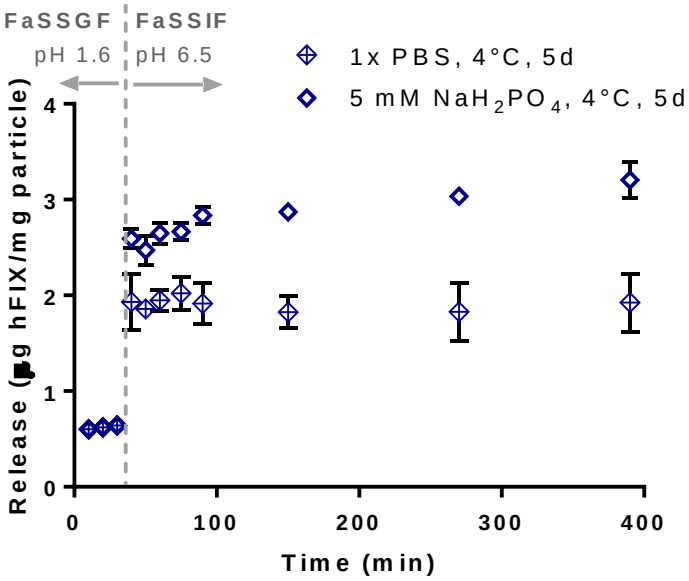

Figure 5-11. Release of hFIX from the PEGDMA1000 formulation using two-stage dissolution in biorelevant conditions shows the desired release profile. Improved hFIX loading (in 5 mM NaH_2PO_4 compared to 1x PBS) resulted in higher release of hFIX in intestinal conditions. (n=3, mean ± SE).

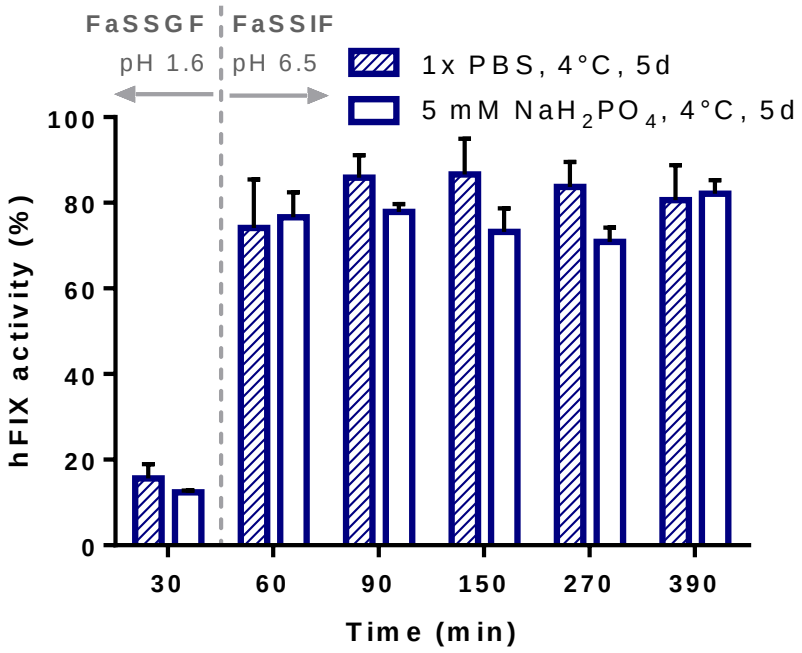

Figure 5-12. Activity of released hFIX is maintained in intestinal conditions. (n=3, mean ± SE).

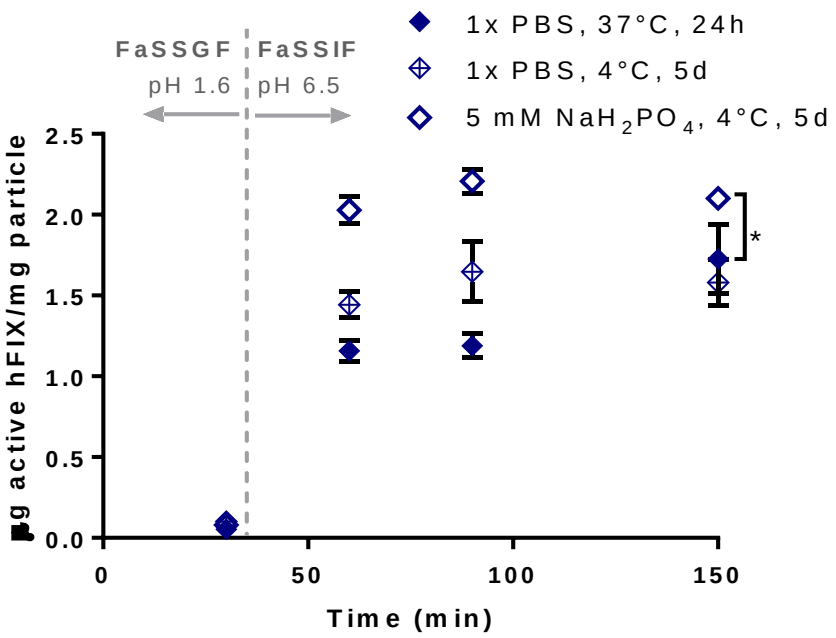

Figure 5-13. Improved hFIX loading resulted in significantly higher release of active hFIX in intestinal conditions, which can improve the efficacy of an orally delivered therapy. (n=3, mean ± SE, *p<0.05).

5.3.3 Dose Calculation

The dose for FIX depends on the patient's severity of hemophilia B, body weight, age, and type of treatment required (e.g. prophylactic and on-demand for minor, moderate, or major surgeries/trauma). The amount of factor IX international units (IU) required in units of IU can be calculated as:

$$FIX\ IU\ required = body\ weight \times desiredFIX\ increase \times reciprocal\ of\ recovery \quad \text{(Eq. 5-2)}$$

where the body weight is in kg, desired FIX increase in units of % or IU/dL and reciprocal of recovery is in IU/kg per IU/dL. [8] The international unit (IU) for hFIX is defined as the activity of hFIX in 1 mL of normal plasma, and normal hFIX plasma concentrations are 2.5-5 µg/mL, and therefore 1 IU equals 2.5-5 µg. The reciprocal of observed recovery is

commonly defined as 1 IU/kg per IU/dL; however, this value can vary with age and on an individual basis.

Prophylactic treatment regimens are given on a regular weekly basis as a preventative measure for patients with severe (<1%) hemophilia B. The common prophylactic dosage is 25-40% increase in FIX, administered twice per week.[9] However, studies have shown that tailoring the dosing of FIX according to an individual patient and increasing the dosage intervals to determine the minimum effective dose can markedly improve the cost-effectiveness of the prophylactic treatment, as well as maintain a certain trough level. For a patient with relatively unaffected joints, a 1% increase in FIX is generally recommended since a 1% activity level can eliminate spontaneous bleeding episodes.[9] However, an individual with joint damage typically require a high target level, where a 3% increase has been suggested for preventing further joint function deterioration. Another study found at a 2% increase in FIX for prophylactic treatments is clinically effective and cost-effective.[10] For a minimum effective prophylactic treatment, requiring 1% hFIX increase, an average 10 year old male (35 kg) requires 35 IU or 1750 μg of hFIX, assuming a conversion of 2.5 μg per IU. Based on our results, we can assume an intestinal release of 3 μg hFIX/mg particle and 5% bioavailability, meaning that 583 mg of particles would need to be administered. This dose of particles will fit approximately into two size 2 capsules.

5.3.4 Factor IX Transport Studies

In vitro transport studies are used to screen for potentially successful candidates and determine the effect of the presence of microparticles on the hFIX absorption. We evaluated the transport of hFIX using two intestinal epithelial monolayers of Caco-2 cells only or a co-culture of Caco-2 and HT29-MTX cells. The Caco-2 cell line is well-

characterized intestinal epithelial model that is the most widely used standard in the pharmaceutical industry to predict oral drug absorption. Permeability data obtained using Caco-2 cells often correlates well with *in vivo* results. However, Caco-2 cells do not secret mucus, a key component of the intestinal epithelial layer. Co-cultures of Caco-2 cells and mucus-secreting goblet-like HT29-MTX cells are commonly used as an intestinal epithelial model for predicting oral drug absorption, particularly paracellular transport *in vivo*.[11] A co-culture model better mimics the physiological conditions of the intestine, containing three major absorption barriers—tight junctions, membranes of absorptive epithelia, and a mucus layer. Additionally, HT29-MTX cells modulate the tight junction geometry, resulting in a "tightness", indicated by TEER values (~300 Ω cm^2), closer to *in vivo* conditions which range from 20 to 100 Ω cm^2 (Figure 5-14).[11] While the co-culture model is more physiologically relevant, the drug permeability is typically lower due to higher TEER values.

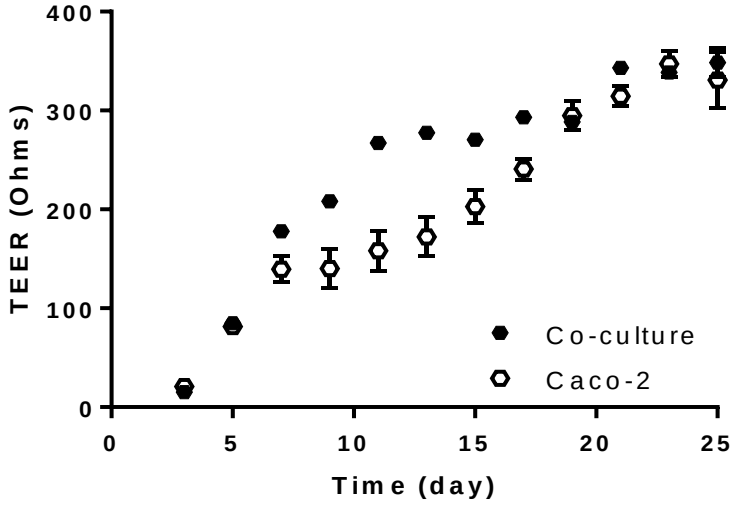

Figure 5-14. TEER of *in vitro* epithelial monolayers during culturing. (n=12, mean ± SE).

Transport studies were conducted to determine the permeability of hFIX across an intestinal epithelial monolayer. Prior to the transport studies, hFIX was endotoxin depleted (final endotoxin concentration < 2.5 EU mL^{-1}). For experimental groups, a suspension of 0.04 mg mL^{-1} hFIX and 0.875 mg mL^{-1} microparticles (the same surface area coverage of 0.391 mg cm^{-2} as the 1.25 mg mL^{-1} concentration used in the cytocompatibility studies and determined as non-cytotoxic) was initially added to the apical chamber, and a 0.04 mg mL^{-1} hFIX solution was also included as a control. The presence of the P(MAA-g-EG) microparticles promoted the apical-to-basolateral transport of hFIX as compared to the hFIX only for both culture types (Figures 5-15 and 5-16). For the Caco-2 only monolayers, PEGDMA1000 formulation resulted in the highest amount of hFIX transported to the basolateral side (Figure 5-15). For the co-culture model, there was no significant difference in hFIX transported among the microparticle formulations (Figure 5-16). Overall, the amount of hFIX transported was higher in the co-culture model.

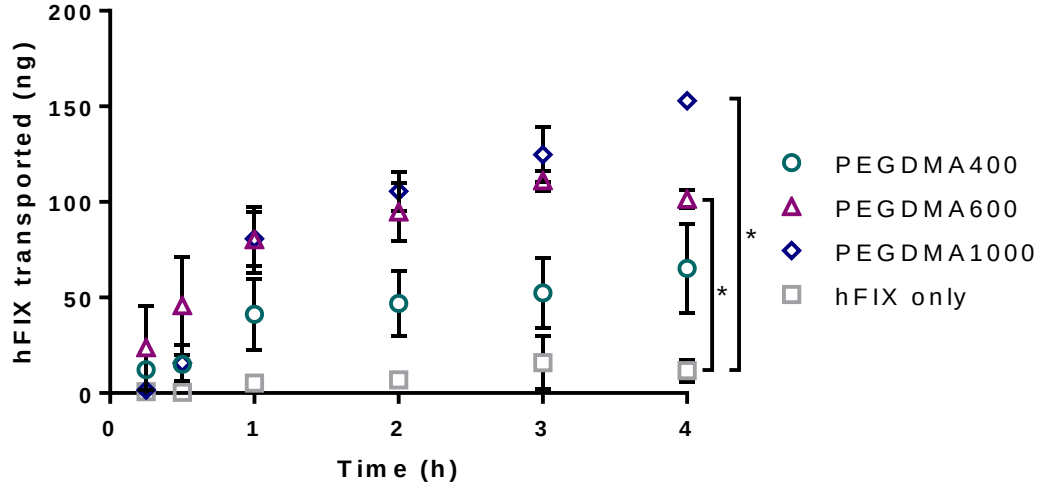

Figure 5-15. The amount of hFIX transported across the Caco-2 intestinal epithelial monolayer over time shows that the presence of the microparticles improved hFIX transport. The PEGDMA1000 formulation resulted in the highest levels of hFIX transported. (n=3, mean ± SE, *p<0.05).

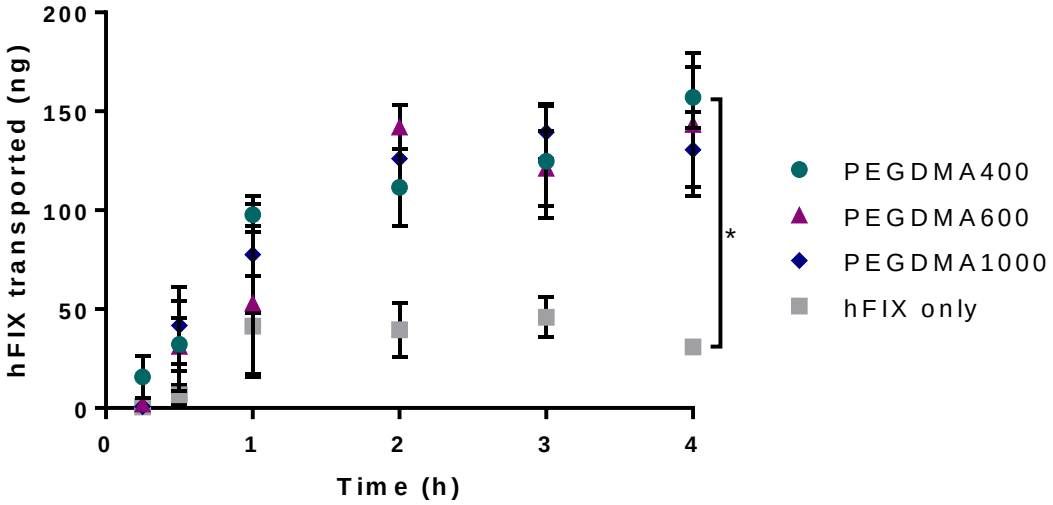

Figure 5-16. The amount of hFIX transported across the co-culture intestinal epithelial monolayer over time shows that the presence of the microparticles improved hFIX transport. (n=3, mean ± SE, *p<0.05).

The permeability of the protein across the monolayer was calculated by:

$$P_{app} = \frac{dQ(t)}{dt} \times \frac{1}{A \times C_{AO}} \quad \text{(Eq. 5-3)}$$

where *Q(t)* is the cumulative protein release (ng) at time *t* (s), *A* is the area of the cell monolayer (cm^2), and C_{AO} is the initial protein concentration (ng/mL). hFIX permeability was calculated after the first 2 hours, where the amount of hFIX transported over time follows a linear relationship. The overall permeability (4 hours) was also calculated; however, values are decreased due to the plateauing of hFIX transported after 2 hours, similar to previous reported trends.[12] The presence of the microparticles resulted in permeability values at least 2.4-fold higher than hFIX only (Figures 5-17 and 5-18). For the Caco-2 model, increasing the PEGDMA crosslinking length resulted in increased hFIX permeability (Figure 5-17). However, results with the co-culture model did not show a significant distinction among formulations (Figure 5-18). Previous studies showed the same trends for insulin, where microparticle presence improved permeability, possibly due to Ca^{2+} chelation.[13] Ichikawa *et al*. hypothesized that PMAA-based microparticles can chelate Ca^{2+}, leading to an opening of tight junctions and increasing permeability.[14]

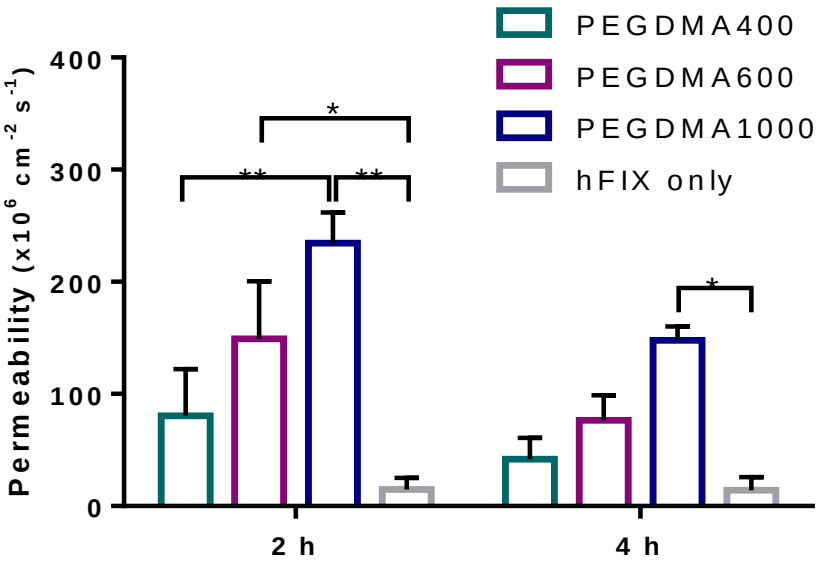

Figure 5-17. The presence of the microparticles enhances the permeability of hFIX (2h and 4h) as compared to hFIX only for the Caco-2 model. Increasing the PEGDMA crosslinking length increased hFIX permeability. (n=3, mean ± SE, *p<0.05, **p<0.01).

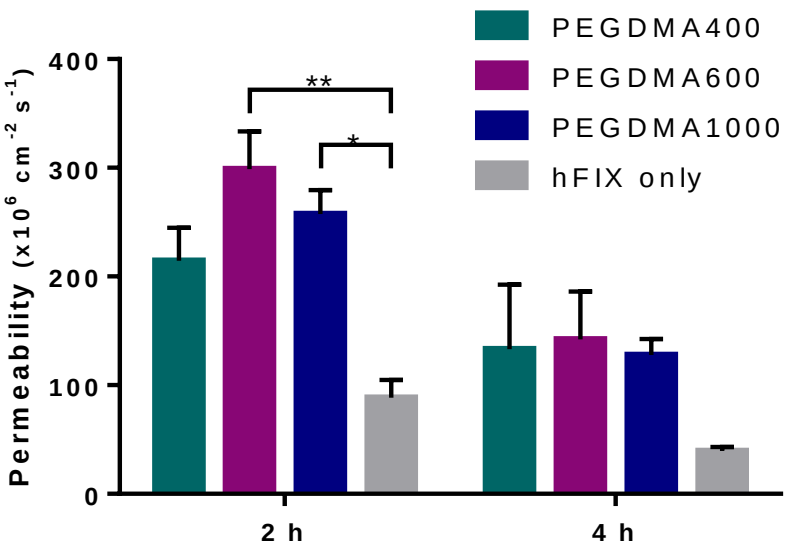

Figure 5-18. The presence of the microparticles enhances the permeability of hFIX (2h and 4h) as compared to hFIX only for the co-culture model. (n=3, mean ± SE, *p<0.05, **p<0.01).

Additionally, the TEER was monitored for the study duration to determine the effect of the microparticles on the monolayer integrity. Similar to previous studies,[13] the TEER values remained relatively constant over the 4-hour exposure for both the Caco-2 and co-culture model, indicating that the tight junctions remained intact (Figures 5-19 and 5-20). As hypothesized by Wood *et al*., the microparticles may have a Ca^{2+} chelating effect, but the mucus layer provides barrier between the cells and microparticles, reducing the effect of the microparticles on TEER.[13] The monolayers also recovered after the removal of the microparticles, as indicated by the 24-hour TEER measurements.

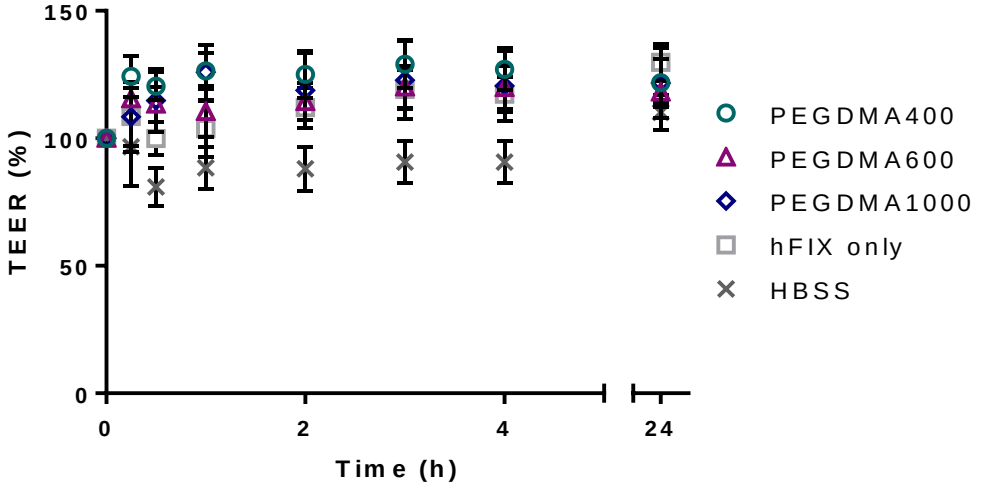

Figure 5-19. TEER remained constant during the transport study, indicating that the tight junctions remained intact for the Caco-2 model. TEER measurements at 24 h post study showed that the monolayers fully recovered after removal of microparticles. (n=4, mean ± SE, *p<0.05, and **p<0.01).

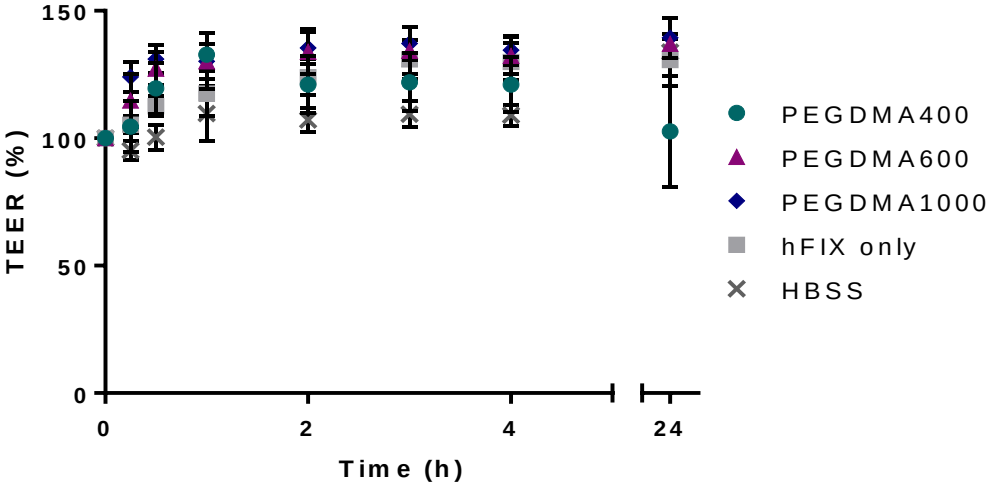

Figure 5-20. TEER remained constant during the transport study, indicating that the tight junctions remained intact for the co-culture model. TEER measurements at 24 h post study showed that the monolayers fully recovered after removal of microparticles. (n=4, mean ± SE, *p<0.05, and **p<0.01).

5.4 CONCLUSIONS

Addressing the medical need, we have developed a delivery system based on pH-responsive P(MAA-g-EG) hydrogel networks for the oral delivery of hematological factor IX. Tailoring the biomaterial formulation by varying the length of the PEGDMA crosslinking agent resulted in improved performance of the microcarriers. Increasing the mesh size increased loading and distribution of hFIX within the microparticles, offering more protection in gastric conditions. Furthermore, improved hFIX protection resulted in higher release of active protein in intestinal conditions. Based on the results presented, P(MAA-g-EG) crosslinked with 1 mol% of PEGDMA1000 is the best performing formulation. Further optimization of loading conditions (i.e., reduced ionic strength of buffer and increased time to 5 days at 4°C) significantly improved the loading efficiency and the amount of active hFIX released.

The ability of the microcarriers to modulate the oral absorption of hFIX further shows the potential of such oral delivery systems. The presence of the microparticles increased hFIX permeability without causing damage to the *in vitro* intestinal epithelial layer. The combination of well-maintained hFIX activity and its enhanced permeability is expected to promote overall bioavailability.

The promising work presented here can lead to an orally administered treatment for hemophilia that can replace needle-based options, offering improved quality of life for patients and global access to therapy.

5.5 REFERENCES

1. Kessler, C. M., Mariani G, Clinical manifestations and therapy of the hemophilias. In Hemostasis and Thrombosis: Basic Principles and Clinical Practice, 5 ed.; Colman, R. W., J Hirsh, VJ Marder, AW Clowes, JN George, Ed. Lippincott-Raven: Philadelphia, **2006**; pp 887-904.
2. White, G. C., 2nd; Rosendaal, F.; Aledort, L. M.; Lusher, J. M.; Rothschild, C.; Ingerslev, J., Definitions in hemophilia. Recommendation of the scientific subcommittee on factor VIII and factor IX of the scientific and standardization committee of the International Society on Thrombosis and Haemostasis. *J. Thromb. Haemost.* **2001**, 85 (3), 560.
3. Mancuso, M. E.; Berardinelli, L.; Beretta, C.; Raiteri, M.; Pozzoli, E.; Santagostino, E., Improved treatment feasibility in children with hemophilia using arteriovenous fistulae: the results after seven years of follow-up. *Haematologica* **2009**, 94 (5), 687-92.
4. Darby, S. C.; Kan, S. W.; Spooner, R. J.; Giangrande, P. L. F.; Hill, F. G. H.; Hay, C. R. M.; Lee, C. A.; Ludlam, C. A.; Williams, M.; Doctors, U. K. H. C., Mortality rates, life expectancy, and causes of death in people with hemophilia A or B in the United Kingdom who were not infected with HIV. *Blood* **2007**, 110 (3), 815-825.
5. Peppas, N. A.; Horava, S. D., Polymers for Delivery of Factor VIII and/or Factor IX. [Patent Pending].
6. Brannon-Peppas, L.; Peppas, N. A., Equilibrium swelling behavior of dilute ionic hydrogels in electrolytic solutions. *J. Control. Release* **1991**, 16 (3), 319-329.
7. Koetting, M. C.; Peppas, N. A., pH-Responsive poly(itaconic acid-co-N-vinylpyrrolidone) hydrogels with reduced ionic strength loading solutions offer improved oral delivery potential for high isoelectric point-exhibiting therapeutic proteins. *Int. J. Pharm.* **2014**, 471 (1–2), 83-91.
8. Inc., W. P. BeneFIX- coagulation factor IX (recombinant). http://labeling.pfizer.com/showlabeling.aspx?id=492.
9. Björkman, S., Prophylactic dosing of factor VIII and factor IX from a clinical pharmacokinetic perspective. *Haemophilia* **2003**, 9, 101-110.
10. Kisker, C. T.; Eisberg, A.; Schwartz, B.; the Mononine Study, G., Prophylaxis in factor IX deficiency product and patient variation. *Haemophilia* **2003**, 9 (3), 279-284.
11. Hilgendorf, C.; Spahn-Langguth, H.; Regardh, C. G.; Lipka, E.; Amidon, G. L.; Langguth, P., Caco-2 versus Caco-2/HT29-MTX co-cultured cell lines:

permeabilities via diffusion, inside- and outside-directed carrier-mediated transport. *J. Pharm. Sci.* **2000**, 89 (1), 63-75.

12. Gupta, V.; Doshi, N.; Mitragotri, S., Permeation of Insulin, Calcitonin and Exenatide across Caco-2 Monolayers: Measurement Using a Rapid, 3-Day System. *PLoS ONE* **2013**, 8 (2), e57136.

13. Wood, K. M.; Stone, G. M.; Peppas, N. A., The effect of complexation hydrogels on insulin transport in intestinal epithelial cell models. *Acta Biomater.* **2010**, 6 (1), 48-56.

14. Ichikawa, H.; Peppas, N. A., Novel complexation hydrogels for oral peptide delivery: In vitro evaluation of their cytocompatibility and insulin-transport enhancing effects using Caco-2 cell monolayers. *J. Biomed. Mater. Res. A* **2003**, 67A (2), 609-617.

Chapter 6: Stability Testing

6.1 INTRODUCTION

Stability testing is critical for predicting shelf life of a drug substance or drug product and determining recommended storage conditions. The FDA provides guidelines for storage conditions of a drug substance to test its thermal stability and its sensitivity to moisture, as well as additional stress testing.[1] In general, stability testing studies are designed to cover storage, shipment, and subsequent use for a new drug substance/product. For the general case, the FDA guidelines for stability testing of a drug substance/product are outlined in Table 6-1. The FDA guidelines also include stability testing conditions for drug substances intended for storage in a refrigerator (Table 6-2).

Table 6-1. FDA guidelines for stability testing for the general case.[1]

Study	Storage Conditions	Minimum Time Period
Accelerated	40°C ± 2°C/75% RH ± 5% RH	6 months
Intermediate	30°C/± 2°C/65% RH ± 5% RH	6 months
Long-term	25°C/± 2°C/60% RH ± 5% RH	12 months

Table 6-2. FDA guidelines for stability testing of a drug substance intended for storage in a refrigerator.[1]

Study	Storage Conditions	Minimum Time Period
Accelerated	25°C ± 2°C/60% RH ± 5% RH	6 months
Long-term	5°C± 3°C	12 months

According to the FDA guidelines, for drug substances intended for storage in a freezer, long-term storage at -20°C ± 5°C should be included in addition to the storage conditions in Table 6-2 for obtaining data at elevated temperatures. The recommended

testing frequency is every 3 months with a minimum of three time points for the accelerated study and four time points for the intermediate study. At the long-term storage conditions, the frequency of testing should be every 3 months over the first year, followed by every 6 months over the second year, and annually thereafter.[1]

In assessing acceptance criteria for a solid oral drug product, the stability testing procedures included several tests as listed:

- *Dissolution*- Measure the release of drug substance from the drug product
- *Disintegration*- Substitute for dissolution for rapidly dissolving products only
- *Hardness/friability*- Only if critical impact on drug product quality (e.g., chewable tablet)
- *Uniformity of dosage unit*- Mass of dosage form and the content of the active substance
- *Water content*- Measure amount of water to determine effects of hydration or water absorption on the drug product
- *Microbial limits*- Measure the amounts of aerobic microorganisms, yeasts and molds, and specific objectionable bacteria (e.g., E. coli, Salmonella, etc.).[2]

For biological products, an assessment of the biological activity is an essential step in determining shelf life. The capacity of a product to achieve a defined biological effect relies on a biologically active therapeutic. Examples of recommended procedures to measure biological activity include:

- *Biochemical assays*- Measure enzymatic reaction rates or biological responses induced by immunological interactions
- *Cell culture-based assays*- Measure biochemical or physiological response at cellular level
- *Animal-based assays*- Measure an organism's biological response to the product.[3]

The potency of the drug during stability testing is critical in determining the recommended storage conditions and predicting shelf life.

A pharmaceutical product is expected to have adequate stability over at least an 18-month shelf life. The stability of most molecules normally increases in the order of solution < glassy solid < crystalline solid due to the increasingly restricted mobility of reacting species.[4, 5] Drying techniques include lyophilization, spray drying, spray freeze drying, vacuum drying, and supercritical fluid technology.

Due to slowed rates of the reactions that involve water as a reactant, lyophilization can enhance pharmaceutical stability and desired shelf life. Lyophilization is the general method of choice due to the following advantages:

- Low temperature process, less thermal degradation
- No terminal sterilization step necessary as it maintains sterility and particle free characteristics of product
- Controlled residual moisture content and headspace gas composition in the vial
- Easy scale-up and reasonable yield process.[4]

We have selected to use lyophilization for drying the hFIX-loaded microparticles due to the aforementioned advantages.

In this Chapter, we outline the stability testing of lyophilized hFIX-loaded microparticles composed of P(MAA-g-EG) crosslinked with 1 mol% PEGDMA1000, previously described in Chapters 4 and 5. The storage conditions tested were selected based on the FDA guidelines for the general case and refrigerated storage. In order to gain an understanding of the drug product stability, we evaluated the effect of temperature and humidity on the dissolution, biological activity, and water content after storage at a maximum of 3 months. This short-term study was designed to assess the stability of the hFIX-loaded microparticles only without additional stabilizing agents.

6.2 Materials and Methods

6.2.1 Polymer Synthesis

P(MAA-g-EG) hydrogels were synthesized by bulk UV-polymerization as previously described in Chapter 4. Briefly, the feed composition of the pre-polymer was MAA and PEGMMA1000 at a 2:1 molar ratio of hydrogen bonding groups, PEGDMA1000 at 1.0 mol% of total monomers, and Irgacure 184® at 1.0 wt. % of total monomers in a 1:1 (w/w) mixture of deionized water and ethanol. After sonicating for 20 minutes, the pre-polymer mixture was needle purged with nitrogen for 5 minutes in the nitrogen-rich environment of a glove box. The mixture was then dispensed between two quartz glass plates, separated with a 0.7 mm Teflon® spacer, and then polymerized for 30 minutes under 35 mW cm^{-2} UV light using a UV flood source. After synthesis, the resulting polymer was removed from the plates, and then washed in deionized water for a total of 10 water exchanges. The polymer was dried for 3 days in air and then for 3 additional days under vacuum at 37°C. Dried films were crushed and sieved into microparticles, sized 30-45 μm.

6.2.2 Protein Loading Studies

Loading studies were conducted using the optimized loading conditions as described in Chapter 5. Dried particles were added to a 0.5 mg mL^{-1} hFIX solution (5 mM NaH_2PO_4) to a final concentration of 5 mg mL^{-1} and pH of 7.4. hFIX loading was carried out by equilibrium partitioning for 5 days with particle/protein suspensions under constant end-to-end rotation at 4°C. After 5 days, particles were collected by Buchner filtration using Whatman 50 filter paper. Particles were then collapsed with 0.1 N HCl and then triple rinsed with 0.1 N HCl, DI water, and 0.1 N HCl. Samples were collected after each step—end of loading, collapse, and rinse—for protein quantification using hFIX ELISAs.

Protein-loaded particles were then lyophilized overnight. Three separate batches of loaded microparticles were prepared.

6.2.3 Storage Conditions

For stability testing, samples included hFIX-loaded particles to determine drug release and activity after storage and empty particles to determine water uptake during storage. All samples (5-6 mg) of either hFIX-loaded particles or empty particles (n=3 for each sample type and storage condition) were placed in Type I borosilicate glass E-C sample vials with PTFE faced 14B Rubber-lined black phenolic caps (Wheaton, VWR, Radnor, PA).

Prior to use, the glass vials and caps were autoclaved. These Type I borosilicate vials conform to USP requirements.[6] Type I borosilicate glass, which has a high hydrolytic resistance and a high thermal shock resistance, is recommended for most products for parenteral and nonparenteral use.

For this stability testing study, we selected three storage conditions according to USP and FDA guidelines. Table 6-3 outlines the conditions for the stability testing, which were adapted based on recommendations for general drug products and drug substances intended for storage in a refrigerator.

Table 6-3. Stability testing conditions.

Study	Storage Conditions	Time Period
Accelerated	40°C/75% RH	30 days (1 month)
Long-term	25°C/60% RH	90 days (3 months)
Long-term, Refrigerated	4°C	90 days (3 months)

The vials with samples were stored protected from light in all conditions. For the accelerated and long-term studies, the samples with loosened caps were stored in the Darwin Chamber Company stability chambers (St. Louis, MO) at the specified conditions. The stability chambers are strictly maintained and monitored by THERAPEUTEX of the Drug Dynamics Institute at the UT Austin Dell Pediatric Research Institute. For the long-term, refrigerated study, samples with the caps tightened were stored in a refrigerator. At the end of the storage time period, samples were immediately tested for drug release and water content.

6.2.4 Dissolution and Biological Activity

In order to determine the release profile, the total amount of drug released, and the total amount of active drug released, protein release studies were conducted immediately following storage. For the t=0 condition, release studies were performed immediately after loading and lyophilization. Protein release studies were conducted following a two-stage dissolution procedure using biorelevant media as previously described in Chapter 5. Biorelevant media were prepared using a FaSSIF, FeSSIF & FaSSGF powder which contains bile salts and phospholipids. Fasted-state simulated gastric fluid (FaSSGF) was prepared at a 1x concentration with a final pH of 1.6 according to the manufacturer's protocol (Biorelevant). Fasted-state simulated intestinal fluid (FaSSIF) was prepared at 2x concentration with a final pH of 6.9. For the two-stage dissolution procedure, a 1:1 (v/v) FaSSGF:FaSSIF mixture at a final pH of 6.5 is required for the intestinal condition.

Dissolution testing was performed using an USP apparatus 2 (paddles) setup for small volume (100 mL vessel) with low evaporation mini vessel covers using a Distek 2100B dissolution apparatus (North Brunswick, NJ). A 5 mg sample of hFIX-loaded microparticles was added to a Sigmacoted (i.e., siliconized) vessel containing 30 mL of

SGF (1x, pH 1.6) at 37°C. After 30 minutes, 30 mL of FaSSIF (2x) at 37°C was added, raising the pH to 6.5. The solution was continuously stirred at 75 rpm and maintained at 37°C for both stages. The FaSSIF stage was carried out for up to 2 h. Over the course of the dissolution, 1 mL samples were taken using a 1/8 cannula sample probe (Distek, Inc.) with a 10 micron polyethylene filter tip (Agilent Technologies, Santa Clara, CA). Samples were replaced with an equal volume of appropriate prewarmed media. hFIX released was quantified by hFIX ELISAs. The biological activity of the released hFIX was measured by hFIX chromogenic activity assays for the 2 h FaSSIF sample only.

6.2.5 Thermogravimetric Analysis (TGA)

Thermogravimetric analysis (TGA) was conducted using a TA Instruments TGA Q500 (New Castle, DE) to determine the water content of the empty particles (2-5 mg) after storage. For the t=0 condition, vacuum dried particles were tested to determine the initial water content. Decomposition profiles were recorded from 25°C ramped at 10°C/min to 550°C in nitrogen and then isothermal at 550°C for 5 minutes.

6.2.6 Statistical Analysis

Data are reported as mean ± standard error. Comparisons between groups were performed using a Student's two-tailed t-test, and comparisons among multiple groups were performed using an ANOVA. Significant differences were considered when $*p < 0.05$ and $**p < 0.01$. All statistical analysis was computed using GraphPad Prism 6.

6.3 Results and Discussion

6.3.1 Protein Loading

Microparticles (30-45 μm) of P(MAA-g-EG) crosslinked with 1 mol% PEGDM1000 were loaded with hFIX using optimized loading conditions.[7] The final amount of protein loaded was calculated based on the concentration of the supernatant after incubation, collapse, and triple rinse. Protein lost during the collapse and rinse was likely surface loaded. The loading level (μg hFIX mg^{-1} particles) was calculated as:

$$Loading = \frac{c_0 V_0 - c_f V_f}{c_p V_0} \quad \text{(Eq. 6-1)}$$

where c_0 is the initial protein concentration (μg mL^{-1}), V_0 is the initial volume (mL), c_f is the final protein concentration (μg mL^{-1}) after rinsing, V_f is the final volume (mL) after rinsing, and c_p is the particle concentration (mg mL^{-1}). The average loading level for the three batches of particles is 50.9 ± 2.5 μg hFIX/mg particle.

6.3.2 Effect of Storage Conditions on Drug Release and Activity

Release studies were conducted to quantify the effects of storage on the stability of hFIX. The release of hFIX from microparticles of P(MAA-g-EG) crosslinked with 1 mol% PEGDMA1000 was tested using a two-stage dissolution procedure in biorelevant media. As shown in Figure 6-1, the initial release profile of hFIX from the t=0 samples matches the trends of previously reported hFIX release curves in Chapter 5. In the t=0 curve, the release is minimal in the fasted-state simulated gastric fluid (FaSSGF) and is significantly increased in the fasted-state simulated intestinal fluid (FaSSIF) as desired. The activity of hFIX released is well maintained (Figure 6-2), which allow agrees with previously reported results.

Based on the hFIX stability study reported in Chapter 5, we expect increased temperature and time to result decreased hFIX activity and stability. The previously reported study was conducted in solution, and the stability is expected to increase for the lyophilized form.[4] Based on the release profiles in Figure 6-1, hFIX was significantly affected by the storage conditions. Samples in both the long-term (25°C/60% RH for 90 days) and the accelerated (40°C/75% for 30 days) studies have significantly reduced release which may be attributed to the degradation of hFIX due to elevated temperature and humidity. However, the release profile from samples in the long-term, accelerated (5°C for 90 days) closely matches that of the initial release profile at t=0. The amount of hFIX released was quantified by hFIX-specific ELISAs. Detection by ELISA required antibodies to bind to hFIX, which confers the native conformation to a degree. In the case of the long-term, refrigerated study, the hFIX likely remained stability in structure. However, the activity of hFIX released from particles stored at 5°C for 90 days is significantly reduced likely due to instability in the Gla domain and its function to bind Ca^{2+} ions (Figure 6-2).[8] Maintenance of the biological activity of hFIX is critical for its therapeutic use in protein replacement therapy.

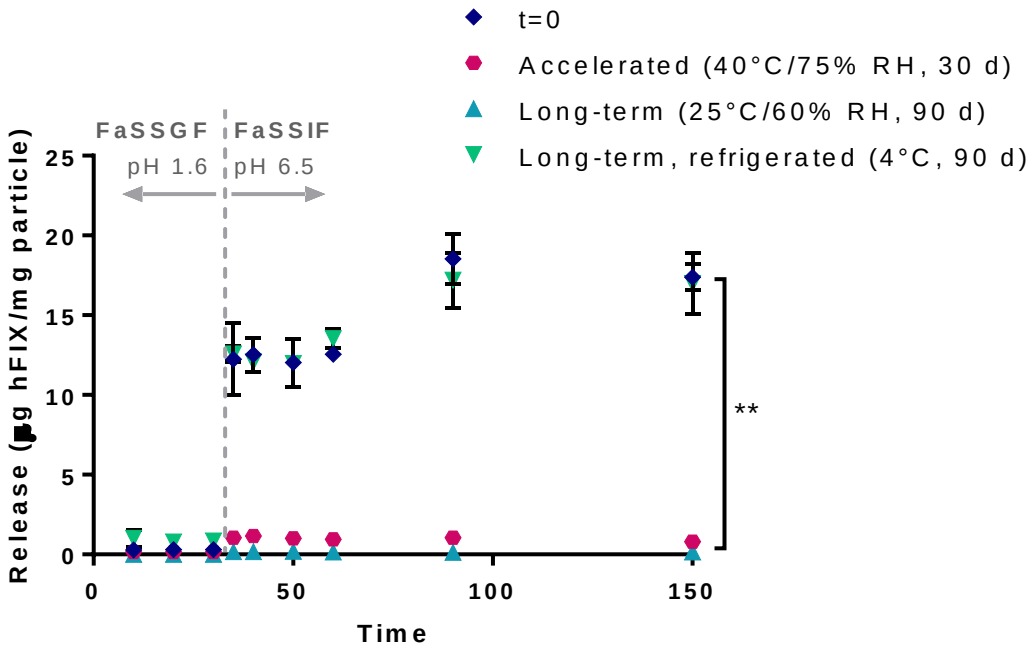

Figure 6-1. Release profile of hFIX from P(MAA-g-EG) microparticles after various storage conditions.

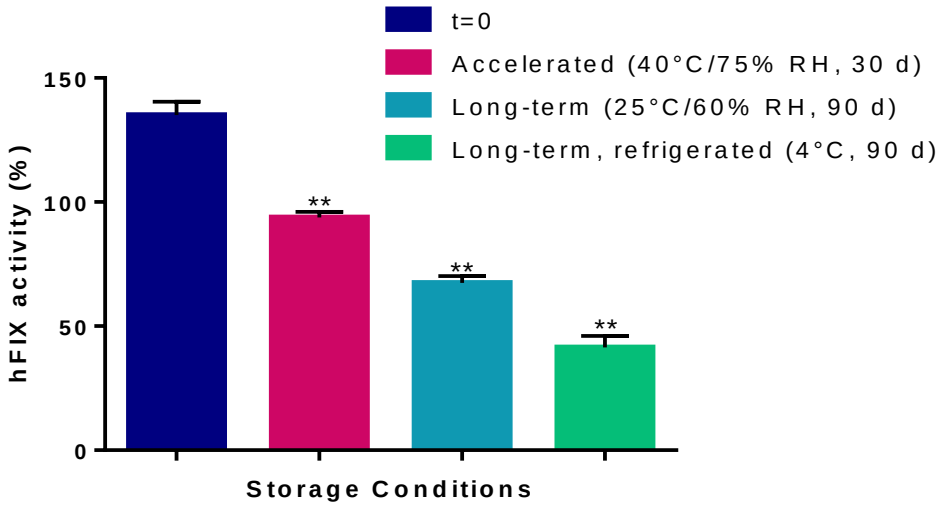

Figure 6-2. Activity (%) of hFIX released (150 min in FaSSIF samples) from P(MAA-g-EG) after various storage conditions.

6.3.3 Effect of Storage Conditions on Sample Water Uptake

During storage, the dried hydrogel particles are susceptible to water uptake, especially in elevated humidity. Water uptake in the sample can lead to protein instability due to hydrolysis. Hydrolytic reactions that occur in proteins include deamidation, aspartate (Asp) isomerization, proteolysis, and β elimination,[9] all of which can affect hFIX (see amino acid sequence in Chapter 2). Deamidation, one of the most common hydrolytic reactions of proteins, occurs primarily at asparagine (Asn) residues, converting them to Asp. Isomerization at Asp sites produces isoAsp, which introduces a methylene group into the peptide backbone and perturbs the local conformation.

Proteolysis is the hydrolysis of amide bonds connecting amino acids in the protein backbone. A single proteolytic reaction splits the protein backbone in two pieces. β-elimination can result in the thermal decomposition of cysteine residues which can lead to additional reactions contributing to intermolecular crosslinking and formulation of covalent protein aggregates.[10] However, β-elimination typically occurs at alkaline conditions, meaning this hydrolytic reaction is unlikely in the present case. The rates of hydrolytic reactions are accelerated at increased temperatures. In addition to chemical degradation by hydrolysis, water uptake in the sample may result in phase separation. At interfaces, proteins tend to denature, losing tertiary and secondary structure.

The water uptake in the sample was quantified by a thermal decomposition analysis using TGA. Representative decomposition curves of empty microparticles from each study show differences in the amount of water removed at 100°C (Figure 6-3). The weight % of the sample was determined at 100°C (averaged over $99.50°C < T < 100.50°C$) to quantify the amount of water in the sample (the weight % removed at 100°C). During storage for all conditions, the microparticle samples did uptake water, and those stored at elevated humidity resulted in at least 2.3-fold increase in water content (Figure 6-4).

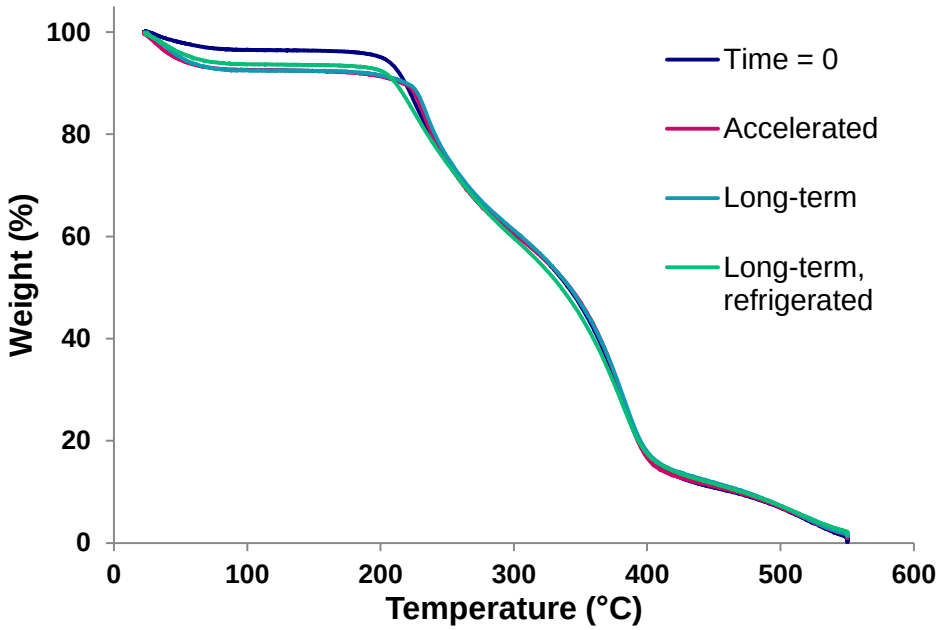

Figure 6-3. Representative decomposition curves of P(MAA-g-EG) microparticles after storage at various conditions.

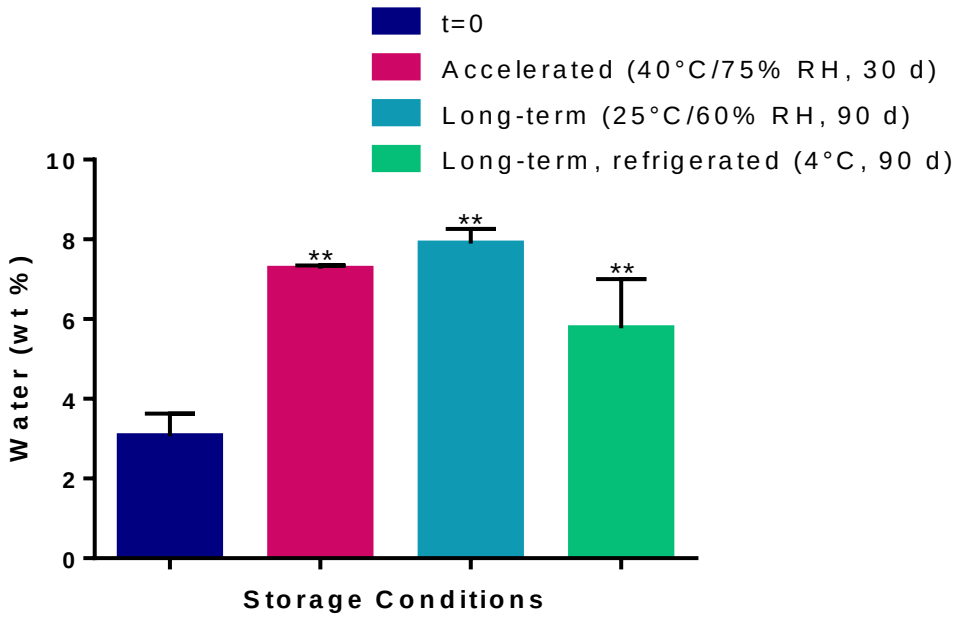

Figure 6-4. Water content (wt. %) of P(MAA-g-EG) microparticles show water uptake during storage under various conditions.

6.3.4 Stability Analysis

In order to predict shelf-life, stability testing is conducted at various temperatures, particularly higher values, to calculate long-term product stability at lower temperatures. The effect of temperature on reaction rates is given by the Arrhenius equation as:

$$k = Ae^{-E_a/RT} \quad \text{(Eq. 6-1)}$$

Where k is the reaction rate constant, A is the Arrhenius factor, E_a is the energy of activation (cal mol^{-1}), R is the ideal gas constant (1.987 cal K^{-1} mol^{-1}), and T is the absolute temperature (K). The Arrhenius equation can be applied regardless of the order of the reaction kinetics.

The reaction rate constant *k* can be determined based on the percent of drug remaining as a function of time. The drug loss as a function of time shows zero-order degradation kinetics for each isotherm. In this case, the reaction rate *k* is defined as:

$$k = \frac{d(drug\ \%)}{dt} \qquad \text{(Eq. 6-2)}$$

which is the slope of the drug % versus time plot. One limitation of this study is the reaction rate *k* was calculated using only two time points due to limited resources. The reaction rate constant was calculated based on both the total amount of hFIX released and the amount of active hFIX released for each temperature (Table 6-4).

Table 6-4. Drug loss and reaction rate constants *k* based on total hFIX released and active hFIX released for three temperatures.

Temperature	Time (days)	Drug (%)	k (drug %/day)	Active Drug (%)	k (drug %/day)
---	0	100.00	---	100.0	---
40°C (313 K)	30	4.67	-3.17	3.34	-3.22
25°C (298 K)	90	0.88	-1.10	0.45	-1.11
4°C (277 K)	90	97.67	-0.03	30.86	-0.77

The energy of activation is critical to applying accelerated stability testing data to predict the product shelf life. To determine the energy of activation, the Arrhenius equation can be rearranged in a linear form as:

$$\ln(k) = \frac{-E_a}{RT} + \ln(A) \qquad \text{(Eq. 6-3)}$$

and an Arrhenius plot of *ln(k)* versus *1/T* has a slope of $-E_a/R$ and an x-intercept of *ln(A)*. Based on the Arrhenius plot using the total hFIX released, the energy of activation E_a is 23.60 ± 4.39 kcal mol^{-1} (Figure 6-5), while the energy of activation E_a is 6.50 ± 2.79 kcal

mol^{-1} for the active hFIX released (Figure 6-6). The E_a for drug decomposition is generally in the range of 12 to 24 kcal mol^{-1}.[11, 12]

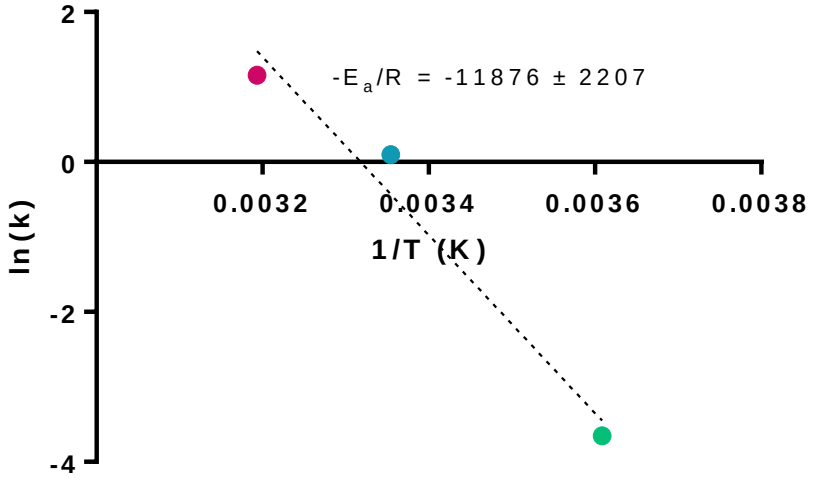

Figure 6-5. Arrhenius plot for the total hFIX released.

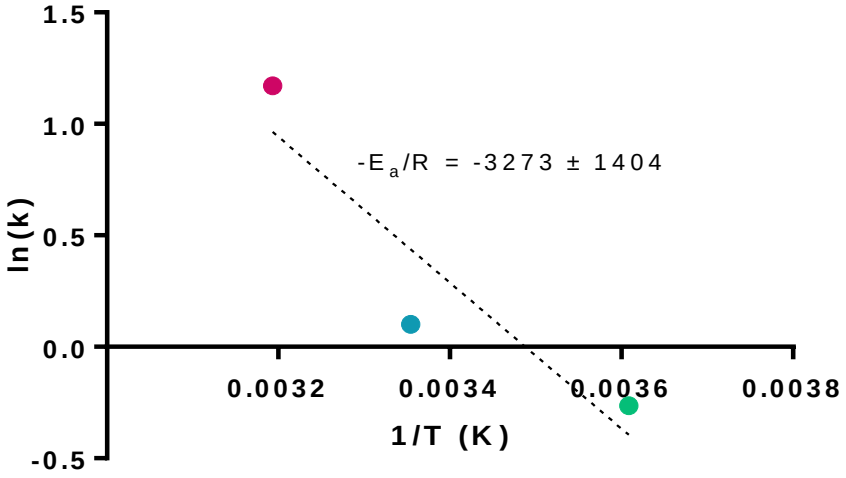

Figure 6-6. Arrhenius plot for the active hFIX released.

6.4 RECOMMENDATIONS FOR IMPROVING STABILITY

Based on the Arrhenius kinetic analysis, the lyophilized hFIX drug product requires additional stabilizing agents to enhance its shelf life. While lyophilization can improve pharmaceutical stability, this process consists of three phases—freezing, drying, and storage—during which stresses can cause product instabilities.

In the freezing phase, the two common mechanisms of denaturation are cryoconcentration[13] and ice-liquid surface denaturation.[14] In the cryoconcentration mechanism, as the water freezes, turning into ice, the solutes can reach concentrations as high as 20-50 times their initial concentration.[4, 13] Despite the reduced temperature, increased protein concentrations can promote degradation. Additionally, increased salt concentrations can contribute to protein instability due to exposure to high ionic strengths.[15] Furthermore, increased salt concentrations at decreased temperatures can lead to selective crystallization, causing pH shifts.[16] While possible pH effect is not evident for use immediately after lyophilization, we recommend monitoring the pH during lyophilization and assessing the potential pH effect on long-term stability.[17]

Ice-liquid surface is a potential site for protein denaturation, as proteins tend to denature at interfaces, losing tertiary and secondary structure. However, increasing the cooling rate, decreasing the time for the system to phase separate, can reduce interface denaturation. In order to minimize degradation due to phase separation, we remove water and buffer by filtration, leaving the microparticles in a collapsed state with minimal liquid remaining. These microparticles are then flash frozen in liquid nitrogen. Additionally, some proteins undergo cold denaturation (i.e., spontaneous unfolding at low temperatures).[18] While hFIX is not a known cold-labile protein, degradation studies at low temperatures could be performed to assess potential instabilities and denaturation.

In the drying phase, additional stresses due to the removal of bound water and elevated temperatures can lead to further protein instability. Reducing moisture levels to ≤1%-2% can unbalance the hydrogen bonding in the protein's native conformation, leading to reversible or irreversible unfolding.[19, 20] Incorporating hydrogen-bonding excipients in the formulation is a common approach to enhancing the stabilization of the protein's structure in the solid state.[21] While no new stresses develop during the storage phase, the stress developed in the lyophilization process will continue to pose challenges to the storage stability.[4] We recommend incorporating additional stabilizing agents, such as cryoprotectants and lyoprotectants, to reduce protein denaturation.

Cryoprotectants are solutes, such as sugars, polyols, certain amino acids, methylamines, and "salting out" salts, used to prevent conformational changes and degradation during freezing.[4] At concentrations of 300-600 mM, these cryoprotectants work by a mechanism called preferential exclusion of solutes.[22] The solutes are excluded from the vicinity of protein, and therefore, their presence increases the chemical potential of the protein. Chemical potential is directly related to surface area. As a protein unfolds, the surface area increases, which in turn increases the chemical potential. Due to the lower chemical potential in the native form, the native form is more thermodynamically stable than the denatured form.[4]

Polymers, particularly poly(ethylene glycol) (PEG), are included in formulations to stabilize biotherapeutics. PEG is a cryoprotectant that stabilizes proteins during freezing through preferential exclusion of PEG from the surface of the protein.[23, 24] The inclusion of PEG in polymer formulation may attribute to the stabilization of hFIX. However, polymers are less effective lyoprotectants, as they are sterically hindered in forming hydrogen-bonds with proteins.

Lyoprotectants serve as "water substitutes" that allow for hydrogen-bonding interactions with the protein similar to such interactions between water and the protein.[4] The stabilization mechanism of lyoprotectants has been interpreted both thermodynamically and kinetically. Thermodynamically, stabilization by hydrogen bonding maintains or restores the free energy of unfolding such that the native conformation is preferred over the unfolded form. In the kinetic interpretation, the protein has restricted mobility due to being dispersed in a viscous microenvironment of the stabilizer. The protein is stabilized due to the significantly reduced or arrest rate of conformational changes leading to protein unfolding.[4]

Nonreducing di- and tri-saccharides, such as sucrose, trehalose, or raffinose, are typically good lyoprotectants that can function as water substitutes and good glass formers.[19, 20] These sugars can replace the hydrogen bonds at the exposed polar groups of the protein, which preserves the native structures of proteins in the dried state and during subsequent storage.[13, 19, 22] Inert stabilizers are critical, where reducing sugars, such as lactose, maltose, and glucose, can chemically react with the protein. Sucrose at a level of approximately 1-9% is widely accepted as a cryoprotectant for lyophilized protein formulations.[4] However, trehalose is a more effective stabilizer under acidic conditions, especially below pH 5, as it is less susceptible to hydrolysis. Since the hFIX-loaded microparticles are in the collapsed state, the microenvironment in the polymer is acidic. We would recommend testing several sugars, particularly trehalose which is an effective stabilizer under acidic conditions, as a lyoprotectant. The desired weight ratio of saccharide to protein is between 1:1 and 10:1 for stabilization during drying and storage. However, one issue that may arise is freeze-concentration-induced phase separation, which could result in protein denaturation.[25] Phase separation can be reduced by increasing the cooling rate.

Commercially available lyophilized hFIX products include trehalose to enhance stability.[26] The addition of 1% trehalose stabilized the calcium binding ability of hFIX and maintained its biological activity. The Gla domain of hFIX is responsible for Ca^{2+} binding which is required for its clotting activity. Binding to Ca^{2+} ions induces a conformational change in the protein that exposes the previously buried hydrophobic binding sites to facilitate binding to phospholipids to achieve efficient coagulation.[8] Previous results show that trehalose decreases the rate of decay at 40°C/75% RH by almost 20-fold and the rate of decay at 25°C/60% by 5-fold for lyophilized hFIX. Likewise, trehalose reduces the rate of decay in biological function to a similar extent. Furthermore, trehalose (1 vol. %) substantially prevents hFIX aggregation during storage of the lyophilized product.[26] We recommend testing the addition of trehalose at 0.5 to 5 vol. % to determine an optimal formulation for lyophilized hFIX-loaded microparticles.

Other components in commercially available lyophilized hFIX products are a buffering agent, a bulking agent, and surfactant. In the patent, the optimal formulation contained 10 mM histidine as a buffering agent, 3 vol. % mannitol as a bulking agent, and 0.0075 vol. % polysorbate 80 as a surfactant. Lyophilized hFIX prepared using this formulation (including 1 vol. % trehalose) maintained at least 90% of its activity when stored at 2-8°C for at least two years and at 25°C/60% RH for 6 months.[26] While results showed that trehalose was key in stabilizing lyophilized hFIX and preserving its activity, we also recommend testing the other additives used in this patented formulation composition.

Gaining a better understanding of the structure and stability of hFIX will be critical for improving drug product stability. FTIR is often used as an analytical tool for identifying the ideal sugar stabilizer for dry powder formulations.[4, 27] Additionally, differential scanning calorimetry (DSC) is a technique used to study the unfolding of secondary

structures of proteins and to characterize the conformational stability of proteins in different conditions (solid and liquid states). Protein unfolding is detected as an endothermic event by DSC, while protein aggregation produces an exothermic peak. DSC analysis can be used to determine the optimal freezing and annealing temperatures during a lyophilization cycle.[4] In formulation development, DSC can be used to measure the effect of an additive on the protein's thermal stability. An increase in the protein's melting temperature indicates that the additive improves protection.

6.5 CONCLUSIONS

Stability testing of a drug product, which in this case is lyophilized hFIX-loaded P(MAA-g-EG) microparticles, is critical for predicting shelf life. After storage, the dissolution, biological activity, and water content were evaluated. Based on these stability testing results, we determined that elevated temperature and humidity can lead to drug loss and water uptake. While the hFIX release profile after storage at 4°C for 90 days nearly matched that of t=0, the biological activity of released hFIX was significantly reduced. Based on these exploratory studies, we recommend storage at 4°C with humidity control. However, enhancing the biological activity of hFIX, which could be achieved by the addition of trehalose,[26] is critical for lyophilized hFIX-loaded microparticles. Further investigations of the effects of additives, particularly trehalose, are recommended to stabilize hFIX in the lyophilized formulation, leading to an improved shelf life.

6.6 REFERENCES

1. FDA Guidance for Industry Q1A(R2) Stability Testing of New Drug Substances and Products.

http://www.fda.gov/downloads/drugs/guidancecomplianceregulatoryinformation/guidances/ucm073369.pdf.

2. ICH, Specifications: Test Procedures and Acceptance Criteria for New Drug Substances and New Drug Products: Chemical Substances Q6A. ICH Harmonised Tripartite Guideline.
3. ICH, Specifications: Test Procedures and Acceptance Criteria for Biotechnological/Biological Products Q6B. ICH Harmonised Tripartite Guideline.
4. Jameel, F.; Hershenson, S., Formulation and Process Development Strategies for Manufacturing Biopharmaceuticals. John Wiley & Sons: Hoboken, **2010**; Vol. 1.
5. Pikal, M. J.; Dellerman, K. M., Stability testing of pharmaceuticals by high-sensitivity isothermal calorimetry at 25°C: cephalosporins in the solid and aqueous solution states. *International Journal of Pharmaceutics* **1989**, 50 (3), 233-252.
6. Containers- Glass. In United States Pharmacopeia, United States Pharmacopeial Convention: Rockville, MD, 2014; Vol. USP 37: The National Formulary: NF 32.
7. Horava, S. D.; Peppas, N. A., Design of pH-Responsive Biomaterials to Enable the Oral Route of Hematological Factor IX. *Annals of Biomedical Engineering* **2016**, 1-13.
8. Gui, T.; Lin, H.-F.; Jin, D.-Y.; Hoffman, M.; Straight, D. L.; Roberts, H. R.; Stafford, D. W., Circulating and binding characteristics of wild-type factor IX and certain Gla domain mutants in vivo. *Blood* **2002**, 100 (1), 153-158.
9. Manning, M. C.; Patel, K.; Borchardt, R. T., Stability of protein pharmaceuticals. *Pharm Res* **1989**, 6 (11), 903-18.
10. Volkin, D. B.; Klibanov, A. M., Thermal destruction processes in proteins involving cystine residues. *Journal of Biological Chemistry* **1987**, 262 (7), 2945-2950.
11. Duncan, M.; Zaretsky, I., Do the Math for Shelf Life. *Pharmaceutical Formulation and Quality* **2011**, 13 (2), 22-28.
12. Connors, K. A.; Amidon, G. L.; Stella, V. J., Chemical stability of pharmaceuticals: a handbook for pharmacists. John Wiley & Sons: **1986**.
13. Rey, L., Freeze-drying/lyophilization of pharmaceutical and biological products. CRC Press: **2010**.
14. Strambini, G. B.; Gabellieri, E., Proteins in frozen solutions: evidence of ice-induced partial unfolding. *Biophysical journal* **1996**, 70 (2), 971.
15. Ahmad, F.; Bigelow, C. C., Thermodynamic stability of proteins in salt solutions: A comparison of the effectiveness of protein stabilizers. J*ournal of protein chemistry* **1986**, 5 (5), 355-367.

16. Murase, N.; Franks, F., Salt precipitation during the freeze-concentration of phosphate buffer solutions. *Biophysical chemistry* **1989**, 34 (3), 293-300.

17. Croyle, M. A.; Roessler, B. J.; Davidson, B. L.; Hilfinger, J. M.; Amidon, G. L., Factors that influence stability of recombinant adenoviral preparations for human gene therapy. *Pharmaceutical development and technology* **1998**, 3 (3), 373-383.

18. Privalov, P. L., Cold denaturation of protein. *Critical reviews in biochemistry and molecular biology* **1990**, 25 (4), 281-306.

19. Carpenter, J. F.; Chang, B. S.; Garzon-Rodriguez, W.; Randolph, T. W., Rational design of stable lyophilized protein formulations: theory and practice. Springer: **2002**.

20. Pikal, M. J., Mechanisms of protein stabilization during freeze-drying and storage: The relative importance of thermodynamic stabilization and glassy state relaxation dynamics. *Drugs and the Pharmaceutical Sciences* **2004**, 137, 63-108.

21. Hageman, M. J., The role of moisture in protein stability. *Drug Development and Industrial Pharmacy* **1988**, 14 (14), 2047-2070.

22. Carpenter, J. F.; Crowe, J. H., The mechanism of cryoprotection of proteins by solutes. *Cryobiology* **1988**, 25 (3), 244-255.

23. Mi, Y.; Wood, G.; Thoma, L.; Rashed, S., Effects of polyethylene glycol molecular weight and concentration on lactate dehydrogenase activity in solution and after freeze-thawing. *PDA Journal of Pharmaceutical Science and Technology* **2002**, 56 (3), 115-123.

24. Anchordoquy, T. J.; Carpenter, J. F., Polymers protect lactate dehydrogenase during freeze-drying by inhibiting dissociation in the frozen state. *Archives of biochemistry and biophysics* **1996**, 332 (2), 231-238.

25. Randolph, T. W., Phase separation of excipients during lyophilization: effects on protein stability. *Journal of Pharmaceutical Sciences* **1997**, 86 (11), 1198-1203.

26. Mankarious, S.; Griffith, M. J., Stabilized factor ix formulations containing trehalose. Google Patents: **2008**.

27. Prestrelski, S. J.; Tedeschi, N.; Arakawa, T.; Carpenter, J. F., Dehydration-induced conformational transitions in proteins and their inhibition by stabilizers. *Biophysical journal* **1993**, 65 (2), 661.

Chapter 7: Enzymatically Degradable Delivery Systems[3]

7.1 INTRODUCTION

Current treatments for hemophilia B, a hereditary bleeding disorder, require painful IV injections of coagulation factor IX. To overcome the issues with current treatment options, our goal is to develop an oral delivery system for human FIX (hFIX) as a convenient prophylactic treatment for hemophilia B.

We have successfully designed a pH-responsive P(MAA-g-EG) microcarrier system to enable the oral route of factor IX.[1] However, modifications of this delivery system became necessary to improve the oral bioavailability of hFIX. We have incorporated an enzymatically degradable peptide-based crosslinking agent into the pH-responsive P(MAA-g-EG) system to increase release of hFIX in the small intestine. Using enzyme-degradable components in hydrogel systems has been recently explored for oral delivery systems of biologics targeted for delivery to the small intestine.[2-4] Previous work showed promising applications of enzymatically degradable systems for delivering siRNA to treat inflammation of the small intestine.[3]

Enzymatic degradation is an attractive method for site-specific delivery systems due to the localized enzyme concentrations in the GI tract and the specificity of enzyme-catalyzed reactions (Figure 7-1).[2, 3, 5] In the stomach, the primary proteolytic enzyme is pepsin. The human small intestine contains gram quantities of peptidases (e.g. trypsin, α-chymotrypsin, pancreatic elastase, etc.) secreted from the pancreas and cellular peptidases from the mucosal cells.[6, 7] In order to achieve targeted degradation in the small intestine, the peptide crosslinking agent can be designed with cleavage sites specific to intestinal

[3] Portions of this chapter have been previously published in Horava, S. D.; Moy, K.J.; Peppas, N. A., Biodegradable Hydrophilic Carriers for Delivering Hematological Factor IX for Hemophilia B Treatment. International Journal of Pharmaceutics 2016.

enzymes, while avoiding sites for pepsin (see Table 1 for enzyme cleavage sites).[7] We have selected a peptide crosslinking agent composed primarily of arginine (Arg, R) residues, as well as glycine (Gly, G) and lysine (Lys, K), for targeted cleavage by trypsin and resistance to degradation by pepsin.

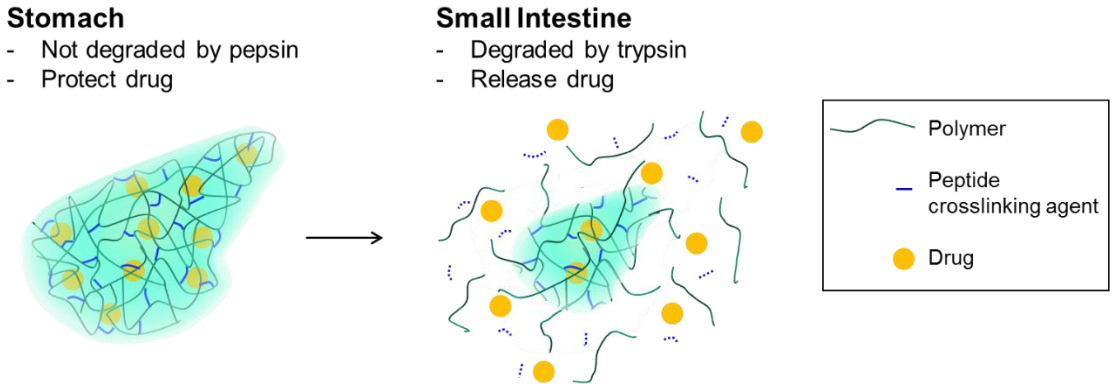

Figure 7-1. Schematic of a biodegradable microcarrier containing peptide crosslinks shows the enzyme-specific degradation. In the stomach, the peptide crosslinking agent is not degraded by pepsin, and the particle remains intact, protecting the drug. In the small intestine, the peptide crosslinking agent is degraded by trypsin, which allows for the release of the drug.

Table 7-1. Cleavage sites of the primary proteolytic enzymes in the stomach and small intestine. (Note: Xaa = amino acid).[7]

	Enzyme	**Cleavage sites**
Stomach	pepsin	Phe-|-Xaa, Tyr-|-Xaa, Leu-|-Xaa, Trp-|-Xaa, ideally Xaa = Phe, Trp, Tyr
Small intestine	trypsin	Arg-|-Xaa, Lys-|-Xaa
	α-chymotrypsin	Tyr-|-Xaa, Trp-|-Xaa, Phe-|-Xaa, Leu-|-Xaa, Met-|-Xaa
	pancreatic elastase	Ala-|-Xaa, Gly-|-Xaa, Val-|-Xaa, Ser-|-Xaa

Here, we describe the design and development of an enzymatically degradable and pH-responsive P(MAA-g-EG) system for the oral delivery of hFIX. As previously described, the pH-responsive swelling behavior allows for protection of the protein in the stomach and release in the small intestine. Additionally, the release of protein is triggered by enzymatic degradation by trypsin in the small intestine. Degradation of the microcarriers is expected to improve the release of hFIX as compared to the diffusion-based release of crosslinked P(MAA-g-EG) systems. Increased release is expected to promote the overall bioavailability of orally administered hFIX. Synthesis, characterization, and cytocompatibility of biodegradable P(MAA-g-EG), as well as an evaluation of hFIX loading, release, and *in vitro* transport, are detailed herein.

7.2 METHODS

7.2.1 Materials

Methacrylic acid (MAA), Irgacure 184® (1-hydroxy-cyclohexyl-phenylketone), N-(3-dimethylaminopropyl)-N′-ethylcarbodiimide (EDC), N-hydroxysulfosuccinimide (NHS), trypsin from bovine pancreas, and trypsin inhibitor type III-O (free of ovoinhibitor) were purchased from Sigma-Aldrich (St. Louis, MO). Poly(ethylene glycol) (MW=1000) mono methyl ether monomethacrylate (PEGMMA1000) was purchased from Polysciences (Warrington, PA). The custom sequence oligopeptide was synthesized by CHI Scientific (Maynard, MA). Plasma-derived human factor IX (hFIX) was purchased from Haematologic Technologies Inc. (Essex Junction, VT). Human factor IX ELISA kits were purchased from AssayPro LLC. (St. Charles, MO), and the BIOPHEN factor IX activity assays were purchased from HYPHEN Biomed SAS (Neuville-sur-Oise, France). FaSSIF, FeSSIF & FaSSGF Powder was purchased from Biorelevant.com (London, England, UK).

All reagents were used as received. All other solvents and buffers were purchased from Fisher Scientific (Waltham, MA).

7.2.2 Uncrosslinked Polymer Synthesis, Purification, and Characterization

Uncrosslinked P(MAA-g-EG) polymer was synthesized by bulk UV polymerization (Figure 7-2). MAA and PEGMMA1000 were added at 2:1 molar ratio of hydrogen bonding groups to a 1:1 (w/w) mixture of deionized water and ethanol to result in a 1:1 (w/w) ratio of total monomer to solvent in a 10 mL round bottom flask. Irgacure 184® photoinitiator was added at 1 wt. % of the total monomers, and then the prepolymer mixture was sonicated for 20 minutes in a Bransonic® CPX3800 ultrasonic digital bath (Branson Ultrasonics Corporation, Danbury, CT). After sealing the flask with a rubber septum, the prepolymer mixture was nitrogen purged for 20 minutes to remove oxygen, which is a free radical scavenger, while stirring. With constant stirring, the mixture was polymerized for 90 minutes under 100 mW/cm^2 UV light using a Dymax BlueWave 200 UV point source (Dymax, Torrington, CT).

In order to purify the polymer from any unreacted monomers, the uncrosslinked polymer was purified by precipitation with acetone and then dialyzed. In order to precipitation of the polymer, 1 N NaOH was added to ionize the polymer and acetone (dielectric constant ε=20.7) was added to induce ionomer collapse.[8] The precipitated polymer suspension was then centrifuged at 20,000 x g and then resuspended in deionized water. This precipitation procedure was carried out a total of three times, followed by dialysis using 3.5 kDa MWCO Spectra/Por Regenerated Cellulose Dialysis Tubing (Spectrum Laboratories Inc.) in 1 mL of deionized water, changed daily 10 times. After purification, the polymer was frozen with liquid nitrogen and then lyophilized for at least 72 hours.

Potentiometric titration was used to quantify the MAA content of the uncrosslinked polymer. Uncrosslinked P(MAA-g-EG) was dissolved in 10 mM NaCl at a concentration of 1 mg/mL, and then titrated to a pH of 2.5 using 0.05 N HCl at 25°C with constant stirring. HCl was added (10-60 μL) to the polymer solution, and the pH was measured until reaching a steady value (three consecutive readings within ± 0.02) at each step using a Thermo Scientific Orion Star A211 pH benchtop meter (Waltham, MA). The molar amount of MAA was calculated based on equivalence point and a charge balance.

The composition of the uncrosslinked polymer was further analyzed using proton nuclear magnetic resonance (^{1}H NMR) spectroscopy and Fourier transform infrared (FTIR) spectroscopy (see section 2.4). For NMR, a sample of uncrosslinked polymer was prepared in deuterium oxide (D_2O) at 10 mg/mL. The ^{1}H NMR spectra were collected using an Agilent Technologies 400-MR NMR spectrometer (Santa Clara, CA) with a resonance frequency of 400 MHz, with 64 scans collected at 1 second relaxation delay and 90° pulse angle.

7.2.3 Crosslinking via EDC-NHS Chemistry

Post polymerization, P(MAA-g-EG) polymer was crosslinked with a GRRRGK peptide via EDC-NHS chemistry (Figure 7-2). Uncrosslinked polymer was dissolved in a 1:1 (v/v) mixture of deionized water and ethanol. To activate the carboxyl groups, EDC (50 mg/mL in ethanol) and NHS (16.66 mg/mL in ethanol) were added at a mass ratio of 6:3:1 polymer: EDC: NHS, which is an approximate molar ratio of 2.2:1 MAA groups:EDC and 1.8:1 EDC:NHS. The mixture was then allowed to react for 3 minutes at room temperature while under constant rotation. The activated polymer was then titrated to pH 7 by adding 1 N NaOH. To crosslink the activated polymer, GRRRGK peptide (100 mg/mL in ethanol) was added at a mass ratio of 2:1 polymer: peptide. To further facilitate

the reaction, the pH was reduced to 4.5-5 using 1 N HCl. The reaction was then allowed to proceed for 24 hours at room temperature under constant rotation.

The peptide crosslinked polymer was purified by washing with deionized water and centrifuging at 10,000 x g for 5 minutes for three times, and then lyophilized overnight. The resulting P(MAA-g-EG) polymer crosslinked with GRRRGK peptide was then crushed and sieved into microparticles of the desired size range, and then stored at 4°C in a desiccator.

To quantify the amount of GRRRGK peptide crosslinking agent in the final polymer, the peptide content in the supernatant after the reaction and after each wash was quantified using a fluorescamine assay. Briefly, the fluorescamine reagent (3 mg/mL fluorescamine dissolved in filtered acetone) was add at a 1:3 ratio by volume to supernatant samples, and then samples were mixed for 15 minutes at room temperature. The fluorescence was measured at an excitation of 400 nm and an emission of 430 nm using a BioTek Cytation 3 multi-mode reader (Winooski, VT).

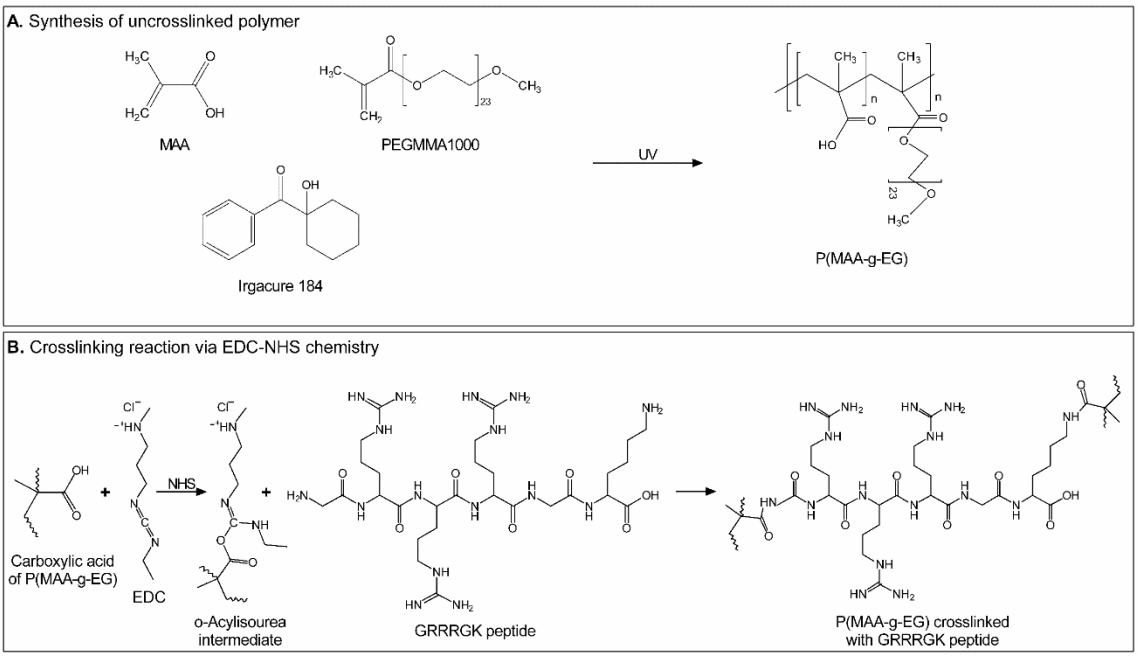

Figure 7-2. (A) Synthesis of uncrosslinked P(MAA-g-EG) polymer by UV polymerization. (B) Crosslinking reaction of P(MAA-g-EG) via EDC-NHS chemistry. EDC reacts with the carboxylic acid groups of the PMAA backbone to form an active O-acylisourea intermediate which is easily displace by nucleophilic attack from a primary amine groups of the GRRRGK peptide. The primary amine forms an amide bond with the original carboxyl group, releasing an isourea by-product. (Figure adapted from Knipe *et al*.[3])

7.2.4 FTIR-ATR Spectroscopy

Fourier transform infrared-attenuated total reflectance (FTIR-ATR) spectroscopy was used to determine the composition of peptide crosslinked microparticles as compared to the uncrosslinked P(MAA-g-EG) polymer and the GRRRGK peptide. FTIR-ATR spectra were collected using a Thermo Scientific Nicolet^{TM} iS10 FT-IR spectrometer (Waltham, MA) with an accessory germanium crystal at an incidence angle of 45°C. A background spectra was acquired immediately prior to each individual sample. Prior to

analysis, the uncrosslinked polymer and the microparticles were dried in a vacuum at 37°C for at least 24 hours. The GRRRGK peptide was used as provided from the manufacturer. For each sample, 128 scans were performed with a resolution of 4 cm^{-1} and a gain of four.

7.2.5 SEM

Scanning electron microscopy was used to examine the morphology and size distribution of the peptide crosslinked microparticles. For sample preparation, dried microparticles were dusted onto carbon tape-covered aluminum stubs and then coated with 12 nm of Pt/Pd using a Cressington 208 Benchtop sputter coater (Watford, England, UK). SEM images were obtained using a Zeiss Supra 40VP Scanning Electron Microscope (Oberkochen, Germany).

7.2.6 Microparticle Swelling Studies and Enzyme Degradation

The time scale of microparticle swelling and degradation is determined by kinetic turbidimetric studies in biorelevant media. Biorelevant media were prepared using FaSSIF, FeSSIF & FaSSIF Powder (Biorelevent.com, London, England, UK). Fasted-state simulated gastric fluid (FaSSGF) was prepared at a 1x concentration according to the manufacturer's protocol, while fasted-state simulated intestinal fluid (FaSSIF) was prepared at a 2x concentration. For all turbidity, microscopy, and release studies, a 1:1 (v/v) mixture of FaSSGF and FaSSIF buffers at a final pH of 6.5 were used for intestinal conditions.

Microparticle suspensions (5 mg/mL) were prepared with FaSSGF buffer (pH 1.6), 3.2 mg/mL pepsin in FaSSGF buffer, 1:1 FaSSGF:FaSSIF buffer (pH 6.5), and 0.625 mg/mL trypsin in FaSSGF:FaSSIF buffer. Immediately following suspension, 200 μL of either particle suspension or buffer only was added in triplicate to a 96-well plate. The absorbance was then measured at 520 nm in 1 minute intervals with 20 seconds of shaking

prior to each read at 37°C for 2 hours using a BioTek Cytation 3 multi-mode reader (Winooski, VT).

To further confirm the pH-responsive swelling behavior, microparticles in the FaSSGF and FaSSIF buffers were visually examined by bright-field microscopy. Additionally, bright-field microscopy is used to visualize degradation of the microparticles by trypsin and resistance to degradation by pepsin. Bright-field images were captured using an Olympus IX 73 inverted microscope using the 10x objective.

7.2.7 Cytocompatibility Studies

To determine the cytocompatibility of the peptide crosslinked microparticles and the degradation products, cell proliferation (MTS) assays were conducted using two intestinal epithelial model cell lines. Human epithelial colorectal adenocarcinoma (Caco-2) and mucus-secreting goblet-like human colorectal adenocarcinoma (HT29-MTX) were cultured in modified Dulbecco's Eagle Medium (DME) supplemented with 10% fetal bovine serum (FBS). Caco-2 cells (at passages 65-75) or HT29-MTX cells (at passages 15-20) were plated on a 96-well plate, coated with fibronectin, at an initial seeding density of $5x10^6$ cells per well and then cultured to 80% confluence.

Prior to use, microparticles (30-45 μm) were added to DMEM without phenol red with 10% FBS at concentrations of 0.625, 1.25, and 2.5 mg/mL and allowed to swell for 1 hour at 37°C under constant rotation. To prepare the degradation products, microparticles were added to 0.625 mg/mL of trypsin in 1X PBS (sterile filtered) and then allowed to degrade for 6 hours at 37°C under constant rotation. To quench trypsin activity, trypsin inhibitor Type III-O (free of ovoinhibitor) was added 1:1 mass ratio to trypsin, and then further incubated for 1 hour at 37°C under constant rotation. The degradation products were further diluted 1:6 with DMEM with 10% FBS to final concentrations of 0.625, 1.25,

and 2.5 mg/mL. Samples of trypsin and inhibitor in media at the same ratios were prepared as a control.

For the cytocompatibility study, growth media was removed from the cell and replaced with 100 μL of solution—microparticle suspensions, degradation product suspensions, media (positive control), media with trypsin and inhibitor, or lysis buffer (negative control). The cells were incubated for 6 hours. For the CellTiter 96® Aqueous One Solution Cell Proliferation (MTS) assay (Promega Corporation, Madison, WI), MTS reagent (20 μL/well) for was added after 6 h exposure, and then incubated for an additional 90 minutes. The absorbance was measured at 490 nm for the MTS and 690 nm for the background using a BioTek Cytation 3 multi-mode reader (Winooski, VT).

7.2.8 Factor IX Loading Studies

Previously optimized loading conditions for hFIX were used with the peptide crosslinked P(MAA-g-EG) microparticles. Dried particles (5 mg/mL) and hFIX (0.5 mg/mL) were suspended in 5 mM NaH_2PO_4 buffer, adjusted to a final pH of 7.4. hFIX was loaded by equilibrium partitioning for 5 days at 4°C under constant rotation. After incubation, particles were collected by Buchner filtration using Whatman 50 filter paper, then collapsed with 0.1 N HCl, and then triple rinsed with 0.1 N HCl, then water, and lastly 0.1 N HCl. Samples were collected after each step for analysis using hFIX ELISAs. The hFIX-loaded particles were then lyophilized overnight.

7.2.9 Factor IX Release Studies

Release studies were conducted using two-stage dissolution in biorelevant media (prepared described above). Dissolution testing was performed using a Distek 2100B dissolution apparatus (North Brunswick, NJ) with a USP apparatus 2 (with paddles) setup for small volumes (100 mL vessels) with low evaporation mini vessel covers. A 5 mg

sample of hFIX-loaded microparticles was added to a Sigmacoted (i.e., siliconized) vessel containing 30 mL of FaSSGF buffer (pH 1.6) at 37°C with continuous stirring at 75 rpm. At 10 minute intervals, three 1 mL samples were taken using a 1/8 cannula sample probe (Distek, Inc.) with a 10 micron polyethylene filter tip (Agilent Technologies, Santa Clara, CA). Samples were replaces with an equal volume of appropriate pre-warmed media. After 30 minutes for the FaSSGF stage, 30 mL of 1.25 mg/mL trypsin in FaSSIF (2x) at 37°C was added, raising the pH to 6.5 ad bringing the final trypsin concentration to 0.625 mg/mL. Similarly, samples were taken over the course of the 2 hour FaSSIF stage. Release samples were analyzed by hFIX ELISAs.

7.2.10 Factor IX Transport Studies

In order to determine the effect of the microparticles and degradation products on the transport of factor IX across an intestinal epithelium, *in vitro* transport studies were conducted using an intestinal epithelial model. Caco-2 and HT29-MTX cells at 1:1 mixture were seeded on the apical side of 12-well Transwell® plates (12 mm diameter, 0.4 μm pores, Corning, Corning, NY) at 10^5 cells per well. Monolayers were cultures for 17-21 days with media (DMEM with 10% FBS) changes every other day. The transepithelial electrical resistance (TEER) was measured 2 hours post media change using an EVOM^2 epithelial voltohmmeter and chopstick electrode (World Precision Instruments, Sarasota, FL).

Prior to *in vitro* use, hFIX was endotoxin-depleted for cell culture standards. Endotoxins were removed using Thermo Scientific™ Pierce™ High-Capacity Endotoxin Removal Spin Columns according to the manufacturer's protocol. For maximum endotoxin removal, the hFIX was incubated in the spin column for 24 hours at 4°C. After endotoxin

depletion, a Thermo Scientific™ Pierce™ LAL (limulus amebocyte lysate) was used to measure the amount of endotoxin in hFIX samples.

Prior to the start of the transport study, microparticle samples were added to Hank's balanced salt solution (HBSS) with 0.5 mg/ml bovine serum albumin (BSA) (HBSS/BSA) and allowed to swell for 1 hour at 37°C under constant rotation. To prepare the degradation products, microparticles were added to 0.625 mg/mL of trypsin in 1X PBS (sterile filtered) and then allowed to degrade for 6 hours at 37°C under constant rotation. To quench trypsin activity, trypsin inhibitor Type III-O (free of ovoinhibitor) was added 1:1 mass ratio to trypsin, and then further incubated for 1 hour at 37°C under constant rotation. The degradation products were further diluted 1:6 with HBSS/BSA with 10% FBS to final concentrations of 0.625, 1.25, and 2.5 mg/mL. Samples of trypsin and inhibitor in HBSS/BSA at the same ratios were prepared as a control.

One hour before the transport study, media was removed and replaced with HBSS/BSA at 37°C to allow the cells to equilibrate. The TEER was measured in HBSS/BSA after the 1 hour incubation, and then HBSS/BSA was removed from the apical side. Microparticles (0.875 mg/mL = 0.391 mg/cm^2) with hFIX, degradation products (0.875 mg/mL) with hFIX, neat hFIX, HBSS/BSA, or trypsin and inhibitor in HBSS/BSA were added to the apical side. hFIX was tested at two different concentrations—0.04 mg/mL and 0.4 mg/mL (10x)—for the microparticles, degradation products, and neat hFIX samples. In addition to the HBSS/BSA control, samples with trypsin and inhibitor in HBSS/BSA were also included to determine if trypsin and inhibitor affected TEER measurements. For the duration of the 4 hour study, TEER was measured, and then 200 µL samples were collected from the basolateral side and replaced with HBSS/BSA at 37°C for each time point. After 4 hours, final apical and basolateral samples were collected, then cells were rinsed with media, and fresh media was added to both sides. To monitor the

recovery of the monolayers, final TEER measurements were taken 24 hours post study completion. The amount of hFIX transported to the basolateral side was quantified by hFIX ELISAs.

7.2.11 Statistical Analysis

Data are reported as mean ± standard error. All statistical analysis, either a Student's two-tailed t-test for two groups or an ANOVA for multiple groups, were computed using GraphPad Prism 6. Significant differences were considered when $*p < 0.05$ and $**p < 0.01$.

7.3 Results and Discussion

7.3.1 Uncrosslinked Polymer Synthesis, Purification, and Characterization

The composition of the resulting uncrosslinked P(MAA-g-EG) polymer was confirmed by titration and FTIR (see Section 7.3.3). Based on titration, the uncrosslinked polymer is composed of 93 ± 0.5 mol % MAA. Similarly, the uncrosslinked polymer is composed of 6.60 mol% PEG and therefore 93.5 mol% MAA as calculated from peak ratios of the ^{1}H NMR spectrum (Figure 7-3). Both results agree closely of the monomer feed of 97 mol % MAA.

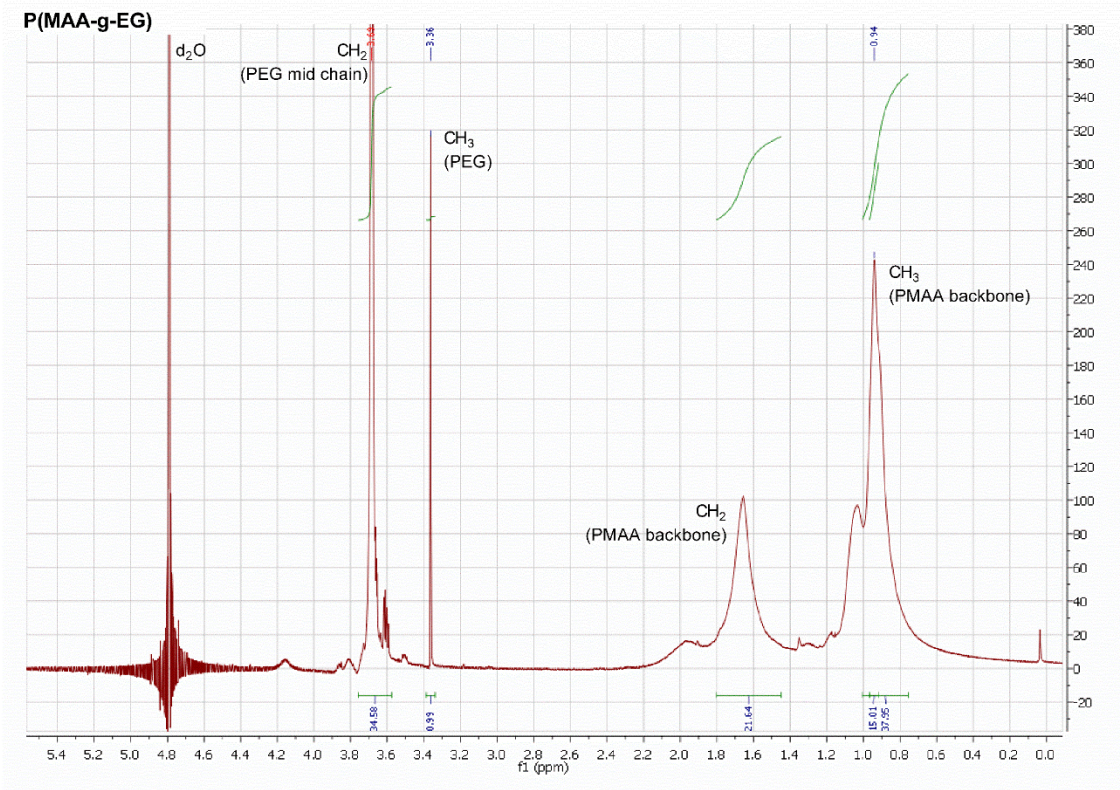

Figure 7-3. ^{1}H NMR spectrum of P(MAA-g-EG) polymer dissolved in d_2O shows the integration of the peaks of interest.

7.3.2 Peptide Crosslinking via EDC-NHS Chemistry

Immediately following the addition of GRRRGK peptide, the mixture became cloudy, indicating crosslinking of the P(MAA-g-EG). After the 24 hour incubation, a single opaque mass had formed and the remaining liquid was clear. After each wash step, the mass of crosslinked polymer slightly decreased due to the removal of uncrosslinked polymer. The resultant lyophilized crosslinked polymer was white and denser than lyophilized uncrosslinked polymer. Based on results from the fluorescamine assay, the final amount of peptide incorporated was 1.32 ± 0.24 mol % of total moles of polymer. The

dried peptide crosslinked polymer was crushed into microparticles of 30-45 μm, and the particles showed irregular morphology due to the crushing process (Figure 7-4).

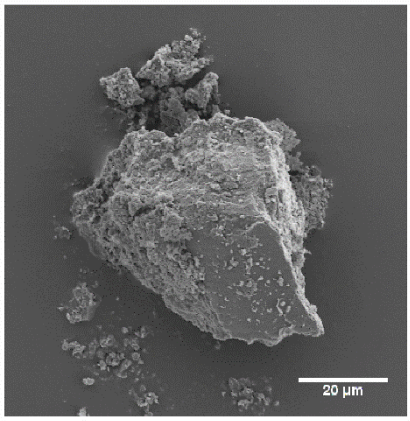

Figure 7-4. A representative SEM image shows the irregular morphology of a 30-45 μm peptide crosslinked P(MAA-g-EG) microparticle (scale bar = 20 μm).

7.3.3 FTIR-ATR Spectroscopy

In order to confirm the incorporation of the GRRRGK peptide into the microparticles, FTIR-ATR spectra were collected for uncrosslinked P(MAA-g-EG) polymer, GRRRGK peptide, and peptide crosslinked microparticles. As shown in Figure 7-2, the peptide spectrum shows the amide I region (1700-1600 cm^{-1}), corresponding to the carbonyl (C=O) stretching vibration of a peptide bond, and the amide II region (1575-1480 cm^{-1}) due to CN stretching and NH bending.[9, 10] Additional characteristic bands of the peptide can be attributed to CN stretching (1250 and 1140 cm^{-1}) and NH_2 stretching (800 cm^{-1}).[2] For the uncrosslinked P(MAA-g-EG) spectra, peaks are characteristic of COOH stretching (1730 cm^{-1}), C-O stretching (1200 cm^{-1}), and asymmetric stretching of the ether group (C-O-C) of PEG (1100 cm^{-1}).[11] The spectra of P(MAA-g-EG) crosslinked with

peptide shows characteristic peaks from both the uncrosslinked P(MAA-g-EG) polymer and the GRRRGK peptide, notably the broadening of the peak at 1750-1600 cm^{-1} and 1250-1140 cm^{-1} (Figure 7-5).

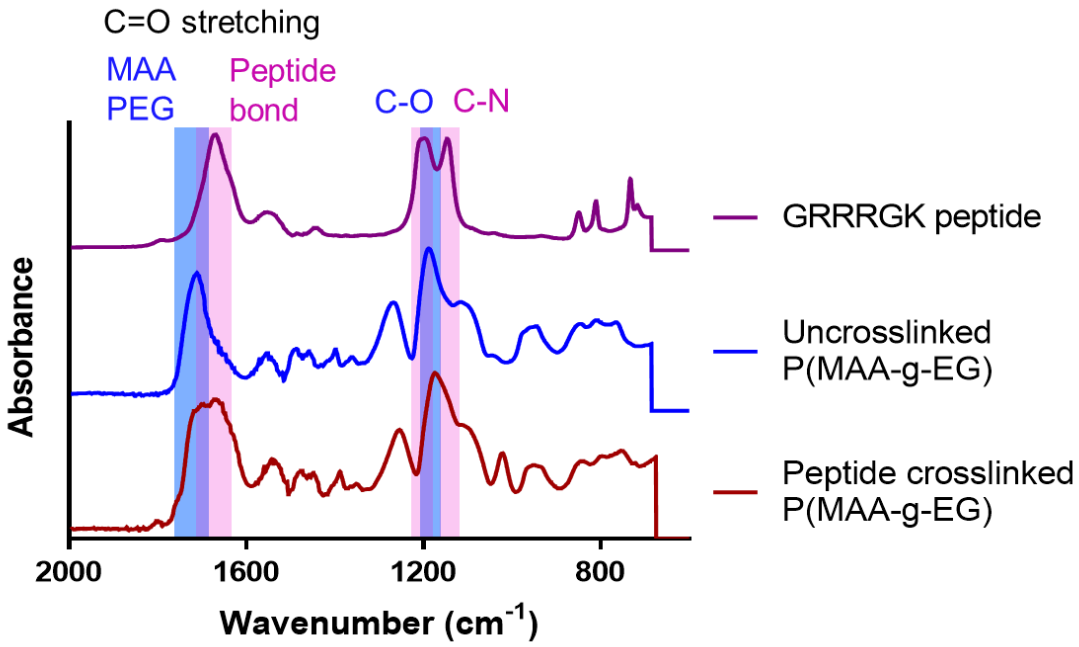

Figure 7-5. FTIR-ATR spectra of uncrosslinked P(MAA-g-EG), GRRRGK peptide, and peptide crosslinked P(MAA-g-EG).

7.3.4 Microparticle Swelling and Enzyme Degradation

Kinetic turbidimetric studies were conducted to determine the timescale of microparticle swelling and degradation. Previous studies have demonstrated the use of turbidity for analysis of microparticle swelling[1] and microparticle degradation.[2] The turbidity of a microparticle dispersion decreases as a result of microparticle swelling due to the increased transparency of the microparticles. Similarly, as microparticles degrade,

the turbidity of the dispersion decreases. In the case of microparticle swelling and degradation, the relative refractive index of the particles to the solvent decreases and reduces the turbidity measurement. As previously derived by Klinger et al., turbidity can be expressed as:

$$\tau = [A_t - A_0]\ \ln 10 \qquad \text{(Eq. 7-1)}$$

where A_t is the absorbance of the sample and A_0 is the absorbance of the pure solvent. [12] For kinetic turbidity measures for an individual sample, the relative turbidity is defined as:

$$\tau_{rel} = \frac{\tau_t}{\tau_{t=0}} \qquad \text{(Eq. 7-2)}$$

where τ_t is the turbidity at time, t, and τ_t is the initial turbidity.

The kinetics of degradation and swelling are shown in Figure 7-6 where the rate of degradation (sample in FaSSIF with 0.625 mg/mL trypsin) is occurs more rapidly than the rate of swelling (samples in FaSSIF). The microparticles (90-150 μm) are nearly completed degraded by one hour. The turbidity of samples in FaSSGF with 3.2 mg/mL pepsin remain relatively constant indicating that the particles remain intact and do not swell. The kinetic turbidity results are as expected since this system is designed for targeted degradation by trypsin (prominent in the small intestine), not by pepsin (prominent in the stomach).

In addition to turbidity results, microscopy was used to visually confirm the pH-responsive swelling behavior of peptide-crosslinked P(MAA-g-EG). At intestinal conditions (pH 6.5), the microparticles were swollen as shown by the increase in size compared to microparticles at gastric conditions (pH 1.6). In addition, the microparticles remained intact at pH 6.5 confirming that the P(MAA-g-EG) polymer was crosslinked by the GRRRGK peptide (Figure 7-7). Uncrosslinked polymer would dissociate at a pH above 4.8, which is the pKa of MAA.

Microscopy was further used to confirm the specificity of the enzymatic degradation and the corresponding timescale. As visually confirmed, the microparticles

were not degraded by pepsin in FaSSGF medium, while microparticles were degraded by trypsin (0.625 mg/mL) in FaSSIF medium (Figure 7-7). The majority of microparticles were degraded within 30 minutes with small pieces remaining, and within an hour, the microparticles were fully degraded.

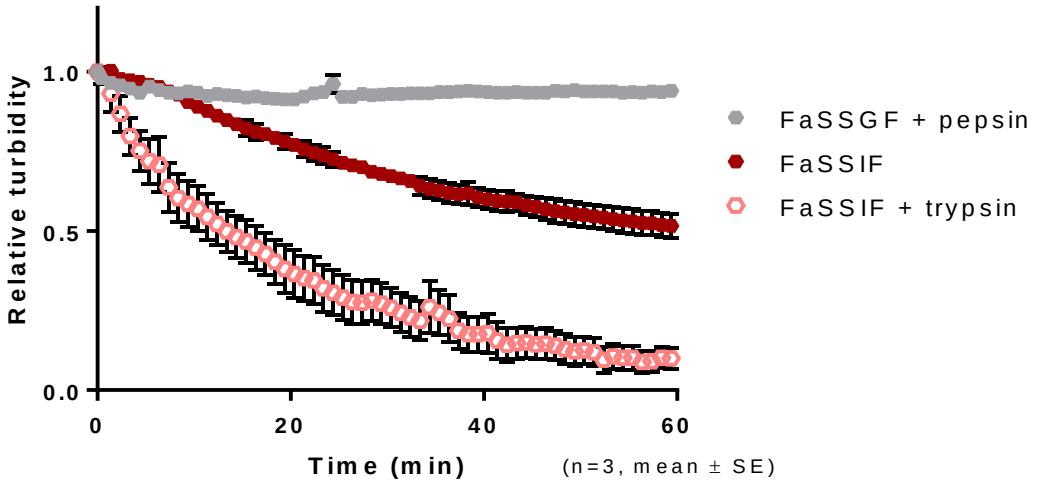

Figure 7-6. Kinetic turbidimetric measurements show the timescale of microparticle swelling and degradation by trypsin, while confirming that the microparticles are not degraded by pepsin (mean ± SE, n=3).

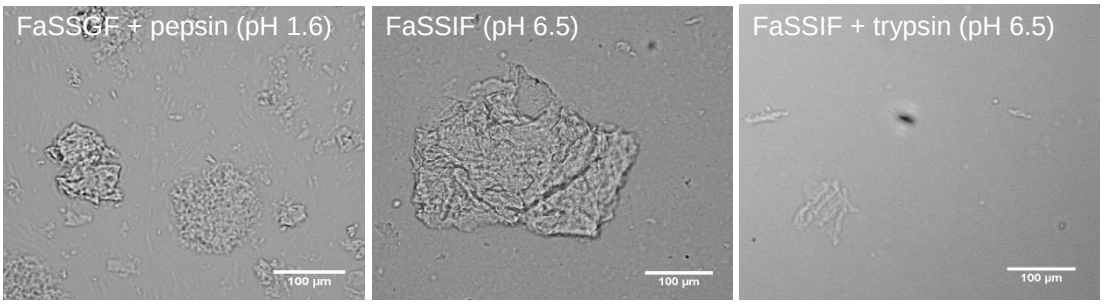

Figure 7-7. Bright-field images of microparticles (90-150 µm) after 30 minutes in biorelevant conditions (scale bar = 100 µm). Microparticles in the gastric conditions with pepsin remained intact. In the intestinal conditions with enzymes, the microparticles are swollen and intact. The microparticles are degraded by trypsin, leaving some debris behind.

7.3.5 Cytocompatibility

The cytocompatibility of the microparticles and degradation products was determined using an MTS cell proliferation assay. The cytocompatibility was found to be concentration dependent with the effect more profound for Caco-2 cells (Figure 7-8) compared to HT29-MTX (Figure 7-9). At all concentrations, both the microparticles and the degradation products are cytocompatible (80% cell viability) in both cell lines. As the microparticles degrade in the small intestine, the degradation products are also cytocompatible as there is no significant difference between the two groups. Additionally, the presence of trypsin and inhibitor in the media showed no negative effects on cell viability (103.5 ± 5.1% for Caco-2 cells and 100.2 ± 1.9% for HT29-MTX cells).

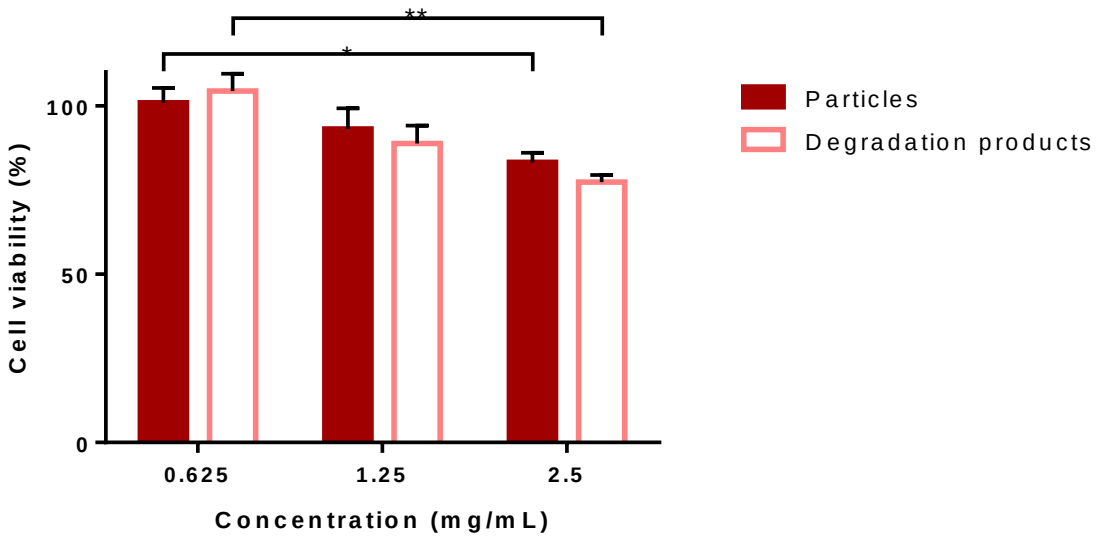

Figure 7-8. Cytocompatibility of peptide crosslinked P(MAA-g-EG) particles and degradation products (6 h exposure) was evaluated in Caco-2 cells using a cellular metabolic activity MTS assay. (n=3, mean ± SE, *p<0.5).

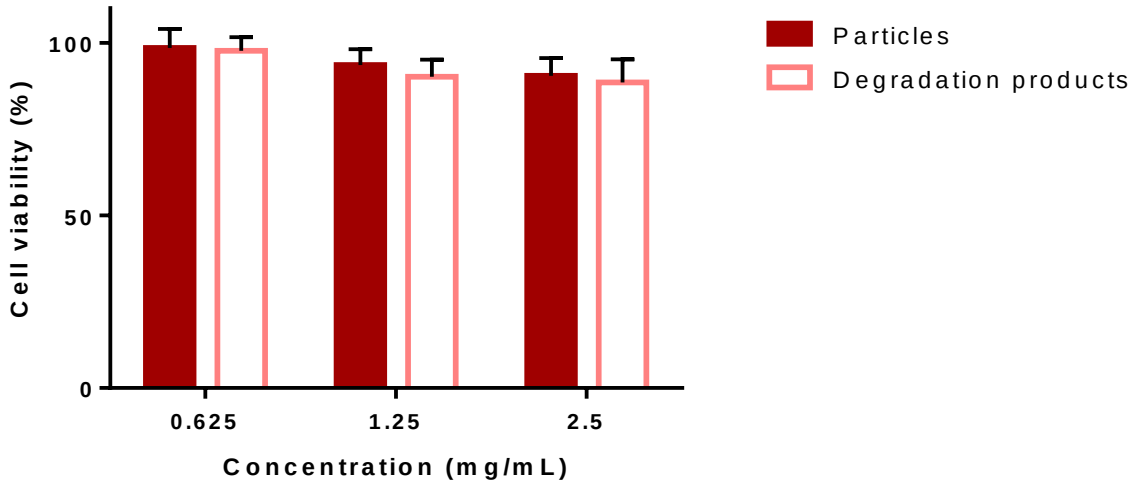

Figure 7-9. Cytocompatibility of peptide crosslinked P(MAA-g-EG) particles and degradation products (6 h exposure) was evaluated in HT29-MTX cells using a cellular metabolic activity MTS assay. (n=3, mean ± SE, *p<0.5).

7.3.6 Factor IX Loading and Release

We designed a biodegradable system for improved release of hFIX as compared to previously tested systems using P(MAA-g-EG) crosslinked with PEGDMA (MW of PEG ranging from 400 to 1000). The final amount of protein loaded takes into account the concentration of supernatant after incubation, collapse, and triple rinse. Protein lost during collapse and rinse was likely surface loaded. The loading level tor the peptide-crosslinked P(MAA-g-EG) microparticles is 37.02 ± 0.21 µg hFIX/mg particles, which is similar to the loading amount (39.91 ± 1.91 µg hFIX/mg particles) for P(MAA-g-EG) crosslinked with 1% PEGDMA1000 using the same loading conditions.[1]

Release from the biodegradable system showed the desired trends with minimal release in gastric conditions (FaSSGF) and increased release in intestinal conditions

(FaSSIF), as shown in Figure 7-10. hFIX release from the biodegradable system continued to increase over the first hour in FaSSIF conditions which may be attributed to both the pH-responsive swelling and enzymatic degradation. As the microparticles swell, the peptide crosslinks become more accessible to trypsin, which can increase the rate of degradation of the microparticle and allow for increased release of hFIX from the internal sections of the microparticle. By combining pH-responsive behavior and enzymatic degradation, we have improved the amount of hFIX released in intestinal conditions by 1.7-fold as compared to PEGDMA crosslinked pH-responsive systems.

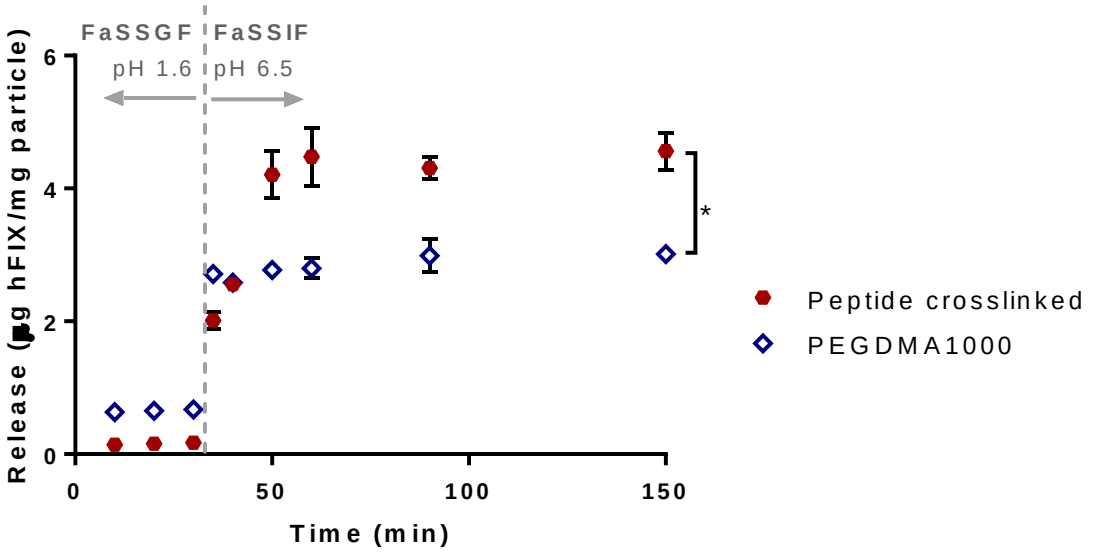

Figure 7-10. Release profile of hFIX from P(MAA-g-EG) microparticles using two-stage dissolution in biorelevant media. Enzymatically degradable particles crosslinked with peptide showed increased hFIX release compared to particles crosslinked with PEGMDA1000 (data from Horava and Peppas[1]). Note that FaSSGF = fasted-state simulated gastric fluid and FaSSIF = fasted-stated simulated intestinal fluid. (n=3, mean ± SE, *$p<0.05$).

7.3.7 Transport Studies

In vitro transport studies using an intestinal epithelial model are used as a tool to predict the oral drug absorption. Co-cultures of Caco-2 cells and mucus-secreting goblet-like HT29-MTX cells are a commonly used as physiologically relevant intestinal epithelial models for predicting oral drug absorption.[13] As previously noted, co-culture models contain three major absorption barriers—tight junctions, membranes of absorptive epithelia, and a mucus layer. While the tight junctions (*in vitro* TEER values of ~250-300 Ω cm^2, Figure 7-11) are closer to *in vivo* values (20-100 Ω cm^2), the *in vitro* drug permeability is typically lower than *in vivo*.[13]

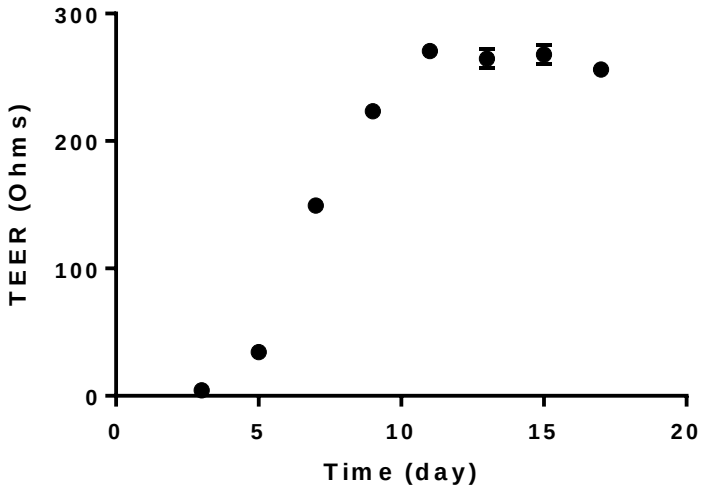

Figure 7-11. TEER of *in vitro* intestinal epithelial monolayers (co-culture of Caco-2 and HT29-MTX cells) during culturing. (n=24, mean ± SE).

Transport studies using an *in vitro* intestinal epithelial model were conducted to determine the effect of the microparticles and degradation products on the transport of hFIX. We further examined the effect of apical hFIX concentration on absorption. Prior to

in vitro use, hFIX was endotoxin depleted to a final concentration of < 1.5 EU/mL, as quantified by LAL assay. Suspensions of microparticles and degradation products were added at a concentration of 0.875 mg/mL, which is the same surface coverage of 0.391 mg/cm^2 as the 1.25 mg/mL concentration tested in cytocompatibility studied and found as non-cytotoxic. Two hFIX concentrations, 0.04 mg/mL and 0.40 mg/mL (10x), were tested. For both hFIX concentrations, the presence of the microparticles and degradation products significantly increased the apical-to-basolateral transport of hFIX as compared to hFIX only (Figures 7-12 and 7-13). Similar to previously reported results,[1, 14] protein transport begins to plateau after 2 hours. For an initial hFIX concentration of 0.04 mg/mL at the apical side, the microparticles and degradation products have the same effect on the transport of hFIX (Figure 7-12). At the higher initial hFIX concentration of 0.40 mg/mL, the effect of the microparticles and degradation products deviate at times greater than 2 hours (Figure 7-13). The decreased transport at later times for the microparticles may be attributed to hFIX loading into the microparticles on the apical side. In order to improve bioavailability, increasing the initial amount of hFIX can drive the transport of hFIX by increasing the protein gradient across the monolayer.

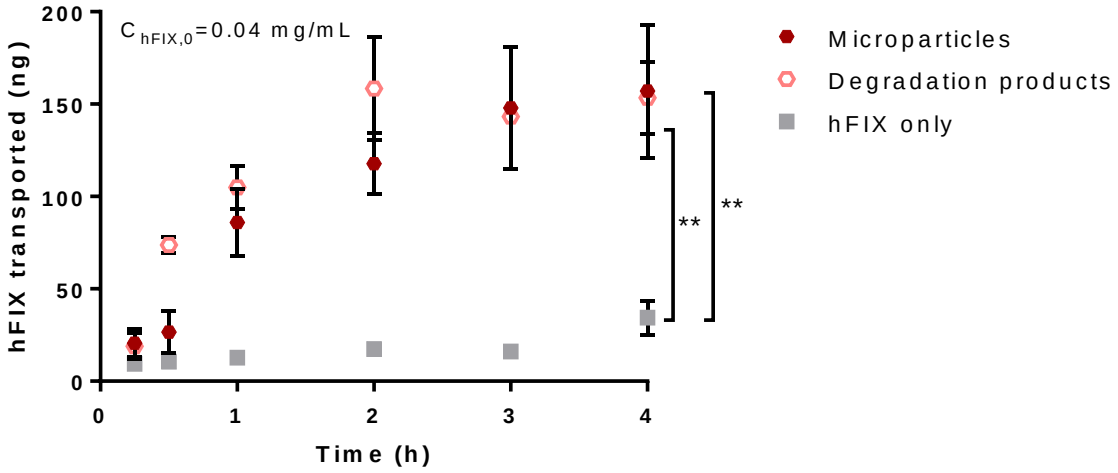

Figure 7-12. The amount of hFIX transported across the co-culture intestinal epithelial monolayer over time shows that the presence of the microparticles and degradation products improved hFIX transport. (n=3, mean ± SE, **p<0.001).

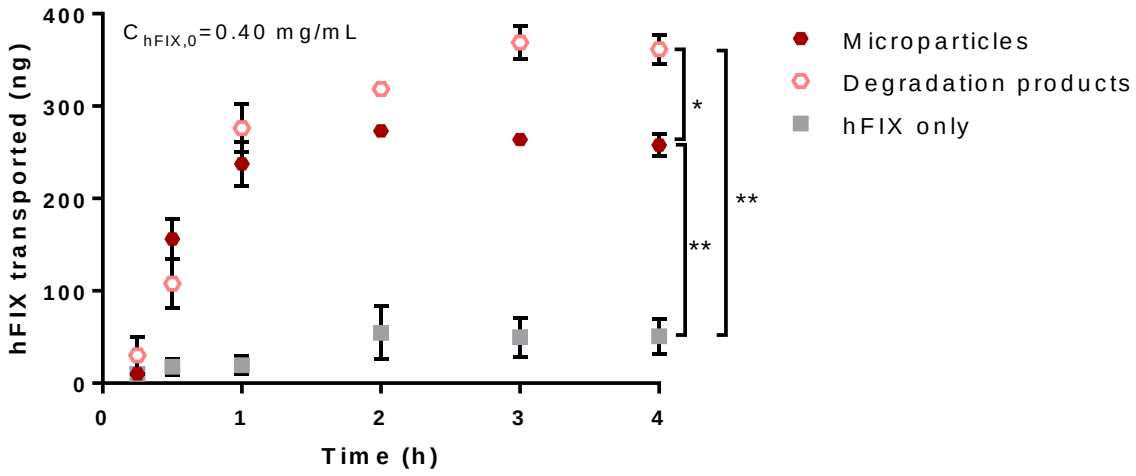

Figure 7-13. The amount of hFIX transported across the co-culture intestinal epithelial monolayer over time shows that the presence of the microparticles and degradation products improved hFIX transport. (n=3, mean ± SE, *p<0.05, **p<0.01).

We further evaluated the effect of the microparticles and degradation products, as well as the initial hFIX concentration, on the permeability of hFIX. The permeability of protein across the monolayer was calculated by:

$$P_{app} = \frac{dQ(t)}{dt} \times \frac{1}{A \times C_{AO}} \quad \text{(Eq. 3-1)}$$

where $Q(t)$ is the cumulative protein release (ng) at time t (s), A is the area of the cell monolayer (cm^2), and C_{AO} is the initial protein concentration (ng/cm^3) at the apical side. The permeability of hFIX was calculated over 1 hour, 2 hours, and 4 hours (Table 7-2). We examined the permeability at these time points, since the amount of hFIX transported over time ($dQ(t)/dt$) follows a linear relationship for 1 hour at the initial concentration of 0.04 mg/mL and for 2 hours at the initial concentration of 0.04 mg/mL. The permeability of hFIX is significantly increased by the presence of microparticles and degradation

products as compared to hFIX only for all cases. These trends are the same as previously reported results where PMAA-based microparticles improve protein permeability, which may be due to Ca^{2+} chelation.[1, 15] While higher initial hFIX concentrated improved transport, the amount of hFIX transported was only two-fold higher for a 10x initial concentration, resulting in reduced permeability values.

Table 7-2. In vitro permeability of hFIX across the intestinal epithelial monolayer is improved by the presence of the microparticles and degradation products.

	For $C_{hFIX,0}$ =0.04 mg/mL			**For $C_{hFIX,0}$ =0.40 mg/mL**		
	Micro-particles	**Degradation Products**	**hFIX only**	**Micro-particles**	**Degradation Products**	**hFIX only**
$P_{app,\ 1\ h}$	513.7±101.8	600.8±43.2	24.9±7.2	164.7±15.0	191.5±21.0	6.5±5.1
$P_{app,\ 1\ h}$	326.4±59.8	404.3±77.0	25.4±12.7	74.4±3.2	93.2±5.8	14.4±8.4
$P_{app,\ 1\ h}$	210.9±42.1	171.2±20.8	30.7±7.2	28.4±3.5	47.7±0.8	6.8±2.9

To evaluate the integrity of the intestinal epithelial monolayers, the TEER was measured for the study duration (Figure 7-140. As previously reported,[1] the TEER values for all conditions were relatively constant over the 4-hour study, indicating that the tight junctions remained intact. Exposure to trypsin and inhibitor did not affect the TEER measurements. Furthermore, the presence of the microparticles and degradation products did not have negative effects on the monolayer integrity. While the Ca^{2+} chelating effect is expected to open the tight junctions, the mucus layer is hypothesized to act as a barrier between the cells and microparticles and therefore reduce the effect on TEER measurements. Additionally, the monolayers fully recovered 24 hours after the removal of the microparticles and degradation products. In an oral delivery system application, any

effect of the particles and their degradation products is expected to only be temporary and not cause any permanent damage to the intestinal tract.

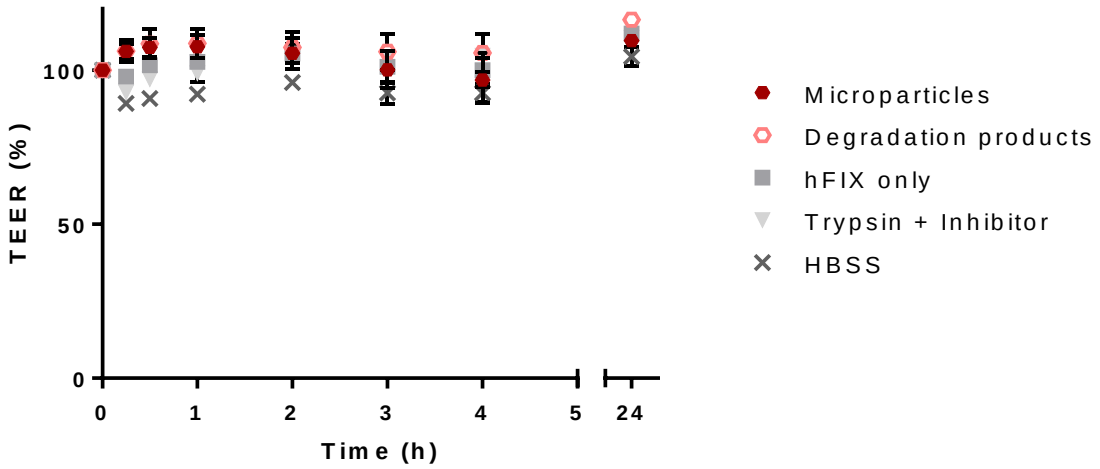

Figure 7-14. TEER remained constant during the transport study, indicating that the tight junctions remained intact with when exposed to microparticles and degradation products. TEER measurements at 24 h post study showed that the monolayers fully recovered after removal of microparticles. (n=6, mean ± SE).

7.4 CONCLUSIONS

We have successfully developed a microcarrier system based on an enzymatically degradable and pH-responsive P(MAA-g-EG) hydrogel for the oral delivery of hFIX. In order to improve upon previously described pH-responsive systems, we incorporated an enzymatically degradable peptide crosslinking agent to achieve a higher delivery potential. We have demonstrated the enzyme-specific degradation reaction of such microcarriers on a physiologically relevant time scale. Both the microparticles and degradation products

were found to be cytocompatibility which is necessary for the end use in therapeutic applications.

The peptide crosslinked P(MAA-g-EG) microparticles are capable of loading hFIX and releasing it in response to environmental stimuli. Incorporation of a biodegradable component allowed for increased levels of hFIX released under intestinal conditions. Improving the delivery potential of hFIX is important for promoting the oral bioavailability of hFIX. Additionally, we have demonstrated that the presence of the microparticles and degradation products enhances the *in vitro* absorption of hFIX. Based on the result reported here, enzymatically degradable and pH-responsive P(MAA-g-EG) microcarriers are an ideal candidate for an oral drug delivery system for hFIX.

7.5 REFERENCES

1. Horava, S. D.; Peppas, N. A., Design of pH-Responsive Biomaterials to Enable the Oral Route of Hematological Factor IX. *Annals of Biomedical Engineering* **2016**, 1-13.
2. Knipe, J. M.; Chen, F.; Peppas, N. A., Enzymatic Biodegradation of Hydrogels for Protein Delivery Targeted to the Small Intestine. *Biomacromolecules* **2015**, *16* (3), 962-972.
3. Knipe, J. M.; Strong, L. E.; Peppas, N. A., Enzyme-and pH-responsive microencapsulated nanogels for oral delivery of siRNA to induce TNF-α knockdown in the intestine. *Biomacromolecules* **2016**.
4. Koetting, M. C.; Guido, J. F.; Gupta, M.; Zhang, A.; Peppas, N. A., pH-responsive and enzymatically-responsive hydrogel microparticles for the oral delivery of therapeutic proteins: Effects of protein size, crosslinking density, and hydrogel degradation on protein delivery. *Journal of Controlled Release* **2016**, *221*, 18-25.
5. Glangchai, L. C.; Caldorera-Moore, M.; Shi, L.; Roy, K., Nanoimprint lithography based fabrication of shape-specific, enzymatically-triggered smart nanoparticles. *Journal of Controlled Release* **2008**, *125* (3), 263-272.

6. Woodley, J. F., Enzymatic barriers for GI peptide and protein delivery. *Critical reviews in therapeutic drug carrier systems* **1993**, *11* (2-3), 61-95.

7. Vlieghe, P.; Lisowski, V.; Martinez, J.; Khrestchatisky, M., Synthetic therapeutic peptides: science and market. *Drug Discovery Today* **2010**, *15* (1), 40-56.

8. Khokhlov, A. R.; Kramarenko, E. Y., Polyelectrolyte/ionomer behavior in polymer gel collapse. *Macromolecular theory and simulations* **1994**, *3* (1), 45-59.

9. Kong, J.; Yu, S., Fourier transform infrared spectroscopic analysis of protein secondary structures. *Acta biochimica et biophysica Sinica* **2007**, *39* (8), 549-559.

10. Jameel, F.; Hershenson, S., Formulation and Process Development Strategies for Manufacturing Biopharmaceuticals. John Wiley & Sons: Hoboken, **2010**; Vol. 1.

11. Torres-Lugo, M.; Peppas, N. A., Preparation and characterization of P (MAA-g-EG) nanospheres for protein delivery applications. *Journal of Nanoparticle Research* **2002**, *4* (1-2), 73-81.

12. Klinger, D.; Landfester, K., Enzymatic- and light-degradable hybrid nanogels: Crosslinking of polyacrylamide with acrylate-functionalized Dextrans containing photocleavable linkers. *J. Polym. Sci. A Polym. Chem.* **2012**, *50* (6), 1062-1075.

13. Hilgendorf, C.; Spahn-Langguth, H.; Regardh, C. G.; Lipka, E.; Amidon, G. L.; Langguth, P., Caco-2 versus Caco-2/HT29-MTX co-cultured cell lines: permeabilities via diffusion, inside- and outside-directed carrier-mediated transport. *J. Pharm. Sci.* **2000**, *89* (1), 63-75.

14. Gupta, V.; Doshi, N.; Mitragotri, S., Permeation of Insulin, Calcitonin and Exenatide across Caco-2 Monolayers: Measurement Using a Rapid, 3-Day System. *PLoS ONE* **2013**, *8* (2), e57136.

15. Wood, K. M.; Stone, G. M.; Peppas, N. A., The effect of complexation hydrogels on insulin transport in intestinal epithelial cell models. *Acta Biomater.* **2010**, *6* (1), 48-56.

Chapter 8: In Vivo Safety of P(MAA-g-EG) Microcarriers[4]

8.1 INTRODUCTION

The oral delivery of factor IX for the treatment of hemophilia B is a highly desirable alternative to needle-based treatment options, especially for patients with moderate and severe hemophilia B taking multiple injections per week for prophylaxis. We have developed pH-responsive P(MAA-g-EG) microcarriers to enable the oral route of factor IX.[1, 2] However, before safe use of these P(MAA-g-EG) in a clinical setting, their biocompatibility must be evaluated in preclinical studies.[3] As previously reported, the *in vivo* safety of oral delivery systems has been tested in rodent models and assessed by clinical biochemical tests and tissue examination.[4, 5]

In this Chapter, we investigated the acute and long-term *in vivo* safety of P(MAA-g-EG) microcarriers. The safety study consisted of two separate studies: (1) acute and (2) long-term. The goal of the acute study was to evaluate the acute inflammatory response 24 hours post administration of the P(MAA-g-EG) microcarriers. The second study evaluated the long-term effects of dosing microparticles every other day for 14 days to mimic a prophylactic regimen with the shortest dosing intervals (and therefore, maximum exposure to the P(MAA-g-EG) microparticles). For both studies, the P(MAA-g-EG) microparticles were administered by oral gavage. The control group received sterile distilled water by oral gavage, which should cause no adverse effects. To establish the biocompatibility of P(MAA-g-EG) microparticles, we evaluated cytokine levels for inflammatory and immune responses, performed biochemical analysis of serum and urine for kidney and liver function, and examined tissue morphology for damage and inflammation.

[4] The *in vivo* safety studies presented here were conducted as part of a study testing the safety of three hydrogel formulations. The safety studies were performed by the author and Stephanie Steichen.

8.2 Materials and Methods

8.2.1 Polymer Synthesis

P(MAA-g-EG) hydrogels were synthesized by bulk UV-polymerization as previously described in Chapter 4. Briefly, the feed composition of the pre-polymer was MAA and PEGMMA1000 at a 2:1 molar ratio of hydrogen bonding groups, PEGDMA1000 at 1.0 mol% of total monomers, and Irgacure 184® at 1.0 wt. % of total monomers in a 1:1 (w/w) mixture of deionized water and ethanol. After sonicating for 20 minutes, the pre-polymer mixture was needle purged with nitrogen for 5 minutes in the nitrogen-rich environment of a glove box. The mixture was then dispensed between two quartz glass plates, separated with a 0.7 mm Teflon® spacer, and then polymerized for 30 minutes under 35 mW cm^{-2} UV light using a UV flood source. After synthesis, the resulting polymer was removed from the plates, and then washed in deionized water for a total of 10 water exchanges. The polymer was dried for 3 days in air and then for 3 additional days under vacuum at 37°C. Dried films were crushed and sieved into microparticles, sized 30-45 μm.

8.2.2 Animals and Treatment

Female C57BL/6J mice (4-6 weeks old) were purchased from The Jackson Laboratory. C57BL/6J mice were selected since the hemophilia B mice are derived from this background. For both the acute and long-term studies, adult mice entered the UT animal facility in the ARC building and were given at least three days to acclimate themselves to their new environment. Upon arrival mice were housed four per cage, and mice received ear punches as an identification marker.

One day prior to administration, a baseline blood sample was collected via saphenous vein. For the blood sample, the mice were restrained manually while the hind

leg was shaved using electric clippers and then the blood (up to 0.15 mL) was collected from the saphenous vein using a sterile 27G needle to puncture and a blood-collection tube.

For the acute study, mice were fasted by the removal of solid food in the morning for two hours prior to administration. The P(MAA-g-EG) microparticles were suspended in sterile distilled water prior to administration. The microparticle suspension (6.67 mg particle/mL distilled water) (n=8) or the sterile distilled water (control, n=8) were administered via oral gavage using a 22 gauge metal feeding tube (gavage needle) about 1.5 inches in length with a rounded tip. The dosing volume was 0.15 mL for a 15 g mouse (based on the recommended 10 mL/kg). Mice were administered 30-45 μm microparticle suspensions at a dose of 66.7 mg particle/kg body, which was 1 mg for a 15 g mouse. This dosing level was based on a minimum effective prophylactic treatment requiring a 1% increase in factor IX and assumed 2% bioavailability and a delivery potential of 3 μg hFIX/mg particle. The mouse was manually restrained and the proper length of the gavage tube was determined. A dose of either particle suspension or water was administered by a syringe attached to the end of the tube. After dosing, the tube was removed gently following the same angle as insertion. Each mouse was monitored for signs of labored breathing or distress for 5-10 minutes after oral gavage. Animals were monitored for the duration of the study. Twenty-four hours post administration, a urine sample was collected. The mice were then sacrificed by an overdose of CO_2 and then exsanguinated by heart stick.

For the long-term study, mice were fasted every other day in the morning for two hours prior to administration. As in the acute study, mice received either a microparticle suspension (6.67 mg particle/mL distilled water) (n=8) or the sterile distilled water (control, n=8) at a dosing volume of 0.15 mL via oral gavage. In addition to monitoring the mice for physical signs of labored breathing or distress, mice were weighted after each

administration. Mice received a dose of microparticle suspension or water every other day for 14 days (a total of seven doses). On day 15 (24 hours post the final administration), a urine sample was collected, and mice were then sacrificed by an overdose of CO_2 and then exsanguinated by heart stick.

8.2.3 Serum Cytokine Analysis

The serum cytokine analysis was performed using a Bio-Rad Bio-Plex Pro™ Assay (Hercules, CA) for mouse cytokines. The assay was selected for quantification of seven cytokines: interleukin-1β (IL-1β), IL-2, IL-6, IL-10, IL-12 (p70), interferon-γ (IFN-γ), and tumor necrosis factor-α (TNF-α). Serum samples were diluted 1:4 with sample diluent, and the assay was carried out according to the manufacturer's protocol. The wash steps were automated using a Bio-Rad Bio-Plex Pro™ wash station. The plate was read using low PMT voltage and low RPI target using the Bio-Rad Bio-Plex 200 multiplex system.

8.2.4 Blood Urea Nitrogen (BUN) Analysis

To assess kidney and level function, serum samples were analyzed to determine the blood urea nitrogen (BUN) using a Sigma-Aldrich urea assay kit. Serum samples were diluted 1:100 with assay buffer, and the assay was performed according to the manufacturer's protocol. In the urea assay, the amount of urea was determined by a coupled enzyme reaction that results in a colorimetric product. The absorbance at 570 nm was read using a BioTek Cytation 3 multi-mode reader (Winooski, VT).

8.2.5 Urine Creatinine Analysis

To determine the effect of the microparticles on the kidney function, the creatinine levels were evaluated. The amount of creatinine in the urine was determined using a Sigma-Aldrich creatinine assay kit. Urine samples were diluted 1:100 with assay buffer. The assay was performed following the manufacturer's protocol for fluorometric detection. After

incubating at 37°C for 60 minutes, the fluorescence was measured at 535 nm excitation and 587 nm emission using a BioTek Cytation 3 multi-mode reader (Winooski, VT).

8.2.6 Histological Analysis

Histological studies were performed for the long-term study to determine the effect of repeated dosing microparticles at the tissue level. The spleen, liver, kidneys, and GI tract (including stomach, small intestine, cecum, and large intestine) were removed from each animal. Organs were immersion-fixed in formalin at room temperature for at least 24 h. After fixing, each organ was cleaned up by removing any remaining fat and then was placed in a tissue cassette, and then dehydrated in 70% ethanol. The GI tract was split up into the stomach, small intestine (further sectioned into three pieces of equal length of 8-9 cm to represent the duodenum, jejunum, and ileum), and cecum with the ascending colon.

Tissues were embedded in paraffin, then sectioned using a microtome, and stained with hematoxylin and eosin (H&E). Embedding, sectioning, and staining were performed by the Histology/Immunohistochemistry Laboratory, Department of Pathology at UT Health Science Center San Antonio. The sections were also examined and scored blindly by Dr. Robert Reddick, MS, MD, Department of Pathology at UT Health Science Center San Antonio. Bright-field images of stained sections were captured using an Olympus IX 73 inverted microscope with the 4x objective.

8.2.7 Statistical Analysis

Data are reported as mean ± standard error. Comparisons between groups were performed using a Student's two-tailed t-test, and comparisons among multiple groups were performed using an ANOVA. Significant differences were considered when $*p < 0.05$ and $**p < 0.01$. All statistical analysis was computed using GraphPad Prism 6.

8.3 Results and Discussion

8.3.1 Oral Administration

The acute and long-term biocompatibility of P(MAA-g-EG) microparticles was assessed *in vivo* by the oral administration of microparticles in C57BL/6J mice. Mice were treated with a single dose of microparticles for the acute study and multiple doses given every other day for 14 days for the long-term study. The microparticles were administered via oral gavage to mimic the intended route of administration and to control the dose. When administered orally, the microparticles pass through the different regions of the GI tract where they are exposed to different physiological pH and enzymatic conditions. No differences in clinical signs (e.g. diarrhea, fever, or other systemic symptoms) between the experimental and control groups were observed, and no significant differences in body weight between the two groups were found. Additionally, there was no mortality over the course of the study.

8.3.2 Cytokine Analysis

In order to determine whether administration of P(MAA-g-EG) microparticle resulted in inflammation or an immune response, the serum levels of various cytokines (listed in Table 8-1) were quantified. No significant differences between the experimental and control groups were found. Based on the results from the cytokine analysis, administration of P(MAA-g-EG) microparticles did not cause an inflammatory or immune response for both a single dose and repeated doses. (See below for specific details about each cytokine).

Table 8-1. Cytokine analytes in the Bio-plex assay. (Note that MHC = major histocompatibility complex.)[6]

Cytokine	Source	Principle Target	Property	Principle Effects
IL-1β	Macrophages, LGLs, B cells, endothelium fibroblasts, astrocytes, etc.	T cells, B cells, macrophages, endothelium tissue cells	Pro-inflammatory	Lymphocyte activation, macrophage simulation, ↑ leukocyte/endothelial adhesion, pyrexia, acute phase proteins
IL-2	T cells	T cells	Hematopoietic, immune response, tolerance, immunity	T cell proliferation and differentiation, activation of cytotoxic lymphocytes and macrophages
IL-6	T cells, B cells, fibroblasts, macrophages	B cells, hepatocytes	Pro-inflammatory, hematopoietic	B cell differentiation, induces acute phase proteins
IL-10	T cells	Th 1 cells	Anti-inflammatory (pro-inflammatory from muscle)	Inhibition of cytokine synthesis
IL-12	Monocytes	T cells	Pro- or anti-inflammatory, anti-angiogenic	Induction of Th 1 cells
IFN-γ	T cells, NK cells, epithelia, fibroblasts	Leukocytes, tissue cells, Th 2 cells	Innate and adaptive immunity	MHC class I and II induction, macrophage activation, ↑ endothelial cell/lymphocyte adhesion. monocyte cytokine synthesis, antiviral state, anti-proliferation (Th2 cells)
TNF-α	Macrophages, mast cells, lymphocytes	Macrophages, granulocytes, tissue cells	Pro-inflammatory, innate immunity	Activation of macrophages, granulocytes and cytotoxic cells, leukocyte/endothelial cell adhesion, cachexia, pyrexia, induction of acute phase protein, stimulation of angiogenesis, enhanced MHC class I production

8.3.2.1 Interleukin-1β

IL-1β plays an important role in the innate and adaptive immunity. As a pro-inflammatory cytokine, IL-1 β is a crucial mediator of the host inflammatory response.[7] Results for both the acute and long-term studies show that oral administration of P(MAA-g-EG) microparticles did not affect IL-1β serum levels as compared to the control group (Figure 8-1). There are no significant differences IL-1β concentrations between the experimental and control groups in each study.

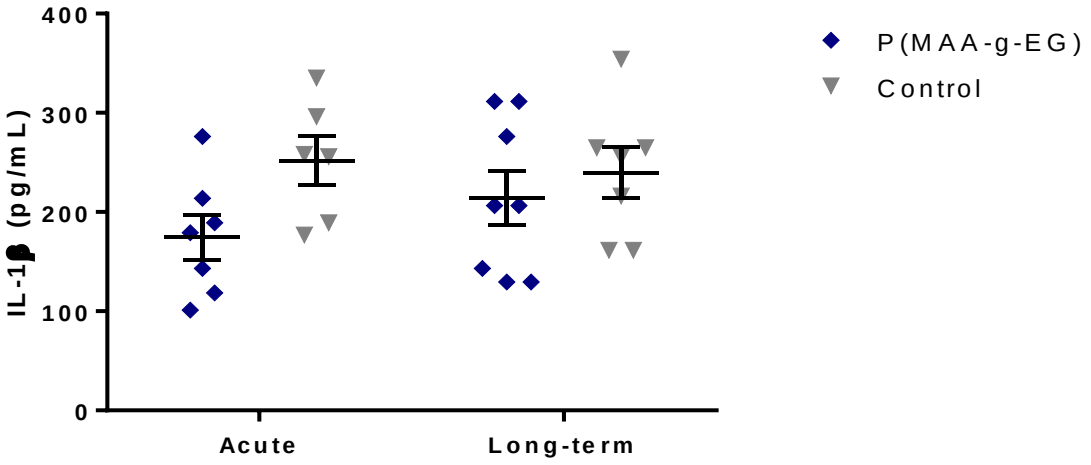

Figure 8-1. Serum concentrations of IL-1β for mice that received P(MAA-g-EG) microparticles or water (control) via oral gavage. For the acute study, mice received a single dose and serum was collected 24 h after. For the long-term study, mice received a dose every other day for 14 days and serum was collected 24 h after the final dose. (Points represent individual mice, mean ± SE).

8.3.2.2 Interleukin-2

IL-2 plays a variety of roles in the immune system related to immune response, tolerance, immunity, and hematopoiesis. IL-2 supports the proliferation and differentiation

of cells with high-affinity IL-2 receptors, such as stimulated T lymphocytes and T helper (T_H) cells. Binding of IL-2 to its specific receptors on T_H cells stimulated their proliferation along with the release of numerous cytokines. IL-2 is required for the generation of $CD8^+$ cytolytic T cells, which are important in antiviral responses. Additionally, IL-2 enhances the immune system's ability to kill tumor cells and may also interfere with blood flow to tumors.[7]

For both studies, the serum concentrations of IL-2 were not significantly different between the experimental and control groups (Figure 8-2). The administration of P(MAA-g-EG) microparticles did not affect the IL-2 levels which indicates that the microparticles do not produce an immune response.

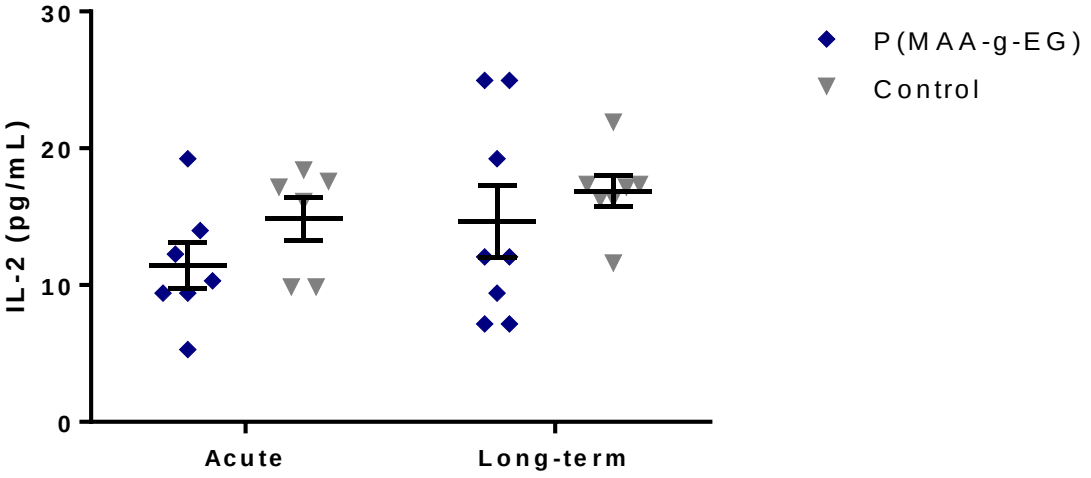

Figure 8-2. Serum concentrations of IL-2 for mice that received P(MAA-g-EG) microparticles or water (control) via oral gavage for both the acute and long-term studies. (Points represent individual mice, mean ± SE).

8.3.2.3 Interleukin-6

IL-6 is a pro-inflammatory cytokine that affects various processes including the immune response, reproduction, bone metabolism, and aging. IL-6 is produced in response to trauma, tissue damage, inflammation, IL-1, and TNF-α.[7] As shown in Figure 8-3, IL-6 serum levels remained unchanged after P(MAA-g-EG) microparticle administration, with no significant differences between the experimental and control groups for each study. The IL-6 concentrations indicate that there is no tissue damage nor inflammation after dosing of P(MAA-g-EG) microparticles.

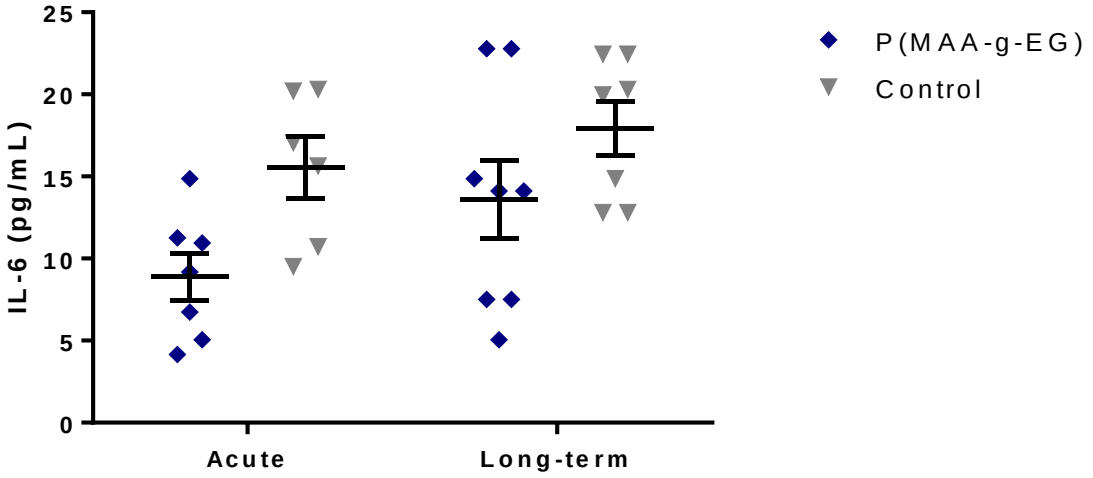

Figure 8-3. Serum concentrations of IL-2 for mice that received P(MAA-g-EG) microparticles or water (control) via oral gavage for both the acute and long-term studies. (Points represent individual mice, mean ± SE).

8.3.2.4 Interleukin-10

IL-10 is an anti-inflammatory cytokine and an important immunoregulatory cytokine. IL-10 inhibits the production of pro-inflammatory cytokines and augments the production of anti-inflammatory factors. The major role of IL-10 is to regulate the Th1/Th2 (cellular/humoral) balance. Additionally, IL-10 is involved in assisting against intestinal parasitic infection and local mucosal infection, and indirectly helps neutralize bacterial toxins.[7] Serum concentrations of IL-10 were not significantly affected by the single dose and multiple doses of P(MAA-g-EG) microparticles as compared to the control (Figure 8-4).

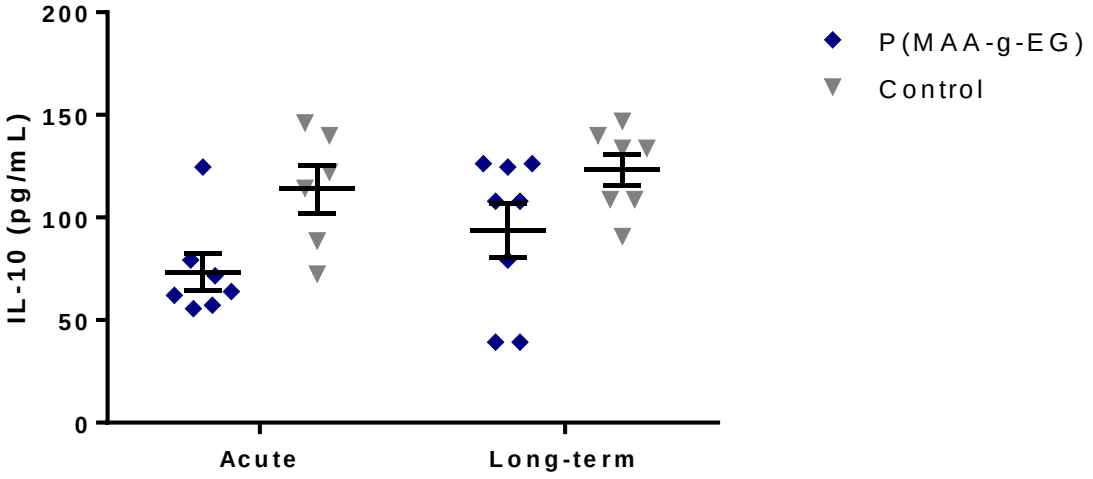

Figure 8-4. Serum concentrations of IL-10 for mice that received P(MAA-g-EG) microparticles or water (control) via oral gavage for both the acute and long-term studies. (Points represent individual mice, mean ± SE).

8.3.2.5 Interleukin-12

IL-12 has both pro- and anti-inflammatory effects. IL-12 induces the production of INF-γ which can mediate the pro-inflammatory activities of IL-12. Additionally, IL-12 has an important role in the Th1 response where it functions as an immunoregulatory cytokine. IL-12 promotes the differentiation of T helper 1 (T_H1) cells, forming a link between innate resistance and adaptive immunity.[8]. IL-12 is a heterodimer formed by a 35-kDa light chain (p35) and a 40-kDa heavy chain (p40), and the heterodimer form is denoted IL-12 (p70).[7] Similar to other interleukin serum levels, there were no significant differences in IL-12 concentrations between the experimental and control groups for each study (Figure 8-5).

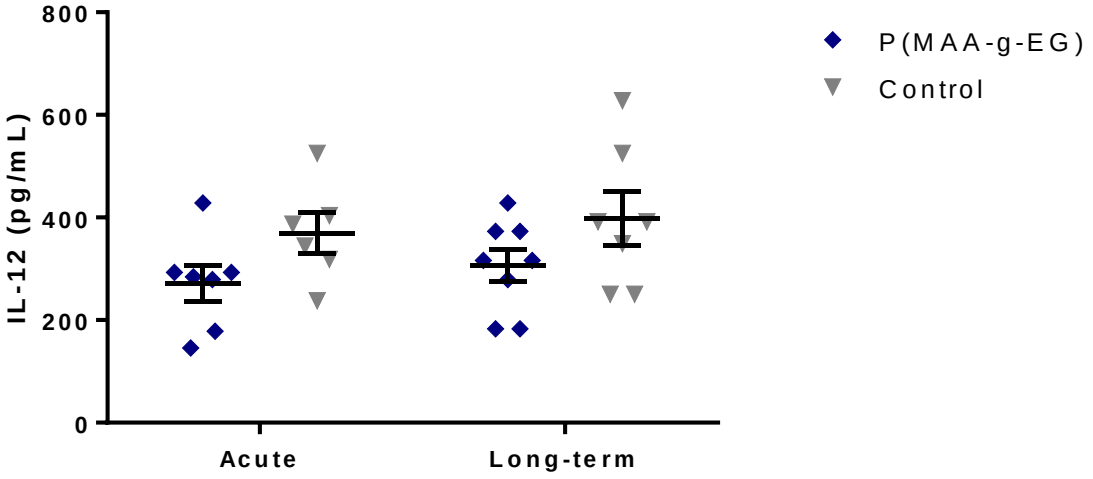

Figure 8-5. Serum concentrations of IL-12 for mice that received P(MAA-g-EG) microparticles or water (control) via oral gavage for both the acute and long-term studies. (Points represent individual mice, mean ± SE).

8.3.2.6 Interferon-γ

IFN-γ modulates various components in the immune response. IFN-γ is important for host response to intracellular pathogens by increasing cytotoxic T cell recognition and therefore promoting the induction of cell-mediated immunity. Produced from Th1 cells, IFN-γ favors a Th1 response by promoting innate cell-mediated immunity, specific cytotoxic immunity, and macrophage activation. IFN-γ induces Th1 differentiation and indirectly inhibits Th2 proliferation and differentiation. Additionally, IFN-γ induces key antiviral enzymes and such immunoregulatory activities of IFN-γ are important in establishing an antiviral state for longer term control.[9] The serum levels of IFN-γ for mice that received P(MAA-g-EG) microparticles were not significantly different from that of the control group in the same study (Figure 8-6).

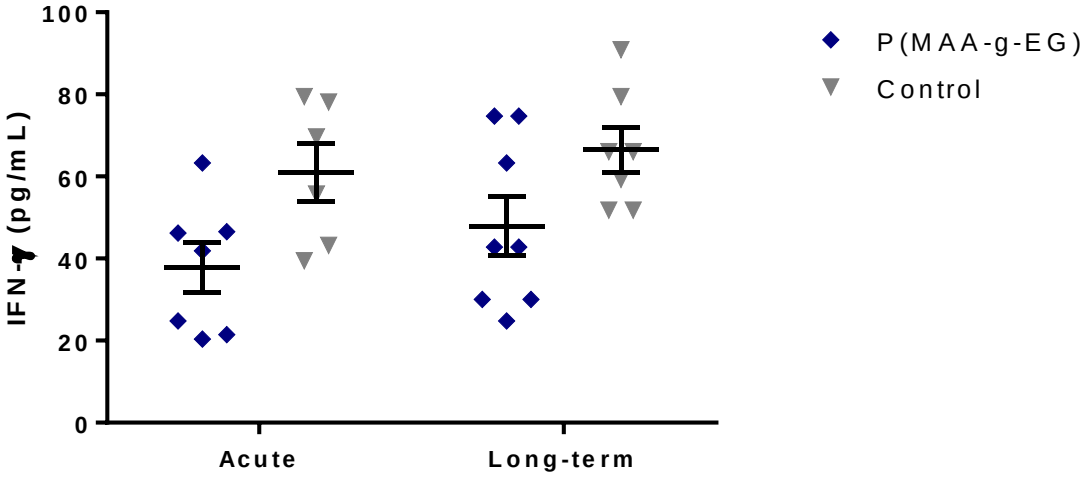

Figure 8-6. Serum concentrations of IFN-γ for mice that received P(MAA-g-EG) microparticles or water (control) via oral gavage for both the acute and long-term studies. (Points represent individual mice, mean ± SE).

8.3.2.7 Tumor Necrosis Factor-α

TNF-α is another pro-inflammatory cytokine that mediates the natural and acquired immunity. Although the main cell source of TNF-α is macrophage, it can also be produced as a result of tissue damage. Increased local concentrations of TNF-α cause heat, swelling, redness, and pain. TNF-α further causes an inflammatory response by inducing the production of pro-inflammatory cytokines (IL-1, IL-6, and itself) and chemokines through stimulation of macrophages. In response to an infection, TNF-α induces acute-phase responses by activating hepatocytes.[6, 7] Serum concentrations of TNF-α shown in Figure 8-7 indicate that administration of P(MAA-g-EG) microparticles did not induce an inflammatory response. For each study, no significant differences between the experimental and control groups were found.

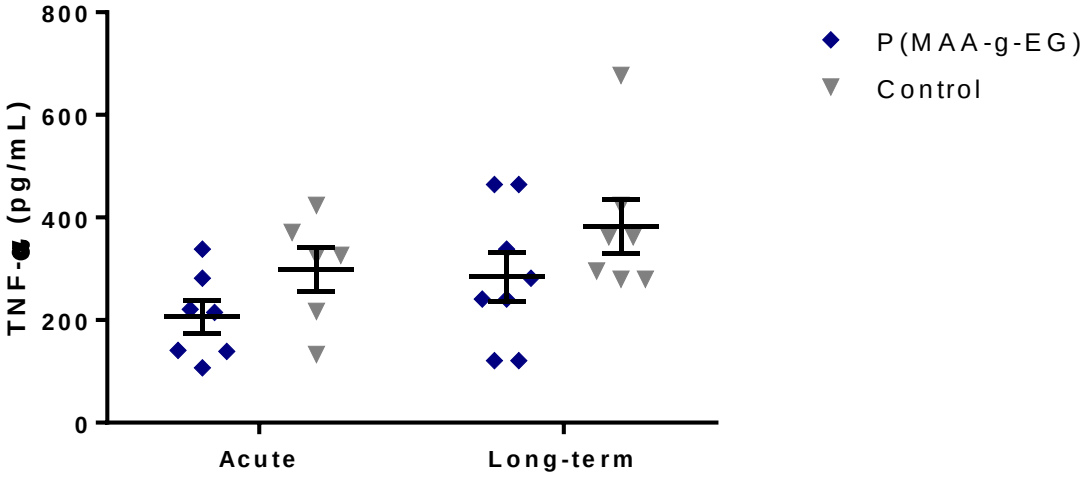

Figure 8-7. Serum concentrations of TNF-α for mice that received P(MAA-g-EG) microparticles or water (control) via oral gavage for both the acute and long-term studies. (Points represent individual mice, mean ± SE).

8.3.3 Blood Urea Nitrogen (BUN) Analysis

Urea is a major waste product of nitrogen metabolism and is produced from the urea cycle of the digestion of proteins in the liver. In the urea cycle, ammonia is converted to urea, which is dissolved in the blood and transported to the kidneys. Urea is then excreted by the kidneys as component of urine. High levels of urea in the blood may indicate renal failure. Other causes of elevated urea levels include decreased kidney filtration due to dehydration or congestive heart failure. Additionally, decreased blood urea levels can be indicative of liver disease or malnutrition.[10]

A blood urea nitrogen (BUN) test is commonly used to determine kidney health and, to a lesser extent, liver health.[10] We measured the amount of urea in serum samples from individual mice that were administered either P(MAA-g-EG) microparticles or water. The concentration of urea can be converted to BUN levels by:

$$BUN = [urea] \times \frac{2\ mmol\ N}{1\ mmol\ urea} \times MW_N \quad \text{(Eq. 8-1)}$$

where BUN is in units of mg dL^{-1}, the concentration of urea is in units of mmol dL^{-1}, molar ratio of nitrogen to urea is 2, and MW_N is the molar mass of nitrogen (14 mg $mmol^{-1}$).

Based in the BUN analysis shown in Figure 8-8, the oral administration of P(MAA-g-EG) microparticles does not affect renal function. Furthermore, repeated doses of P(MAA-g-EG) microparticles showed no negative signs of kidney and liver health. No significant differences between the experimental and control groups for each study were found.

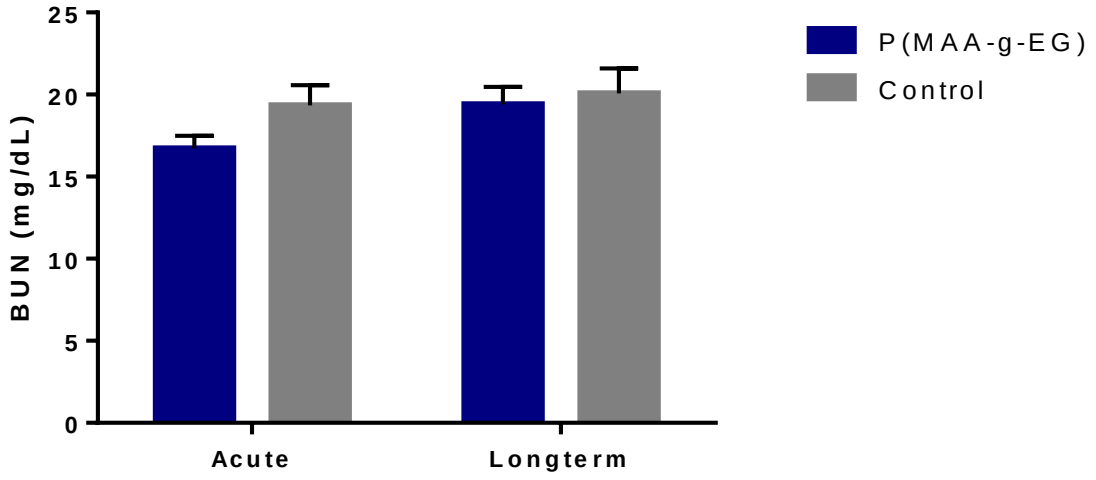

Figure 8-8. Blood urea nitrogen (BUN) concentrations for mice that received P(MAA-g-EG) microparticles or water (control) via oral gavage for both the acute and long-term studies. ($n \geq 7$, mean ± SE).

8.3.4 Creatinine Analysis

To further evaluate the effect of dosing P(MAA-g-EG) microparticles on renal function, we also quantified creatinine levels in urine samples. Creatinine is generated from creatine by nonenzymatic dehydration in muscles. Creatinine is produced at a fairly constant rate, depending on muscle mass, and is excreted from the body through kidney glomerular filtration.[10] Decreased kidney function can affect the filtration rate of creatinine, which can be used a measure of kidney health. In the case of decreased renal function, the inability of the kidneys to eliminate creatinine through urine excretion results in increased serum creatinine levels and decreased urine creatinine levels.[11]

Results from the creatinine analysis (Figure 8-9) indicate that kidney function is not affected by administration of P(MAA-g-EG) microparticles, which agrees with the findings from the BUN analysis. Urine creatinine levels of mice that received

microparticles showed no significant difference compared to that of mice in the control group. Both a single dose of microparticles and repeated doses over 14 days had no negative effects on renal function.

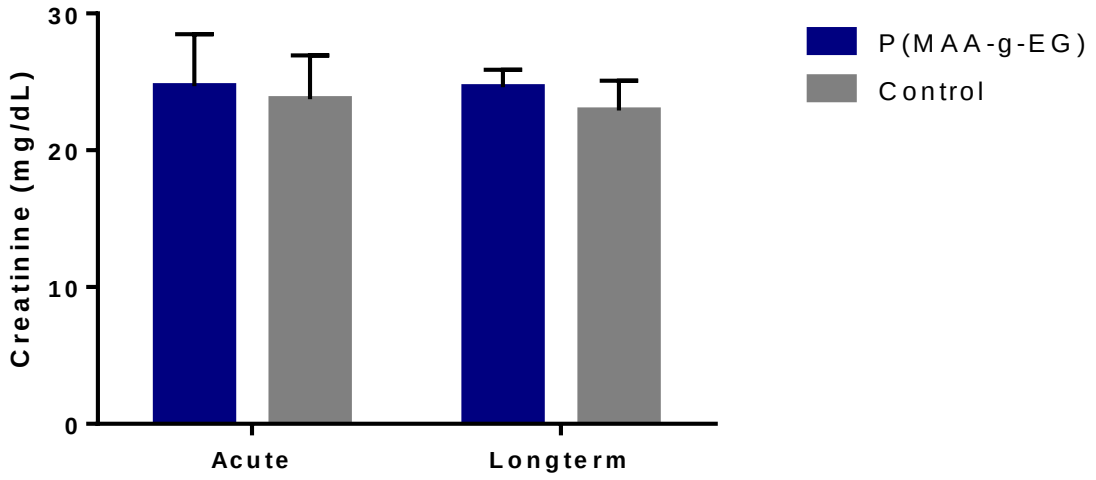

Figure 8-9. Urine creatinine concentrations for mice that received P(MAA-g-EG) microparticles or water (control) via oral gavage for both the acute and long-term studies. ($n \geq 7$, mean ± SE).

8.3.5 Histological Analysis

Although the administration of P(MAA-g-EG) microparticles show no signs of inflammation and immune response (cytokine analysis) and cause no negative effects on kidney and liver function (BUN and creatinine analysis), we evaluated the spleen, liver, kidney, and GI tract for any changes in tissue pathology due to long-term, repeated microparticle administration. In a blind study, a pathologist examined the tissue sections stained with H&E. Overall, the general appearance and morphology of the tissues from the experimental group were similar to that of the control group. Histological analysis

indicated that the repeated administration of P(MAA-g-EG) did not result in any tissue damage/inflammation, which agrees with the biochemical analysis. (Further analysis of the histology images can be found in Appendix B.)

8.3.5.1 Spleen

The two main functions of the spleen are filtration and immunological processing and destruction. Structurally, the spleen consists of the white pulp (contains lymphocytes) and red pulp (composed of sinusoids lined by macrophages).[12] A morphometric analysis of a rodent spleen is typically included in toxicity studies to determine changes in the cellular immune system.[13] According to the pathologist's examination, the findings for the spleen were normal. There was no evidence of morphological changes due to an immune response.

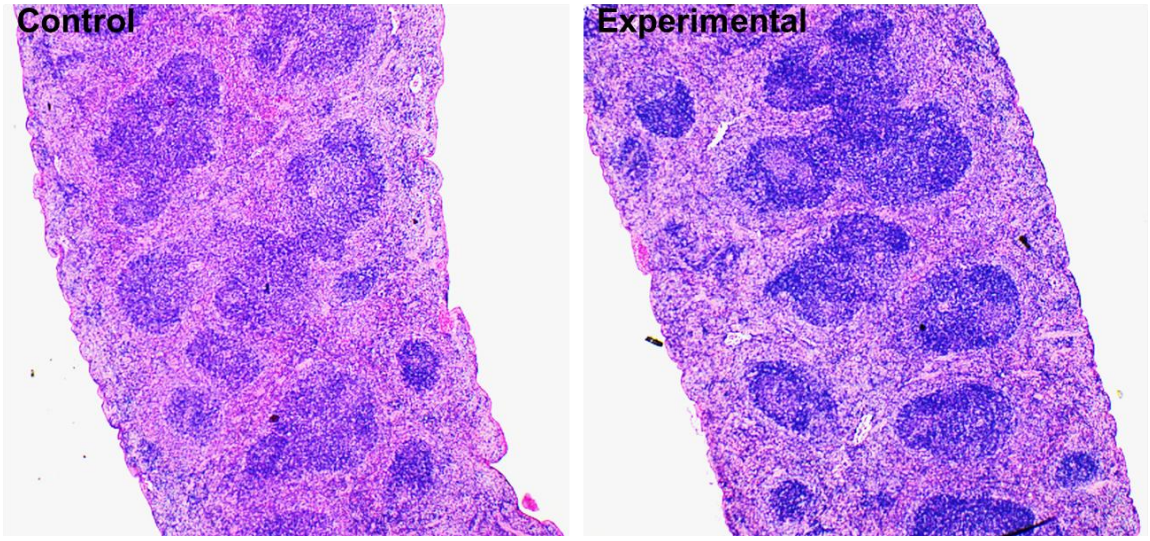

Figure 8-10. Representative images of spleen sections (H&E staining, magnification 4x) of mice that received water (control) and mice that were orally administered P(MAA-g-EG) microparticles (experimental).

8.3.5.2 Liver

The liver, which is the largest gland in the body, produces and secretes bile along with serving numerous metabolic functions for normal homeostasis.[14] Hepatocytes compose about 60% of the liver, and such cells have a polyhedral morphology with the six facets covered with microvilli.[13] For both the experimental and control groups, histological analysis showed normal liver architecture, as well as component of basic liver lobules with portal area (includes portal vein, hepatic artery, and small bile duct) and central venule (Figure 8-12).[15] Additionally, the pathologist noted the presence of focal small collections of chronic inflammatory cells, which is often seen in murine liver. Results indicated that repeated doses of P(MAA-g-EG) microparticles do not cause any liver damage.

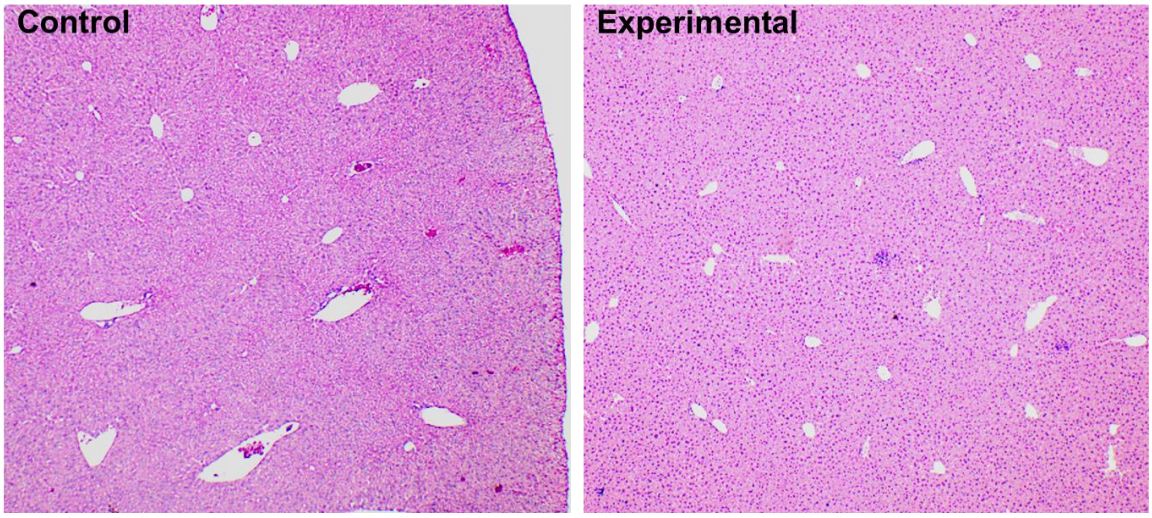

Figure 8-11. Representative images of liver sections (H&E staining, magnification 4x) of mice that received water (control) and mice that were orally administered P(MAA-g-EG) microparticles (experimental).

8.3.5.3 Kidney

As part of the urinary system, kidneys are responsible for filtration and waste excretion. Additional homeostatic functions of the kidneys include regulation of water-soluble molecules and electrolytes, maintenance of acid-base balance, and regulation of blood pressure. The kidneys are a frequent site of toxic injury in rodent toxicity studies. Renal toxicity in preclinical studies is a good predictor of adverse renal effects in patients.[13] In general, examination of the kidneys showed normal findings for both the experimental and control groups (Figure 8-12).

In addition to the normal findings, the pathologist noted a few cases of mild hydronephrosis. Hydronephrosis is the swelling of a kidney due to the build-up of urine caused by a blockage or obstruction. The histopathology of hydronephrosis show marked loss of renal parenchyma, which is more evident in severe cases. Additionally, characteristic morphology of hydronephrosis can be detected in the medullar area (innermost part of the kidney) showing dilation of tubules ad widened interstitial space with interstitial fluid.[16]

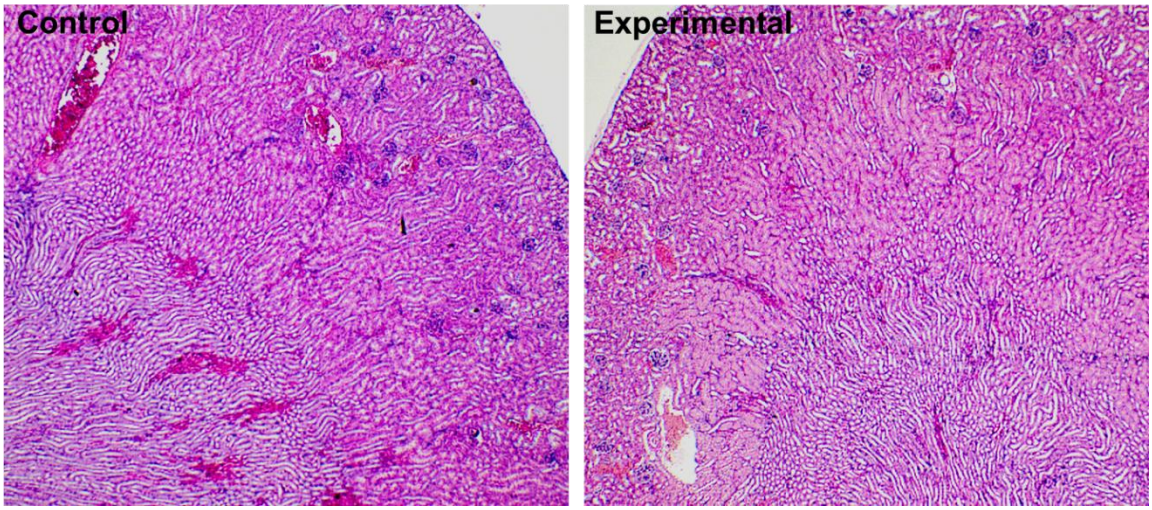

Figure 8-12. Representative images of kidney sections (H&E staining, magnification 4x) of mice that received water (control) and mice that were orally administered P(MAA-g-EG) microparticles (experimental).

8.3.5.4 Stomach

In the oral route of administration, the administered drug delivery system remains in contact with the stomach mucosa at relatively high concentrations for up to several hours. The mouse stomach contains two regions, a forestomach and a glandular stomach, which are separated by a limiting ridge (an elevated mucosal fold at the junction of the two regions). The forestomach, which receives the esophagus at the cardiac antrum, is lined by stratified squamous epithelium. Humans lack a forestomach, and therefore, the relevance of changes by drugs and their carrier systems in the rodent forestomach is disputed. The glandular stomach, which opens into the pylorus and duodenum, is covered by a columnar epithelium containing gastric glands. Gastric glands are tubular structures that are lined by columnar epithelium and form deep gastric pits. Additionally, the columnar epithelium of the mucosal surface contains mucus-secreting cells for protection against self-digestion.[13]

Safety studies in rodents can generally be used to predict adverse effects in patients.[13] Normal findings were reported for the forestomach (Figure 8-13) and glandular stomach (Figure 8-14) sections of mice from both the experimental and control groups, indicating that repeated exposure to P(MAA-g-EG) microparticles does not negatively affect the stomach.

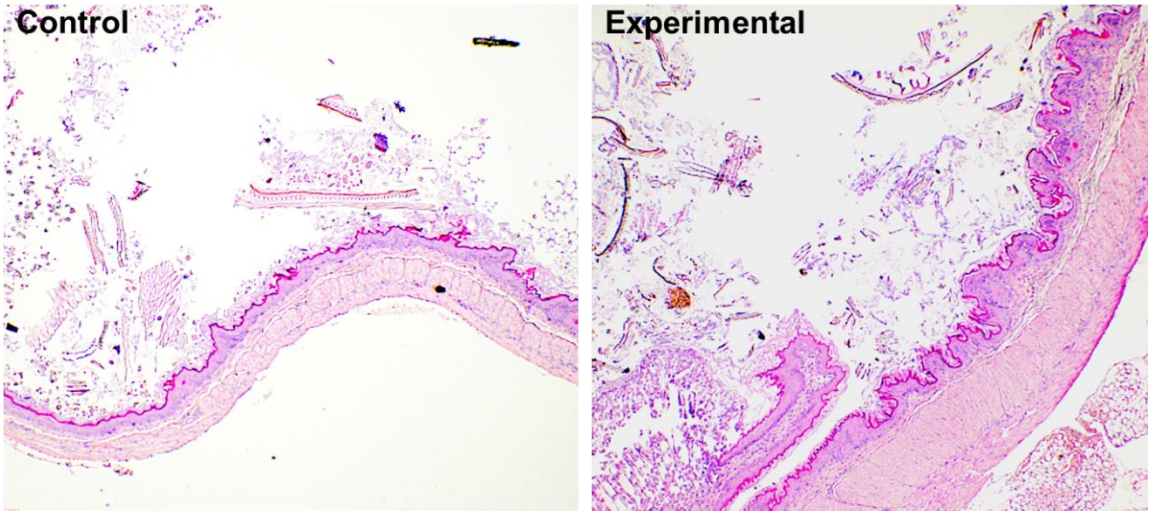

Figure 8-13. Representative images of forestomach sections (H&E staining, magnification 4x) of mice that received water (control) and mice that were orally administered P(MAA-g-EG) microparticles (experimental).

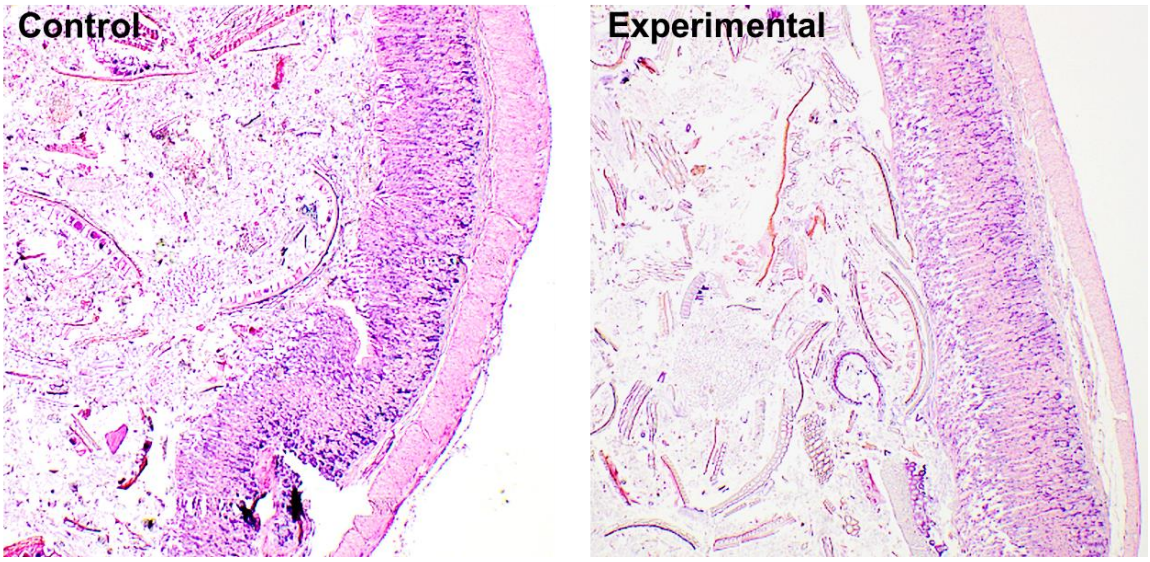

Figure 8-14. Representative images of glandular stomach sections (H&E staining, magnification 4x) of mice that received water (control) and mice that were orally administered P(MAA-g-EG) microparticles (experimental).

8.3.5.5 Small Intestine

The small intestine is particularly important in the safety evaluation of oral drug delivery systems. In the case the P(MAA-g-EG) system, the residence time in the small intestine is increased due to PEG tethers. Generally, gastrointestinal findings in preclinical studies in rodents are reasonable predictors of gastrointestinal adverse effects in patients.[13] The main cell population of the epithelium is absorptive enterocytes with microvilli on the apical surface, allowing the small intestine to function as an absorptive surface. However other epithelial cell types, mucous (goblet) cells, Paneth cells, and endocrine cells are also present and serve important functions. Additionally, the small intestinal mucosa functions as a barrier to potentially pathogenic substances and micro-organisms. The gut associated lymphoid tissue (GALT) plays an important role of the protective system in the intestine. Peyer's patches are prominent aggregates of lymphoid tissue. In humans, Peyer's patches

are more common in the ileum, but in mice, they are more uniformly distributed.[17] In Peyer's patches, lymphoid follicles are surrounded by a corona of small lymphocytes, principally B cells, and the overlaying epithelium (dome area) contains specialized epithelial cells called microfold (also membranous or M) cells.[13]

Histologically, the mucosa of the small intestine forms villi (finger-like projections) ad crypts (deep cavities between the villi).[18] For the histological analysis, small intestine was divided into three sections—duodenum, jejunum, and ileum. The duodenum is characterized by tall, left-shaped villi and the submucosal Brunner's glands. The mucosa of the duodenum is thick and forms permanent circular fold (plicae circulares). About halfway along the length of the duodenum, there are openings of common bile and pancreatic ducts in the medial wall. The jejunum and ileum are more histologically similar with minor differences in villi structure. In the jejunum, the villi are tall and cylindrical, while the villi are short and cylindrical in the ileum. Generally, the jejunum tends to be thicker-walled with more prominent plicae circulares and more numerous Peyer's patches than the ileum.[14] In mice, Paneth cells with very prominent granules are especially found in the jejunum.

Examination of H&E stained sections of the duodenum (Figure 8-15), jejunum (Figure 8-16), and ileum (Figure 8-17) showed normal findings for both experimental and control groups. The absence of villae and crypts would be indicative of toxicity or damage to the small intestine,[19] which is not the case for results presented here. However, lymphoid nodules along the small intestine were noted. As previously mentioned, Peyer's patches (aggregates of lymphoid tissue) are commonly distributed along the small intestine. Histologically findings indicated that repeated dosing of P(MAA-g-EG) microparticles does not cause inflammation of the small intestine, which is critical for its application as an oral drug delivery vehicle.

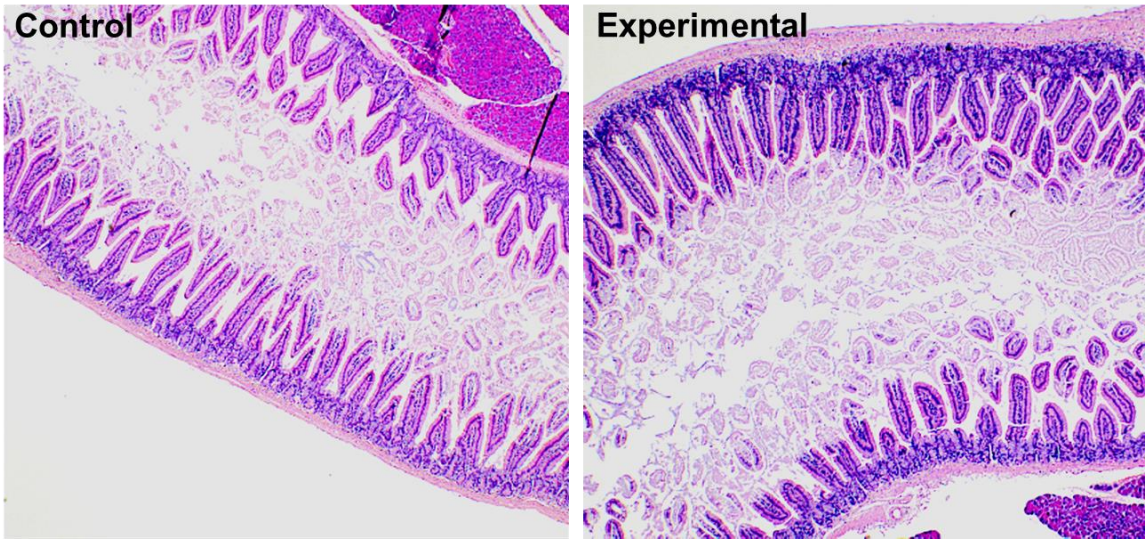

Figure 8-15. Representative images of duodenum sections (H&E staining, magnification 4x) of mice that received water (control) and mice that were orally administered P(MAA-g-EG) microparticles (experimental).

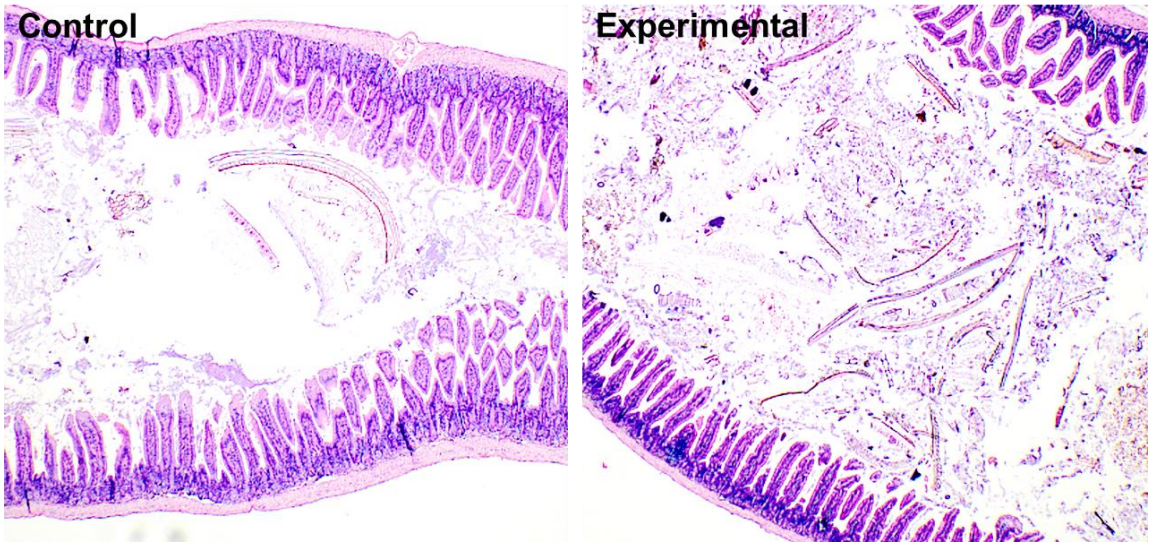

Figure 8-16. Representative images of jejunum sections (H&E staining, magnification 4x) of mice that received water (control) and mice that were orally administered P(MAA-g-EG) microparticles (experimental).

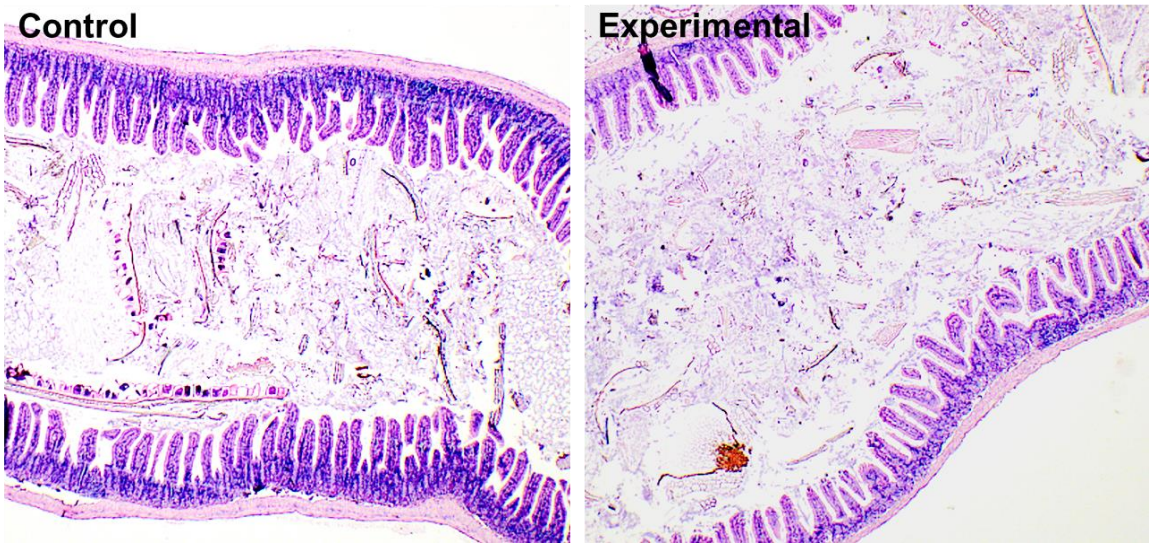

Figure 8-17. Representative images of ileum sections (H&E staining, magnification 4x) of mice that received water (control) and mice that were orally administered P(MAA-g-EG) microparticles (experimental).

8.3.5.6 Cecum and Colon

The large intestine of mice consists of the cecum, colon (ascending colon), and rectum (descending colon), where there is a lack of clearly defined transverse colon and an appendix as found in humans. The cecum of humans is a small diverticulum, but the enlarged cecum in mice is necessary for the breakdown of cellulose due to their omnivorous diets. The cecum, which is a kidney-shaped pouch, functions as a fermentation organ.[13] Histologically, the cecum and colon are lined by a relatively uniform mucosa distinctly without villi. The mucosa of the cecum is thin with short crypts and transverse folds, while the mucosa of the colon has long crypts and forms longitudinal folds.[13, 14]

Safety evaluation in rodents does not always indicate safety in humans. While some substances do not show inflammation in mice, they may still result in an inflammatory response in humans. However, inflammation is mice is typically predictive of a similar

response in humans.[13] Histologically, the cecum (Figure 8-18) and the colon (Figure 8-19) of mice from the experimental group were not different from the normal tissues from the control group. Similar to previously discussed results, the repeated dosing of P(MAA-g-EG) microparticles does not cause inflammation in the large intestine.

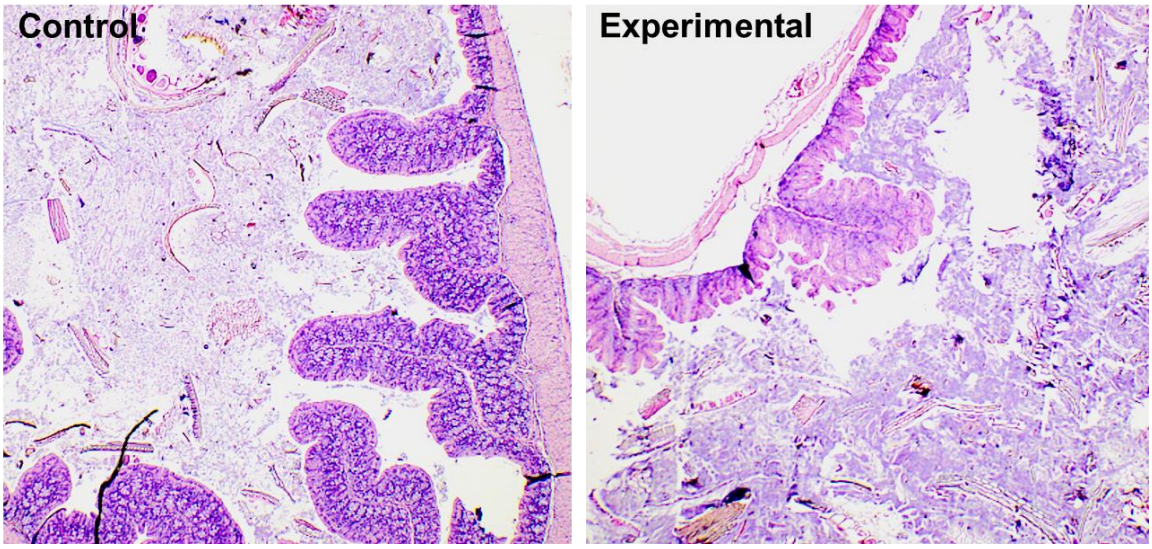

Figure 8-18. Representative images of cecum sections (H&E staining, magnification 4x) of mice that received water (control) and mice that were orally administered P(MAA-g-EG) microparticles (experimental).

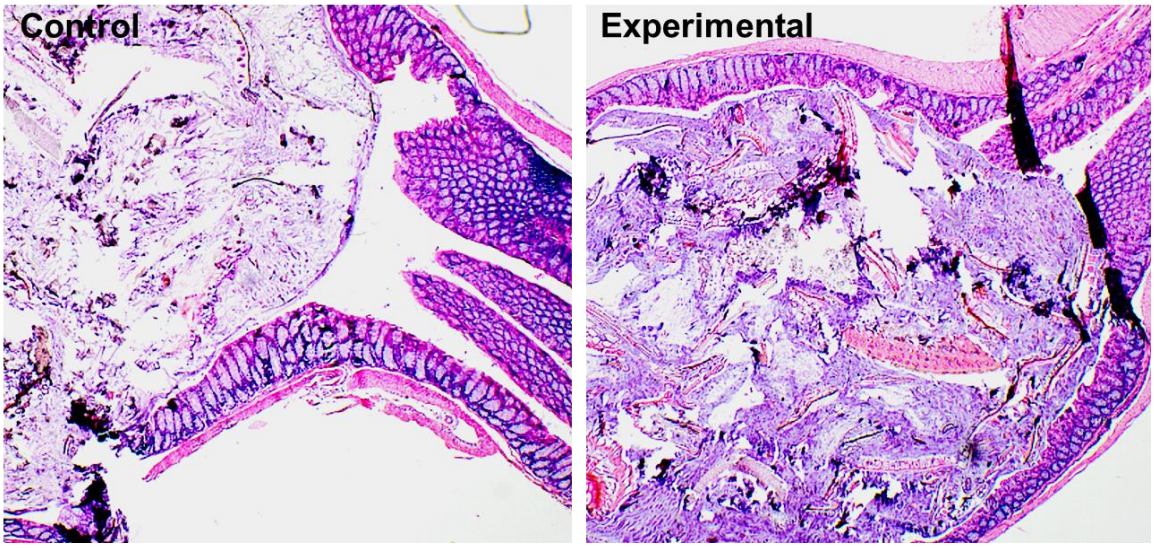

Figure 8-19. Representative images of colon sections (H&E staining, magnification 4x) of mice that received water (control) and mice that were orally administered P(MAA-g-EG) microparticles (experimental).

8.4 CONCLUSIONS

Developing an orally administered hFIX therapy for the treatment of hemophilia B requires the use of a drug delivery system. As previously discussed, P(MAA-g-EG) hydrogel microcarriers have been designed for protection of hFIX in the stomach and site-specific release of hFIX in the small intestine. While such systems have been evaluated in *in vitro* cytocompatibility studies, an evaluation of the *in vivo* biocompatibility is critical for establishing the clinical safety of P(MAA-g-EG) microparticles. Based on cytokine levels, the short-term and long-term administration of P(MAA-g-EG) microparticles did not cause any inflammatory reactions or immune response. Biochemical analysis (BUN and creatinine concentrations) indicated that the microparticles had no effects on kidney and liver health. Further histological examination of the spleen, liver, kidneys, and GI tract supported the findings of the cytokine and biochemical analyses. Based on the results

reported here, P(MAA-g-EG) microparticles are biocompatible *in vivo* and are safe for long-term, repeated use necessary for prophylactic regimens in protein replacement therapy applications.

8.5 REFERENCES

1. Peppas, N. A.; Horava, S. D., Polymers for Delivery of Factor VIII and/or Factor IX. [Patent Pending].
2. Horava, S. D.; Peppas, N. A., Design of pH-Responsive Biomaterials to Enable the Oral Route of Hematological Factor IX. *Annals of Biomedical Engineering* **2016**, 1-13.
3. Kunzmann, A.; Andersson, B.; Thurnherr, T.; Krug, H.; Scheynius, A.; Fadeel, B., Toxicology of engineered nanomaterials: focus on biocompatibility, biodistribution and biodegradation. *Biochimica et Biophysica Acta (BBA)-General Subjects* **2011**, *1810* (3), 361-373.
4. Golla, K.; Reddy, P. S.; Bhaskar, C.; Kondapi, A. K., Biocompatibility, absorption and safety of protein nanoparticle-based delivery of doxorubicin through oral administration in rats. *Drug delivery* **2013**, *20* (3-4), 156-167.
5. Sonaje, K.; Lin, Y.-H.; Juang, J.-H.; Wey, S.-P.; Chen, C.-T.; Sung, H.-W., In vivo evaluation of safety and efficacy of self-assembled nanoparticles for oral insulin delivery. *Biomaterials* **2009**, *30* (12), 2329-2339.
6. Male, D. K., Immunology. Elsevier/Saunders: United States, **2013**; Vol. 8th.
7. Khan, M. M., Immunopharmacology. Springer: New York, **2008**.
8. Trinchieri, G., Interleukin-12 and the regulation of innate resistance and adaptive immunity. *Nature Reviews Immunology* **2003**, *3* (2), 133-146.
9. Schroder, K.; Hertzog, P. J.; Ravasi, T.; Hume, D. A., Interferon-γ: an overview of signals, mechanisms and functions. *Journal of leukocyte biology* **2004**, *75* (2), 163-189.
10. Gowda, S.; Desai, P. B.; Kulkarni, S. S.; Hull, V. V.; Math, A. A.; Vernekar, S. N., Markers of renal function tests. *N Am J Med Sci* **2010**, *2* (4), 170-173.
11. Zuo, Y.; Wang, C.; Zhou, J.; Sachdeva, A.; Ruelos, V. C., Simultaneous determination of creatinine and uric acid in human urine by high-performance liquid chromatography. *Analytical Sciences* **2008**, *24* (12), 1589-1592.

12. Cesta, M. F., Normal structure, function, and histology of the spleen. *Toxicologic pathology* **2006**, *34* (5), 455-465.

13. Greaves, P. M. B. C. B.; NetLibrary, I., Histopathology of preclinical toxicity studies: interpretation and relevance in drug safety evaluation. Academic Press: Amsterdam, **2007**; Vol. 3rd;4th;3;4;.

14. Cameron, R. I.; Allen, D. C.; NetLibrary, I., Histopathology specimens: clinical, pathological and laboratory aspects. Springer: New York;London;, **2004**.

15. Baratta, J. L.; Ngo, A.; Lopez, B.; Kasabwalla, N.; Longmuir, K. J.; Robertson, R. T., Cellular organization of normal mouse liver: a histological, quantitative immunocytochemical, and fine structural analysis. *Histochemistry and cell biology* **2009**, *131* (6), 713-726.

16. Seseke, F.; Thelen, P.; Hemmerlein, B.; Kliese, D.; Zöller, G.; Ringert, R., Histologic and molecular evidence of obstructive uropathy in rats with hereditary congenital hydronephrosis. *Urological research* **2000**, *28* (2), 104-109.

17. Cornes, J., Number, size, and distribution of Peyer's patches in the human small intestine: Part I The development of Peyer's patches. *Gut* **1965**, *6* (3), 225.

18. Treuting, P. M.; Dintzis, S. M., Comparative Anatomy and Histology: A Mouse and Human Atlas. Academic Press: US, **2012**; Vol. Expert Consult: Online and Print.

19. Paris, F.; Fuks, Z.; Kang, A.; Capodieci, P.; Juan, G.; Ehleiter, D.; Haimovitz-Friedman, A.; Cordon-Cardo, C.; Kolesnick, R., Endothelial apoptosis as the primary lesion initiating intestinal radiation damage in mice. *Science* **2001**, *293* (5528), 293-297.

Chapter 9: In Vivo Biodistribution of P(MAA-g-EG) Microcarriers[5]

9.1 INTRODUCTION

The oral delivery of factor IX is a highly desirable alternative to needle-based options for prophylactic therapy for hemophilia B patients. We have developed pH-responsive P(MAA-g-EG) microcarriers to enable the oral route of factor IX.[1, 2] For eventual clinical applications, understanding the biodistribution and clearance of microcarriers is important. Visualizing the passage of the microparticles through the GI tract provides critical details about the residence time in the small intestine as well as the time scale for clearance. The residence time in the small intestine affects the local concentration of the protein released, which will in turn affect the amount of protein in circulation. Increased residence time in the small intestine due to the mucoadhesive properties of the microparticles can improve the bioavailability of the therapeutic protein. Knowledge of the kinetic distribution of the microparticles in the GI tract can also provide insight into the pharmacokinetics of an orally administered drug using such microcarriers.

An *in vivo* model is required to validate the performance of an oral delivery system. The IVIS® *in vivo* imaging system (PerkinElmer, Inc., Hopkinton, MA) allows for *in vivo* real-time imaging without radiation. This non-invasive method allows for visualization and quantification of microparticles moving through the GI tract after oral delivery.[3] Alternative *ex vivo* techniques, such as an everted rat intestinal sac, can be used to determine mucoadhesive properties of orally delivered microparticles. However, differences in the *ex vivo* and *in vivo* extracellular environments, as well as differences due

[5] The *in vivo* biodistribution studies presented here were conducted as part of a study testing the safety of three hydrogel formulations. The biodistribution studies were performed by the author and Stephanie Steichen.

to the segmentation of the intestine, result in inaccuracies and may fail to predict what occurs *in vivo*.[3]

In this Chapter, we determined the *in vivo* biodistribution of P(MAA-g-EG) microparticles post oral administration using a mouse model. Fluorescently-tagged P(MAA-g-EG) microparticles were tracked over time using the IVIS® *in vivo* imaging system. Furthermore, the specific location of the microparticles along the GI tract were evaluated by removing and imaging the GI tract.

9.2 Materials and Methods

9.2.1 Polymer Synthesis

P(MAA-g-EG) hydrogels were synthesized by bulk UV-polymerization as previously described in Chapter 4. Briefly, the feed composition of the pre-polymer was MAA and PEGMMA1000 at a 2:1 molar ratio of hydrogen bonding groups, PEGDMA1000 at 1.0 mol% of total monomers, and Irgacure 184® at 1.0 wt. % of total monomers in a 1:1 (w/w) mixture of deionized water and ethanol. After sonicating for 20 minutes, the pre-polymer mixture was needle purged with nitrogen for 5 minutes in the nitrogen-rich environment of a glove box. The mixture was then dispensed between two quartz glass plates, separated with a 0.7 mm Teflon® spacer, and then polymerized for 30 minutes under 35 mW cm^{-2} UV light using a UV flood source. After synthesis, the resulting polymer was removed from the plates, and then washed in deionized water for a total of 10 water exchanges. The polymer was dried for 3 days in air and then for 3 additional days under vacuum at 37°C. Dried films were crushed and sieved into microparticles, sized 30-45 μm.

9.2.2 Quantum Dot-Microparticle Conjugation

After synthesis, microparticles were fluorescently labeled with near-infrared (NIR) quantum dots (QD) for biomedical imaging. Using NIR (700-1000 nm) light for *in vivo* imaging eliminates the auto-fluorescence of tissue. Furthermore, QDs are preferential to organic fluorophores due to their resistance to photobleaching.[4] Microparticles were surface decorated with carboxyl QDs (Qdot® 705 ITK Carboxyl Quantum Dots, Life Technologies, Carlsbad, CA) via EDC-NHS chemistry using an ethylene diamine linkage (Figure 9-1).

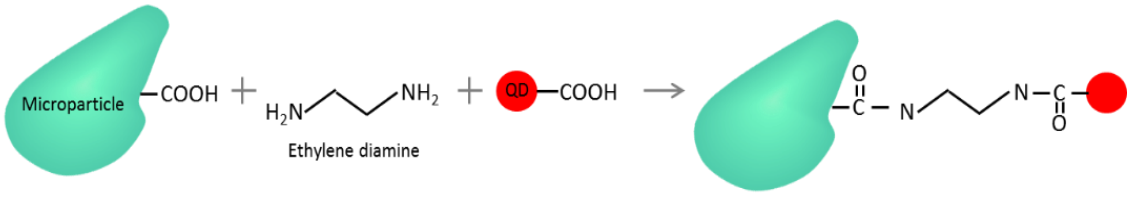

Figure 9-1. Simplified schematic of the QD-microparticle conjugation.

The carboxyl QDs were first conjugated with ethylene diamine via EDC chemistry to add a prime amine to the QDs. Ethylene diamine and EDC where added at a 1:80:3000 molar ratio of QD:ethylene diamine:EDC to a QD solution in 10 mM borate buffer (pH 7.4), and the mixture was allowed to react for 1 h at room temperature while constantly stirring. After 1 h, the conjugate solution was filtered through a 0.2 µm PES syringe filter to remove any aggregates. Then the solution was transferred to a centrifugal ultrafiltration unit (10 kDa cutoff) and centrifuged for 10 minutes at 4696 x g. To remove any unbound ethylene diamine, the solution was purified by six buffer exchanges of 50 mM borate buffer (pH 8.3), added at 10-fold volume concentration, and centrifugation cycles. Immediately after the final ultracentrifugation, the solution was filtered through a 0.8/0.2 µm

combination PF syringe filter to remove any aggregates. The primary amine functionalized QD solution was stored at 4°C until further use.

Separately, the carboxylic acids groups on the P(MAA-g-EG) microparticles were activated by EDC-NHS chemistry. Based on titration results previously reported, the amount of carboxylic acid (COOH) groups is approximately 1 x 10^{-5} mol COOH/mg microparticle. EDC and NHS were added at a molar ratio of 1.5:1:1 NHS:EDC:COOH in deionized water (pH 5.0), and the mixture was allowed to react for 30 minutes at room temperature under constant rotation. After the 30 minute incubation, the activated particles were collected by centrifugation at 8000 x g for 5 minutes, and the supernatant was removed. To further remove any excess EDC and NHS, the microparticles were resuspended in 50 mM MES buffer (pH 5.0) and centrifuged for three cycles.

Immediately after carboxylic acid activation, the microparticles were conjugated with QDs. The primary amine functionalized QDs were added at 0.025 nmol QD/mg microparticle (1.33 x 10^{-6} mol QD/mol COOH) to the activated microparticles in a 50 mM MES buffer (pH 5.0). The coupling reaction was allowed to proceed for 10-12 h at room temperature under constant rotation. After the incubation, the QD-conjugated particles were collected by centrifugation at 8000 x g for 5 minutes, and the supernatant was removed. To remove any unbound QDs, 1x PBS with 0.05 (v/v) % Tween-20 was added to the microparticles, then vortexed for 30 seconds, and centrifuged. This wash step was repeated a total of three times. A second wash step with distilled water was completed at least three times. The QD-conjugated microparticles were stored in distilled water at 4°C until further use.

9.2.3 Animals and Treatment

Female C57BL/6J mice (4-6 weeks old) were purchased from The Jackson Laboratory. We selected C57BL/6J mice since the hemophilia B mice are derived from this background. Adult mice entered the UT animal facility in the ARC building and were given at least three days to acclimate themselves to their new environment. Upon arrival mice were housed five per cage, and mice received ear punches as an identification marker. Mice were feed an alfalfa-free diet (2019 Teklad Global 19% Protein Extruded Rodent Diet) for at least 4 days prior to the imaging study to reduce intestinal auto-fluorescence.[5, 6]

Prior to administration, mice were fasted by the removal of solid food in the morning for two hours. The microparticle suspension (6.67 mg particle/mL distilled water) (n=3) for each time point were administered via oral gavage using a 22 gauge metal feeding tube (gavage needle) about 1.5 inches in length with a rounded tip. The dosing volume was 0.15 mL for a 15 g mouse (based on the recommended 10 mL/kg). Based on the dosing for the safety studies, mice were administered 30-45 μm microparticle suspensions at a dose of 66.7 mg particle/kg body, which was 1 mg for a 15 g mouse. Additionally, a control group (n=3) was included in the study, where mice received 0.15 mL of distilled water via oral gavage. The mouse was manually restrained and the proper length of the gavage tube was determined. A dose of either microparticle suspension or water was administered by a syringe attached to the end of the tube. After dosing, the tube was removed gently following the same angle as insertion. Each mouse was monitored for signs of labored breathing or distress for 5-10 minutes after oral gavage. Animals were monitored for the duration of the study.

9.2.4 IVIS Live Imaging

Mice were imaged over the course of 24 h post administration. In mice, the gastric emptying time is 1-2 hours and the clearance time of the small intestine is 1-4 hours after gastric emptying.[7] Mice were imaged at 1.5 h post administration to confirm that microparticles were localized in the stomach. To determine the residence time of the microparticles in the small intestine, mice were imaged at 4 h and 7 h post administration. Mice were also imaged at 24 h to ensure clearance. For each time point, three individual mice were imaged, and then sacrificed for further image analysis. The control mice were imaged 4 h post administration of water.

Mice were anesthetized 20 minutes prior to the pre-designated imaging time points. Mice were first placed in an induction chamber using 2% isoflurane-mixed oxygen, and then moved to nose cones, placed on their backs, in the IVIS imaging system. While under anesthesia, hair from the abdominal region was removed with depilatory cream (Nair) to reduce the light scattering/block effect.[8] Fluorescent images were captured using the spectral unmixing protocol for QD705 (excitation at 640 nm and emission at 700, 720, 740, 760, 780, and 800 nm) and a 5 second exposure. Additionally, photographs were captured. After imaging, mice were euthanized with an overdose of CO_2, and the secondary measure was a bilateral thoracotomy.

9.2.5 IVIS Imaging of Organs

Immediately after sacrifice, the GI tract (starting at the stomach and ending at the colon), liver, and kidneys were removed and subsequently imaged using the IVIS. The GI tract was imaged to determine the location and distribution of microparticles along the length of the GI tract. The liver and kidneys were also imaged to confirm that the microparticles were confined to the GI tract and were not accumulating in these organs. Fluorescent images were captured using the spectral unmixing protocol for QD705

(excitation at 640 nm and emission at 700, 720, 740, 760, 780, and 800 nm) and a 5 second exposure. Additionally, photographs were captured.

9.2.6 Image Processing

The fluorescent signal was converted to radiant efficiency with units of $(p/sec/cm^3/sr)/(\mu W/cm^2)$. A common scale (minimum radiant efficiency = 1.00e7 and maximum = 1.50e8) was used to compare all images of the organs.

9.3 Results and Discussion

9.3.1 QD-Microparticle Conjugation

After conjugation of the QDs to the surface of the P(MAA-g-EG), the series of washes were completed until the supernatant was visible clear. The fluorescence (excitation at 640 nm and emission at 740) of a sample of QD-microparticles was confirmed using a BioTek Cytation 3 multi-mode reader (Winooski, VT).

9.3.2 IVIS Live Imaging

Visualizing the transit of the microparticles through the GI tract after administration is critical for determine the residence time of the microcarriers in the small intestine (target site of drug delivery) and their clearance time. Images of the abdominal region of live mice were collected at 1.5, 4, 7, and 24 h post administration of QD-conjugated microparticles. A representative image shows the microparticles are localized in the abdominal region 4 h post administration (Figure 9-2). However, the exact location of the microparticles cannot be discerned from the live mice images. Similar images were collected for all time points, and the location of the microparticles along the GI was further determined by removal of the relevant organs.

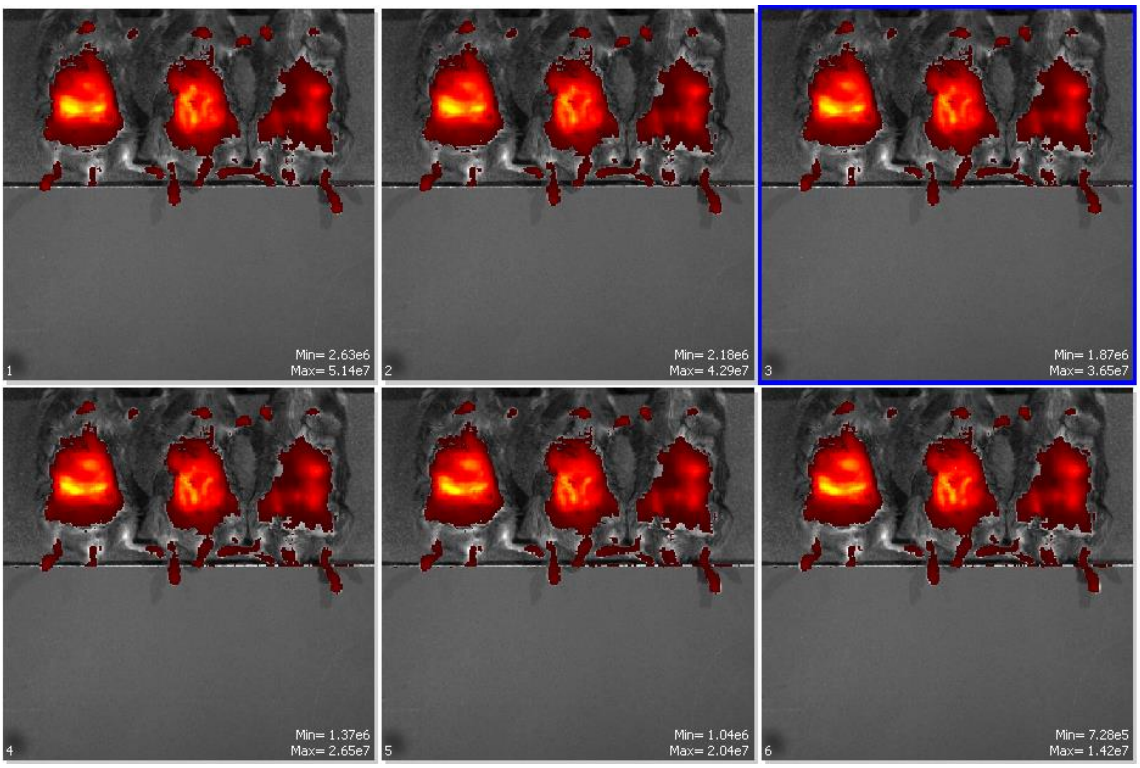

Figure 9-2. Images of an overlap of the fluorescent image and photograph of live mice taken 4 h post administration of QD-conjugated microparticles at an excitation of 640 nm. The different images are shown with different emission filters at 700, 720, 740, 760, 780, and 800 nm.

Additionally, some mice had skin pigmentation (darkened areas, dark gray/black color) which interfered with the live imaging. For example, the right mouse in Figure 9-2 had pigmented skin. The growth phase of the hair affects the skin pigmentation. In the anagen phase (active hair growth), the darkened skin color is from the melanin in the hair follicles in that area.[9]

9.3.3 Imaging of Organs

In order to locate the microparticles along the GI tract, the GI tract from the stomach to the colon was removed and imaged. Additionally, the liver and kidneys were removed and imaged. Figure 9-3 shows the labeled organs.

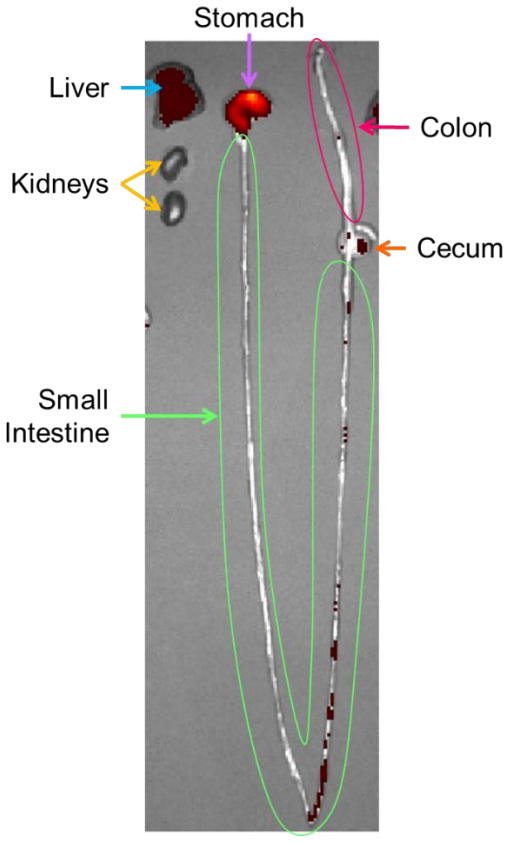

Figure 9-3. Image of organs labelled for the liver, kidneys, stomach, small intestine, cecum, and colon.

As shown in Figure 9-4, the mice administered distilled water (blank) have a low fluorescent signal in the stomach, indicating that the stomach has auto-fluorescence. Additionally, the low fluorescent signal (indicated by dark red) in the lower GI tract is

likely due to auto-fluorescence. The kidneys show no fluorescent signal, while the liver sections have a low fluorescent signal, likely due to auto-fluorescence.

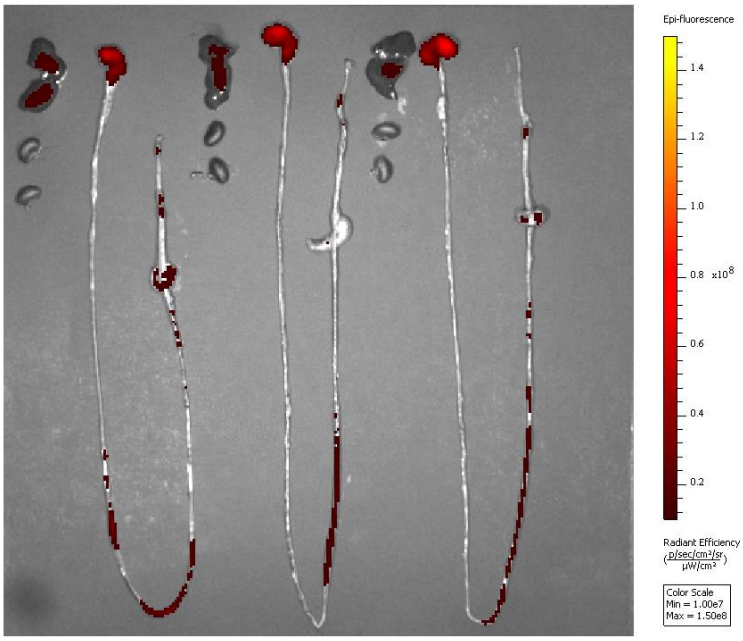

Figure 9-4. Fluorescent images of the liver, kidneys, and GI tract. Organs were removed from mice 3 h post administration of distilled water (blank).

Over the course of 24 h post administration, the transit of the QD-conjugated microparticles was visualized through the GI tract. Images were taken at 1.5, 4, 7, and 24 h post administration of the QD-conjugated microparticles via oral gavage. As shown in Figure 9-5, the microparticles are mostly confined in the stomach 1.5 h post administration. Similar to the blank organs, there is a low fluorescent signal (indicated by dark red) in the lower GI tract and liver, while there is no fluorescence in the kidneys. It is important to note that the 1.5 h time point was administered a different batch of QD-conjugated microparticles than the later time points, and this batch for the 1.5 h time point had reduced

fluorescence. Mice used for the time points at 4, 7, and 24 h post administration received the same batch of QD-conjugated microparticles.

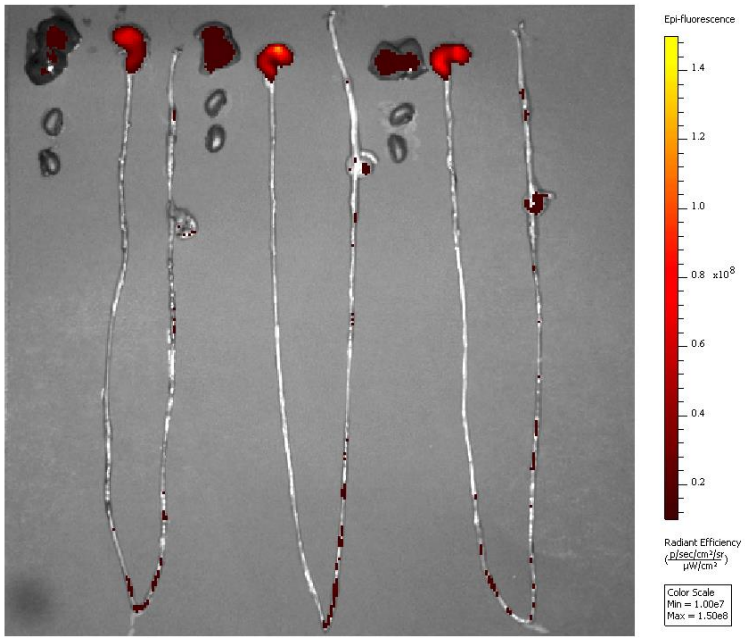

Figure 9-5. Fluorescent images of the liver, kidneys, and GI tract. Organs were removed from mice 1.5 h post administration of QD-microparticles. Microparticles remain in the stomach 1.5 h post administration.

At 4 h post administration, the microparticles have traveled through the small intestine, reaching the jejunum (middle section) and the ileum (final section), and passed through to the cecum and colon (Figure 9-6). However, the microparticles still remained in the stomach as indicated by the high fluorescent signal, which can be attributed to the feeding patterns in mice. Due to short delays between successive food intakes, the contents of the stomach are successively diluted. The gastric emptying in mice is nonlinear, unlike in humans where gastric empty is linear. Humans achieve nearly complete gastric emptying before each meal due to habits of eating three meals per day.[10]

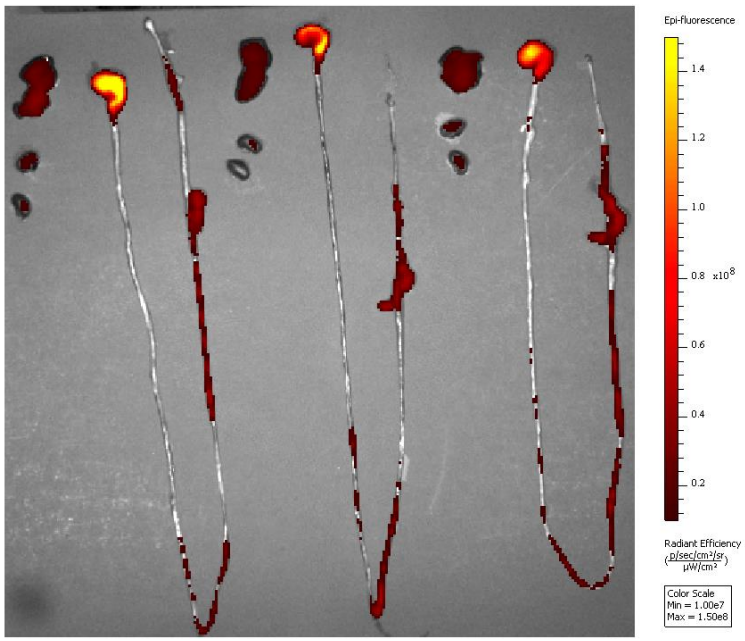

Figure 9-6. Fluorescent images of the liver, kidneys, and GI tract, imaged at 4 h post administration. Microparticles have traveled to lower small intestine, cecum, and colon, while some still remain in the stomach.

At 7 h post administration, the microparticles can be seen mostly in the jejunum, ileum, cecum, and colon (Figure 9-7). Additionally, the fluorescent signal in the stomach is reduced, indicating that the microparticles have exited the stomach. At 24 h post administration, the microparticles have mostly cleared the small intestine, with some fluorescent signal in the jejunum and ileum (9-8). The some microparticles are still retained in the cecum and colon. As expected, the majority of the microparticles have passed through the GI tract and cleared through excretion by 24 h post administration.

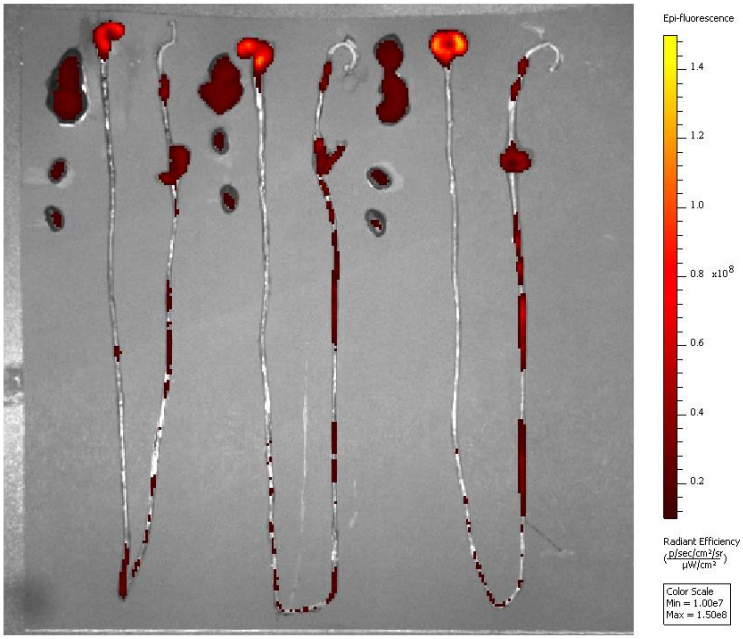

Figure 9-7. Fluorescent images of the liver, kidneys, and GI tract, imaged at 7 h post administration. Microparticles have exited from the stomach and traveled to lower small intestine, cecum, and colon.

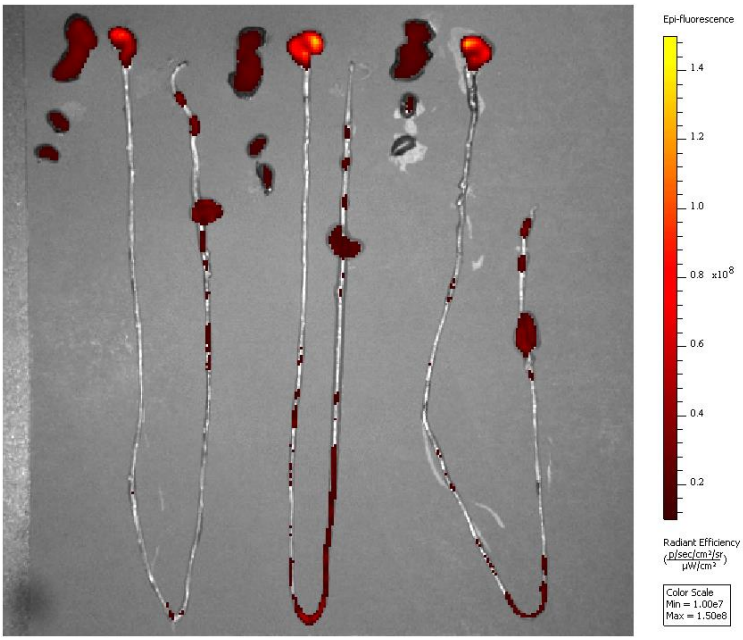

Figure 9-8. Fluorescent images of the liver, kidneys, and GI tract, imaged at 24 h post administration. Microparticles have mostly cleared the small intestine and some remain in the cecum and colon.

Despite an extensive wash procedure to remove any unbound QDs, some unbound QDs appear to have been administered to the mice with the QD-conjugated microparticles. The fluorescence in the kidneys and liver slightly increased over the course of the 24 h study likely due to unbound QDs. While the size of the microparticles (30-45 µm, dried) excludes them from paracellular and transcellular transport and entering circulation, the unbound QDs (~10 nm) could possibly enter circulation.

9.4 CONCLUSIONS

Biodistribution studies can be used to determine the residence time of the microparticles in the small intestine, as well as the clearance time. The P(MAA-g-EG) microcarrier system is designed for targeted release of the drug (hFIX) in the small

intestine. The microparticles were observed in the small intestine at both 4 and 7 h post administration, while some microparticles still remained in the lower small intestine after 24 h. At 24 h post administration, the majority of the microparticles had cleared the GI tract through excretion. Prolonged residence time of the microcarrier in the small intestine can increase the amount of drug released, which can also increase the amount of drug absorbed and therefore improve the overall bioavailability.

9.5 REFERENCES

1. Peppas, N. A.; Horava, S. D., Polymers for Delivery of Factor VIII and/or Factor IX. [Patent Pending].
2. Horava, S. D.; Peppas, N. A., Design of pH-Responsive Biomaterials to Enable the Oral Route of Hematological Factor IX. *Annals of Biomedical Engineering* **2016**, 1-13.
3. Gamboa, J. M.; Leong, K. W., In vitro and in vivo models for the study of oral delivery of nanoparticles. *Advanced Drug Delivery Reviews* **2013**, *65* (6), 800-810.
4. Frangioni, J. V., In vivo near-infrared fluorescence imaging. *Current Opinion in Chemical Biology* **2003**, *7* (5), 626-634.
5. Inoue, Y.; Izawa, K.; Kiryu, S.; Tojo, A.; Ohtomo, K., Diet and abdominal autofluorescence detected by in vivo fluorescence imaging of living mice. *Molecular imaging* **2008**, *7* (1), 21-27.
6. Panthani, M. G.; Khan, T. A.; Reid, D. K.; Hellebusch, D. J.; Rasch, M. R.; Maynard, J. A.; Korgel, B. A., In Vivo Whole Animal Fluorescence Imaging of a Microparticle-Based Oral Vaccine Containing (CuInSe x S2–x)/ZnS Core/Shell Quantum Dots. *Nano letters* **2013**, *13* (9), 4294-4298.
7. Peterson, J. D., Imaging Gastric Emptying with GastroSense 750. *PerkinElmer* **2012**.
8. Tseng, J.-C.; Vasquez, K.; Peterson, J. D., Optical Imaging on the IVIS SpectrumCT System: General and Technical Considerations for 2D and 3D Imaging. *PerkinElmer* **2015**.
9. Curtis, A.; Calabro, K.; Galarneau, J.-R.; Bigio, I. J.; Krucker, T., Temporal variations of skin pigmentation in C57BL/6 mice affect optical bioluminescence quantitation. *Molecular Imaging and Biology* **2011**, *13* (6), 1114-1123.

10. Schwarz, R.; Kaspar, A.; Seelig, J.; Künnecke, B., Gastrointestinal transit times in mice and humans measured with 27Al and 19F nuclear magnetic resonance. *Magnetic resonance in medicine* **2002**, *48* (2), 255-261.

Appendix A: Dissemination of Research

A.1 PUBLICATIONS

1. **Horava SD**, Moy KJ, and Peppas NA. Biodegradable Hydrophilic Carriers for Delivering Hematological Factor IX for Hemophilia B Treatment. *Int. J. Pharm.* 2016, [Submitted].
2. **Horava SD** and Peppas NA. Design of pH-Responsive Biomaterials to Enable the Oral Route of Hematological Factor IX. *Ann. Biomed. Eng.* 2016, doi:10.1007/s10439-016-1566-x. [Advanced online publication].
3. Sharpe LA, Daily AM, **Horava SD**, Peppas NA. Therapeutic Applications of Hydrogels in Oral Drug Delivery. *Expert Opin. Drug Deliv.* 2014, 11 (6): 901-15.

A.2 PATENT

1. Peppas NA and **Horava SD**. Polymers for Delivery of Factor VIII and/or Factor IX. U.S. Patent No. UTSB.P1047US.P1. [Patent Pending].

A.3 PRESENTATIONS

1. **Horava SD**, Moy K, Liou J, Peppas NA. Evaluation of pH-Responsive Hydrogel Networks as Oral Delivery Systems for Hematologic Factor IX. *American Chemical Society National Meeting*, San Diego, CA, March 2016. [Oral].
2. **Horava SD**, Peppas NA. Tailoring Biomaterial Microcarriers for the Improved Delivery of Hemophiliac Factor IX. *American Institute of Chemical Engineers Annual Meeting*, Salt Lake City, UT, Nov 2015. [Oral]

3. **Horava SD**, Peppas NA. Avoiding the Needle: Novel Oral Delivery Systems of Hemophiliac Factor IX. *Society of Women Engineers Annual Conference*, Nashville, TN, Oct 2015. [Poster] ***Competition finalist**
4. **Horava SD**, Liou J, Peppas NA. Optimizing Microcarrier Loading for Oral Delivery Systems. *Texas Biomaterials Day*, Houston, TX, Jun 2015. [Poster]
5. **Horava SD**, Peppas NA. pH-Responsive Novel Carriers for Oral Delivery of Hemophiliac Factor IX. *Society for Biomaterials Annual Meeting*, Charlotte, NC, April 2015. [Oral]
6. **Horava SD**, Peppas NA. Novel Biomaterial-Based Carriers for Oral Delivery of Hemophiliac Factor IX. *Graduate and Industry Networking Event*, Austin, TX, Feb 2015. [Poster] ***1st place award**
7. **Horava SD**, Peppas NA. Characterization of pH-Responsive Polymeric Systems for the Delivery of Hemophiliac Factors. *American Institute of Chemical Engineers Annual Meeting*, Atlanta, GA, Nov 2014. [Oral]
8. **Horava SD**, Peppas NA. Optimization of pH-Responsive Hydrogels for the Delivery of HMW Proteins. *Biomedical Engineering Society Annual Meeting*, San Antonio, TX, Oct 2014. [Poster]
9. **Horava SD**, Peppas NA. Characterization of pH-Sensitive Polymers for the Delivery of High Molecular Weight Proteins. *Texas Biomaterials Day*, College Station, TX, Jun 2014. [Poster]

Appendix B: Histology

Supporting Information for Chapter 8

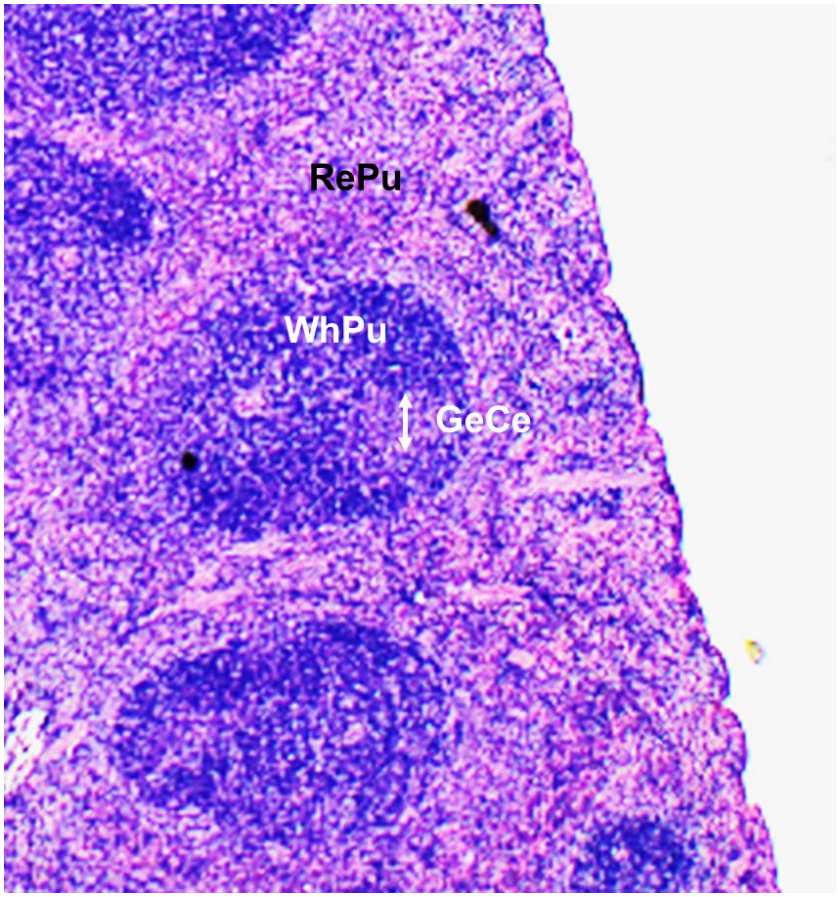

Figure B-1. Spleen. RePu- red pulp (contains macrophages); WhPu- white pulp (contains lymphocytes); GeCe- germinal center.

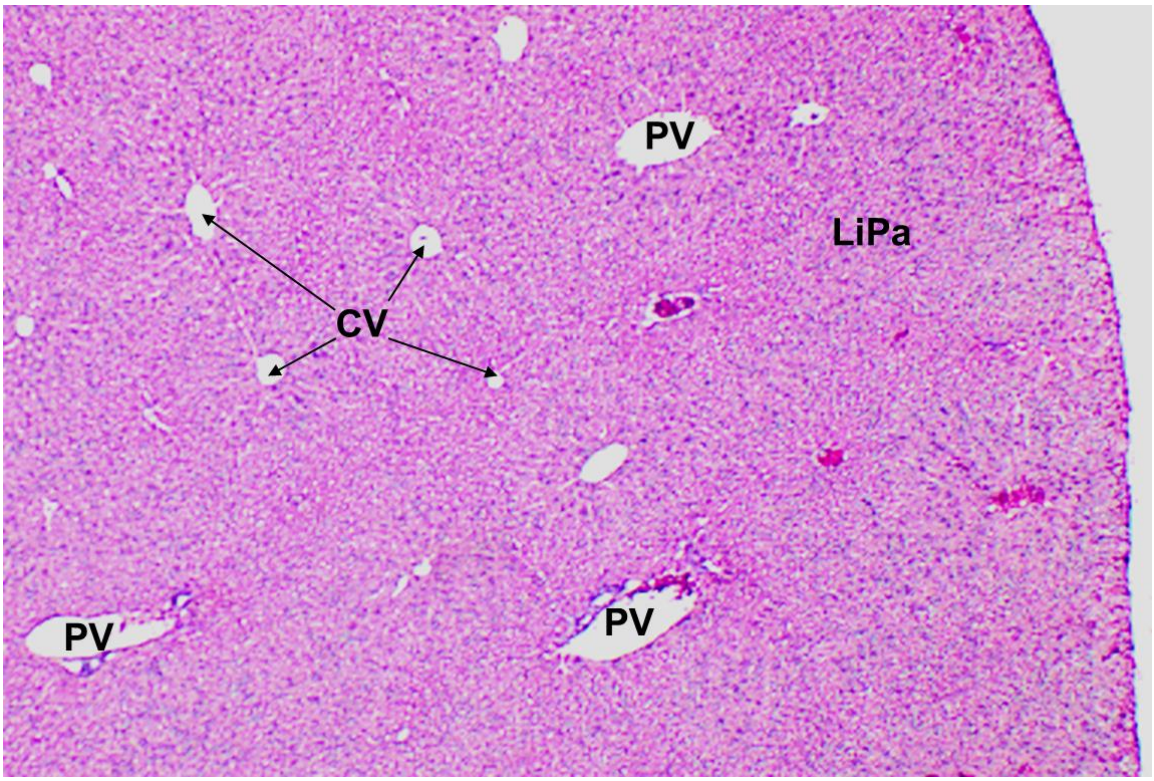

Figure B-2. Liver. CV- central vein; PV- portal vein (portal triad contains the portal vein, hepatic artery, and bile); LiPa- liver parenchyma (consists of hepatocytes arranged in cords).

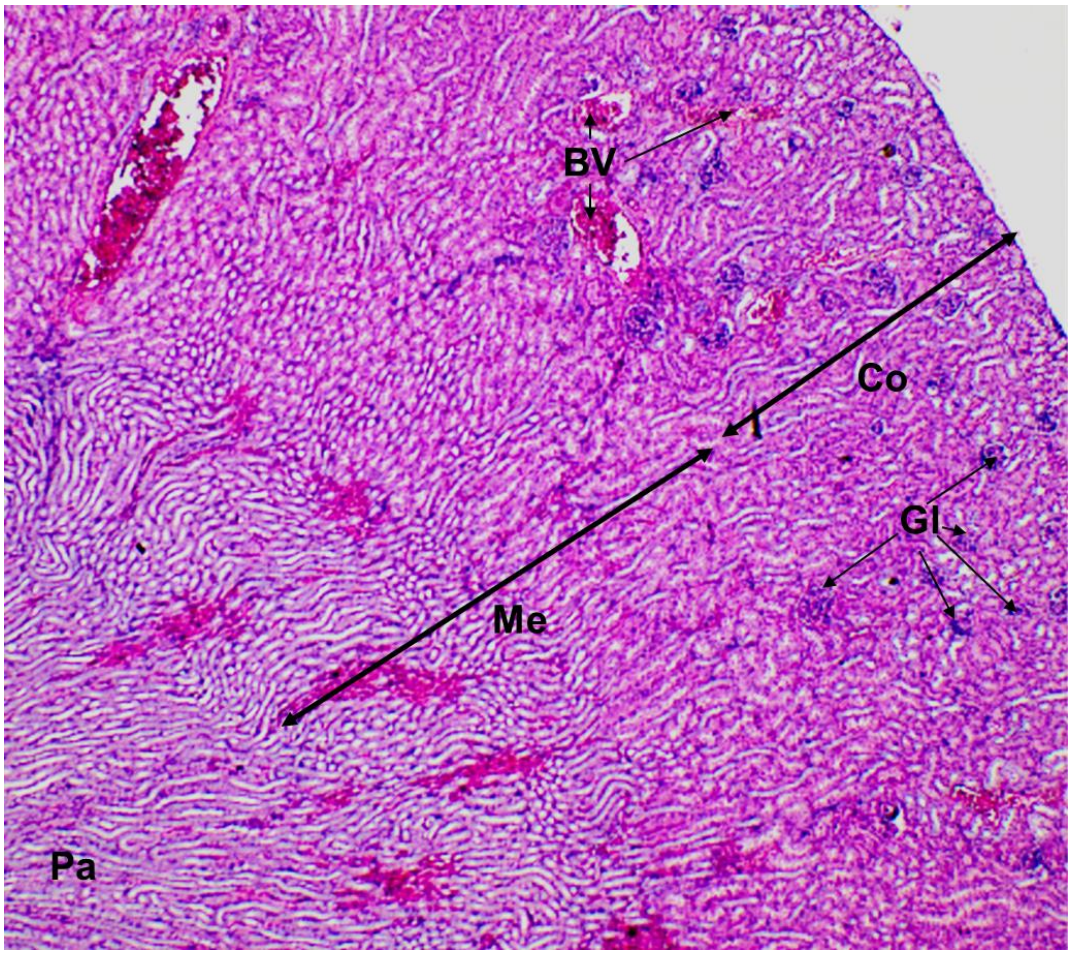

Figure B-3. Kidney. BV- blood vessel; Co- renal cortex containing renal corpuscles (glomerulus surrounded by Bowman's capsule) and proximal convoluted tubules; Gl- glomerulus; Me- renal medulla containing the loop of Henle (leads from proximal convoluted tubule to distal convoluted tubule), collecting tubules, and blood vessels; Pa- renal papilla formed by collecting ducts and blood vessels.

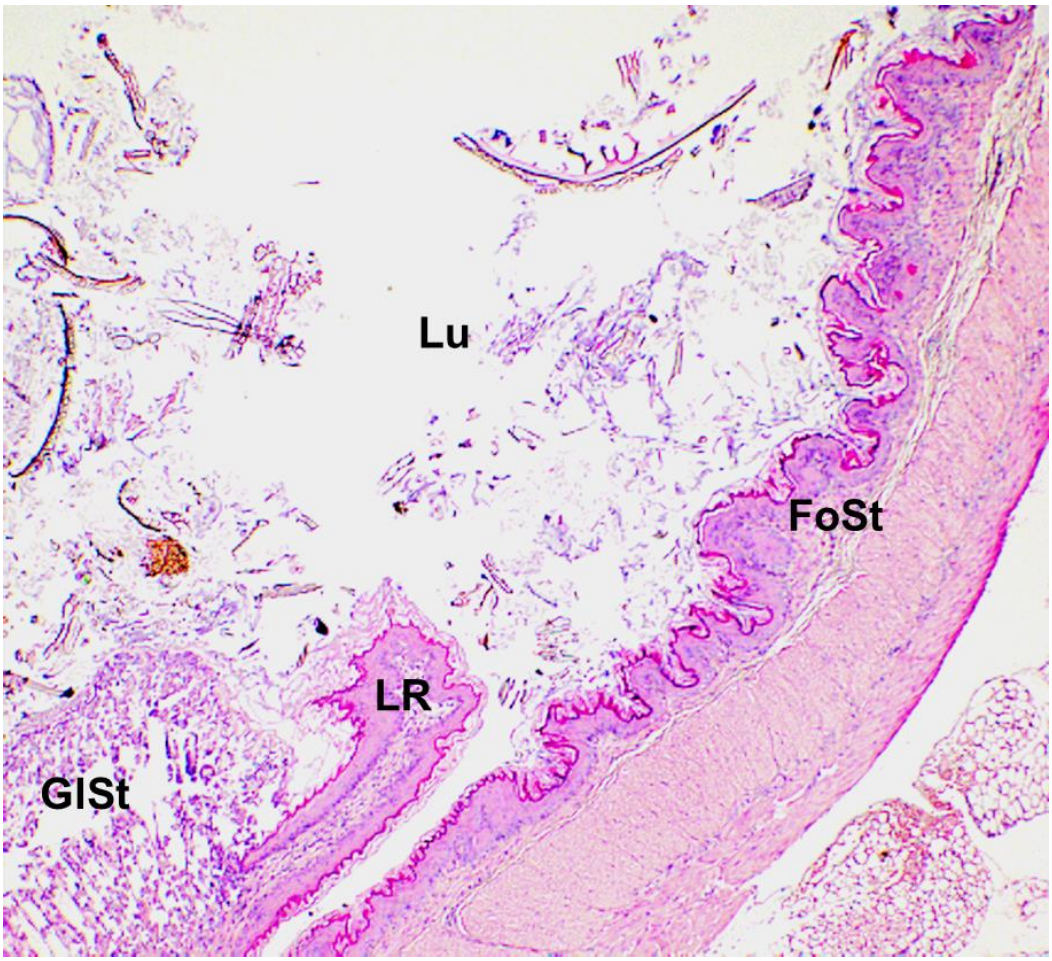

Figure B-4. Forestomach. FoSt- forestomach; LR- limiting ridge (margo plicatus) which separates the forestomach from the glandular stomach; GlSt- glandular stomach; Lu- lumen (with debris). The debris may include plant fragments with cell walls and cellular material, as well as hair fragments.

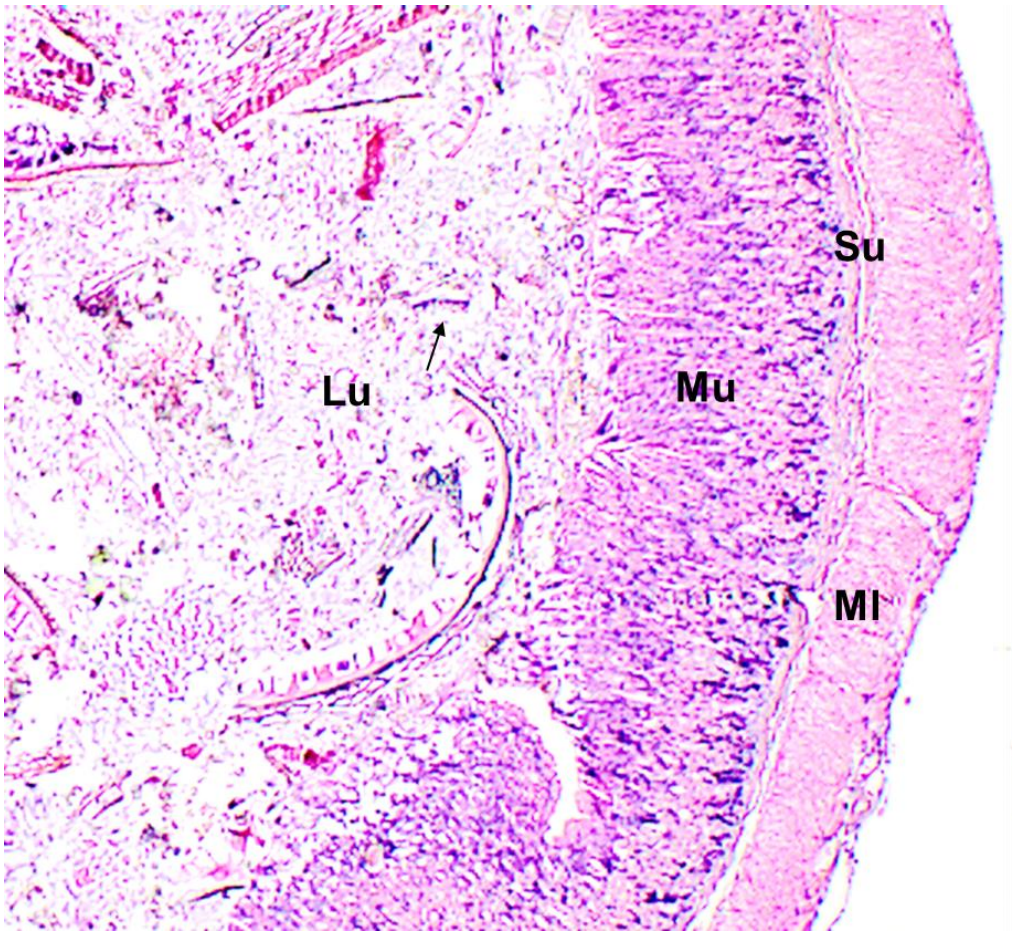

Figure B-5. Glandular stomach. Mu- mucosa with gastric pits; Su- submucosa; Ml- muscularis; Lu- lumen (with debris).

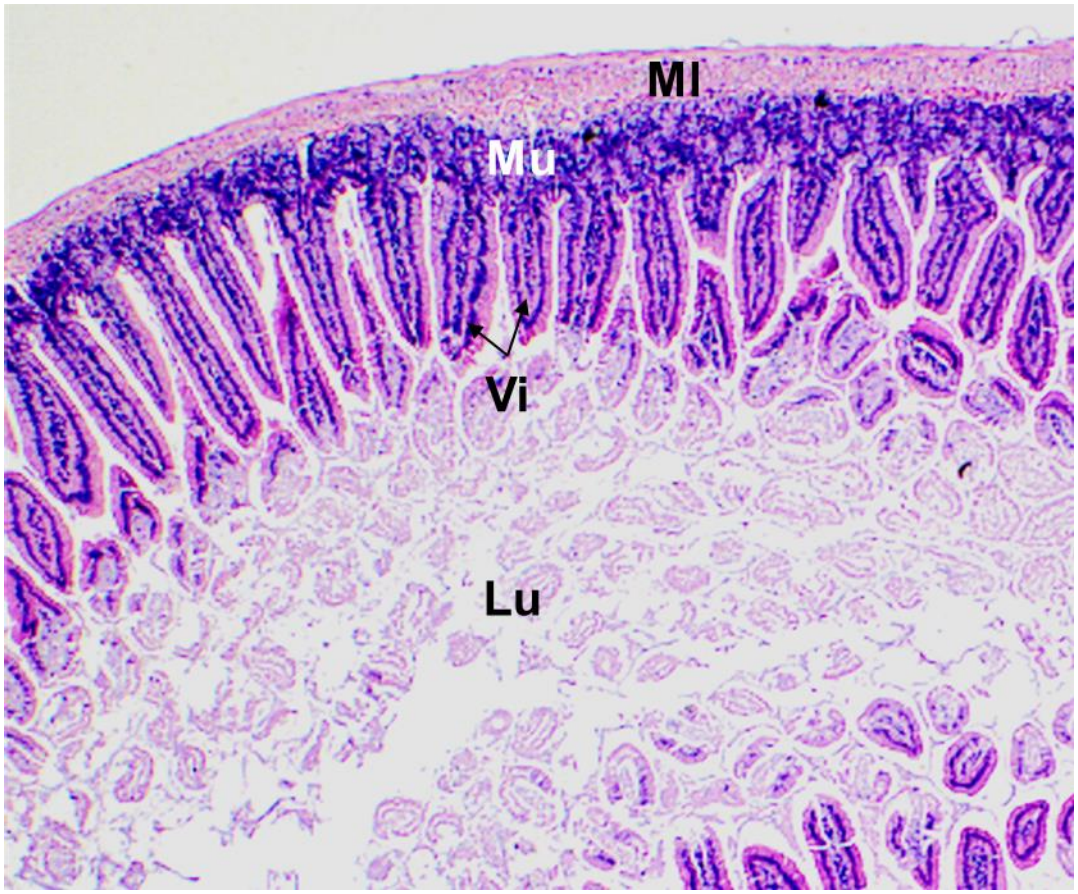

Figure B-6. Duodenum. Vi- villus; Mu- mucosa; Ml- muscularis; Lu- lumen.

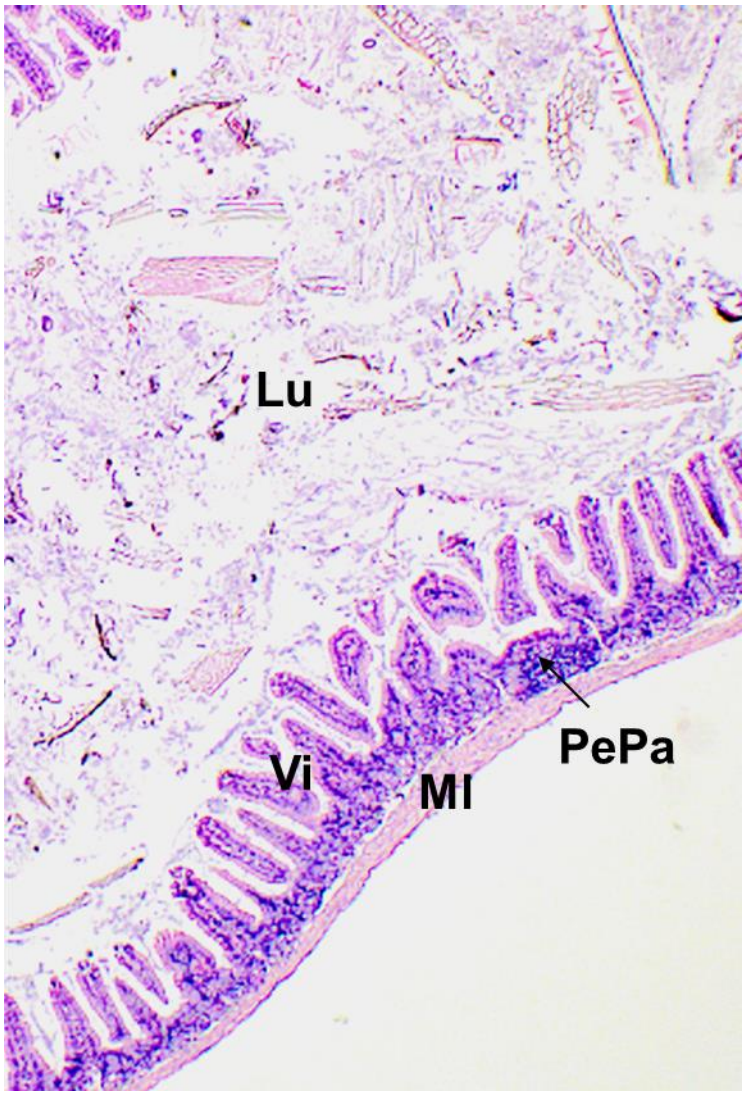

Figure B-7. Ileum. PePa- Peyer's patch; Vi- villus; Mu- mucosa; Ml- muscularis; Lu- lumen (with debris).

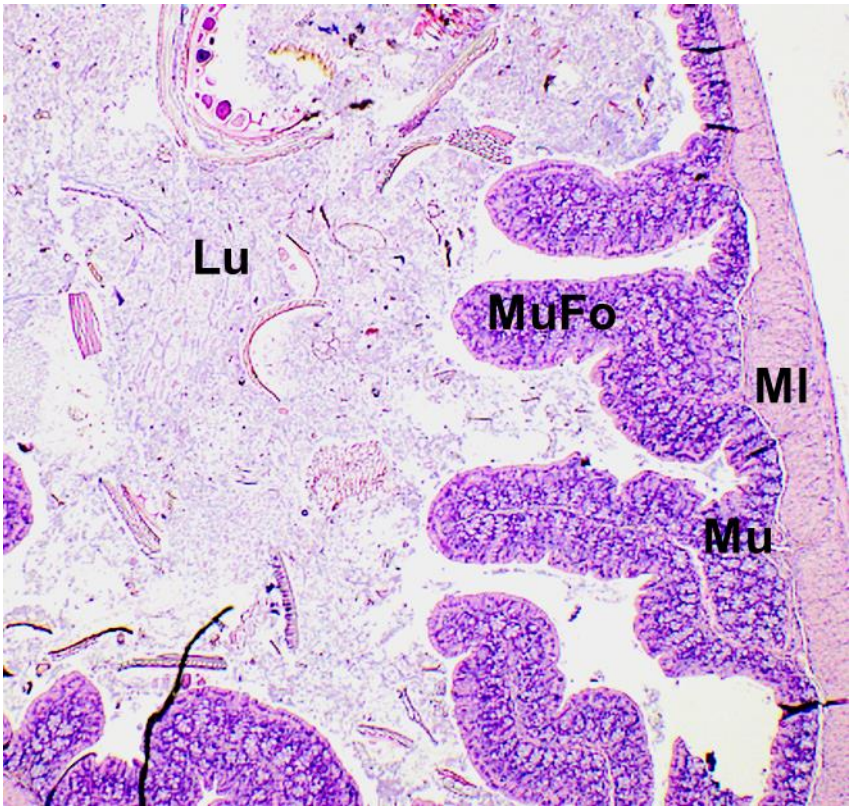

Figure B-8. Cecum. MuFo- mucosal fold; Mu- mucosa; Ml- muscularis; Lu- lumen (with debris).

Figure B-9. Colon. BM- bowel movement; Mu- mucosa; Ml- muscularis; Lu- lumen.

Appendix C: Animal Studies

C.1 Pharmacokinetic Studies

C.1.1 Rationale

In vivo studies will be conducted with male C57BL/6 mice prior to testing in the hemophilia B mouse model (B6.129P2-F9^{tm1Dws}/J, The Jackson Laboratory) to determine the pharmacokinetics of orally administered factor IX. A pilot study will be used to determine a detectable oral dosage. Then a full scale pharmacokinetic study will be conducted using three different oral formulations to determine the best performing one. Using the best performing formulation, a multi-dose study will be conducted to mimic a prophylactic regimen. Prior to all studies, the drug delivery systems will be loaded with factor IX. The amount loaded will be quantified by ELISA.

C.1.2 Pilot Study

Male C57BL/6 mice (The Jackson Laboratory) of 4-6 weeks will be used for a pilot study with varying dosages for one oral formulation. The recommended formulation is P(MAA-g-EG) with 1 mol% PEGDMA1000. Three dosages will be tested: 5 µg, 10 µg, and 20 µg of hFIX, where 5 µg of hFIX has been shown to be sufficient in a previous study. Table 1 provides the conditions and size of experimental and control groups. Prior to the initial treatment, animals will be placed on a liquid diet for 72 hours with the first 24 hours as transition period, and then fasted for 24 hours. Blood will be sampled 1 day prior to treatment by saphenous vein blood collection. Immediately prior to administration, lyophilized hFIX-loaded particles will be suspended in sterile distilled water. Mice will receive hFIX based on group classification as positive control (IV injection) and experimental (oral gavage, particle suspension) (Table C-1).

To maximize the amount of blood per sample, each animal will only have two time points (the first sample taken by tail bleeding and the second by cardiac puncture immediately post euthanasia), see Table C-2. Since the average gastric emptying time for mice is 1-2 hours, the first time point using going be hFIX in plasma samples will be quantified by an ELISA and its activity will be assessed by a chromogenic assay. Additionally, gastrointestinal (GI) tract will be harvested. Each organ—stomach, small intestine, cecum, and colon—will be homogenized and analyzed for factor IX using an ELISA. An optimal dosage and timescale of blood collection will be selected for the pharmacokinetic study.

The total number of animals required for the pilot study is:

Positive control: 1 group X 4 mice = 4 mice

Experimental: 1 formulation X 3 dosages X 6 mice = 18 mice

Total for pilot study: 22 mice

Table C-1. Groups for *in vivo* pharmacokinetic studies.

Group	**Positive Control**	**Negative Control**	**Experimental**
Administration	Tail vein injection of hFIX concentrate	Oral gavage of sterile distilled water	Oral gavage of hFIX-loaded particles + sterile distilled water
# Groups- Pilot	1 (n=4)	0	1 formulation x 3 dosages (n=4)
# Groups- Pharmacokinetic	1 (n=16)	1 (n=4)	3 formulations (n=16)
# Groups- Multi-dose	1 x 5 doses (n=4)	0	1 formulation x 5 doses (n=8)

Table C-2. Schedule for staggered blood draws.

Animal #	**1st Sample**	**2nd Sample**
Mouse 1	2 h	6 h
Mouse 2	3 h	7 h
Mouse 3	4 h	8 h
Mouse 4	5 h	24 h

C.1.3 Pharmacokinetic Study- Single Dose

The pharmacokinetics of three oral formulations (at the dosage determined in the pilot study) will be determined using the protocol described above. Table C-1 provides the conditions and size of experimental and control groups. Similarly, each animal will only have two time points based on the results of the pilot study. For each time point, there will be four blood samples from independent animals. Therefore, there will be eight total time points collected for each formulation (i.e., for one formulation: 16 mice x 2 time points/4 mice = 8 time points). Analysis will be carried out as previously described above. The total number of animals required for the single dose study is:

Positive control: 1 group X 16 mice = 16 mice

Negative control: 1 group X 4 mice = 4 mice

Experimental: 1 formulation X 3 dosages X 16 mice = 48 mice

Total for single dose study: 68 mice

C.1.4 Pharmacokinetic Study- Multiple Doses

Using the best performing oral formulation, a multi-dose study will be conducted where the treatment is administered every other day for ten days (i.e., five doses over 10 days). The multi-dose study is designed to mimic the prophylactic regimen and to determine if a therapeutic concentration can be maintained overtime. Table 1 provides the

conditions and size of experimental and control groups. Similarly, each animal will only have two time points based on previous results. For each time point for each dose, there will be four blood samples from independent animals and a total of four time points after each dose. Analysis will be carried out as previously described above. The total number of animals required for the multiple dose study is:

Positive control: 1 group X 5 doses X 4 mice = 20 mice

Experimental: 1 formulation X 5 doses X 8 mice = 60 mice

Total for pilot study: 60 mice.

C.1.5 Expected Results

The oral delivery hFIX using P(MAA-g-EG) microcarriers is expected to increase the amount of hFIX in circulation. Based on the pilot study, a detectable dose level will be selected. The pharmacokinetic curve for the orally administered hFIX is expected to look similar to a controlled release formulation, unlike the curve for the IV injection which is expected to show an immediate spike. The multiple dose study will be used to determine dosing intervals necessary to sustain therapeutically relevant levels of hFIX.

C.2 THERAPEUTIC EFFICACY STUDY

C.2.1 Rationale

In order to determine the clinical relevance of P(MAA-g-EG) microcarrier systems, using a hemophilia B model is necessary to access *in vivo* therapeutic efficacy. Testing the oral administration of hFIX-loaded microparticles in a humanized hemophilia B mouse can be used to determine *in vivo* bioactivity of hFIX. This experimental treatment is expected

to restore hemostasis in humanized hemophilia B, providing evidence of a novel clinically relevant treatment.

C.2.2 Efficacy Studies

Hemophilia B male mice (Strain B6.129P2-F9^{tmDws}/J, The Jackson Library) with targeted deletion of endogenous F9 ("null" mutation for hFIX) will be used. Animals will be housed under pathogen-free conditions and will be 8-10 weeks old at the onset of experiments. The conditions and size of experimental and control groups will the same as in Table C-2. The procedure is the same as the pharmacokinetic studies. Blood samples will be collected based on the timescale determined in the pharmacokinetic studies. Using plasma samples, hFIX will be quantified by an ELISA and its activity will be assessed by a chromogenic assay. Clotting time will be assessed by an activated partial thromboplastin time (aPTT) assay, used for clinical detection of hemophilia. The normal time to form a thrombus is 25 -35 seconds using the aPTT assay, while deficiency of FIX results in a prolonged time with up to a 2.5 times increase.

C.2.3 Expected Results

It is expected that the mice orally administered hFIX-loaded microparticles will have increased levels of active hFIX in the circulation, which will restore hemostasis. Prophylactic treatment regimens increase circulating FIX by 10%; however, a one percent increase in FIX for severe hemophilia can reduce spontaneous bleeding episodes. Ideally, mice given the experimental treatment will have at least a 10% increase in active hFIX in the circulation as compared to the negative control groups and baseline measurements. Experimental treatment will also reduce the partial thromboplastin time to a normal level, which will also be seen with the positive control group.

References

Chapter 2

1. DeLoughery, T. G., *Hemostasis and Thrombosis*. Springer Verlag: Cham, 2015; Vol. 3;3;3rd 2015;.
2. Francischetti, I. M. B., Does activation of the blood coagulation cascade have a role in malaria pathogenesis? *Trends in Parasitology* **2008,** *24* (6), 258-263.
3. Stenflo, J., Contributions of Gla and EGF-like domains to the function of vitamin K-dependent coagulation factors. *Critical reviews in eukaryotic gene expression* **1998,** *9* (1), 59-88.
4. Wilcox, J. N.; Smith, K. M.; Schwartz, S. M.; Gordon, D., Localization of tissue factor in the normal vessel wall and in the atherosclerotic plaque. *Proceedings of the National Academy of Sciences* **1989,** *86* (8), 2839-2843.
5. Banner, D. W.; D'Arcy, A.; Chene, C.; Winkler, F. K.; Guha, A.; Konigsberg, W. H.; Nemerson, Y.; Kirchhofer, D., The crystal structure of the complex of blood coagulation factor VIIa with soluble tissue factor. *Nature* **1996,** *380*, 41-46.
6. Mosesson, M. W.; Siebenlist, K. R.; Meh, D. A., The structure and biological features of fibrinogen and fibrin. *Annals of the New York Academy of Sciences* **2001,** *936* (1), 11-30.
7. Bajzar, L., Thrombin activatable fibrinolysis inhibitor and an antifibrinolytic pathway. *Arteriosclerosis, thrombosis, and vascular biology* **2000,** *20* (12), 2511-2518.
8. Fantony, J. J.; Inman, B. A., Thromboembolism and bleeding in bladder cancer. *Oncology* **2014,** *28* (10), 847-847.
9. Ruggeri, Z., Von Willebrand factor, platelets and endothelial cell interactions. *Journal of Thrombosis and Haemostasis* **2003,** *1* (7), 1335-1342.
10. Kessler, C. M., Mariani G, Clinical manifestations and therapy of the hemophilias. In *Hemostasis and Thrombosis: Basic Principles and Clinical Practice*, 5 ed.; Colman, R. W., J Hirsh, VJ Marder, AW Clowes, JN George, Ed. Lippincott-Raven: Philadelphia, 2006; pp 887-904.
11. Hemophilia. http://www.cdc.gov/ncbddd/hemophilia/facts.html.
12. About Bleeding Disorders: Hemophilia. http://www.wfh.org/en/page.aspx?pid=646.
13. Hemophilia B. https://www.hemophilia.org/Bleeding-Disorders/Types-of-Bleeding-Disorders/Hemophilia-B.

14. Darby, S. C.; Kan, S. W.; Spooner, R. J.; Giangrande, P. L. F.; Hill, F. G. H.; Hay, C. R. M.; Lee, C. A.; Ludlam, C. A.; Williams, M.; Doctors, U. K. H. C., Mortality rates, life expectancy, and causes of death in people with hemophilia A or B in the United Kingdom who were not infected with HIV. *Blood* **2007,** *110* (3), 815-825.

15. White, G. C., 2nd; Rosendaal, F.; Aledort, L. M.; Lusher, J. M.; Rothschild, C.; Ingerslev, J., Definitions in hemophilia. Recommendation of the scientific subcommittee on factor VIII and factor IX of the scientific and standardization committee of the International Society on Thrombosis and Haemostasis. *J. Thromb. Haemost.* **2001,** *85* (3), 560.

16. Colman, R. W., Are hemostasis and thrombosis two sides of the same coin? *J Exp Med* **2006,** *203* (3), 493-5.

17. Manco-Johnson, M. J.; Abshire, T. C.; Shapiro, A. D.; Riske, B.; Hacker, M. R.; Kilcoyne, R.; Ingram, J. D.; Manco-Johnson, M. L.; Funk, S.; Jacobson, L., Prophylaxis versus episodic treatment to prevent joint disease in boys with severe hemophilia. *New England Journal of Medicine* **2007,** *357* (6), 535-544.

18. Chalmers, E. A., Haemophilia and the newborn. *Blood reviews* **2004,** *18* (2), 85-92.

19. Kulkarni, R.; Soucie, J.; Lusher, J.; Presley, R.; Shapiro, A.; Gill, J.; MANCO-JOHNSON, M.; Koerper, M.; Mathew, P.; Abshire, T., Sites of initial bleeding episodes, mode of delivery and age of diagnosis in babies with haemophilia diagnosed before the age of 2 years: a report from The Centers for Disease Control and Prevention's (CDC) Universal Data Collection (UDC) project. *Haemophilia* **2009,** *15* (6), 1281-1290.

20. Lee, C. A.; Berntorp, E. E.; Hoots, K.; Ebooks, C., *Textbook of Hemophilia*. John Wiley & Sons, Ltd: Chichester, 2010; Vol. 2nd;2;.

21. Sellner, L. N.; Taylor, G. R., MLPA and MAPH: new techniques for detection of gene deletions. *Human mutation* **2004,** *23* (5), 413-419.

22. KWON, M. J.; YOO, K. Y.; KIM, H. J.; KIM, S. H., Identification of mutations in the F9 gene including exon deletion by multiplex ligation-dependent probe amplification in 33 unrelated Korean patients with haemophilia B. *Haemophilia* **2008,** *14* (5), 1069-1075.

23. Yoshitake, S.; Schach, B. G.; Foster, D. C.; Davie, E. W.; Kurachi, K., Complete nucleotide sequences of the gene for human factor IX (antihemophilic factor B). *Biochemistry* **1985,** *24* (14), 3736-3750.

24. Schmidt, A. E.; Bajaj, S. P., Structure–Function Relationships in Factor IX and Factor IXa. *Trends in Cardiovascular Medicine* **2003,** *13* (1), 39-45.

25. College, D. o. B. D. Coagulation Factor IX. Structure–Function Relationships in Factor IX and Factor IXa.

26. Fay, P. J., Activation of factor VIII and mechanisms of cofactor action. *Blood reviews* **2004,** *18* (1), 1-15.

27. Brandstetter, H.; Bauer, M.; Huber, R.; Lollar, P.; Bode, W., X-ray structure of clotting factor IXa: active site and module structure related to Xase activity and hemophilia B. *Proceedings of the National Academy of Sciences* **1995,** *92* (21), 9796-9800.

28. Hopfner, K.-P.; Lang, A.; Karcher, A.; Sichler, K.; Kopetzki, E.; Brandstetter, H.; Huber, R.; Bode, W.; Engh, R. A., Coagulation factor IXa: the relaxed conformation of Tyr99 blocks substrate binding. *Structure* **1999,** *7* (8), 989-996.

29. Rao, Z.; Handford, P.; Mayhew, M.; Knott, V.; Brownlee, G. G.; StuartZ, D., The structure of a Ca 2+-binding epidermal growth factor-like domain: its role in protein-protein interactions. *Cell* **1995,** *82* (1), 131-141.

30. Huang, M.; Furie, B. C.; Furie, B., Crystal structure of the calcium-stabilized human factor IX Gla domain bound to a conformation-specific anti-factor IX antibody. *Journal of Biological Chemistry* **2004,** *279* (14), 14338-14346.

31. Shen, B. W.; Spiegel, P. C.; Chang, C.-H.; Huh, J.-W.; Lee, J.-S.; Kim, J.; Kim, Y.-H.; Stoddard, B. L., The tertiary structure and domain organization of coagulation factor VIII. *Blood* **2008,** *111* (3), 1240-1247.

32. Ngo, J. C. K.; Huang, M.; Roth, D. A.; Furie, B. C.; Furie, B., Crystal structure of human factor VIII: implications for the formation of the factor IXa-factor VIIIa complex. *Structure* **2008,** *16* (4), 597-606.

33. Autin, L.; Miteva, M.; Lee, W.; Mertens, K.; RADTKE, K. P.; Villoutreix, B., Molecular models of the procoagulant factor VIIIa–factor IXa complex. *Journal of Thrombosis and Haemostasis* **2005,** *3* (9), 2044-2056.

34. Koeberl, D. D.; Bottema, C.; Buerstedde, J.; Sommer, S. S., Functionally important regions of the factor IX gene have a low rate of polymorphism and a high rate of mutation in the dinucleotide CpG. *American journal of human genetics* **1989,** *45* (3), 448.

35. Green, P.; Saad, S.; Lewis, C.; Giannelli, F., Mutation rates in humans. I. Overall and sex-specific rates obtained from a population study of hemophilia B. *The American Journal of Human Genetics* **1999,** *65* (6), 1572-1579.

36. Saunders, R. E.; Perkins, S. J., CoagMDB: a database analysis of missense mutations within four conserved domains in five vitamin K–dependent coagulation serine proteases using a text-mining tool. *Human mutation* **2008,** *29* (3), 333-344.

37. Thompson, A.; Bajaj, S. P.; Chen, S.-H.; MacGillivray, R., " Founder" effect in different families with haemophilia B mutation. *The Lancet* **1990,** *335* (8686), 418.

38. Anagnostopoulos, T.; Morris, A.; Ayres, K. L.; Giannelli, F.; Green, P., DNA variation in a 13-Mb region including the F9 gene: inferring the genealogical

history and causal role of a hemophilia B mutation (IVS 5+ 13 A→ G). *Journal of Thrombosis and Haemostasis* **2003,** *1* (12), 2609-2614.

39. Jenkins, P.; Egan, H.; Keenan, C.; O'SHEA, E.; Smith, O.; Nolan, B.; White, B.; O'DONNELL, J., Mutation analysis of haemophilia B in the Irish population: increased prevalence caused by founder effect. *Haemophilia* **2008,** *14* (4), 717-722.

40. Ljung, R.; Nilsson, I. M., Hemophilia B Leyden and a similar variant of hemophilia A. *The New England journal of medicine* **1982,** *307* (14), 897.

41. Crossley, M.; Ludwig, M.; Stowell, K. M.; De Vos, P.; Olek, K.; Brownlee, G. G., Recovery from hemophilia B Leyden: an androgen-responsive element in the factor IX promoter. *Science* **1992,** *257* (5068), 377-379.

42. DiMichele, D., Inhibitor development in haemophilia B: an orphan disease in need of attention. *British Journal of Haematology* **2007,** *138* (3), 305-315.

43. Jameel, F.; Hershenson, S., *Formulation and Process Development Strategies for Manufacturing Biopharmaceuticals*. John Wiley & Sons: Hoboken, 2010; Vol. 1.

44. Biogen-Idec Press Release. http://www.biogenidec.com/press_release_details.aspx?ID=14712&Action=1&NewsId=2303&M=NewsV2&PID=61997.

45. Berntorp, E.; Shapiro, A. D., Modern haemophilia care. *Lancet* **2012,** *379* (9824), 1447-56.

46. Ljung, R. C., Aspects of haemophilia prophylaxis in Sweden. *Haemophilia* **2002,** *2*, 34-7.

47. Yee, T. T.; Beeton, K.; Griffioen, A.; Harrington, C.; Miners, A.; Lee, C. A.; Brown, S. A., Experience of prophylaxis treatment in children with severe haemophilia. *Haemophilia* **2002,** *8* (2), 76-82.

48. Mancuso, M. E.; Berardinelli, L.; Beretta, C.; Raiteri, M.; Pozzoli, E.; Santagostino, E., Improved treatment feasibility in children with hemophilia using arteriovenous fistulae: the results after seven years of follow-up. *Haematologica* **2009,** *94* (5), 687-92.

49. Healthcare Observer Jan 2013: The Hemophilia B Market. *Morningstar* **2013**.

50. Mullard, A., Biogen Idec enters hemophilia B market. *Nature biotechnology* **2014,** *32* (6), 506-506.

51. Peters, R. T.; Low, S. C.; Kamphaus, G. D.; Dumont, J. A.; Amari, J. V.; Lu, Q.; Zarbis-Papastoitsis, G.; Reidy, T. J.; Merricks, E. P.; Nichols, T. C., Prolonged activity of factor IX as a monomeric Fc fusion protein. *Blood* **2010,** *115* (10), 2057-2064.

52. Østergaard, H.; Bjelke, J. R.; Hansen, L.; Petersen, L. C.; Pedersen, A. A.; Elm, T.; Møller, F.; Hermit, M. B.; Holm, P. K.; Krogh, T. N.; Petersen, J. M.; Ezban, M.;

Sørensen, B. B.; Andersen, M. D.; Agersø, H.; Ahmadian, H.; Balling, K. W.; Christiansen, M. L. S.; Knobe, K.; Nichols, T. C.; Bjørn, S. E.; Tranholm, M., *Prolonged half-life and preserved enzymatic properties of factor IX selectively PEGylated on native N-glycans in the activation peptide*. 2011; Vol. 118, p 2333-2341.

53. Karpf, D. M.; Sørensen, B. B.; Hermit, M. B.; Holmberg, H. L.; Tranholm, M.; Bysted, B. V.; Groth, A. V.; Bjørn, S. E.; Stennicke, H. R., Prolonged half-life of glycoPEGylated rFVIIa variants compared to native rFVIIa. *Thrombosis Research* **2011,** *128* (2), 191-195.

54. Stennicke, H. R.; Ostergaard, H.; Bayer, R. J.; Kalo, M. S.; Kinealy, K.; Holm, P. K.; Sørensen, B. B.; Zopf, D.; Bjørn, S. E., Generation and biochemical characterization of glycoPEGylated factor VIIa derivatives. *Thrombosis and haemostasis* **2008,** *100* (5), 920-928.

55. Product Pipeline: Factor IX. http://www.hemophilia.ca/en/.

56. Zhou, Z.-Y.; Koerper, M. A.; Johnson, K. A.; Riske, B.; Baker, J. R.; Ullman, M.; Curtis, R. G.; Poon, J.-L.; Lou, M.; Nichol, M. B., Burden of illness: direct and indirect costs among persons with hemophilia A in the United States. *Journal of medical economics* **2015,** *18* (6), 457-465.

57. Eldar-Lissai, A.; Hou, Q.; Krishnan, S., The Changing Costs of Caring for Hemophilia Patients in the US: Insurers' and Patients' Perspectives. *Blood* **2014,** *124* (21), 199-199.

58. Hemophilia Insight Report. https://www.optum.com/content/dam/optum/resources/brochures/Rx/m53018_n_hemophilia_insight_report_0424a.pdf.

59. Dimichele, D. M., Immune tolerance: critical issues of factor dose, purity and treatment complications. *Haemophilia* **2006,** *12*, 81-86.

60. Thorland, E. C.; Drost, J. B.; Lusher, J. M.; Warrier, I.; Shapiro, A.; Koerper, M. A.; Dimichele, D.; Westman, J.; Key, N. S.; Sommer, S. S., Anaphylactic response to factor IX replacement therapy in haemophilia B patients: complete gene deletions confer the highest risk. *Haemophilia* **1999,** *5* (2), 101-105.

61. Pannier, A. K.; Shea, L. D., Controlled release systems for DNA delivery. *Mol Ther* **2004,** *10* (1), 19-26.

62. Ginn, S. L.; Alexander, I. E.; Edelstein, M. L.; Abedi, M. R.; Wixon, J., Gene therapy clinical trials worldwide to 2012 – an update. *The Journal of Gene Medicine* **2013,** *15* (2), 65-77.

63. High, K. H.; Nathwani, A.; Spencer, T.; Lillicrap, D., Current status of haemophilia gene therapy. *Haemophilia* **2014,** *4*, 43-9.

64. Kotterman, M. A.; Schaffer, D. V., Engineering adeno-associated viruses for clinical gene therapy. *Nat Rev Genet* **2014,** *15* (7), 445-451.

65. Dose-escalation study of a self complementary adeno-associated viral vector of gene transfer in hemophilia B. In *ClinicalTrials.gov*, 2009; Vol. Identifier: NCT00979238.

66. Hemophilia B gene therapy – Spark. In *ClinicalTrials.gov* 2012; Vol. Identifier: NCT01620801.

67. Open-Label Single Ascending Dose of Adeno-associated Virus Serotype 8 Factor IX Gene Therapy in Adults with Hemophilia B. In *ClinicalTrials.gov*, 2012; Vol. Identifier: NCT01687608.

68. Wright, J., Product-Related Impurities in Clinical-Grade Recombinant AAV Vectors: Characterization and Risk Assessment. *Biomedicines* **2014,** *2* (1), 80-97.

69. Skinner, M. W., Gene Therapy for Hemophilia: Addressing the Coming Challenges of Affordability and Accessibility. *Mol Ther* **2013,** *21* (1), 1-2.

70. Verma, D.; Moghimi, B.; LoDuca, P. A.; Singh, H. D.; Hoffman, B. E.; Herzog, R. W.; Daniell, H., Oral delivery of bioencapsulated coagulation factor IX prevents inhibitor formation and fatal anaphylaxis in hemophilia B mice. *Proc. Natl. Acad. Sci. U.S.A.* **2010,** *107* (15), 7101-6.

71. Kwon, K.-C.; Verma, D.; Singh, N. D.; Herzog, R.; Daniell, H., Oral delivery of human biopharmaceuticals, autoantigens and vaccine antigens bioencapsulated in plant cells. *Adv. Drug Deliv. Rev.* **2013,** *65* (6), 782-799.

72. Guan, Z. J.; Guo, B.; Huo, Y. L.; Guan, Z. P.; Dai, J. K.; Wei, Y. H., Recent advances and safety issues of transgenic plant-derived vaccines. *Appl. Microbiol. Biotechnol.* **2013,** *97* (7), 2817-40.

73. Sherman, A.; Su, J.; Daniell, H.; Herzog, R. W., Mechanism Of Oral Tolerance Induced By Bioencapsulated Coagulation Factor IX In Hemophilia B Mice. *Blood* **2013,** *122* (21), 30-30.

74. Wang, X.; Su, J.; Sherman, A.; Rogers, G. L.; Liao, G.; Hoffman, B. E.; Leong, K. W.; Terhorst, C.; Daniell, H.; Herzog, R. W., Plant-based oral tolerance to hemophilia therapy employs a complex immune regulatory response including LAP+ CD4+ T cells. *Blood* **2015,** *125* (15), 2418-2427.

75. Su, J.; Zhu, L.; Sherman, A.; Wang, X.; Lin, S.; Kamesh, A.; Norikane, J. H.; Streatfield, S. J.; Herzog, R. W.; Daniell, H., Low cost industrial production of coagulation factor IX bioencapsulated in lettuce cells for oral tolerance induction in hemophilia B. *Biomaterials* **2015,** *70*, 84-93.

76. Daugherty, A. L.; Mrsny, R. J., Transcellular uptake mechanisms of the intestinal epithelial barrier - Part one. *Pharmaceutical Science & Technology Today* **1999,** *2* (4), 144-151.

77. Peppas, N. A.; Bures, P.; Leobandung, W.; Ichikawa, H., Hydrogels in pharmaceutical formulations. *Eur. J. Pharm. Biopharm.* **2000,** *50* (1), 27-46.

78. Lowman, A. M.; Dziubla, T.; Bures, P.; Peppas, N. A., Structural and dynamic response of neutral and intelligent networks in biomedical environments. In *Advances in Chemical Engineering: Molecular and cellular foundations of biomaterial*, Peppas, N. A.; Sefton, M., Eds. Elsevier: San Diego, 2004; Vol. 29, pp 75-130.

79. Lowman, A. M.; Morishita, M.; Kajita, M.; Nagai, T.; Peppas, N. A., Oral delivery of insulin using pH-responsive complexation gels. *J. Pharm. Sci.* **1999,** *88* (9), 933-937.

80. Nakamura, K.; Murray, R. J.; Joseph, J. I.; Peppas, N. A.; Morishita, M.; Lowman, A. M., Oral insulin delivery using P(MAA-g-EG) hydrogels: effects of network morphology on insulin delivery characteristics. *J. Control. Release* **2004,** *95* (3), 589-599.

81. Morishita, M.; Goto, T.; Nakamura, K.; Lowman, A. M.; Takayama, K.; Peppas, N. A., Novel oral insulin delivery systems based on complexation polymer hydrogels: Single and multiple administration studies in type 1 and 2 diabetic rats. *J. Control. Release* **2006,** *110* (3), 587-594.

82. Wood, K. M.; Stone, G. M.; Peppas, N. A., Wheat Germ Agglutinin Functionalized Complexation Hydrogels for Oral Insulin Delivery. *Biomacromolecules* **2008,** *9* (4), 1293-1298.

83. Wood, K. M.; Stone, G. M.; Peppas, N. A., The effect of complexation hydrogels on insulin transport in intestinal epithelial cell models. *Acta Biomater.* **2010,** *6* (1), 48-56.

84. Sharpe, L. A.; Daily, A. M.; Horava, S. D.; Peppas, N. A., Therapeutic applications of hydrogels in oral drug delivery. *Expert Opin. Drug Deliv.* **2014,** *11* (6), 901-15.

85. Kamei, N.; Morishita, M.; Chiba, H.; Kavimandan, N. J.; Peppas, N. A.; Takayama, K., Complexation hydrogels for intestinal delivery of interferon beta and calcitonin. *J. Control. Release* **2009,** *134* (2), 98-102.

86. Carr, D. A.; Gomez-Burgaz, M.; Boudes, M. C.; Peppas, N. A., Complexation Hydrogels for the Oral Delivery of Growth Hormone and Salmon Calcitonin. *Ind. Eng. Chem. Res.* **2010,** *49* (23), 11991-11995.

Chapter 4

1. Lowman, A. M.; Morishita, M.; Kajita, M.; Nagai, T.; Peppas, N. A., Oral delivery of insulin using pH-responsive complexation gels. *J. Pharm. Sci.* **1999**, *88* (9), 933-937.

2. Nakamura, K.; Murray, R. J.; Joseph, J. I.; Peppas, N. A.; Morishita, M.; Lowman, A. M., Oral insulin delivery using P(MAA-g-EG) hydrogels: effects of network morphology on insulin delivery characteristics. *J. Control. Release* **2004**, *95* (3), 589-599.

3. Morishita, M.; Goto, T.; Nakamura, K.; Lowman, A. M.; Takayama, K.; Peppas, N. A., Novel oral insulin delivery systems based on complexation polymer hydrogels: Single and multiple administration studies in type 1 and 2 diabetic rats. *J. Control. Release* **2006**, *110* (3), 587-594.

4. Wood, K. M.; Stone, G. M.; Peppas, N. A., Wheat Germ Agglutinin Functionalized Complexation Hydrogels for Oral Insulin Delivery. *Biomacromolecules* **2008**, *9* (4), 1293-1298.

5. Wood, K. M.; Stone, G. M.; Peppas, N. A., The effect of complexation hydrogels on insulin transport in intestinal epithelial cell models. *Acta Biomater.* **2010**, *6* (1), 48-56.

6. Peppas, N. A.; Bures, P.; Leobandung, W.; Ichikawa, H., Hydrogels in pharmaceutical formulations. *Eur. J. Pharm. Biopharm.* **2000**, *50* (1), 27-46.

7. Sharpe, L. A.; Daily, A. M.; Horava, S. D.; Peppas, N. A., Therapeutic applications of hydrogels in oral drug delivery. *Expert Opin. Drug Deliv.* **2014**, *11* (6), 901-15.

8. Kamei, N.; Morishita, M.; Chiba, H.; Kavimandan, N. J.; Peppas, N. A.; Takayama, K., Complexation hydrogels for intestinal delivery of interferon beta and calcitonin. *J. Control. Release* **2009**, *134* (2), 98-102.

9. Carr, D. A.; Gomez-Burgaz, M.; Boudes, M. C.; Peppas, N. A., Complexation Hydrogels for the Oral Delivery of Growth Hormone and Salmon Calcitonin. *Ind. Eng. Chem. Res.* **2010**, *49* (23), 11991-11995.

10. Torres-Lugo, M.; Peppas, N. A., Preparation and characterization of P (MAA-g-EG) nanospheres for protein delivery applications. *Journal of Nanoparticle Research* **2002**, *4* (1-2), 73-81.

11. Ho, B.-C.; Lee, Y.-D.; Chin, W.-K., Thermal degradation of polymethacrylic acid. *Journal of Polymer Science Part A: Polymer Chemistry* **1992**, *30* (11), 2389-2397.

12. Brandrup, J.; Immergut, E. H., Polymer handbook. Wiley: New York, **1989**; Vol. 3rd.

13. Lowman, A. M.; Peppas, N. A., Analysis of the complexation/decomplexation phenomena in graft copolymer networks. *Macromolecules* **1997**, *30* (17), 4959-4965.

14. Brannon-Peppas, L.; Peppas, N. A., Equilibrium swelling behavior of dilute ionic hydrogels in electrolytic solutions. *J. Control. Release* **1991**, *16* (3), 319-329.

15. Erickson, H. P., Size and shape of protein molecules at the nanometer level determined by sedimentation, gel filtration, and electron microscopy. *Biological procedures online* **2009**, *11* (1), 32.

16. Knipe, J. M.; Chen, F.; Peppas, N. A., Enzymatic Biodegradation of Hydrogels for Protein Delivery Targeted to the Small Intestine. *Biomacromolecules* **2015**, *16* (3), 962-972.

17. Klinger, D.; Landfester, K., Enzymatic- and light-degradable hybrid nanogels: Crosslinking of polyacrylamide with acrylate-functionalized Dextrans containing photocleavable linkers. *J. Polym. Sci. A Polym. Chem.* **2012**, *50* (6), 1062-1075.

18. Hoffman, A. S., Stimuli-responsive polymers: Biomedical applications and challenges for clinical translation. *Advanced Drug Delivery Reviews* **2013**, *65* (1), 10-16.

Chapter 5

1. Kessler, C. M., Mariani G, Clinical manifestations and therapy of the hemophilias. In Hemostasis and Thrombosis: Basic Principles and Clinical Practice, 5 ed.; Colman, R. W., J Hirsh, VJ Marder, AW Clowes, JN George, Ed. Lippincott-Raven: Philadelphia, **2006**; pp 887-904.

2. White, G. C., 2nd; Rosendaal, F.; Aledort, L. M.; Lusher, J. M.; Rothschild, C.; Ingerslev, J., Definitions in hemophilia. Recommendation of the scientific subcommittee on factor VIII and factor IX of the scientific and standardization committee of the International Society on Thrombosis and Haemostasis. *J. Thromb. Haemost.* **2001**, 85 (3), 560.

3. Mancuso, M. E.; Berardinelli, L.; Beretta, C.; Raiteri, M.; Pozzoli, E.; Santagostino, E., Improved treatment feasibility in children with hemophilia using arteriovenous fistulae: the results after seven years of follow-up. *Haematologica* **2009**, 94 (5), 687-92.

4. Darby, S. C.; Kan, S. W.; Spooner, R. J.; Giangrande, P. L. F.; Hill, F. G. H.; Hay, C. R. M.; Lee, C. A.; Ludlam, C. A.; Williams, M.; Doctors, U. K. H. C., Mortality

rates, life expectancy, and causes of death in people with hemophilia A or B in the United Kingdom who were not infected with HIV. *Blood* **2007**, 110 (3), 815-825.

5. Peppas, N. A.; Horava, S. D., Polymers for Delivery of Factor VIII and/or Factor IX. [Patent Pending].

6. Brannon-Peppas, L.; Peppas, N. A., Equilibrium swelling behavior of dilute ionic hydrogels in electrolytic solutions. *J. Control. Release* **1991**, 16 (3), 319-329.

7. Koetting, M. C.; Peppas, N. A., pH-Responsive poly(itaconic acid-co-N-vinylpyrrolidone) hydrogels with reduced ionic strength loading solutions offer improved oral delivery potential for high isoelectric point-exhibiting therapeutic proteins. *Int. J. Pharm.* **2014**, 471 (1–2), 83-91.

8. Inc., W. P. BeneFIX- coagulation factor IX (recombinant). http://labeling.pfizer.com/showlabeling.aspx?id=492.

9. Björkman, S., Prophylactic dosing of factor VIII and factor IX from a clinical pharmacokinetic perspective. *Haemophilia* **2003**, 9, 101-110.

10. Kisker, C. T.; Eisberg, A.; Schwartz, B.; the Mononine Study, G., Prophylaxis in factor IX deficiency product and patient variation. *Haemophilia* **2003**, 9 (3), 279-284.

11. Hilgendorf, C.; Spahn-Langguth, H.; Regardh, C. G.; Lipka, E.; Amidon, G. L.; Langguth, P., Caco-2 versus Caco-2/HT29-MTX co-cultured cell lines: permeabilities via diffusion, inside- and outside-directed carrier-mediated transport. *J. Pharm. Sci.* **2000**, 89 (1), 63-75.

12. Gupta, V.; Doshi, N.; Mitragotri, S., Permeation of Insulin, Calcitonin and Exenatide across Caco-2 Monolayers: Measurement Using a Rapid, 3-Day System. *PLoS ONE* **2013**, 8 (2), e57136.

13. Wood, K. M.; Stone, G. M.; Peppas, N. A., The effect of complexation hydrogels on insulin transport in intestinal epithelial cell models. *Acta Biomater.* **2010**, 6 (1), 48-56.

14. Ichikawa, H.; Peppas, N. A., Novel complexation hydrogels for oral peptide delivery: In vitro evaluation of their cytocompatibility and insulin-transport enhancing effects using Caco-2 cell monolayers. *J. Biomed. Mater. Res. A* **2003**, 67A (2), 609-617.

Chapter 6

1. FDA Guidance for Industry Q1A(R2) Stability Testing of New Drug Substances and Products. http://www.fda.gov/downloads/drugs/guidancecomplianceregulatoryinformation/guidances/ucm073369.pdf.
2. ICH, Specifications: Test Procedures and Acceptance Criteria for New Drug Substances and New Drug Products: Chemical Substances Q6A. ICH Harmonised Tripartite Guideline.
3. ICH, Specifications: Test Procedures and Acceptance Criteria for Biotechnological/Biological Products Q6B. ICH Harmonised Tripartite Guideline.
4. Jameel, F.; Hershenson, S., Formulation and Process Development Strategies for Manufacturing Biopharmaceuticals. John Wiley & Sons: Hoboken, **2010**; Vol. 1.
5. Pikal, M. J.; Dellerman, K. M., Stability testing of pharmaceuticals by high-sensitivity isothermal calorimetry at 25°C: cephalosporins in the solid and aqueous solution states. *International Journal of Pharmaceutics* **1989**, 50 (3), 233-252.
6. Containers- Glass. In United States Pharmacopeia, United States Pharmacopeial Convention: Rockville, MD, 2014; Vol. USP 37: The National Formulary: NF 32.
7. Horava, S. D.; Peppas, N. A., Design of pH-Responsive Biomaterials to Enable the Oral Route of Hematological Factor IX. *Annals of Biomedical Engineering* **2016**, 1-13.
8. Gui, T.; Lin, H.-F.; Jin, D.-Y.; Hoffman, M.; Straight, D. L.; Roberts, H. R.; Stafford, D. W., Circulating and binding characteristics of wild-type factor IX and certain Gla domain mutants in vivo. *Blood* **2002**, 100 (1), 153-158.
9. Manning, M. C.; Patel, K.; Borchardt, R. T., Stability of protein pharmaceuticals. *Pharm Res* **1989**, 6 (11), 903-18.
10. Volkin, D. B.; Klibanov, A. M., Thermal destruction processes in proteins involving cystine residues. *Journal of Biological Chemistry* **1987**, 262 (7), 2945-2950.
11. Duncan, M.; Zaretsky, I., Do the Math for Shelf Life. *Pharmaceutical Formulation and Quality* **2011**, 13 (2), 22-28.
12. Connors, K. A.; Amidon, G. L.; Stella, V. J., Chemical stability of pharmaceuticals: a handbook for pharmacists. John Wiley & Sons: **1986**.
13. Rey, L., Freeze-drying/lyophilization of pharmaceutical and biological products. CRC Press: **2010**.
14. Strambini, G. B.; Gabellieri, E., Proteins in frozen solutions: evidence of ice-induced partial unfolding. *Biophysical journal* **1996**, 70 (2), 971.

15. Ahmad, F.; Bigelow, C. C., Thermodynamic stability of proteins in salt solutions: A comparison of the effectiveness of protein stabilizers. J*ournal of protein chemistry* **1986**, 5 (5), 355-367.

16. Murase, N.; Franks, F., Salt precipitation during the freeze-concentration of phosphate buffer solutions. *Biophysical chemistry* **1989**, 34 (3), 293-300.

17. Croyle, M. A.; Roessler, B. J.; Davidson, B. L.; Hilfinger, J. M.; Amidon, G. L., Factors that influence stability of recombinant adenoviral preparations for human gene therapy. *Pharmaceutical development and technology* **1998**, 3 (3), 373-383.

18. Privalov, P. L., Cold denaturation of protein. *Critical reviews in biochemistry and molecular biology* **1990**, 25 (4), 281-306.

19. Carpenter, J. F.; Chang, B. S.; Garzon-Rodriguez, W.; Randolph, T. W., Rational design of stable lyophilized protein formulations: theory and practice. Springer: **2002**.

20. Pikal, M. J., Mechanisms of protein stabilization during freeze-drying and storage: The relative importance of thermodynamic stabilization and glassy state relaxation dynamics. *Drugs and the Pharmaceutical Sciences* **2004**, 137, 63-108.

21. Hageman, M. J., The role of moisture in protein stability. *Drug Development and Industrial Pharmacy* **1988**, 14 (14), 2047-2070.

22. Carpenter, J. F.; Crowe, J. H., The mechanism of cryoprotection of proteins by solutes. *Cryobiology* **1988**, 25 (3), 244-255.

23. Mi, Y.; Wood, G.; Thoma, L.; Rashed, S., Effects of polyethylene glycol molecular weight and concentration on lactate dehydrogenase activity in solution and after freeze-thawing. *PDA Journal of Pharmaceutical Science and Technology* **2002**, 56 (3), 115-123.

24. Anchordoquy, T. J.; Carpenter, J. F., Polymers protect lactate dehydrogenase during freeze-drying by inhibiting dissociation in the frozen state. *Archives of biochemistry and biophysics* **1996**, 332 (2), 231-238.

25. Randolph, T. W., Phase separation of excipients during lyophilization: effects on protein stability. *Journal of Pharmaceutical Sciences* **1997**, 86 (11), 1198-1203.

26. Mankarious, S.; Griffith, M. J., Stabilized factor ix formulations containing trehalose. Google Patents: **2008**.

27. Prestrelski, S. J.; Tedeschi, N.; Arakawa, T.; Carpenter, J. F., Dehydration-induced conformational transitions in proteins and their inhibition by stabilizers. *Biophysical journal* **1993**, 65 (2), 661.

Chapter 7

1. Horava, S. D.; Peppas, N. A., Design of pH-Responsive Biomaterials to Enable the Oral Route of Hematological Factor IX. *Annals of Biomedical Engineering* **2016**, 1-13.
2. Knipe, J. M.; Chen, F.; Peppas, N. A., Enzymatic Biodegradation of Hydrogels for Protein Delivery Targeted to the Small Intestine. *Biomacromolecules* **2015**, *16* (3), 962-972.
3. Knipe, J. M.; Strong, L. E.; Peppas, N. A., Enzyme-and pH-responsive microencapsulated nanogels for oral delivery of siRNA to induce TNF-α knockdown in the intestine. *Biomacromolecules* **2016**.
4. Koetting, M. C.; Guido, J. F.; Gupta, M.; Zhang, A.; Peppas, N. A., pH-responsive and enzymatically-responsive hydrogel microparticles for the oral delivery of therapeutic proteins: Effects of protein size, crosslinking density, and hydrogel degradation on protein delivery. *Journal of Controlled Release* **2016**, *221*, 18-25.
5. Glangchai, L. C.; Caldorera-Moore, M.; Shi, L.; Roy, K., Nanoimprint lithography based fabrication of shape-specific, enzymatically-triggered smart nanoparticles. *Journal of Controlled Release* **2008**, *125* (3), 263-272.
6. Woodley, J. F., Enzymatic barriers for GI peptide and protein delivery. *Critical reviews in therapeutic drug carrier systems* **1993**, *11* (2-3), 61-95.
7. Vlieghe, P.; Lisowski, V.; Martinez, J.; Khrestchatisky, M., Synthetic therapeutic peptides: science and market. *Drug Discovery Today* **2010**, *15* (1), 40-56.
8. Khokhlov, A. R.; Kramarenko, E. Y., Polyelectrolyte/ionomer behavior in polymer gel collapse. *Macromolecular theory and simulations* **1994**, *3* (1), 45-59.
9. Kong, J.; Yu, S., Fourier transform infrared spectroscopic analysis of protein secondary structures. *Acta biochimica et biophysica Sinica* **2007**, *39* (8), 549-559.
10. Jameel, F.; Hershenson, S., Formulation and Process Development Strategies for Manufacturing Biopharmaceuticals. John Wiley & Sons: Hoboken, **2010**; Vol. 1.
11. Torres-Lugo, M.; Peppas, N. A., Preparation and characterization of P (MAA-g-EG) nanospheres for protein delivery applications. *Journal of Nanoparticle Research* **2002**, *4* (1-2), 73-81.
12. Klinger, D.; Landfester, K., Enzymatic- and light-degradable hybrid nanogels: Crosslinking of polyacrylamide with acrylate-functionalized Dextrans containing photocleavable linkers. *J. Polym. Sci. A Polym. Chem.* **2012**, *50* (6), 1062-1075.
13. Hilgendorf, C.; Spahn-Langguth, H.; Regardh, C. G.; Lipka, E.; Amidon, G. L.; Langguth, P., Caco-2 versus Caco-2/HT29-MTX co-cultured cell lines: permeabilities via diffusion, inside- and outside-directed carrier-mediated transport. *J. Pharm. Sci.* **2000**, *89* (1), 63-75.

14. Gupta, V.; Doshi, N.; Mitragotri, S., Permeation of Insulin, Calcitonin and Exenatide across Caco-2 Monolayers: Measurement Using a Rapid, 3-Day System. *PLoS ONE* **2013**, *8* (2), e57136.

15. Wood, K. M.; Stone, G. M.; Peppas, N. A., The effect of complexation hydrogels on insulin transport in intestinal epithelial cell models. *Acta Biomater.* **2010**, *6* (1), 48-56.

Chapter 8

1. Peppas, N. A.; Horava, S. D., Polymers for Delivery of Factor VIII and/or Factor IX. [Patent Pending].

2. Horava, S. D.; Peppas, N. A., Design of pH-Responsive Biomaterials to Enable the Oral Route of Hematological Factor IX. *Annals of Biomedical Engineering* **2016**, 1-13.

3. Kunzmann, A.; Andersson, B.; Thurnherr, T.; Krug, H.; Scheynius, A.; Fadeel, B., Toxicology of engineered nanomaterials: focus on biocompatibility, biodistribution and biodegradation. *Biochimica et Biophysica Acta (BBA)-General Subjects* **2011**, *1810* (3), 361-373.

4. Golla, K.; Reddy, P. S.; Bhaskar, C.; Kondapi, A. K., Biocompatibility, absorption and safety of protein nanoparticle-based delivery of doxorubicin through oral administration in rats. *Drug delivery* **2013**, *20* (3-4), 156-167.

5. Sonaje, K.; Lin, Y.-H.; Juang, J.-H.; Wey, S.-P.; Chen, C.-T.; Sung, H.-W., In vivo evaluation of safety and efficacy of self-assembled nanoparticles for oral insulin delivery. *Biomaterials* **2009**, *30* (12), 2329-2339.

6. Male, D. K., Immunology. Elsevier/Saunders: United States, **2013**; Vol. 8th.

7. Khan, M. M., Immunopharmacology. Springer: New York, **2008**.

8. Trinchieri, G., Interleukin-12 and the regulation of innate resistance and adaptive immunity. *Nature Reviews Immunology* **2003**, *3* (2), 133-146.

9. Schroder, K.; Hertzog, P. J.; Ravasi, T.; Hume, D. A., Interferon-γ: an overview of signals, mechanisms and functions. *Journal of leukocyte biology* **2004**, *75* (2), 163-189.

10. Gowda, S.; Desai, P. B.; Kulkarni, S. S.; Hull, V. V.; Math, A. A.; Vernekar, S. N., Markers of renal function tests. *N Am J Med Sci* **2010**, *2* (4), 170-173.

11. Zuo, Y.; Wang, C.; Zhou, J.; Sachdeva, A.; Ruelos, V. C., Simultaneous determination of creatinine and uric acid in human urine by high-performance liquid chromatography. *Analytical Sciences* **2008**, *24* (12), 1589-1592.

12. Cesta, M. F., Normal structure, function, and histology of the spleen. *Toxicologic pathology* **2006**, *34* (5), 455-465.

13. Greaves, P. M. B. C. B.; NetLibrary, I., Histopathology of preclinical toxicity studies: interpretation and relevance in drug safety evaluation. Academic Press: Amsterdam, **2007**; Vol. 3rd;4th;3;4;.

14. Cameron, R. I.; Allen, D. C.; NetLibrary, I., Histopathology specimens: clinical, pathological and laboratory aspects. Springer: New York;London;, **2004**.

15. Baratta, J. L.; Ngo, A.; Lopez, B.; Kasabwalla, N.; Longmuir, K. J.; Robertson, R. T., Cellular organization of normal mouse liver: a histological, quantitative immunocytochemical, and fine structural analysis. *Histochemistry and cell biology* **2009**, *131* (6), 713-726.

16. Seseke, F.; Thelen, P.; Hemmerlein, B.; Kliese, D.; Zöller, G.; Ringert, R., Histologic and molecular evidence of obstructive uropathy in rats with hereditary congenital hydronephrosis. *Urological research* **2000**, *28* (2), 104-109.

17. Cornes, J., Number, size, and distribution of Peyer's patches in the human small intestine: Part I The development of Peyer's patches. *Gut* **1965**, *6* (3), 225.

18. Treuting, P. M.; Dintzis, S. M., Comparative Anatomy and Histology: A Mouse and Human Atlas. Academic Press: US, **2012**; Vol. Expert Consult: Online and Print.

19. Paris, F.; Fuks, Z.; Kang, A.; Capodieci, P.; Juan, G.; Ehleiter, D.; Haimovitz-Friedman, A.; Cordon-Cardo, C.; Kolesnick, R., Endothelial apoptosis as the primary lesion initiating intestinal radiation damage in mice. *Science* **2001**, *293* (5528), 293-297.

Chapter 9

1. Peppas, N. A.; Horava, S. D., Polymers for Delivery of Factor VIII and/or Factor IX. [Patent Pending].

2. Horava, S. D.; Peppas, N. A., Design of pH-Responsive Biomaterials to Enable the Oral Route of Hematological Factor IX. *Annals of Biomedical Engineering* **2016**, 1-13.

3. Gamboa, J. M.; Leong, K. W., In vitro and in vivo models for the study of oral delivery of nanoparticles. *Advanced Drug Delivery Reviews* **2013**, *65* (6), 800-810.

4. Frangioni, J. V., In vivo near-infrared fluorescence imaging. *Current Opinion in Chemical Biology* **2003**, *7* (5), 626-634.

5. Inoue, Y.; Izawa, K.; Kiryu, S.; Tojo, A.; Ohtomo, K., Diet and abdominal autofluorescence detected by in vivo fluorescence imaging of living mice. *Molecular imaging* **2008**, *7* (1), 21-27.

6. Panthani, M. G.; Khan, T. A.; Reid, D. K.; Hellebusch, D. J.; Rasch, M. R.; Maynard, J. A.; Korgel, B. A., In Vivo Whole Animal Fluorescence Imaging of a Microparticle-Based Oral Vaccine Containing (CuInSe x S2–x)/ZnS Core/Shell Quantum Dots. *Nano letters* **2013**, *13* (9), 4294-4298.

7. Peterson, J. D., Imaging Gastric Emptying with GastroSense 750. *PerkinElmer* **2012**.

8. Tseng, J.-C.; Vasquez, K.; Peterson, J. D., Optical Imaging on the IVIS SpectrumCT System: General and Technical Considerations for 2D and 3D Imaging. *PerkinElmer* **2015**.

9. Curtis, A.; Calabro, K.; Galarneau, J.-R.; Bigio, I. J.; Krucker, T., Temporal variations of skin pigmentation in C57BL/6 mice affect optical bioluminescence quantitation. *Molecular Imaging and Biology* **2011**, *13* (6), 1114-1123.

10. Schwarz, R.; Kaspar, A.; Seelig, J.; Künnecke, B., Gastrointestinal transit times in mice and humans measured with 27Al and 19F nuclear magnetic resonance. *Magnetic resonance in medicine* **2002**, *48* (2), 255-261.